THE AGGREGATION OF α-SYNUCLEIN AND ITS INHIBITION

Thesis submitted in accordance with the requirements of the

University of Liverpool

For the degree of

Doctor in Philosophy

By

James Hilary Torpey

May 2019

UNIVERSITY OF LIVERPOOL

Table of Contents

Figure List

Table list

Abstract

The aggregation of the human brain protein alpha-synuclein is associated with Parkinson's disease and a host of other neurodegenerative diseases termed the synucleinopathies. In this thesis is described aspects of the pathophysiology of alpha-synuclein and that of six point mutants associated with familial Parkinson's disease, as well as strategies aimed at impeding the aggregation process.

A novel ten-residue peptide – KDGIVNGVKA – was identified using NMR spectroscopy as binding to aggregated forms of alpha-synuclein and preventing fibril elongation. Through the use of multiple alanine-scanning variants of the peptide it was determined that a critical three-residue stretch – IVN – was essential for binding to alpha-synuclein aggregates. Through the use of cell viability and NMR metabolomics experiments the impact of these shortened amyloid fibrils formed in the presence of the peptide on SH-SY5Y cells was assessed. The shortened fibrils did not result in an increase in toxicity and the cellular metabolome of the challenged cells was more similar to those of the control samples than of those cells challenged with the fibrils formed without the peptide inhibitor.

In this thesis a hitherto uncharacterized interaction between alpha-synuclein and the peptidyl-prolyl isomerase cyclophilin-D was described. Through a combination of NMR and isothermal titration calorimetry it was shown that cyclophilin-D binds to alpha-synuclein at its acidic C-terminus, and through ThT fluorescence assays that this was sufficient to prevent alpha-synuclein aggregation. The incubation of pre-formed alpha-synuclein fibrils with cyclophilin-D resulted in their dramatic shortening, as seen by TEM, and the restoration of peaks associated with the monomeric protein in the HSQC NMR spectra. These are evidence that cyclophilin-D disaggregates alpha-synuclein fibrils. This disaggregation activity was dependent on the cis-trans isomerase activity of cyclophilin-D and was not observed using the catalytically compromised mutants R55K and R82K.

Through the use of circular dichroism spectroscopy, the lipid-binding affinity of alpha-synuclein, its point mutants, and nitrated forms was probed. Nitration, a post-translational modification identified in Lewy bodies, was found to impair lipid-binding, which may be of importance given recent reports in the literature of large levels of membranes present in Lewy bodies. The rates of alpha-synuclein aggregation were compared using ThT fluorescence, and it was found that nitrated alpha-synuclein was incapable of forming amyloid fibrils. Additionally, through the use of TEM the length and morphology of the fibrils formed by the different mutants was observed, and a lengths analysis was conducted. This revealed that A30P formed extremely long fibrils, whilst G51D and A53E formed particularly short fibrils. Together these experiments shed light on the pathophysiology of alpha-synuclein, with novel findings not shown previously for the six disease-linked mutants.

Acknowledgements

My PhD began five years ago and I have now, at long last, reached the end of the road. I need to thank a great many people without whom this would not have been possible. First and foremost I'd like to thank my supervisors Jill Madine and Dan Rigden, who took me on after a series of unfortunate events in the first years of my PhD. It is thanks to their support and belief in me that I have been able to complete my research project and compile this thesis. I would like to thank Hannah Davies for her vital help and support in the lab, assistance in the lunchtime crossword, and for regular necessary trips to Caffé Nero for a Milano hot chocolate. My thanks also go to Kieran Hand, Kiani Jeacock, Alana Maerivoet, Nathan Cumberbatch and Heike Arnolds for their cheery dispositions in journal club, and also for their help in the lab. I'd also like to thank my flatmate Nick Thomas, and Chris Hill and the AJs crew for maintaining my sanity with drinks after work and for helping me have a great time!

I would like to thank Marie Phelan, Igor Barsukov and Lu-Yun Lian for their invaluable assistance and training in NMR spectroscopy, and to Svetlana Antonyuk for her training of me in crystallography. Amy Wood deserves thanks for preparing CypD. Mark Wilkinson and Philip Brownridge very kindly ran mass spectrometry experiments for me on my synuclein and its mutants. Gaz Wright deserves special credit for training me in the lab in the first years of my PhD.

I owe a great debt of gratitude to Meriel Jones, Linda Marsh, Rob Beynon, Caroline Dart, and Anthony Hollander. These people stepped up for me when I needed it most and as a result I was able to complete my PhD. I similarly would like to thank the following staff at the Synchrotron SOLEIL: Andrew Thompson, Beatriz Guimarães, Serena Sirigu, Pierre Legrand, Leonard Chavas, Nicolas Foos, Denis Duran, Patrick Gourhant, Frank Wien, and Blandine Pineau for being so warm and welcoming of me, and for their own support during the trials and tribulations of my PhD.

Finally I'd like to thank my Mum & Dad (and Pippin the corgi) for simply everything!

Abbreviations

Aβ = Amyloid-β peptide

AD = Alzheimer's disease

AFM = Atomic force microscopy

ANOVA = Analysis of variance

APP = Amyloid-β precursor protein

aSyn = α-synuclein

ATP = Adenosine triphosphate

BSA = Bovine serum albumin

bSyn = β-synuclein

CD = Circular dichroism

CJD = Creutzfeld-Jakob disease

CMC = Critical micelle concentration

CNS = Central nervous system

CPMG = Carr-Purcell-Meiboom-Gill (NMR experiment)

CsA = Ciclosporin A

CTD = C-terminal domain (of α-synuclein)

Cryo-EM = Cryo-electron microscopy

CypD = Cyclophilin-D (*PPIF)*

ddH_2O = double-distilled water

DEPA = diethylenetriaminepentaacetic acid

DLB = Dementia with Lewy bodies

DOPC = 1,2-dioleoyl-*sn*-glycero-3-phosphocholine

DOPE = 1,2-dioleoyl-*sn*-glycero-3-phosphoethanolamine

DOPS = 1,2-dioleoyl-*sn*-glycero-3-phospho-L-serine

EDTA = Ethylenediaminetetraacetic acid

ESI = Electrospray ionization

FBS = Fetal bovine serum

FDR = False discovery rate

FID = Free induction decay

GABA = γ-aminobutyric acid

GCI = Glial cytoplasmic inclusion

GHB = γ-hydroxybutyric acid

gSyn = γ-synuclein

HCD = Higher energy collisional dissociation

HFIP = Hexafluoroisopropanol

HSQC = Heteronuclear single quantum coherence

HT = High tension

IAPP = Islet amyloid polypeptide precursor

IDP = Intrinsically disordered protein

IDR = Intrinsically disordered region

INEPT = Insensitive nuclei enhanced through polarisation transfer

IPTG = Isopropyl-β-D-1-thiogalactopyranoside

ITC = Isothermal titration calorimetry

LB = Lewy body

LBVAD = Lewy body variant of Alzheimer's disease

LC = Liquid chromatography

L-DOPA = L-3,4-dihydroxyphenylalanine

LN = Lewy neurite

LN_2 = Liquid nitrogen

LSD = Least significant difference

MEM = Minimal essential medium

mPTP = mitochondrial permeability transition pore

MPTP = 1-methyl-4-phenyl-1,2,3,6-tetrahydropyridine

MS = Mass spectrometry

MSA = Multiple system atrophy

MTT = 3-(4,5-dimethylthiazol-2-yl)-2,5-diphenyltetrazolium bromide

MWCO = Molecular weight cut-off

NAC = Non amyloid-β component (of α-synuclein)

NFT = Neurofibrillary tangle

NMR = Nuclear magnetic resonance

NOE = Nuclear Overhauser effect

NOESY = Nuclear Overhauser effect spectroscopy

NRMSD = Normalized root mean square deviation

NTD = N-terminal domain (of α-synuclein)

OD_{600} = Optical density (at 600nm)

PBS = Phosphate buffered saline

PCA = Principal component analysis

PD = Parkinson's disease

PDD = Parkinson's disease with dementia

Pen-Strep = Penicillin-Streptomycin

PLS-DA = Partial least squares discriminant analysis

PNS = Peripheral nervous system

PPI = Protein-protein interaction

PPIase = Peptidyl-prolyl isomerase

ppm = parts per million

PrP = Prion protein

PTM = Post-translational modification

RF = Radiofrequency (pulse)

RNS = Reactive nitrogen species

ROS = Reactive oxygen species

SAXS = Small-angle X-ray scattering

SDS-PAGE = Sodium dodecyl sulfate polyacrylamide gel electrophoresis

SOC = Super optimal broth with catabolite repression

SPR = Surface plasmon resonance

SNARE = Soluble N-ethylmaleimide-sensitive factor attachment protein receptor

ssNMR = Solid-state NMR

SUV = Small unilamellar vesicle

TEM = Transmission electron microscopy

ThS = Thioflavin S

ThT = Thioflavin T

TMS = Tetramethylsilane

TSP = Trimethylsilylpropanoic acid

TOCSY = Total correlation spectroscopy

UV = Ultraviolet

VIP = Variable importance in projection (plot)

WaterLOGSY = Water-ligand observed via gradient spectroscopy

WT = Wild-type

1 Introduction

1.1 Definition of amyloid

The International Society of Amyloidosis defines amyloid as a protein that has misfolded to form insoluble fibrils which are largely deposited extracellularly (1). To be deemed amyloid the fibrils must bind to Congo red dye (Figure 1-1) and exhibit green, yellow or orange birefringence when observed under polarized light, and when isolated should exhibit a cross-β X-ray diffraction pattern (1). Amyloid itself is often associated with disease, but functional amyloids have also been discovered (e.g. biofilms) (2). It is also common to use the benzathiazole dyes thioflavin-S (ThS) and thioflavin-T (ThT) (Figure 1-1) to monitor amyloid formation, although neither are considered definitive indicators of amyloid. ThS is maximally excited at 389nm with an emission maxima at 426nm; this fluorescence is dramatically enhanced when the dye is bound to β-sheets. ThT operates in the same way but has a characteristic shift in fluorescence excitation and emission maxima upon binding (from 385 to 450nm and 445 to 482nm, respectively).

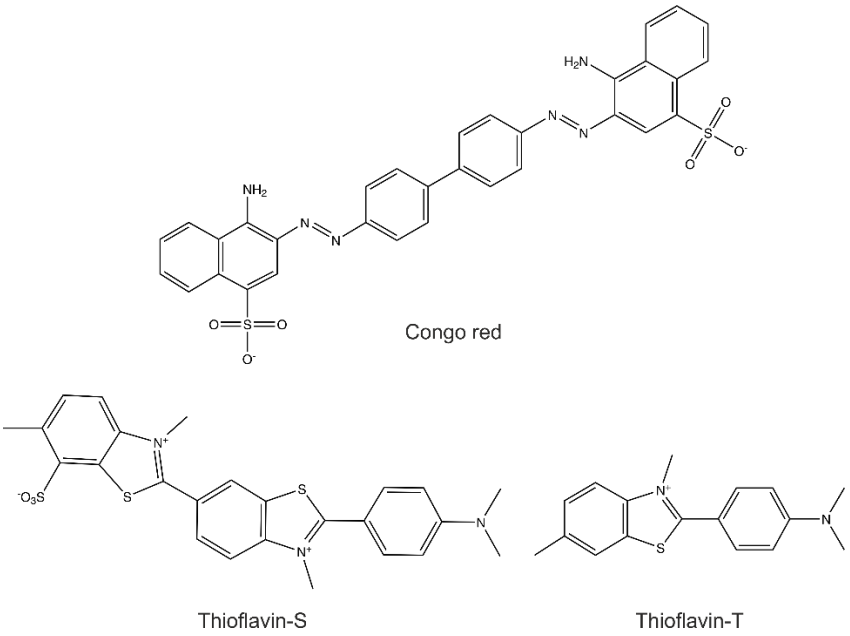

Figure 1-1 - Structure of the amyloid-binding dyes Congo red, ThS, and ThT. *Top) Structure of the dye Congo red. The binding of Congo red is a requirement for aggregates to be deemed true amyloid. Bottom) The structure of the benzothiazole dyes ThS (left) and ThT (right).*

Well-known examples of amyloid include the peptide amyloid-beta (Aβ) – associated with Alzheimer's disease – in which it forms extracellular plaques in the central nervous system (CNS) (3), and also islet amyloid polypeptide (IAPP) – associated with diabetes mellitus type II – in the Islets of Langerhans in the pancreas (4). The proteins alpha synuclein (aSyn) and the microtubule-associated protein tau have traditionally been considered "amyloid-like" or "intracellular amyloid" given the fact that the deposits of these aggregated proteins are found intracellularly within the neurons. However, they have recently been officiated by the International Society of Amyloidosis as true amyloids given the fact that after cell death these deposits may be found extracellularly (1).

1.2 Protein mis-folding and aggregation

In the case of pathological amyloids, life begins as a native protein with a physiological function. These proteins then undergo some sort of change that allows for their aggregation; the cause of this is not always clear. For example, in the case of the amyloid-β precursor protein (APP) the protein is proteolytically processed by beta secretase-I (BACE-I), and subsequently a γ-secretase, to form the Aβ peptide (5–7). In others, off-pathway species are formed during folding which can serve as nucleation points or "seeds", or the protein structure is disturbed in some way by mutations or by changes in the local environment that result in the exposure of normally buried residues that can act as interfaces for aberrant protein-protein interactions (PPIs). This new aggregation-capable species is the "nucleus". The formation of the nucleus is usually a slow and rare event. The length of time needed for the emergence of this nucleus species is termed the "lag-phase", and this is the time-limiting step. This nucleus provides a platform for further mis-folding and aggregation to form higher-order oligomeric species: dimers, trimers, tetramers and onward (Figure 1-2). These oligomers are structurally ambiguous. Some have appeared as: spheres, beads-on-a-string, annular structures or 'tubes', and more (8,9). Their characterization is difficult due to their heterogeneity and that isolation may alter the chemical kinetics enabling their existence. The oligomers begin to take on more and more of a cross-β character, at which point they begin to be

termed “protofibrils” and “protofilaments”. Protofibrils consist of stacks of individual monomeric units that each form β-strands of an overall β-sheet architecture growing in the direction of the fibril axis. Each sheet is held together by hydrogen bonds formed from the backbone amides (and also any sidechain amides) to those above and below the β-strand. The monomeric units may form quite complex motifs (e.g. Greek key) with multiple strand-forming regions (10). Complementary β-strands within the same monomer may interact via electrostatic interactions to form so-called “zippers” that repeat throughout the sheet. These zippers usually exclude water and thus hydrophobics, as well as electrostatics, play an important role in maintaining the stability of the protofilament. The cross-β X-ray fibre diffraction images reveal sharp reflections at 4.7Å and 10Å, corresponding to the inter-strand and inter-sheet spacings respectively (Figure 1-3). Multiple protofilaments ultimately align or twine around each other, depending on local conditions, to form the final fibril. This fibril will be approximately 10nm in diameter and can be considered to be a highly energetically stable, off-pathway form of the protein (11).

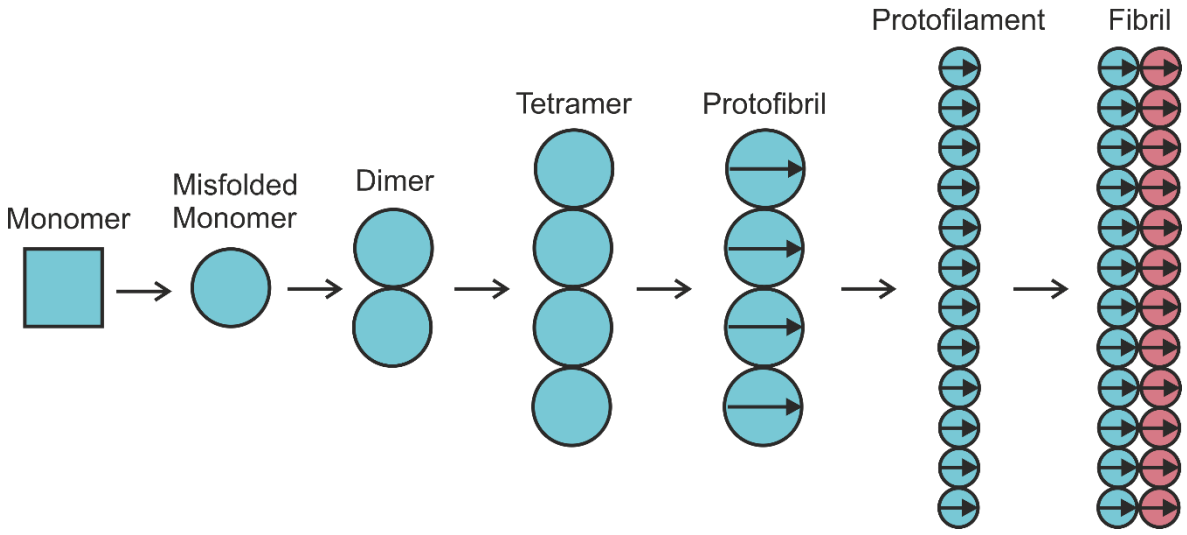

Figure 1-2 - Schematic showing the process of amyloid formation. *A folded monomeric unit misfolds in such a way as to enable aberrant interactions with other misfolded units. These multimeric units grow and take on increasing levels of β-structure. These β-strands ultimately stack to form vast β-sheets, becoming protofibrils and later protofilaments. Multiple protofilaments may associate or intertwine forming a fibril.*

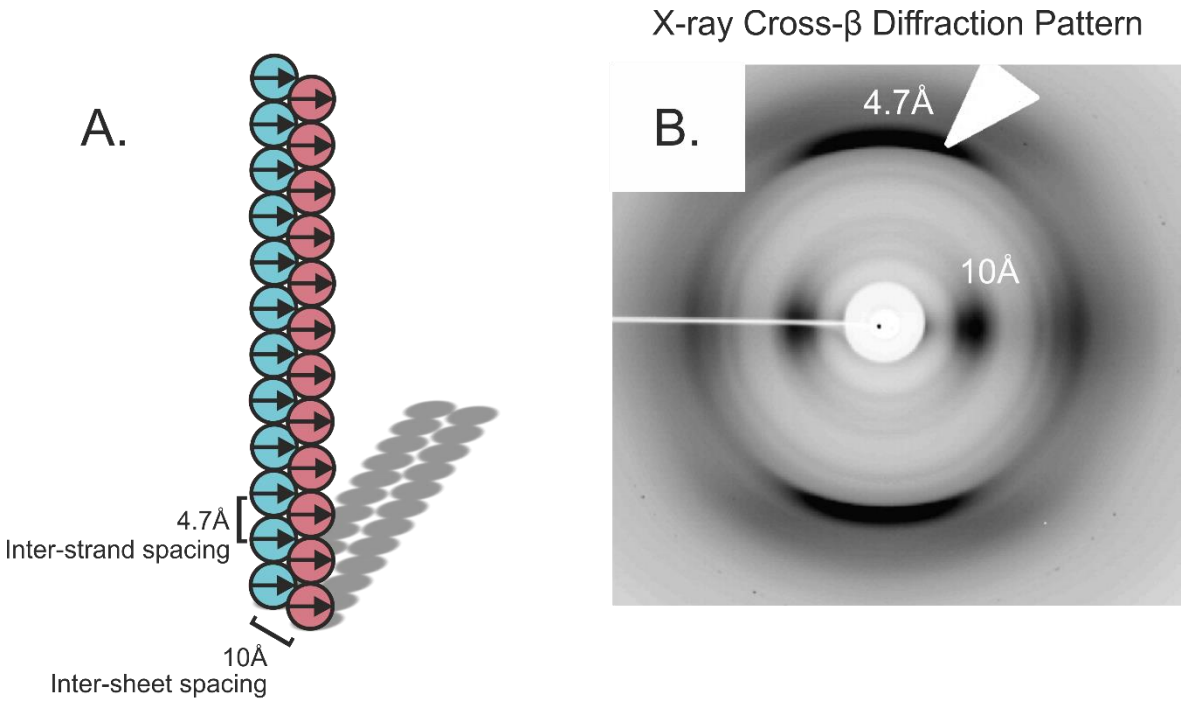

Figure 1-3 - Schematic showing how the inter-strand and inter-sheet spacings of amyloid fibrils give rise to a cross-ß X-ray diffraction pattern. *The image is the diffraction pattern from fibrils of Aβ(1-42). Adapted from* (12).

It is to be noted that a single peptide or protein can form different types of fibril; so-called "strains". These strains may have different structures and toxicities, and as a result are of interest with regards to disease. For example, aSyn has been implicated in a host of neurodegenerative diseases. It remains an open question as to whether and to what extent different strains correspond to different pathologies. Two distinct strains of aSyn with different structures, levels of toxicity and seeding capacities have recently been reported and this may influence pathology, through differing rates of elongation and capacity for seeding (13,14). Different strains seem to be formed under different environmental conditions *in vitro* such as: ionic strength, pH, and the number of 'seeding generations' (14). This is perhaps unsurprising as these factors influence the interactions holding fibrils together dramatically; changes will result in differences in interaction and result in the stabilization of different species.

1.3 Will the toxic species please stand up?

Many neurodegenerative diseases are associated with amyloid. This includes aSyn with Parkinson's disease (PD) and the other synucleinopathies, Aβ with Alzheimer's disease (AD), tau with AD and the tauopathies, and huntingtin with Huntington's disease (HD) (3,15–17). The question of how the amyloids are associated with neuronal cell death is an open one. Disease onset and progression appears to be linked with protein aggregation and it has historically been thought that the amyloid fibrils must be toxic. It was thought that extracellular fibrils could disrupt the cell membrane whilst intracellular fibrils may disrupt axonal transport (18). This view has been challenged in recent years by the discovery that the severity of AD does not correlate with deposition of Aβ fibrils, as shown in patients immunized against $A\beta_{42}$ (19). This has led to the consensus moving in another direction; that it is the prefibrillar oligomeric species that are the arbiters of toxicity (20). Oligomers have been observed to form a variety of different structures and have been shown to be able to interact with, and disrupt, lipid membranes (21). If oligomers are truly the toxic species responsible for mediating cell death then the fibrils may be thought of repositories that sequester the oligomers away, and thus may be protective. Alternatively, the fibrils could be seen as a source of potentially toxic material if the equilibrium were to shift in favour of fibril disassembly.

1.4 Intrinsically disordered proteins

ASyn and the other members of the synuclein family are all intrinsically disordered proteins (IDPs), which is to say that they lack any stable fold or tertiary structure in solution. Recent estimates suggest that ≥30% of all eukaryotic proteins are either IDPs or contain intrinsically disordered regions (IDRs) (22). IDPs and IDRs generally contain very few hydrophobic residues to form any kind of "hydrophobic core" around which the protein could fold. Instead they are rich in polar and charged residues, and display a lack of any defined structure (23). These proteins fly in

the face of the traditional structure-function relationship that has historically underpinned the field of structural biology. As a direct result of this, IDPs and IDRs represent a particular challenge as structural biology has been largely built around the determination of stable tertiary structures using X-ray crystallography and, recently, cryo-electron microscopy (cryo-EM). Nuclear magnetic resonance (NMR) spectroscopy and other "softer" solution-based biophysical techniques, such as circular dichroism (CD) spectroscopy and small angle X-ray scattering (SAXS), have proven to be the most successful techniques with regard to gaining a real understanding of the behaviour of aSyn and other IDPs as they recognize the key role that dynamics plays alongside structure in protein functionality. The structural plasticity of IDPs means that they are capable of a wide-array of different functions. These can be in protein-protein interactions, chaperone activity, lipid-protein interactions, ligand-scavenging, and linker regions. Many reviews have been written on this class of proteins which can go into far greater detail than myself here (24). The role of aSyn, tau and other IDPs in neurodegenerative disease represent something of a clarion call for a field that needs to take IDPs seriously and push for a greater understanding of their physiological and pathophysiological roles.

1.5 The synuclein family

ASyn is a 140-residue protein expressed primarily within the neurons, where it is localized at the presynaptic terminals (25). ASyn belongs to the *synuclein* family of proteins consisting of: aSyn (14.5kDa), beta synuclein (bSyn) (14.3kDa), and gamma synuclein (gSyn) (13.3kDa), the physiological functions of which all remain obscure. Of the three, aSyn is by far the most intensely studied and over the past two decades a picture has gradually been emerging suggesting a role in vesicle docking/replenishment at the synaptic membrane through the promotion of soluble N-ethylmaleimide-sensitive factor attachment protein receptor (SNARE) complex formation (26). BSyn and gSyn exhibit 61.6% and 48.3% sequence identity to aSyn, respectively (Figure 1-4). BSyn

is also found in the presynaptic terminals of the brain and CNS, whilst gSyn appears to be found predominantly in the peripheral nervous system (PNS) (27,28).

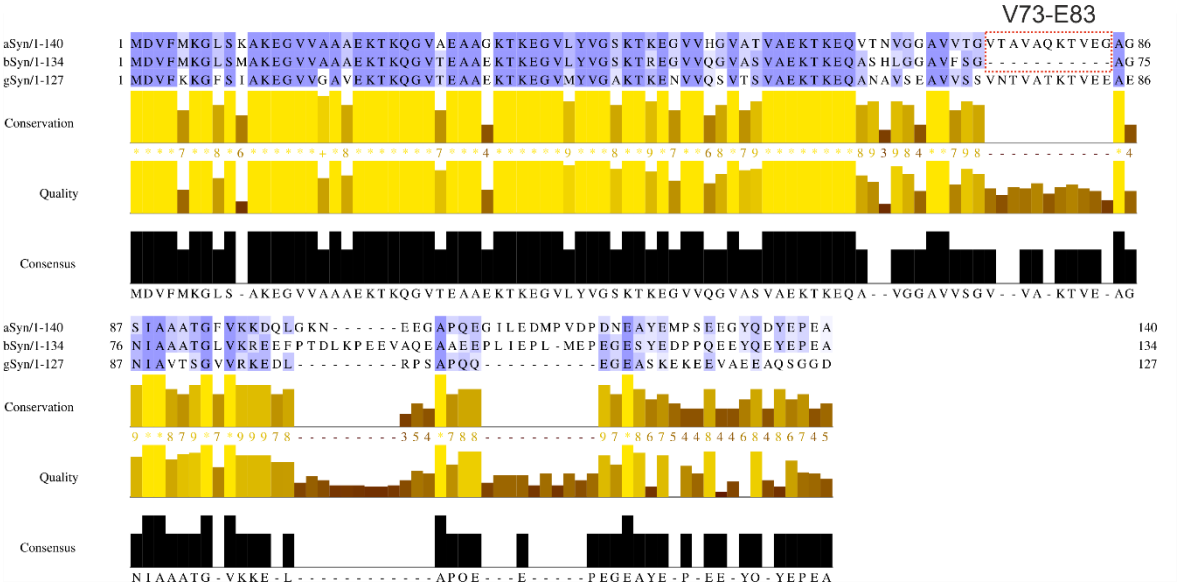

Figure 1-4 - Multiple sequence alignment of aSyn, bSyn, and gSyn. *Those residues highlighted in blue are conserved across all three proteins, whilst lighter blue indicates that the residue is conserved across two of the three proteins. The dashed red box indicates the residues Val73-Glu83 found in the NAC region of aSyn that are absent in bSyn. The alignment was produced in Jalview* (29).

1.5.1 The structure of α-synuclein

ASyn is a 140-residue IDP which is classically divided into three domains: the N-terminal domain (NTD) (1 – 60), the non-Aβ component (NAC) domain (61 – 95), and the C-terminal domain (CTD) (96 – 140) (see Figure 1-5). The NTD is largely positively charged due to the high prevalence of lysine residues. This is because the NTD mediates the interactions with the lipid membranes of synaptic vesicles, which are rich in negatively charged lipid head groups (30–32). The NTD contains seven 11-residue imperfect repeats containing the key KTKEGV motif. The repeats enable the NTD to form a helix that sits across the top of lipid membranes which is thought to be related to aSyn's function. Solution structures of aSyn bound to detergent micelles have been solved using NMR to reveal a broken helix conformation, wherein there is a slight break in the helix between residues 38-45 (see Figure 1-6) (30). It is thought that in contact with synaptic vesicles aSyn forms an

unbroken helix (33). It is also known that N-terminal acetylation, which is a native modification *in vivo*, results in an increase in the helix-forming propensity of aSyn (34). The NAC region has historically been thought to be the main fibril-forming region of aSyn, although the fibril core has since been shown to extend beyond the confines of the NAC domain (10,35). This region is the most hydrophobic part of aSyn and appears to act as a secondary site of lipid interaction (36,37). The CTD is the most dynamic region of aSyn and contains a preponderance of negatively charged aspartic and glutamic acid residues. The function of this domain is unclear, although there have been reports of it transiently "folding over" the hydrophobic NAC domain as a "shield" and of binding to components of the SNARE complex (38,39). C-terminally truncated aSyn (residues 1-123 or 1-120) aggregates more rapidly than the full-length protein and is commonly found in deposits of the protein (40). This may be a result of the loss of a highly soluble portion of the protein and the concomitant loss of "shielding" provided to the NAC region, allowing for aberrant hydrophobic interactions.

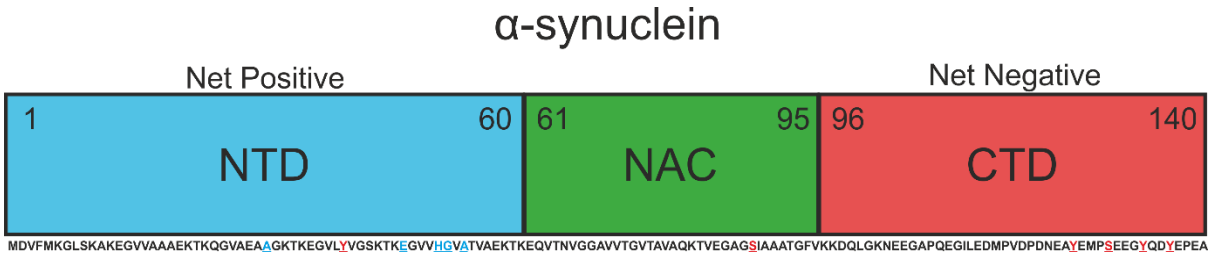

Figure 1-5 - Schematic of aSyn domain organization and mutation/modification sites. *The NTD (1-60), NAC domain (61-95), and the CTD (96-140) are shown. The full length amino acid sequence is written underneath. PD-linked point mutation sites are underlined and highlighted in blue, whilst those sites shown to undergo either nitration or phosphorylation are underlined and highlighted in red.*

Until recently, aSyn has been exclusively reported to exist as a monomer within the cytosol. However this view was challenged in 2011 by *Bartels et al* who reported the discovery of aSyn in a tetrameric form that they believed was the primary and functional form of the protein (41). Indeed, they claimed that the "native" tetrameric form of aSyn was aggregation-resistant and it was the disruption of the tetramer that allowed aSyn to aggregate and ultimately trigger the death of

neurons. The authors claimed that the tetramer had escaped notice due to the extremely harsh purification procedures (e.g. boiling, acidification etc) used in protein preparation. These findings were the target of a wide-degree of suspicion in the scientific community, for a host of reasons. These included criticisms that the aSyn used in the experiment was isolated from erythrocytes rather than brain tissue and the inability of the community to replicate their results. Indeed, after a series of tit-for-tat publications rebutting each other the issue seems to have been put to rest in a publication by *Theillet et al* in which in-cell NMR was used to study aSyn in a more physiologically representative environment; within mammalian neuronal cells (42–44). This study showed that aSyn existed predominantly as an acetylated monomer within the cytosol.

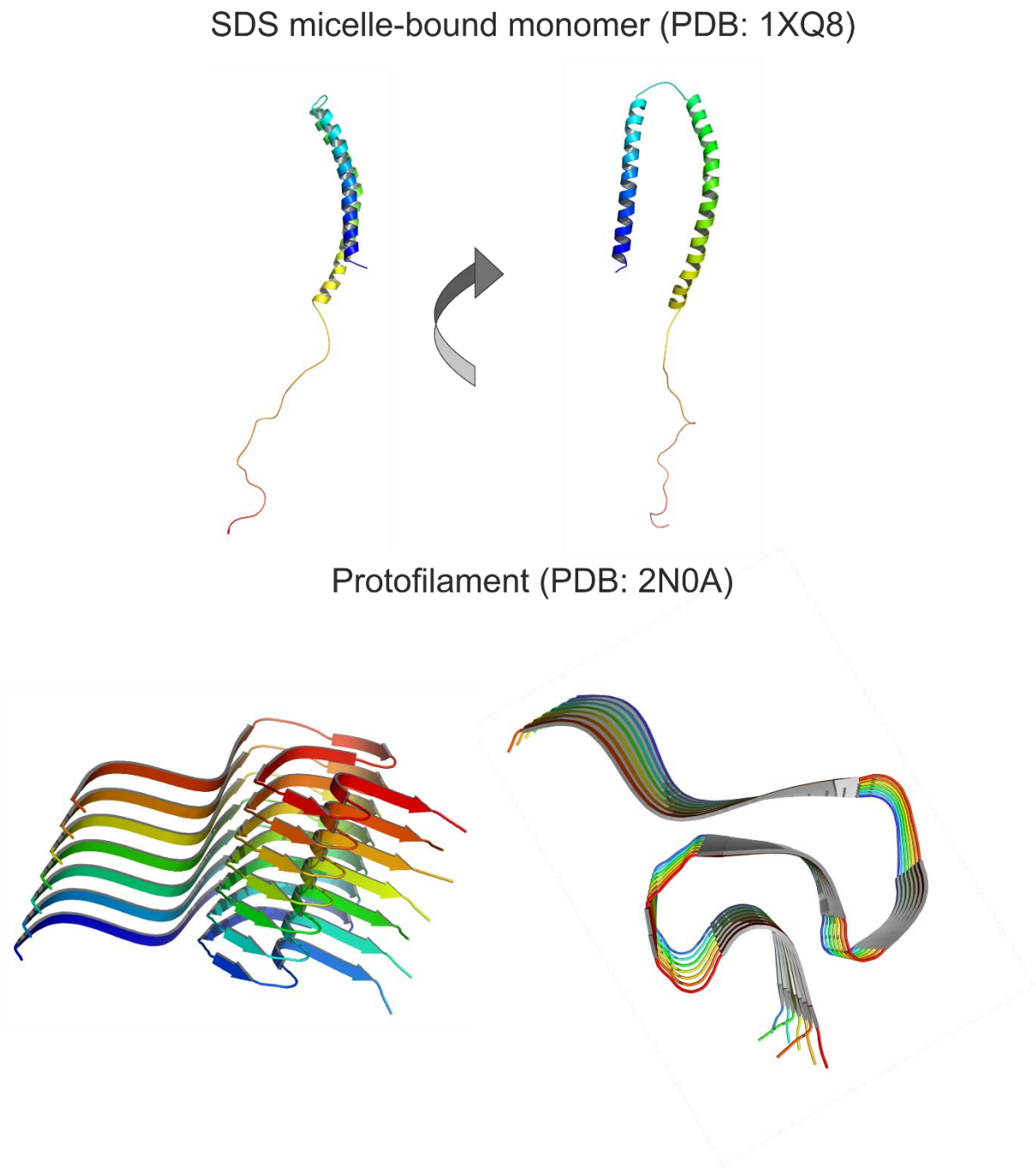

Figure 1-6 - Different structures adopted by aSyn, as solved by solution-state and solid-state NMR. *Top) The structure of monomeric micelle-bound aSyn solved by solution-state NMR. Note the broken helix formed between residues 1-92 that would lie across the surface of the micelle. Bottom) The ssNMR structure of a single aSyn protofilament exhibiting a striking "Greek-key" β-architecture. The N-terminal residues 1-38 and C-terminal residues 97-140 are disordered and have been removed from the image. The leftmost image shows the fibril at a sideways angle, whilst the rightmost image shows a "birdseye view" of the fibril coming out of the page.*

As an amyloid protein aSyn's monomeric form will begin to oligomerize and eventually form fibrils. There has been no successful characterization of aSyn oligomers in high-resolution as they are very heterogenous and extremely condition-dependent, although SAXS has recently been used to obtain low-resolution models over the time course of aggregation (45). Moreover any attempt

to isolate these oligomers will disrupt the delicate equilibrium in which they exist, and thus they could change. Until very recently the fibrils of aSyn were also very poorly characterized. However, with the latest advances in solid-state NMR (ssNMR) and cryo-EM the mystery has begun to be picked apart. *Tuttle et al* showed in a landmark paper that the aSyn protofilament adopts a "Greek-key" motif (Figure 1-6) (10). This structure was solved by ssNMR and has since been validated by cryo-EM (46). Impressively, the N- and C-termini of the protein remain completely disordered even in the fibril structure. Cryo-EM has been particularly helpful in probing the structure of whole fibrils and different polymorphs. The paper by *Li et al*, for example, looked at so-called "rod" and "twister" polymorphs (46). They showed that each fibril was composed of two protofilaments and that in the rod fibrils those protofilaments adopted the Greek-key conformation identified by ssNMR. However, in the twister polymorph the Greek-key was incompletely formed and was instead a "β-arch". This also meant that fewer residues were involved in the actual fibril and it was suggested by the authors that this is what contributed to the "twister" morphology, as there were more residues extending out into space (46).

1.5.2 The function of α-synuclein

Despite intense study for 30 years, aSyn remains something of an enigma. This is especially so with regards to its physiological function which is still poorly understood. ASyn is predominantly expressed in the brain and localized to presynaptic terminals (25). Here it is thought to play a role in the regulation of the docking of synaptic vesicles to the presynaptic membrane (26,47). Despite being a widely conserved protein, the deletion of aSyn in mice was not lethal. Instead these mice displayed a vastly reduced synaptic response to a prolonged train of stimulation (47). Examination by transmission electron microscopy (TEM) revealed a stark reduction in the number of vesicles in the "reserve pool" – those vesicles standing by to dock to the presynaptic membrane after those already docked fuse when the synapse fires (47). Headway has been made recently with several high-profile publications. It was described by *Burré et al* that aSyn at the presynaptic membrane

binds to the N-terminal of synaptobrevin-2 via its CTD and that this instigated the formation of SNARE complexes, which themselves promote vesicle fusion (39) . The same group later showed that aSyn at the membrane multimerizes and that it was this form of the protein – not cytosolic monomeric aSyn – that promoted SNARE formation (26).

1.5.3 The structure and function of β- and γ-synuclein

BSyn and gSyn are both poorly characterized. Neither protein is aggregation prone. GSyn is the most substantially different from the others, but the main difference between aSyn and bSyn lies in the fact that bSyn lacks the Val73-Glu83 portion of the NAC domain (Figure 1-4). Intriguingly, the addition of these residues to bSyn does not result in it becoming amyloidogenic and the formation of fibrils as may have been expected (48). It is thought that the role of this 11-residue patch in aSyn aggregation is as much a feature of its location in the sequence as its relative hydrophobicity and simply inserting this into the corresponding region in bSyn is not enough. This case emphasizes the point that comparatively simple changes made to IDPs don't always have the expected consequence, despite the lack of any 3D structure that may be distorted. This point is also evident with respect to point mutations in aSyn. As stated earlier, there are six known pathogenic mutations in aSyn that are associated with PD. Despite these only being single point mutations and the mutation sites all being very close together (five of the six mutation sites are within seven residues of each other – see Figure 1-5) the effects are quite different. For example H50Q reportedly results in a late-onset form of PD, whilst G51D leads to an early-onset form (49,50). It is clearly of great importance to have a comprehensive and complete understanding of aSyn and how minor changes affect it – as they can clearly have quite radically different clinical effects.

1.6 Lewy bodies, Lewy neurites, and glial cytoplasmic inclusions

Lewy bodies (LBs) are named after Fritz Heinrich Lewy who studied them in detail in the early 20th century. LBs are intracellular proteinaceous inclusions found within neurons and are the

pathological hallmark of PD and some other synucleinopathies (Figure 1-7 A). They are composed primarily of misfolded forms of aSyn and are immuno-reactive to the protein. Immunohistochemistry reveals a dense "core" region and a lighter "halo" surrounding it (51). Approximately 90% of the aSyn deposited within LBs is phosphorylated at S129, whilst only 5% of protein is phosphorylated at the residue outside of the LBs (52). Nitrated and C-terminally truncated forms of aSyn have also been identified in LBs (53,54). It is unclear whether these modifications encourage the protein's deposition into LBs – hence their enrichment over homeostatic levels – or whether they occur post-deposition. Ubiquitin colocalizes with aSyn in LBs. This suggests that aSyn within LBs has been marked for degradation, but that perhaps the cellular degradation machinery is overwhelmed or incapable of removing the fibrillar aSyn (55).

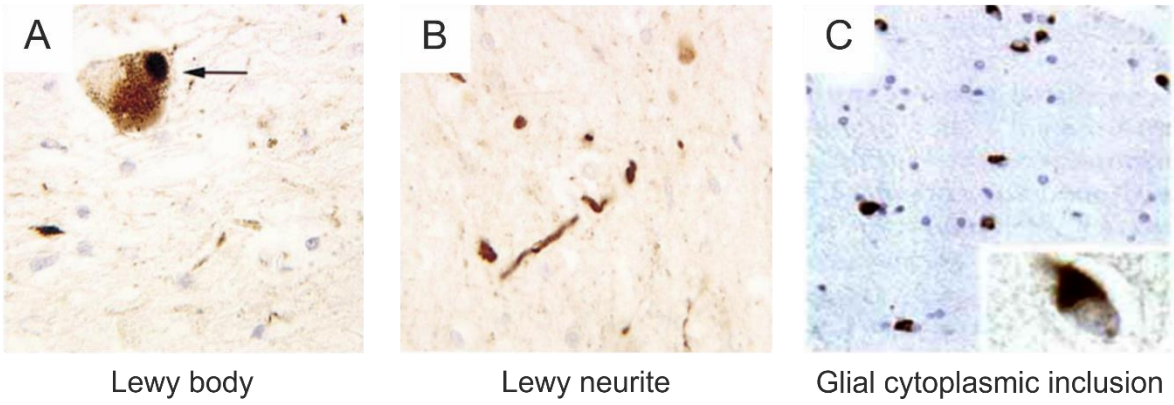

Figure 1-7 - Lewy bodies, Lewy neurites and glial cytoplasmic inclusions. *A) Lewy bodies immunostained for aSyn in neurons of the subtantia nigra. B) Lewy neurite immunostained for aSyn in neurons of the substantia nigra. C) Glial cytoplasmic inclusions immunostained for aSyn in the frontal cortex. Images taken from* (17,56).

Neurites are projections from neuronal cells and Lewy neurites (LNs) are those projections that contain aggregated aSyn (Figure 1-7 B). In this sense they are similar to LBs and are also found in the synucleinopathies.

Glial cytoplasmic inclusions (GCIs), also known as Papp-Lantos bodies, are a distinct pathological feature from LBs and LNs (Figure 1-7 C). GCIs are also composed of aggregated aSyn, but unlike LBs and LNs which are found within the neurons GCIs are found within oligodendrocytes, a type of glial cell (56). GCIs are generally crescent or cone-shaped, but some have a flame-like

shape similar to neurofibrillary (NFTs) in AD. GCIs are not found in PD or AD, and are a hallmark of the brutal disease multiple system atrophy (MSA) (57).

1.7 The synucleinopathies

The huge level of interest in aSyn stems not from the mystery of its physiological function, but rather from its pathophysiology. The discoveries in 1997 by *Spillantini et al* and *Polymeropoulos et al* that aSyn was the main component of LBs and that mutations in the *SNCA* gene were found in rare familial forms of PD together acted as a starting gun to research into the ties between aSyn and neurodegeneration (17,58). Since this time a total of six point mutations in the protein sequence (A30P, E46K, H50Q, G51D, A53T, and A53E) have been linked to familial PD. The involvement of aSyn aggregation has now been tied to a whole host of fatal, progressive and currently incurable neurodegenerative diseases, collectively termed the "*synucleinopathies*" (Figure 1-8). These diseases include, but are not limited to: PD, Parkinson's disease dementia (PDD), dementia with Lewy bodies (DLB), the Lewy body variant of Alzheimer's disease (LBVAD), and MSA. MSA is not a Lewy pathology, instead forming GCIs, and thus is not part of the continuum shown in Figure 1-8.

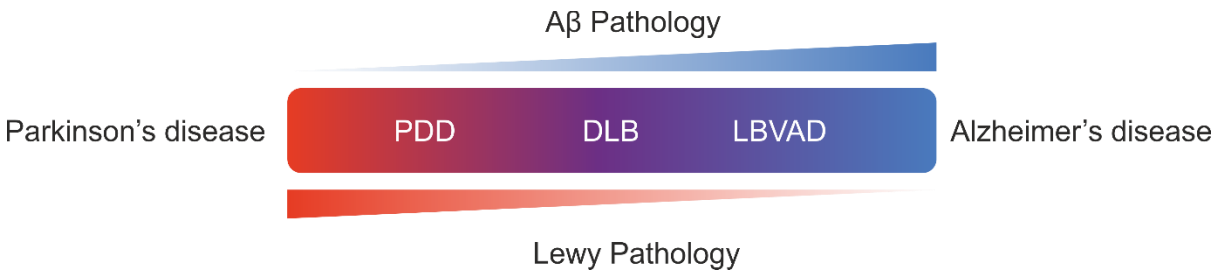

Figure 1-8 - Alzheimer's and Parkinson's exist on a spectrum. *There is a high-degree of overlap between Lewy and Aβ pathology, and which of these predominates determines the course and type of the disease.*

1.7.1 Parkinson's disease

PD – named after James Parkinson who first described the disease in his 1817 piece *An Essay on the Shaking Palsy* – is a progressive and fatal neurodegenerative disease afflicting 1% of

the population over the age of 60 (59). This makes it the second most common neurodegenerative disease after AD. It is characterized by a number of symptoms referred to under the umbrella term "parkinsonism" (60). These symptoms include: a resting tremor, a stooped gait, difficulty walking, bradykinesia, and muscular rigidity. There are also varying levels of non-motor symptoms including: loss of sense of smell, constipation, sleep disorders, and psychiatric issues. The symptoms become more severe as the disease progresses and are caused by the progressive loss of neurons in the brain. The motor symptoms are caused specifically by the loss of dopaminergic neurons in the *substantia nigra pars compacta* in the midbrain (60). The degree and movement of the Lewy pathology throughout the brain is classified by the Braak stages (see Figure 1-9 and Table 1-1) (61). The Braak stage and the extent of Lewy pathology is correlated with disease severity. The only treatment is the administration of the dopamine precursor L-3,4-dihydroxyphenylalanine (L-DOPA), which rescues motor symptoms but has no impact on disease progression (62).

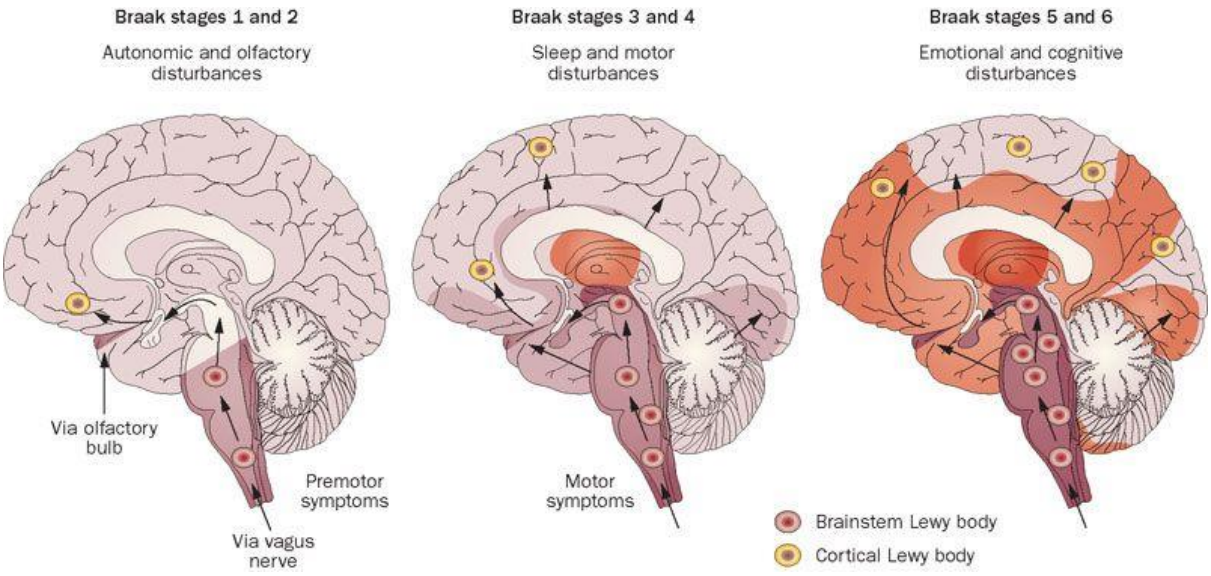

Figure 1-9 - Schematic showing the progression of Lewy pathology throughout the brain at different Braak stages. *The shading indicates the pattern and degree of Lewy pathology. Image taken from* (63).

Table 1-1: The Braak stages of Lewy pathology. *Stages defined by Braak et al* (61).

Braak stage	Location of Lewy pathology
1	Medulla oblongata
2	Stage 1 plus pontine tegmentum
3	Stage 2 plus emergence into the midbrain, including notably the substantia nigra pars compacta
4	Stage 3 plus basal prosencephalon and mesocortex
5	Stage 4 plus neocortex (high order sensory association areas)
6	Stage 5 plus neocortex (first order sensory association areas and premotor areas)

1.7.1.1 Sporadic, environmental, and familial Parkinson's disease

The majority (~90%) of cases of PD are sporadic in nature. This is to say that patients do not have any family history of the disease and onset is as a result of factors that are as yet not well understood. Approximately one in ten patients, however, have genetic mutations that result in the development of PD (64). This is so-called familial PD. Despite its comparative rarity, the ability to tie disease onset to specific genetic defects has been used as an opportunity to study the wider disease mechanisms in more detail. Mutations in multiple genes have been identified and some of these are listed in Table 1-2 (64,65).

Table 1-2 - The different familial PD-linked loci and the associated genes involved. *Loci beyond PARK9 have not been included due to their poor characterization.*

Locus	Chromosome	Protein (Gene)	Protein function	Autosomal Dominant /Recessive
PARK1	4q21.3	α-synuclein (*SNCA)*	Precise role unknown. Involvement in synaptic vesicle docking to presynaptic membrane	Dominant
PARK2	6q25.2-27	Parkin (*PRKN*)	E3 ubiquitin ligase	Recessive
PARK3	2p13	Unknown	Unknown	Dominant
PARK4	4q21.3	α-synuclein (*SNCA*)	See PARK1	Dominant
PARK5	4p14	UCHL1 (*UCHL1*)	Ubiquitin carboxyl terminal hydrolase	Dominant
PARK6	1p35-p36	PINK1 (*PINK1*)	Serine/threonine kinase	Recessive
PARK7	1p36	DJ-1 (*PARK7*)	Unknown	Recessive
PARK8	12p11q13.1	LRRK2 (*LRRK2*)	Serine/threonine kinase	Dominant
PARK9	1p36	ATP13A2 (*ATP13A2*)	Cation transport	Recessive

It is thought that mutations in LRRK2 are the most common cause of familial PD (66), whilst the others are much rarer. Intriguingly, many of the proteins identified in familial PD are associated with ubiquitin-mediated protein degradation (parkin, UCHL1 and PINK1) and mitochondrial quality control (ATP13A2, LRRK2 and DJ-1) and may operate on the same biochemical pathways (67–72). However, such mutations can have wildly different effects on the age of onset of PD, disease severity and pathology.

Also, a few cases of PD are environmental in origin. Exposure to pesticides such as 1-methyl-4-phenyl-1,2,3,6-tetrahydropyridine (MPTP), rotenone and paraquat has been linked to oxidative stress and the development of PD (73,74).

1.7.1.2 Parkinson's disease-linked point mutations in α-synuclein

Polymeropoulos et al identified that point mutations in the *SNCA* gene encoding aSyn were found in an Italian family – "the Contursi kindred" – with a history of Parkinson's disease (58). In members of this family there was a single nucleotide substitution (G209A) in *SNCA* that resulted in the substitution of the alanine at position 53 of the protein being replaced with a threonine (A53T). Since then the total number of known PD-linked point mutations in aSyn has reached six. These are: A30P, E46K, H50Q, G51D, A53T, and A53E (49,50,58,75–77). These point mutations are rare, but represent a powerful opportunity for studying the mechanisms of PD. Despite all being located in close proximity to each other they have quite wildly differing effects. For example, H50Q and G51D are changes in immediately adjacent residues and yet H50Q is associated with accelerated fibrillation and late disease onset, whilst G51D is associated with a greater tendency for oligomerization and an earlier age of onset. The effects of these mutations are particularly difficult to understand as aSyn itself is an unstructured protein and thus lacks a native structure that can be perturbed. Understanding how these mutations result in the onset of PD is important in understanding how PD arises sporadically and for a wider understanding of the underlying disease mechanisms.

It is known that some of the mutations in particular (e.g. A53T) enhance the rate of aSyn aggregation (78). It is also known that some of the mutations have an impact on the protein's intrinsic ability to associate with lipid bilayers (e.g. A30P) (79). What the work in this thesis provides is a comprehensive study of the different PD-linked mutants that have been analysed under identical conditions and at the same time. The hope is that this will fill in some of the gaps in the literature regarding the mutants, particularly those for those only discovered recently, and help resolve any contradictions. I also hope that this information will provide insight into how these different mutants result in remarkably different disease phenotypes.

1.7.2 Dementia with Lewy bodies, Parkinson's disease dementia, and the Lewy body variant of Alzheimer's disease

DLB is a disease closely related to PD and is one of the most common dementias. Due to its similarity with AD it is thought to be significantly under-diagnosed. According to official figures it makes up 4% of all cases of dementia, but according to the Alzheimer's Society may make up as much as 15% of all dementia based upon studies of brain tissue of patients taken *post mortem* (80). Like PD it is characterized by the appearance of LBs in the brain. Dementia is most commonly the presenting feature and patients will commonly exhibit powerful hallucinations, sleep disorders, and also the classic parkinsonian symptoms (e.g. stooped gait, rigidity, resting tremors etc) (80).

PDD and DLB are extremely similar; the diagnosis of a patient is dependent on which symptoms present first (81). A presentation of motor symptoms associated with parkinsonism before the onset of the dementia-like symptoms results in a PDD diagnosis. If the reverse happens then a DLB diagnosis is more likely.

There is some confusion as to whether LBVAD is a separate disease, as some sources use it as an alternative name for DLB (82,83). The synucleinopathies exist on a spectrum with AD on one end and PD at the other (Figure 1-8). The position on the spectrum relates to the extent of Lewy or

Aβ pathology. Those diseases with greater Lewy pathology, or in which Lewy pathology is predominant, are more Parkinson's-like in presentation (e.g. PDD). Others with a greater prevalence of Aβ plaques will be more Alzheimer's-like. LBVAD may exist somewhere on this spectrum, but it must be remembered that each patient and case is unique and trying to pigeonhole every case may prove to be impossible.

1.7.3 Multiple system atrophy

MSA is a fatal and progressive neurodegenerative disease characterized by the pathological hallmark GCIs. These proteinaceous inclusions composed of aggregated aSyn are found within oligodendrocytes and are distinct from the LBs and LNs found in the neurons in patients with PD or DLB. MSA is a rare disease and there are thought to be 3,300 patients in the UK and Ireland; the incidence is generally thought to be around 5 patients in every 100,000 over 50 years of age (84). Symptoms can include parkinsonism – resulting in many cases being initially diagnosed as PD – and cerebellar ataxia (problems with balance and coordination of movement) (85). Despite its similarity to PD it is a faster moving disease and death typically occurs within about 9 years of diagnosis (85). MSA is relatively "new" disease as it has historically been considered as three separate diseases: striatonigral degeneration, sporadic olivopontocerebellar atrophy, and Shy-Drager syndrome. MSA is an umbrella that is subdivided into MSA-P, the Parkinson's-like subtype historically known as striatonigral degeneration, and MSA-C, the subtype associated with cerebellar dysfunction and historically known as sporadic olivopontocerebellar atrophy (86,87). Shy-Drager syndrome is now considered a slightly archaic name, but is sometimes used as an alternative name for MSA as a whole. It is noteworthy to acknowledge that the strain of aSyn found in MSA is distinct from those found in patients with PD and that it is a prion (88). This makes aSyn the second identified human prion in history, subsequent only to the prion protein (PrP) in Creutzfeldt-Jakob disease (CJD).

1.8 Therapeutic strategies against the synucleinopathies

In the fight against neurodegeneration and the synucleinopathies there are a number of therapeutic strategies that are under active investigation and development. Currently, there are no cures and all treatments target symptoms rather than the underlying pathology.

1.8.1 Symptomatic treatments

1.8.1.1 L-DOPA

L-DOPA is a precursor to the neurotransmitter dopamine and is itself formed from the amino acid tyrosine (Figure 1-10) (89,90). L-DOPA is commonly administered to patients with PD in order to alleviate the typical parkinsonian motor symptoms, such as resting tremors. Dopamine cannot be administered itself due to its poor penetrance across the blood-brain barrier. L-DOPA, on the other hand, can cross the blood-brain barrier and its movement is facilitated by the 4F2hc/LAT1 amino acid transport system (91). The recognizable symptoms of PD are caused by the loss of dopaminergic signalling neurons in the *substantia nigra pars compacta* of the brain. L-DOPA offsets this loss by increasing the supply of dopamine available (62). It should be noted that not all patients are receptive to treatment by L-DOPA and in those that are the benefits of the treatment decline over time as the disease progresses.

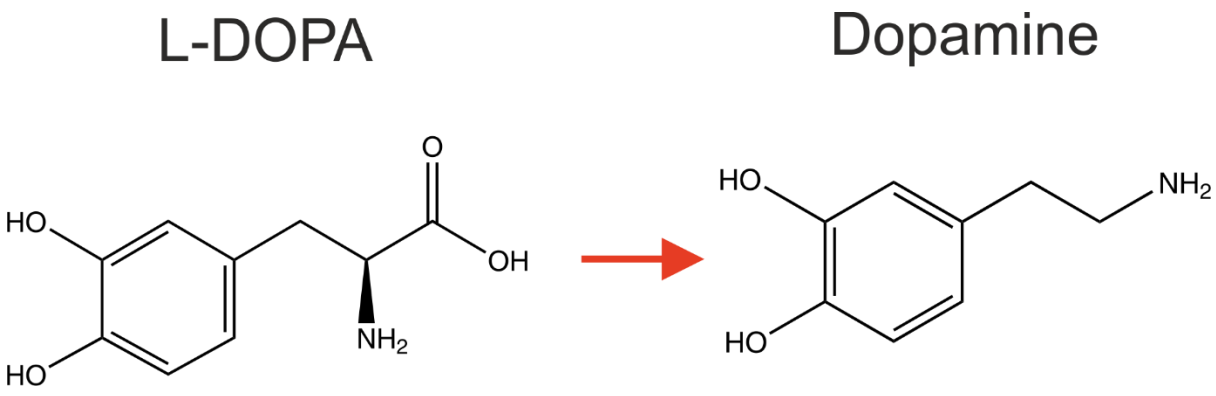

Figure 1-10 - L-DOPA is the precursor to dopamine. *L-DOPA is given to patients with Parkinson's disease in order to ease its associated motor symptoms, which arise as a result of the loss of dopamine signalling neurons in the substantia nigra. The administration of L-DOPA can temporarily make up for the shortfall in dopaminergic signalling in some patients.*

1.8.1.2 Dopamine agonists

Dopamine agonists (e.g. pramipexole) are another form of symptomatic treatment of PD, which may be administered alongside L-DOPA or alone (92). As their name suggests this is a class of compounds that serve to bind to and activate dopamine receptors, and in this way mimic the action of dopamine (93,94). Pramipexole was discovered to significantly improve symptoms in early cases of PD (92) however there are notable side-effects and withdrawal symptoms, especially regarding impulse control (e.g. gambling) (95,96). Like L-DOPA, the aim of these compounds is to mitigate against the loss of overall dopaminergic signalling caused by the death of neurons in the *substantia nigra pars compacta*. However, also like L-DOPA, this form of treatment appears to become less effective over time – this is because the scale of neuronal loss can no longer be compensated for by the administration of greater levels of dopamine mimics.

1.8.2 Non-symptomatic treatments

Non-symptomatic treatments are those that are not aimed at targeting the obvious parkinsonian symptoms of PD, but those that are actually targeting the underlying pathology. This means they are aimed at either preventing the accumulation of aSyn aggregates, or somehow reversing the process. None of these treatments currently exist, yet there are numerous ideas and several of these are currently undergoing clinical trials.

1.8.2.1 Peptide inhibitors of α-synuclein aggregation

The majority of drugs on the market currently are small molecules (<1kDa), however there is an increasing level of interest in the use of peptides as pharmaceuticals. Peptides are generally far more specific to a given target than small molecules and thus are less likely to have prohibitive side-effects. Also, many of the issues that have historically proved an impediment to their clinical use (e.g. proteolytic degradation and localization) are better understood and can now be circumvented (97). Peptides are particularly attractive to neurodegenerative research due to their

specificity and their potential to impede fibril elongation. Some peptides, for example, have been shown to form β-hairpin structures that "cap" fibrils to prevent the addition of further monomeric units and thus blocking their elongation. This has been shown for amylin and aSyn (98). This can be particularly facilitated in N-methylated peptides (i.e. the backbone amides are methylated) as it prevents the formation of hydrogen bonds by one side of the peptide (99).

1.8.2.2 Monoclonal antibodies targeting α-synuclein

Pathological forms of aSyn are now known to move from cell-to-cell in a prion-like manner. Virginia Lee and colleagues very elegantly showed this in mice in 2012, and that aSyn pathology spread from an initial point of injection to anatomically connected regions (100). The same group then showed the potential of antibodies specific to mis-folded aSyn to assuage the spread of the pathology and the consequent cell death and motor symptoms. This is presumably by binding to the pathological species and preventing their movement from one neuron to another in which they could seed the mis-folding of native protein (101). The effectiveness of the antibody-driven approach was also shown by *Masliah et al* who used the passive immunization of a mouse model of PD with the 9E4 (anti aSyn 118-126) antibody to promote aSyn clearance and improved cognitive performance (102). This idea has been picked up by Roche and Prothena who are operating in partnership to develop monoclonal antibodies targeting aSyn with the aim of preventing the spread of aSyn pathology and preventing further loss of neurons. Their anti-synuclein antibody Prasinezumab (PRX002/RG7935) is currently in Phase II clinical trials having just passed through Phase Ib trials in which it was found to be safe and well tolerated (103).

1.8.2.3 Chaperone-mediated disaggregation of aggregates

A number of publications have emerged in recent years describing the ability of different proteins, or a collection of proteins, to either inhibit fibril formation or to actively break-up pre-existing fibrils (104–106). These processes are either passive, requiring no energy input (e.g.

cyclophilin-40), or active and require the hydrolysis of ATP to drive the process (e.g. Hsp70) (105). The viability of these approaches clinically has not been shown. Energy-driven approaches, such as that of the disaggregase formed by Hsp70, DNAJB1 and an Hsp110 nucleotide exchange factor, may place an unacceptable energetic burden on the neurons. The spontaneous processes observed with members of the cyclophilin family may not be realistic either, given that they themselves are big players in cell death and their precise involvement remains poorly understood and controversial (106).

1.8.3 Challenges

The development of therapeutics to be used in the treatment of neurodegenerative disease is fraught with difficulties. These challenges go above and beyond those normally encountered on the bumpy road of drug development. First and foremost is a lack of knowledge. The mechanisms that underlie neuronal cell death are not well understood, and in the case of AD there is even argument as to whether focus should be placed on Aβ pathology or tau pathology. Billions of dollars have been spent by pharmaceutical companies on failed clinical trials (e.g. bapineuzumab) (107) to interrupt pathways that are not understood; as a direct result of this Pfizer announced in early 2018 its departure from research into new therapeutics for AD and PD. This highlights the need for further basic research into neurodegeneration. Additionally, there are problems with a lack of biomarkers. Neurodegenerative disease generally only becomes noticeable after pathology is widespread throughout the patient's brain. This makes a preventative approach difficult.

From the point-of-view of designing clinical trials neurodegenerative disease is difficult because they typically move very slowly. AD and PD, for example, are mostly diagnosed in people over the age of 60. By this stage the pathology may be already well established throughout the brain, yet patients can live with AD or PD for decades. To continuously monitor sufficient numbers of people for such durations to see the impact of a drug candidate is a herculean challenge.

1.9 Project aims

The work here is best considered as several separate projects unified by a common protein of interest, aSyn. The experimental chapters are chapters 4, 5, 6, and 7. Chapter 4 relates to the inhibition of aSyn aggregation using a peptide inhibitor (KDGIVNGVKA) of aSyn aggregation. The inhibition of aSyn aggregation is a strategy of therapeutic interest, and whilst implicit evidence for the interaction between KDGIVNGVKA and aSyn is available in the initial publication by *Cheruvara et al* there is no explicit evidence (108). It was an aim of this project to obtain concrete evidence of an interaction between aSyn and KDGIVNGVKA, and if possible identify the residues (if any) which mediate the interaction. This would primarily be elucidated using NMR and TEM, and would allow the further development of peptide-based inhibitors, which in the long-term could hold therapeutic potential.

Chapter 5 overlaps with and complements the work from chapter 4. The work conducted in this chapter was aimed at identifying the metabolic pathways affected as a result of challenging SH-SY5Y neuroblastoma cells with aSyn. It was hypothesized that differences could be observed in the metabolic profile of cells which had been exposed to aSyn monomers versus fibrils, and fibrils versus aSyn that had been incubated with KDGIVNGVKA. Previous work from the group had shown statistically significant differences in the metabolic profile of cells that had been exposed to different species of aSyn (109), and it was my hypothesiss that the incubation of aSyn with KDGIVNGVKA would result in the formation of alternative species that would result in similarly significant differences. Any information that could be withdrawn regarding metabolic pathways involved could be used to infer the mechanisms of aSyn toxicity (e.g. mitochondrial dysfunction) and if/how the peptide inhibitor mitigates that toxicity.

Chapter 6 explores the properties of the PD-linked aSyn point mutants and the effects of tyrosine nitration via peroxynitrite. The information surrounding the PD-linked mutants in the literature is often patchy or even contradictory. It was my aim to express and purify all of these PD-

linked mutants such that I could conduct experiments investigating their properties at the same time and under identical conditions. This would allow for a comprehensive comparison of the effects of these mutations on the rate of aggregation, lipid interactions, and cell toxicity. Given that some of these mutations have quite different effects on the onset and progression of PD it is important to have clarity on their fundamental properties. The effect of nitration on aggregation and lipid-binding is also of importance as this is a pathologically relevant modification found in LBs (53), and gaining an understanding of whether this is a cause or a consequence of aggregation would potentially help resolve some of the questions regarding causality in PD.

Chapter 7 covers work that was aimed at probing the relationship between aSyn, cyclophilin-D (CypD), and the mitochondria. This came about as a result of work (for which I supplied aSyn) in which it was shown by NMR that CypD and aSyn interact. CypD is a big target and regulator of mitochondrial permeability transition pore (mPTP) opening, whilst there is also evidence that aSyn localizes to the mitochondria and may open the MPTP (110–112). This raises a lot of questions. It is my hypothesis that aSyn aggregates localize to the mitochondria where they interact with CypD, which then initiates the opening of the mPTP to result in cell death. This was probed primarily through NMR spectroscopy and TEM, carried out in conjunction with Prof Lu-Yun Lian.

2 NMR theory

Much of the information and figures in this chapter are adapted from the Second Edition of "Understanding NMR Spectroscopy" by James Keeler (113).

2.1 Chemical shift and spins

NMR spectroscopy is a technique used to study atomic nuclei, and is widely used in chemistry and biophysics/structural biology. It may be used to observe nuclei with a quantum property called "spin". The majority of nuclei observed in NMR have a spin state (S) of $+\frac{1}{2}$ or $-\frac{1}{2}$. This includes ^{1}H (a proton), ^{15}N, ^{31}P and ^{13}C. The most commonly observed in biophysics are ^{1}H, ^{15}N and ^{13}C. ^{1}H is present in everything, whilst recombinantly produced proteins may be enriched in the isotopes ^{15}N and ^{13}C using supplemented bacterial growth media. These nuclei, when placed in a magnetic field, will begin to precess about the magnetic field. It is often said that the individual spins align "with" or "against" the magnetic field – spin up (α) or spin down (β). This is a slightly incomplete picture. It is energetically favourable for spins to align with the magnetic field, however due to thermal fluctuations spins are constantly rearranging. There is only a very slight excess of spins aligned with the magnetic field, but this is sufficient to provide the sample as whole with a net alignment with the field. Thus, the magnetization can be considered across the whole sample rather than just for individual spins in individual molecules.

The spins precess about the applied magnetic field (B_0) at a particular frequency, the Larmor frequency (ω_0 in rad s^{-1} or ν_0 in Hz). The Larmor frequency of the nucleus is given by:

$$\omega_0 = -\gamma B_0 \text{ or } \nu_0 = -\gamma B_0/2\pi$$

The gyromagnetic ratio (γ) is specific to each type of nucleus (e.g. ^{1}H) and describes the relationship between its angular momentum and its magnetic moment. An NMR experiment reports in ppm the degree to which the spins in a sample diverge from the Larmor frequency of a defined standard

(e.g. ^{1}H in the reference compound tetramethylsilane (TMS)). This quantity is the chemical shift (δ). The chemical shift relates to the frequency in Hz as follows:

$$\delta(ppm) = 10^6 \times \frac{\nu - \nu_{ref}}{\nu_{ref}}$$

The reference frequency is often used in NMR as a synonym for magnetic field strength (e.g. an 800MHz magnet). The 10^6 makes the maths come out more simply (hence parts per *million*). The chemical shift is reported rather than the frequency in Hz because the frequency value is dependent on the magnetic field strength, whereas the chemical shift has removed the field dependence. Thus the chemical shift allows for the comparison of data collected on spectrometers with different magnetic field strengths.

The Larmor frequency of spins is affected by the local chemical environment and it is this feature that makes NMR so powerful. The rate of precession about the magnetic field is dependent on how much magnetic field the spins "see". Nuclei surrounded by large clouds of electrons are somewhat protected by a countering magnetic field generated by the electrons. For example, the ^{1}H nuclei within methyl groups (CH_3) are relatively shielded, whilst ^{1}H nuclei adjacent to an electronegative atom such as oxygen or nitrogen will "feel" the magnetic field to a greater extent. Thus the nuclei of these groups will exhibit a different chemical shift on an NMR spectrum. The NMR spectrum shows peaks for each different chemical environment in a sample for a given nucleus.

2.2 Pulses and the free induction decay

The actual output of an NMR experiment is called the FID. This is a signal that arises as a result of the sample magnetization vector being placed in the transverse (x, y) plane and passing through the receiver coils. This induces an electric current within the coils that can be measured. It is an analogue signal, but is recorded as digitized points that are reconstructed into the FID signal

during data processing. As the name suggests, the signal is decaying. The transverse magnetization in the x,y plane relaxes over time into nothing, and this means that the initial part of the FID contains the most signal whilst the latter parts decay into noise. This has implications for data processing. Data processing employs a mathematical operation called a Fourier transform, developed by Joseph Fourier in 1822, which converts the rather uninterpretable time-domain FID signal into a frequency-domain spectrum comprising peaks at all of the different frequencies that make up the FID (Figure 2-1).

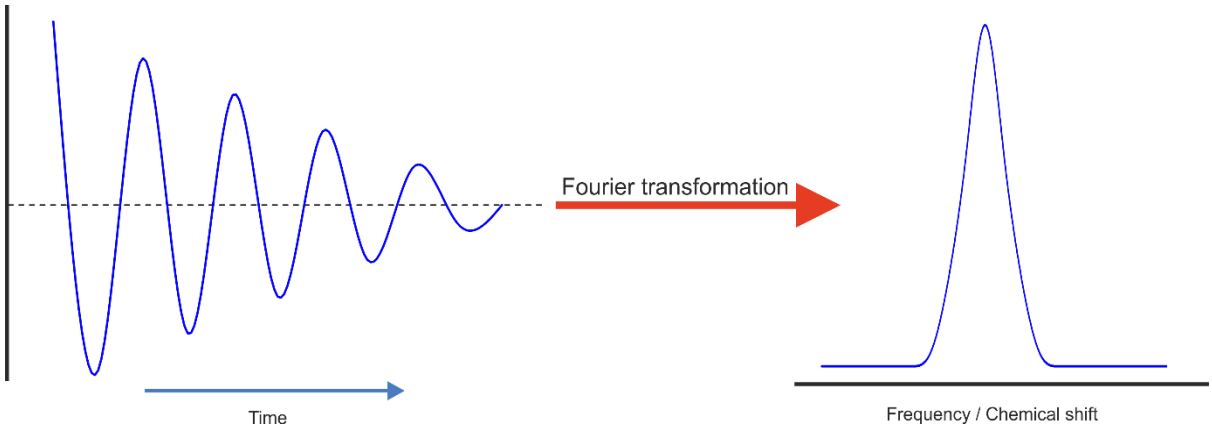

Figure 2-1 - The conversion of the free induction decay into an NMR spectrum. *The free induction decay (left) is the time-domain data collected in an NMR experiment. The majority of the signal is present at the beginning and gradually fades away into the noise due to T_2 relaxation. The data is then made time-independent and converted into the frequency domain via a Fourier transformation. This results in a typical NMR peak (right).*

The magnetization vector is placed into the transverse plane by a radiofrequency (RF) pulse. RF pulses are used due to them having frequencies within a similar range as the Larmor frequencies of the spins in NMR samples. Radio waves are a form of electromagnetic radiation, which is to say that they are composed of an electric component and a magnetic component. This applied magnetic field is generally termed B_1 and is much weaker than the B_o field of the magnet, but at a frequency equal to the Larmor frequency of the spins it achieves resonance which enables it to push the spin magnetization vector into the transverse x,y plane. The duration and power of the pulse affect the degree to which the magnetization is flipped. Most pulses used in pulse sequences are so-called 90° or 180° pulses; meaning that they flip the magnetization vector by 90° or 180°. Before

an experiment is started the parameters to achieve a 90° for the nuclei in the sample must be calibrated. This is done by pulsing until the signal reaches zero (indicating a flip of 180°). A pulse of half this length is then used as the 90°.

Strictly speaking, pulses that are equal in frequency to the Larmor precession are on-resonance pulses. Also utilized in pulse sequences are off-resonance pulses, which do not exactly match the Larmor frequency. Instead, these pulses are useful for targeting multiple spins at once.

2.3 Models of NMR

There are several models used to describe how NMR operates. These are the energy level model, the vector model, and the product operator model. Here is described the energy level model as it is easier to visualize and is a useful teaching tool. However it is an incomplete model and for a more complete understanding of NMR both the vector model and the product operator model are used. However, these are not discussed here as this level of understanding is not necessary to comprehend the work described in this thesis.

2.3.1 Energy level model

When the sample is placed into the magnetic field two energy levels emerge, spin up (α) and spin down (β) mentioned earlier. There is a difference in energy (ΔE) between these energy levels given by:

$$\Delta E = E_\beta - E_\alpha$$

The energy needed to move the spins from one energy level to the other is related through Planck's constant (h) to the frequency of an incoming photon (ν) as given by:

$$\Delta E = h\nu$$

As described in 2.1 the Larmor frequency is dependent on the gyromagnetic ratio of the nucleus (as this determines whether spin state α or β is lower in energy) and the magnetic field strength B_0 (as

a stronger magnetic field will increase the separation between the two energy levels). This means that by applying a pulse of radiation with the same frequency as the Larmor frequency of the spins – the rate of precession – you will induce an energy level transition in the spins and observe a peak in the NMR spectrum (Figure 2-2). Peaks will appear at points corresponding to the Larmor frequency of every spin in the sample. This corresponds to every different chemical environment in the sample.

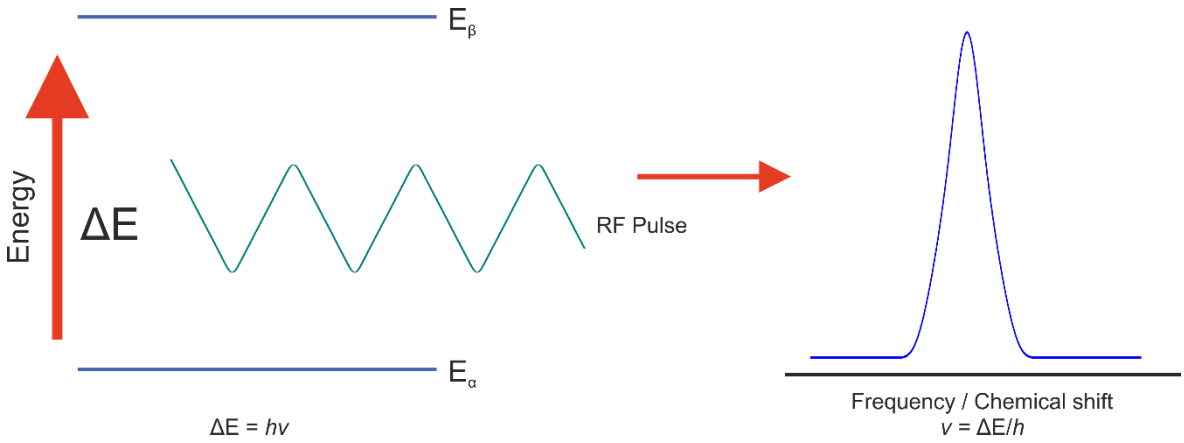

Figure 2-2 - The energy level model of NMR and spin states. *After the sample is placed into the magnetic field spins are separated into α and β spin states. The spins can move between the energy levels through the application of an RF pulse of a frequency matching the difference in energy between them. This will be represented in an NMR spectrum by a peak at the corresponding frequency.*

2.4 1D NMR

2.4.1 1D Proton experiments

1D proton experiments are the simplest type of NMR experiment, but also one of the most valuable. 1D proton experiments (Figure 2-3) consist of a pre-scan delay (d1) to allow the magnetization to reach equilibrium followed by a single pulse and acquisition. One would expect the pulse to be 90° for maximum magnetization, however it is often the case that pulses that rotate the magnetization by just 30° are used. This is because the time it takes for the magnetization to return to equilibrium from 90° is such that by pulsing the sample more frequently with just 30° pulses results in “more bang for your buck” (better signal-to-noise). The pulse sequence shown in

Figure 2-3 is the basic pulse sequence, but it may be modified with additional pulses that fulfil roles such as water suppression (to hide the large water peak at 4.7ppm in aqueous samples).

It is best practice to run a 1D proton experiment on every sample, especially before longer two- and three-dimensional experiments. This allows one to check that various parameters (e.g. spectral-width) are optimized. It also provides a quick-and-easy check of the state of the sample, such as whether it is folded or whether there are any contaminants present.

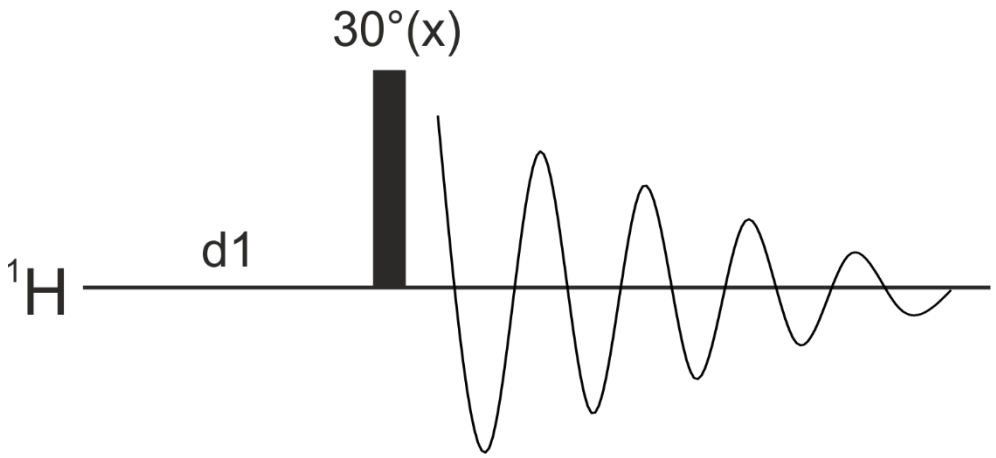

Figure 2-3 - The pulse sequence for a 1D proton experiment. *It consists of an initial delay (d1) that allows the magnetization to reach equilibrium prior to a 30° pulse, followed immediately by the acquisition period.*

2.4.2 WaterLOGSYs

WaterLOGSY experiments are a type of one-dimensional NMR experiment that were designed and are used to study the interaction of weakly-binding ligands to protein molecules. The basic principle of the experiment is that the sample contains a large excess of ligand to protein (e.g. 10µM protein to 200µM ligand). The pulse sequence applies the magnetization to the water of the sample, which is then transferred through a variety of mechanisms to the ligand and protein. These mechanisms include: saturation of H_α resonances; saturation of NH and OH protons in fast exchange with water; and magnetization that has been transferred to bound water trapped in cavities on the surface of the protein and/or at the protein:ligand interface. For these mechanisms to successfully

transfer magnetization to the ligand efficiently it requires the interaction of the ligand with the protein as they are based on nuclear Overhauser effects (NOEs) and spin diffusion, both of which require close proximity between the spins. Additionally, this experiment works best for weakly binding systems, as it means that there is a regular and rapid exchange of bound and unbound ligand. This allows a larger proportion of the total ligand present to acquire magnetization, as opposed to in more tightly binding systems. This is also the reason why the large excess of ligand to protein is used; because the ligand is not being saturated directly. A characteristic of the experiment is that "binders" and "non-binders" will have signals of opposite sign due to their different tumbling rates, resulting in either a positive or negative NOE. The sign change, however, may not be seen if there is a high degree of exchange with the solvent. WaterLOGSYs were used in this thesis to probe the interaction between aSyn and a peptide inhibitor of its aggregation given their widespread usage in the pharmaceutical industry and their increased sensitivity compared to saturation transfer difference (STD) experiments (114).

2.5 Multidimensional NMR

Some spectra, especially for larger molecules like proteins, become very crowded due to the large number of different chemical environments. In these situations it can be difficult to interpret the spectra and it is instead helpful to increase the dimensionality of the experiment. Most commonly two-dimensional experiments (e.g. correlation spectrscopy (COSY), total correlation spectroscopy (TOCSY), heteronuclear single quantum coherence (HSQC)) are used, however higher-dimensional experiments are possible. Multidimensional experiments may be homonuclear (e.g. the 2D COSY) or heteronuclear (e.g. the 2D HSQC). Here the intensity is plotted as a function of more than one frequency; in other words a peak represents two or more nuclei that are coupled together (via bonds or through space).

Two-dimensional experiments are broken down into four parts: preparation, evolution (t_1), mixing, and acquisition (t_2) (Figure 2-4). Preparation refers to the initial step where magnetization

is placed into the transverse plane where it can be manipulated further. During the evolution period the magnetization is allowed to evolve so couplings and chemical shifts may develop. Following this is the mixing time during which the magnetization is primed for acquisition; this may include steps to transfer magnetization onto a more sensitive nucleus (e.g. ^{1}H).

In two-dimensional spectra the first scan is recorded with an evolution time (t_1) of zero. This then gets incrementally increased with every scan. This means that the evolution time (t_1) gets recorded as a function of the acquisition time (t_2). In this way following Fourier transformation the data corresponds to two frequency domains – t_1 and t_2. The Fourier transformation of the data is slightly more involved than that for the one-dimensional NMR spectra as it needs to be processed "both ways" (i.e for t_1 and t_2).

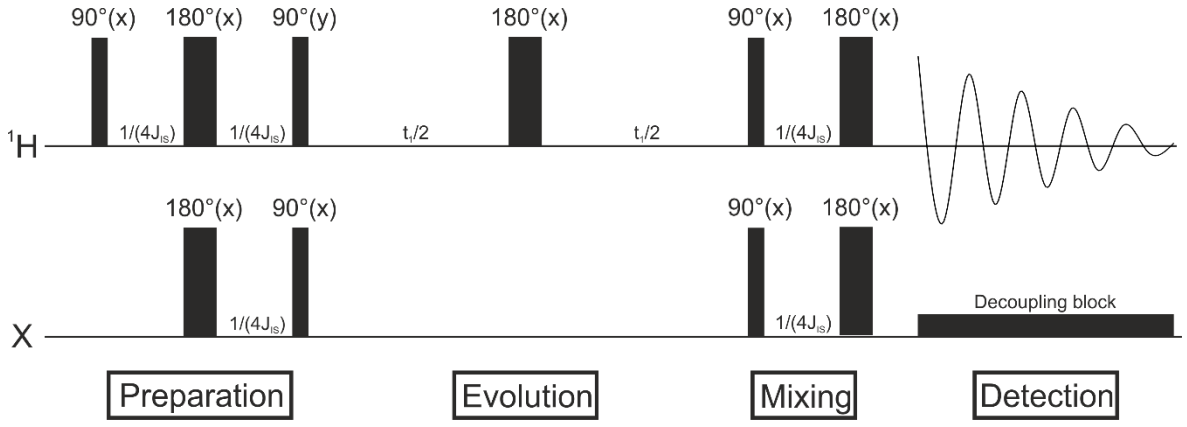

Figure 2-4 - The pulse sequence of a decoupled HSQC experiment. *The preparation part of the HSQC is an INEPT block that transfers magnetization to the X nucleus. During the evolution period there is a single 180° for decoupling of the S nucleus. During the mixing period a second INEPT block is used to transfer magnetization back to the ^{1}H nucleus, for detection. During the detection period a rapid series of pulses is used to remove couplings. This is the decoupling block.*

2.5.1 Heteronuclear Single Quantum Coherence

The HSQC is a heteronuclear NMR experiment commonly used in biomolecular NMR. ^{1}H-^{15}N HSQCs are most common, but ^{1}H-^{13}C HSQCs are also possible. These experiments can be thought of as providing a "fingerprint" of a protein. There are peaks from the backbone amides of every amino acid present in the protein in ^{1}H-^{15}N HSQC spectrum, with the exception of prolines and the N-

terminal residue. Peaks from amide-bearing sidechains may also be present, but these lie away from the backbone peaks. The chemical environment of the backbone amides is heavily dependent on protein conformation and this makes HSQC experiments very useful for observing PPIs and ligand-binding (115–117).

Both ^{15}N and ^{13}C are far less sensitive than ^{1}H due to their gyromagnetic ratios being smaller in magnitude (^{15}N has a negative gyromagnetic ratio, unlike ^{1}H and ^{13}C) and thus the size of the magnetization they produce is much lower. It is thus more common – in biomolecular NMR – to transfer magnetization from the "insensitive" ^{15}N and ^{13}C nuclei onto ^{1}H. This is the principle used in the HSQC experiment and it works through INEPT blocks (Figure 2-5).

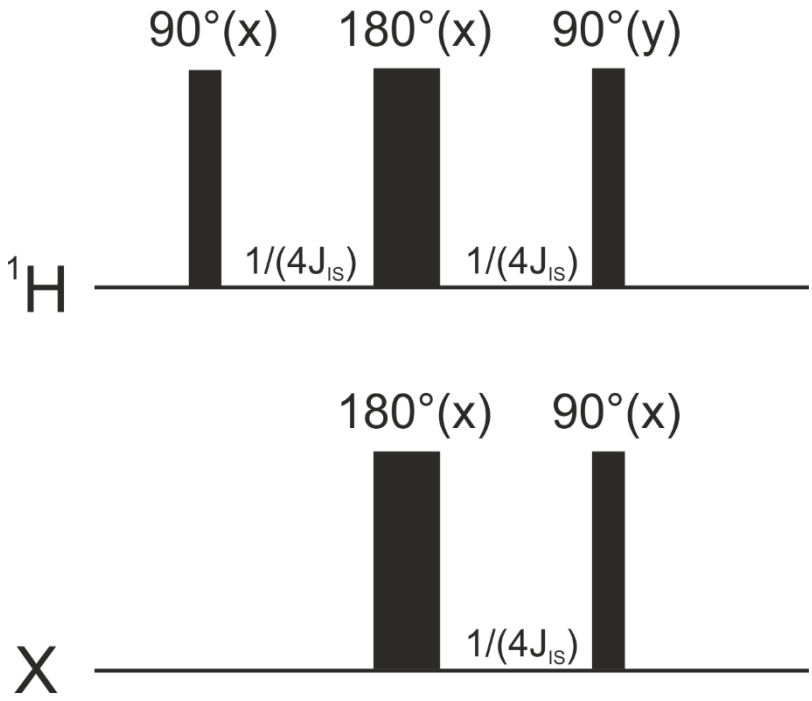

Figure 2-5 - The pulse sequence of the INEPT block, a key component of many multi-dimensional NMR experiments. *The initial 90° pulse places the magnetization into the transverse plane, whilst the two 180° pulses remove the effect of the ^{1}H chemical shift evolution. The final two 90° pulses result in the transfer of the magnetization to the X nucleus and the formation of the antiphase state.*

The INEPT block begins with a 90°(x) pulse on the ^{1}H nucleus to move the magnetization into the transverse plane. This is followed by a delay during which the chemical shift evolves. The issue with this is that it results in a state called "multiple quantum coherence"; in other words that both

the ^{1}H and X nuclear magnetization is in the transverse plane. To rectify this two 180° pulses are applied simultaneously onto the ^{1}H and X nuclei. This removes the effect of the ^{1}H nucleus chemical shift evolution whilst leaving the X nucleus unaffected. The second delay followed by the simultaneous 90° pulses mean that the magnetization is fully transferred to the less sensitive X nucleus, whilst the ^{1}H magnetization is in the transverse plane – this is a state called antiphase.

The remainder of the HSQC pulse sequence (Figure 2-4) is essentially a second INEPT block in reverse to allow the transfer of the magnetization back from the X nucleus to the more sensitive ^{1}H nucleus where it is detected. During the detection period there is also a "decoupling block". This is a train of rapid pulses that are used to remove unwanted ^{1}H-X couplings. This results in the peaks appearing as singlets rather than exhibiting a confusing degree of splitting.

3 Preparation and characterization of alpha-synuclein

3.1 Outline of chapter

In this chapter is described the expression and purification of wild-type (WT) aSyn and each of the point mutations associated with PD. In addition to this is described the process by which the backbone NMR assignment of the WT protein was obtained. In validation of the successful preparation of the PD-linked mutations HSQCs and mass spectra of each were obtained. These confirmed the ability to prepare significant quantities of each of the proteins to high purity, which was essential to carry out the work in this thesis.

3.2 Methods

The procedure used in the expression and purification of WT aSyn is also used for A30P, E46K, H50Q, G51D, A53T, and A53E aSyn.

3.2.1 Expression of α-synuclein

The pRK172 aSyn expression construct (kindly gifted by Michel Goedert) was freshly transformed into *E.coli* BL21 cells, using the heat-shock method. These cells were used to inoculate 1mL of super optimal broth with catabolite repression (SOC) (100ug/mL ampicillin), which was grown at 37°C with shaking at 200rpm for 8 hours. 150µL of this culture was then used to inoculate 50mL of minimal medium (Solution A: 12.5g/L Na_2HPO_4, 7.5g/L KH_2PO_4 pH 7.2; Solution B (for 1L): 4g (^{13}C) glucose, 1g (^{15}N) NH_4Cl, 240mg $MgSO_4 \bullet 7H_2O$, 20mg $CaCl_2 \bullet 2H_2O$, 10mg thiamine), which was grown at 37°C overnight. This starter culture was used to inoculate 1L of minimal medium such that the starting optical density at 600nm (OD_{600}) was 0.1. This culture was then grown at 37°C at 180rpm until the OD_{600} reached 0.8. At this point isopropyl-β-D-1-thiogalactopyranoside (IPTG) was added to the culture to a final concentration of 0.5mM and the culture was then incubated shaking

overnight at 18°C. The next day cells were harvested by centrifugation at 4,000g for 20mins at 4°C. The cell pellets were snap frozen in liquid nitrogen (LN_2) prior to storage at -80°C.

3.2.2 Site-directed mutagenesis of α-synuclein

The QuikChange II kit (Agilent Technologies) was used according to the manufacturer's instructions to prepare the six PD-linked aSyn mutants (A30P, E46K, H50Q, G51D, A53T, and A53E). The WT aSyn pRK172 expression construct was used as the template. The reaction was carried out according to the manufacturer's instructions with the primer sequences shown in Table 3-1.

Table 3-1 - The forward and reverse primers used to generate the PD-linked mutants of aSyn

Mutation	Primer Sequences
A30P	5'-ctcttttgtctttcctggtgcttctgctacaccct-3' 5'-agggtgtagcagaagcaccaggaaagacaaaagag-3'
E46K	5'-catgcaccactccctttcttggttttggagcc-3' 5'-ggctccaaaaccaagaagggagtggtgcatg-3'
H50Q	5'-ctgttgccacaccctgcaccactccctcc-3' 5'-ggagggagtggtgcagggtgtggcaacag-3'
G51D	5'-ccactgttgccacatcatgcaccactccc-3' 5'-gggagtggtgcatgatgtggcaacagtgg-3'
A53T	5'-gtcttctcagccactgtcgtcacaccatgcaccactc-3' 5'-gagtggtgcatggtgtgacgacagtggctgagaagac-3'
A53E	5'-cttctcagccactgtttccacaccatgcaccac-3' 5'-gtggtgcatggtgtggaaacagtggctgagaag-3'

The mutant constructs were subsequently transformed into TOP10 chemically competent cells. Single colonies were used to inoculate 5mL SOC, which were then grown at 37°C overnight

with shaking. The DNA was extracted and amplified using the QIAprep Spin Miniprep Kit (Qiagen), and then sent off for DNA sequencing (Source Bioscience) to confirm successful mutagenesis.

3.2.3 Purification of α-synuclein

The cell pellets were thawed and resuspended in 20mL Buffer A (20mM Tris-HCl pH 8.0, 1mM ethylenediaminetetraacetic acid (EDTA)). Cells were lysed by pressure homogenization, followed by a single cycle of ultra-sonication (30s at 23KHz) to shear DNA. The lysate was incubated at 85°C for 10mins and then clarified by centrifugation at 18,000g for 30mins at 4°C. The clarified lysate was applied directly to a 5mL Q HiTrap anion exchange chromatography column (GE Healthcare Life Sciences) that had been pre-equilibrated with the Buffer A. Protein was eluted from the column via gradient elution with Buffer B (Buffer A + 1M NaCl). Fractions were analysed by SDS-PAGE using a 15% acrylamide gel and the standard Coomassie Brilliant Blue R-250 staining procedure. ASyn is found to elute from the column at approximately 300mM NaCl. The fractions were pooled and filtered through an Amicon Ultra-15 centrifugal filter with a 30kDa molecular weight cut-off (MWCO) (EMD Millipore). The flow-through was collected and applied to a 10kDa MWCO centrifugal filter, and was concentrated to 10mg/mL. The protein concentration was determined using UV absorbance at 280nm (ε = 5600 $M^{-1}cm^{-1}$ and MW = 14.5kDa). Protein purity was assessed by SDS-PAGE and mass spectrometry (MS) was used to verify that the protein was of the expected mass.

3.2.4 Monomerization of α-synuclein

Prior to all experiments, unless explicitly stated, aSyn was buffer exchanged into double-distilled water using a PD-10 desalting column (GE Healthcare Life Sciences). The protein was then snap frozen in liquid nitrogen and transferred to a freeze-drier for lyophilisation. The lyophilised protein was resuspended in 2mL hexafluoroisopropanol (HFIP) (Sigma Aldrich) and thoroughly vortexed until transparent. The HFIP was then evaporated under a stream of nitrogen to leave a

thin “film” of protein lining the sample tube. This film was then resuspended in the buffer of choice for subsequent experiments with the protein in a monomeric-state.

3.2.5 Standard NMR collection procedure

Unless otherwise explicitly stated all NMR spectra were collected on a Bruker Avance III 800MHz spectrometer equipped with a TCI CryoProbe (Bruker) at 298K. Samples were prepared in 5mm glass tubes in “NMR buffer” (10mM sodium phosphate pH 7.0, 100mM KF, 0.05% NaN_3) with a final concentration of 5% D_2O (v/v) for the signal lock. Tuning and matching was carried out as appropriate. The “topshim” automated shimming procedure was used to ensure homogeneity of the magnetic field across the sample. The duration of the 90° pulse was recorded and set for each experiment using the automated “pulsecal” routine. Water suppression was optimized by varying the offset and the pulse power level until the water signal was at a minimum. Samples were left in the magnet for at least 5mins prior to shimming and data collection to allow magnetization to reach equilibrium.

3.2.6 Standard NMR data processing and analysis

NMR data were processed and phased in TopSpin version 3.5 pl 7 (Bruker). Analysis of peak intensities and shifts of 1D spectra was carried out in TopSpin, whilst 2D and 3D NMR spectral analysis was carried out using CcpNmr Analysis version 2.4.2 (CCPN).

3.2.7 Backbone assignment of wild-type α-synuclein

$^{15}N/^{13}C$-labelled aSyn was resuspended in NMR buffer such that the final concentration of protein was 180µM. HNCO, HN(CA)CO, CBCA(CO)NH and HNCACB experiments were recorded for the backbone assignment. 1D proton and ^{1}H-^{15}N HSQC spectra were collected before and after every 3D experiment to monitor the condition of the sample. Backbone resonance assignment was

carried out using CCPN Analysis. To validate the assignment the resonances were followed independently through the carbonyl-amide and the C_α/C_β-amide linkages.

3.3 Results & Discussion

3.3.1 Expression and purification of α-synuclein

ASyn (WT, A30P, E46K, H50Q, G51D, A53T, and A53E) was successfully expressed in minimal growth media and purified using ion-exchange chromatography. Bands of ≥95% purity could be seen for each by SDS-PAGE (Figure 3-1). Additionally, intact masses matching the predicted mass were obtained for each by MS. Unlabelled, ^{15}N-labelled, and $^{13}C/^{15}N$ double-labelled protein was prepared as necessary for the different experiments.

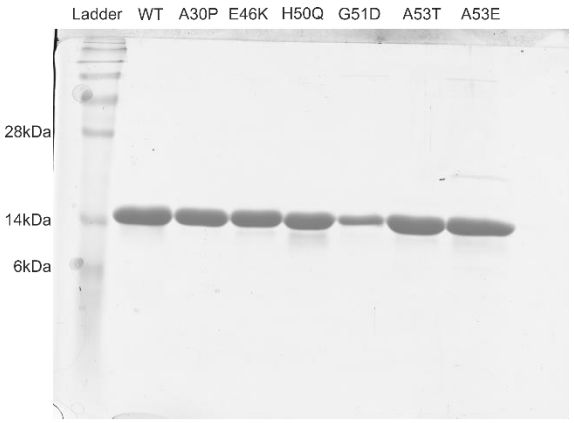

	Predicted mass (Da)	Actual mass (Da)
WT	14460.16	14464.00
A30P	14486.19	14490.00
E46K	14459.21	14463.00
H50Q	14451.15	14454.00
G51D	14518.19	14522.00
A53T	14490.18	14494.00
A53E	14518.19	14522.00

Figure 3-1 - SDS-PAGE gel of purified WT aSyn and the PD-linked mutants and intact MS measurements. *Each of the forms is >95% pure with a single strong band at 14.5kDa, as shown by SDS page gel (left). The intact masses of each were measured by intact MS to confirm that the actual mass of the proteins matched with what was expected. The MS instrument had a 4Da miscalibration, hence each measurement is consistently about 4Da out from the expected value.*

3.3.2 Backbone assignment of wild-type α-synuclein

A reliable backbone assignment is an essential resource because peak shifts are a visible sign of peptide-protein interactions, binding events, and protein conformational changes. By mapping the identity of the different peaks it should therefore be possible to identify the residues involved in these events. For example, in the event of a titration to investigate ligand-binding it

should be possible to identify those residues involved in the binding event (117). There are several previously published assignments of aSyn, however these have often been of samples in different buffers and at different temperatures. These factors can result in peak shifts and thus a new backbone assignment of aSyn in the NMR buffer that would be used in later experiments was desirable. To this end, four different 3D NMR experiments (HNCO, HN(CA)CO, CBCA(CO)NH and HNCACB) were collected. These were interspersed with HSQCs to confirm the state of the protein did not change during the timeframe of the experiments. Through the HNCO and HN(CA)CO it was possible to follow amino acid linkages through the carbonyl groups, whilst through the CBCA(CO)NH and HNCACB spectra linkages through the C_α and C_β peaks could be followed (Figure 3-2). Having the two separate sets of experiments facilitated the assignment process by allowing for validation of assignments made using one set of experiments. Additionally, it was often the case that regions that were difficult to assign in one set of experiments, due to poorly resolved peaks, were better resolved in the other spectra enabling their assignment. Through this process, 122 residues out of a total of 134 assignable residues (140 – (5 prolines + 1 N-terminal residue)) were successfully assigned (Figure 3-3).

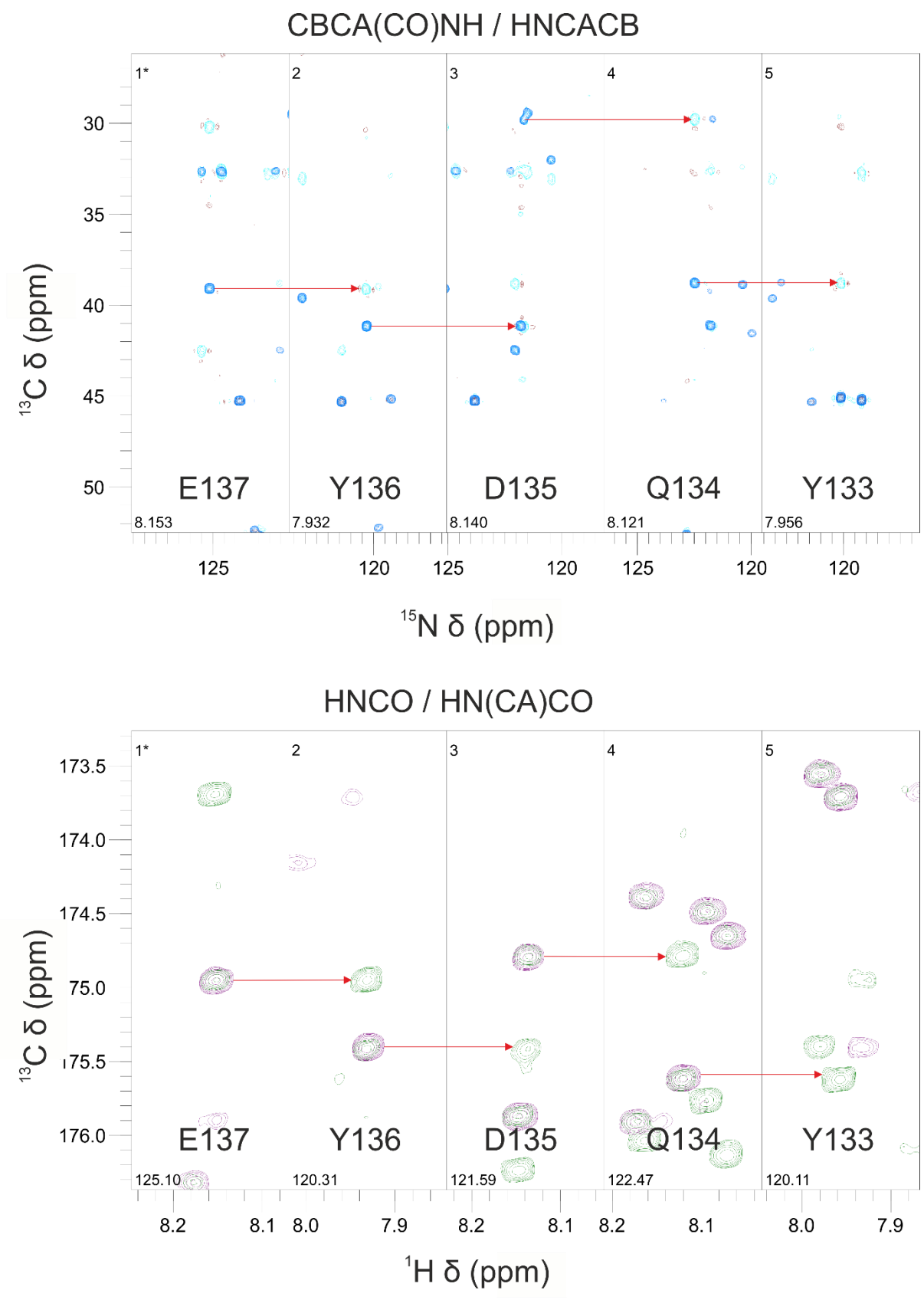

Figure 3-2 - Schematic showing the process of backbone residue assignment of WT aSyn. *Top) Overlaid CBCA(CO)NH (blue) and HNCACB (cyan and brown, positive and negative phasing respectively) spectra showing how the amino acid chain can be followed via the C_α and C_β peaks. Bottom) Overlaid HNCO (purple) and HN(CA)CO (green) spectra showing how the linkages can be independently followed using the carbonyl groups.*

Figure 3-3 - An assigned HSQC spectrum of WT aSyn, and HSQCs of each of the PD-linked mutants. *Left) An assigned HSQC spectrum of WT aSyn. Right) HSQCs of each of the PD-linked aSyn mutants superimposed with the spectrum for WT. Shifts are evident at the mutation site itself and in those residues adjacent to it.*

4 The inhibition of α-synuclein aggregation using a novel peptide-based inhibitor

4.1 Introduction

4.1.1 The plodding advance of neurodegenerative disease

Neurodegenerative diseases, such as PD and AD, arguably represent the most significant challenge to modern medicine. This is in the sense that they are both prevalent and, as yet, remain entirely unconquered. Unlike cancers, with their opportunities for surgical intervention, various chemotherapies or radiotherapy, there are no tools currently available that allow us to fight back against the gradual yet relentless progression of neurodegeneration. In the 21st century, with its vast and ever-growing human population and increased life spans, the impact of neurodegeneration is felt like never before. In the UK 850,000 people are thought to live with dementia to the tune of £26billion per annum (118).

4.1.2 The peptide inhibitor

As discussed previously in 1.8.2.1 there is great interest in the development of new peptide-based inhibitors to combat the toxicity of aggregation-prone proteins, such as aSyn. Collaborators at the University of Bath recently published a paper describing a peptide designed to inhibit the aggregation of aSyn (108). They identified this peptide using a novel intracellular library-screening technique based upon the recombination of dihydrofolate reductase in the event of binding between a peptide candidate and the protein target. Peptides targeting aSyn aggregation have been trialled before (99,119), but *Cheruvara et al* built a library of peptide sequences specifically aimed at the 45-54 region of aSyn in which the majority of the PD-linked point mutations are found. The only criteria needed to be fulfilled by a successful candidate in this screening assay is that it: a) bind to aSyn and b) reduce cytotoxicity. The successful peptide candidate identified was the 10-residue

peptide KDGIVNGVKA, which is acetylated at the N-terminus and amidated at the C-terminus (Figure 4-1). In the publication the group showed via ThT fluorescence assays and atomic force microscopy (AFM) that KDGIVNGVKA abrogated aSyn fibril formation *in vitro*. They also showed that the exposure of cells to aSyn plus peptide reduced cytotoxicity compared to aSyn alone using 3-(4,5-dimethylthiazol-2-yl)-2,5-diphenyltetrazolium bromide (MTT) assays.

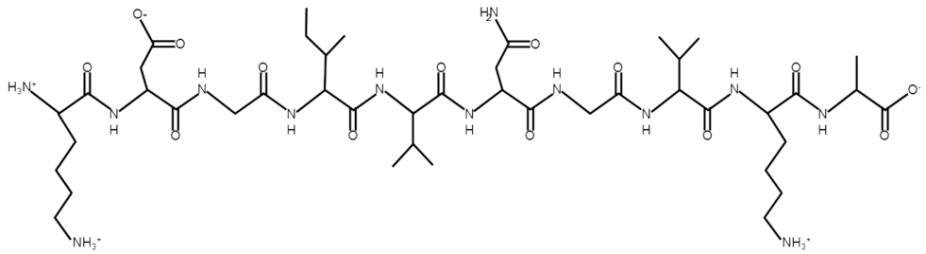

Figure 4-1 – Skeletal formula of the KDGIVNGVKA peptide inhibitor. *This structure was prepared using the PepDraw server* (120)*.*

4.1.3 Aims

The aim in this work was to use NMR to test the hypothesis that KDGIVNGVKA was binding to aSyn, and if possible identify the binding site(s). This was based on the initial observations of *Cheruvara et al* who produced indirect evidence of binding and abrogation of aSyn aggregation (108). To assist in the identification of those residues involved in binding two alanine variants of KDGIVNGVKA were also utilized: KDGIVAGVKA and KAGIVNGVKA.

4.2 Methods

The peptides KDGIVNGVKA, KDGIVAGVKA, and KAGIVNGVKA used in these experiments were either kindly provided by Jody Mason (University of Bath) or purchased from China Peptides (Shanghai, China). All peptides were N-terminally acetylated and C-terminally amidated.

4.2.1 NMR experiments

All NMR experiments were prepared, run and analysed as outlined in sections 3.2.5 and 3.2.6.

4.2.1.1 Peptide-binding NMR titrations

^{15}N-labelled WT aSyn was resuspended in NMR buffer such that the final concentration was 180µM. Initial 1D and ^{1}H-^{15}N HSQC spectra were collected and subsequently KDGIVNGVKA peptide was added to the sample, such that the peptide:protein ratio was 0.25:1. 1D and ^{1}H-^{15}N HSQC experiments were repeated for this molar ratio. This process was repeated and 1D and ^{1}H-^{15}N HSQCs were collected for each of the following peptide:protein ratios: (0.25:1), (0.5:1), (0.75:1), (1:1), (2:1), (6:1), (15:1) and (20:1). 1D proton spectra were collected with 32 scans, 8 dummy scans, 0.557s acquisition time, and sweep width 9.1877ppm. ^{1}H-^{15}N HSQCs were collected with 4 scans, 32 dummy scans, an acquisition time of 0.109s (^{1}H) and 0.061s (^{15}N), and a sweep width of 9.1877ppm (^{1}H) and 26.0000ppm (^{15}N). Spectra were analysed in CCPN Analysis and compared to the assigned WT aSyn spectrum to check for peak shifts or line-broadening. Chemical shift perturbations were expressed as:

$$\Delta\delta = \{(\Delta H)^2 + (0.15\Delta N)^2\}^{1/2}$$

4.2.1.2 Timecourse HSQCs of peptide and α-synuclein

ASyn was resuspended in NMR buffer to a final concentration of 200µM; one sample was of aSyn alone whilst the other contained an equimolar concentration of KDGIVNGVKA peptide. 1D proton spectra and a ^{1}H-^{15}N HSQC were collected on each sample. The samples were then incubated at 37°C with agitation. A further 1D and ^{1}H-^{15}N HSQC spectrum were collected on the samples every 24hours for two weeks. 1D proton spectra were collected with 32 scans, 8 dummy scans, 0.557s acquisition time, and a sweep width of 9.1877ppm. ^{1}H-^{15}N HSQC spectra were collected with 8 scans, 100 dummy scans, an acquisition time of 0.120s (^{1}H) and 0.061s (^{15}N), and a sweep width of 8.3080ppm (^{1}H) and 26.0000ppm (^{15}N). CCPN Analysis was used for data analysis.

4.2.1.3 WaterLOGSY peptide-binding experiments

This experiment was carried out for the following peptides: KDGIVNGVKA, KAGIVNGVKA, KDGIVAGVKA, KDGAVNGVKA, KDGIANGVKA, KDGIVNAVKA, and KDGIVNGAKA. Lyophilized WT aSyn and peptide were reconstituted in NMR buffer with 5% D_2O to a final concentration of 50µM and 1mM respectively. Each experiment required multiple samples: 1mM peptide alone, 50µM WT aSyn alone, 50µM WT aSyn + 1mM peptide. 1D proton and WaterLOGSY spectra were collected on each sample every day for 7 days. The 1D proton spectra were collected with 128 scans, 20 dummy scans, an acquisition time of 0.734s, and a sweep width of 13.9456ppm. WaterLOGSY spectra were collected with 256 scans, 16 dummy scans, an acquisition time of 0.729s, and a sweep width of 14.0396ppm. 1D and WaterLOGSY spectra were compared in TopSpin with the control spectra to check for signs of binding.

4.2.1.4 Natural abundance ^{1}H-^{13}C HSQCs of peptides

The peptides KDGIVNGVKA, KDGIVAGVKA and KAGIVNGVKA were dissolved in D_2O such that the final concentration was 1mM. 1D proton and ^{1}H-^{13}C HSQC spectra were collected for each peptide, and then the samples were incubated at 37°C with agitation for 1 week. Then a further 1D proton and ^{1}H-^{13}C HSQC spectrum was collected for each. 1D proton spectra were collected with 128 scans, 100 dummy scans, an acquisition time of 0.557s, and a sweep width of 9.1877ppm. ^{1}H-^{13}C HSQC spectra were collected with 16 scans, 16 dummy scans, an acquisition time of 0.100s (^{1}H) and 0.014s ($^{13}C0$, and a sweep width of 10.0122ppm (^{1}H) and 65.0005ppm (^{13}C). Spectra were processed in TopSpin and analysed in CCPN Analysis.

4.2.2 "Ageing" of peptides

Stocks of 4mM "aged" KDGIVNGVKA, KDGIVAGVKA, and KAGIVNGVKA were prepared by resuspending the lyophilized peptide into either NMR buffer for NMR studies or PBS pH 7.4 for

aggregation assays and TEM. The peptides were then incubated at 37°C with agitation for 1 week. The stock was then available for use in downstream experiments and assays.

4.2.3 ThT analysis of α-synuclein incubated with KDGIVNGVKA, KDGIVAGVKA, or KAGIVNGVKA

Three samples of 500µL aSyn (WT, A30P, E46K, H50Q, G51D, A53T and A53E) were prepared in PBS pH 7.4 at a concentration of 100µM. One sample was protein alone, whilst the second contained "fresh" KDGIVNGVKA peptide at a final concentration of 100µM. The third sample contained "aged" KDGIVNGVKA at a concentration of 100µM. Each of these tubes was incubated at 37°C with agitation for 1 week. 100µL aliquots were taken and snap frozen in LN_2 on day 0, 1, 3 and 7. These aliquots were then thawed and transferred to a 96-well black-walled, clear bottom plate (Nunc) for endpoint fluorescence measurements on a Flexstation 3 microplate reader (Molecular Devices). Identical samples were simultaneously prepared and measured for the peptides KDGIVAGVKA and KAGIVNGVKA. Each sample was measured in triplicate and the final volume in each well was 50µL. The 50µL was made up using 25µL of sample and 25µL of buffer with 2µM ThT. λ_{ex} = 440nm and λ_{em} = 490nm. Data was processed and analysed using OriginLab. Statistical significance of the differences was assessed using analysis of variance (ANOVA) with the Bonferroni *post hoc* test.

4.2.4 TEM analysis of α-synuclein incubated with KDGIVNGVKA, KDGIVAGVKA, or KAGIVNGVKA

5µL of each sample as used for the ThT assay was mounted onto a carbon-coated copper grid for 2mins. The grid was then gently blotted onto a piece of filter paper to remove excess liquid before applying 4% (w/v) uranyl acetate for 30s. Uranyl acetate was removed and the grid dried by blotting onto a piece of filter paper. Images were collected on a 120kV Tecnai G2 Spirit BioTWIN electron microscope (FEI) with a SIS Megaview III camera. Image and fibril length analysis was

carried out using ImageJ and OriginLab, with the scale bar on each image used as the length reference.

4.2.5 Mass spectrometry analysis of KDGIVNGVKA, KDGIVAGVKA, and KAGIVNGVKA

All MS analysis was carried out by Philip Brownridge and the Centre for Proteome Research at the University of Liverpool. Fresh and aged peptide samples were diluted to a concentration of 1pmol/µL in 50% acetonitrile, 0.1% formic acid and infused at 5µL/min onto the electrospray ionization (ESI) source of an Orbitrap Fusion. Comparison of theoretical and experimental m/z values showed that measurements were accurate to 3ppm. Asn deamidation in KDGIVNGVKA was probed using the corresponding 1Da mass shift and the proportion of Asn deamidated was determined through deconvolution of the isotope (^{13}C) cluster peaks. This was further confirmed through higher-energy C-trap dissociation (HCD) MS-MS. The formation of iso-Asp in the peptides over time was monitored using the KDGIVAGVKA peptide, due to the lack of Asn. KDGIVAGVKA peptide was diluted in 50mM ammonium bicarbonate to a concentration of 0.211µg/µL in 40µL. 0.12µg Asp-N (Roche, Switzerland) was then added to provide an enzyme:substrate ratio of 1:50. The sample was incubated at 37°C and 2µL aliquots of the digest were taken at different timepoints (0hr, 1hr, 3.5hr, 6hr, overnight). Each sample was analysed by ESI on the Q-Exactive HF between 300 and 1500 m/z at 60,000 resolution. The ratio of Ac-KDGIVAGVKA-Amid ions to DGIVAGVKA-Amid ions was used to infer the degree of iso-Asp formation for samples of fresh and aged peptide.

4.3 Results

4.3.1 Peptide-binding NMR titrations

The titration of increasing levels of the KDGIVNGVKA peptide against monomeric aSyn did not result in the expected changes in aSyn's HSQC profile. This was true at a 1:1 peptide:protein molar ratio, and was consistent up to a 20:1 ratio. Using the prepared backbone resonance assignment (Figure 3-3) it had been determined which peak corresponded to which amino acid within the protein. Any changes in the chemical environments of these amino acids induced by, for example, the binding of a peptide to the protein would be clearly visible. With the exception of a shift in the resonance corresponding to His50 no significant changes were seen (Figure 4-2). The change in His50 is likely a result of a minor buffer mis-match between the peptide and protein, especially given the proximity of the buffer pH to the histidine pK_a and the lack of any peak shifts at neighbouring residues. These findings ran marginally contrary to the suggestions of the paper by *Cheruvara et al* (108). In this paper the KDGIVNGVKA peptide was identified using a novel intracellular screening assay on the basis that it bound to monomeric aSyn – specifically the 45-54 region of the protein – and reduced cytotoxicity. In the original publication the peptide was described as being powerfully inhibitory of aSyn aggregation at even 1:1 concentration. The lack of peak shifts seen here at even 20:1 molar ratio strongly suggest that there is no binding between monomeric aSyn and KDGIVNGVKA.

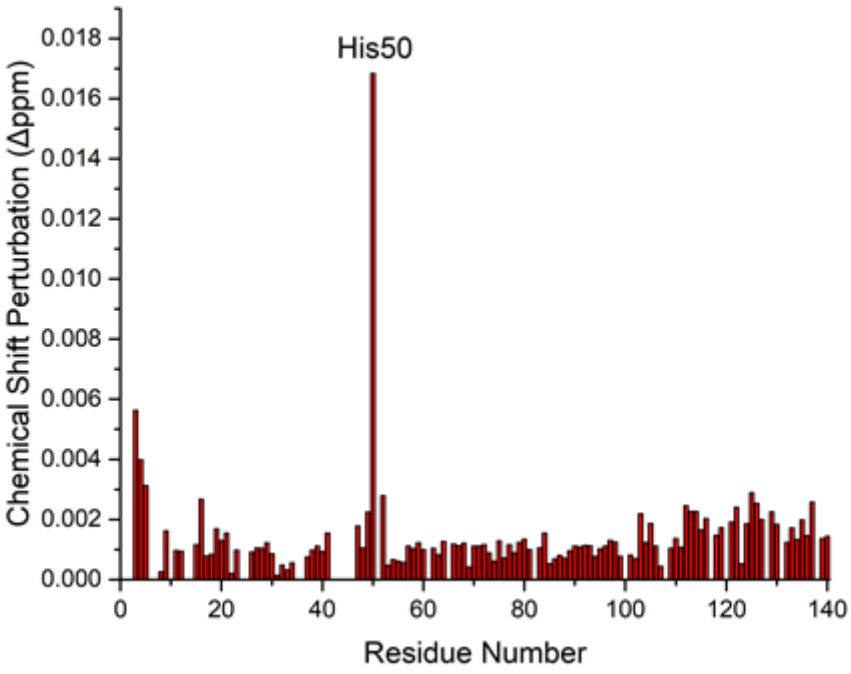

Figure 4-2 - Bar chart showing the HSQC peak shifts of WT aSyn upon addition of KDGIVNGVKA. *The peak shift distances were measured following the addition of KDGIVNGVKA peptide to a 20-fold molar excess of the peptide versus the protein. Gaps indicate those residues that are either unassigned or for which the chemical shift perturbation could not be accurately determined due to overlapping peaks.*

There are several possible explanations for this apparent lack of peptide-protein interaction:

1) There is no interaction.
2) They interact on a timescale that is not conducive to NMR.
3) The interaction takes place between the peptide and an aSyn species that is "NMR-invisible".

Of the three options it is the possibility of an interaction between the peptide and an NMR-invisible species (e.g. oligomers or fibrils) that seemed the most likely and most probe-able. Oligomers and fibrils both exceed the size-limit of NMR (~35kDa), exhibiting prohibitive line-broadening, and thus are not seen on the HSQC spectrum.

4.3.2 Timecourse HSQCs of α-synuclein and KDGIVNGVKA

HSQC spectra of 200µM WT aSyn, with and without 200µM KDGIVNGVKA peptide, were collected every day for a period of two weeks. In between measurements the samples were incubated at 37°C with agitation to allow the formation of fibrils. During this timeframe excessive line-broadening caused by the formation of large aggregates results in the loss of many peaks. Some visible signals did remain, primarily belonging to residues within the CTD and thus that lie outside the core of the aggregated species – oligomers or maybe protofibrils – and therefore have independent dynamic properties (see Figure 4-3). The observed changes in the HSQC were near-identical between the samples of aSyn alone versus that incubated with the inhibitor. This fact is supportive of the hypothesis following the titrations of KDGIVNGVKA against aSyn that KDGIVNGVKA does not bind to monomeric aSyn and may instead be binding to a species that lies beyond the size-limit of NMR and is thus unobservable.

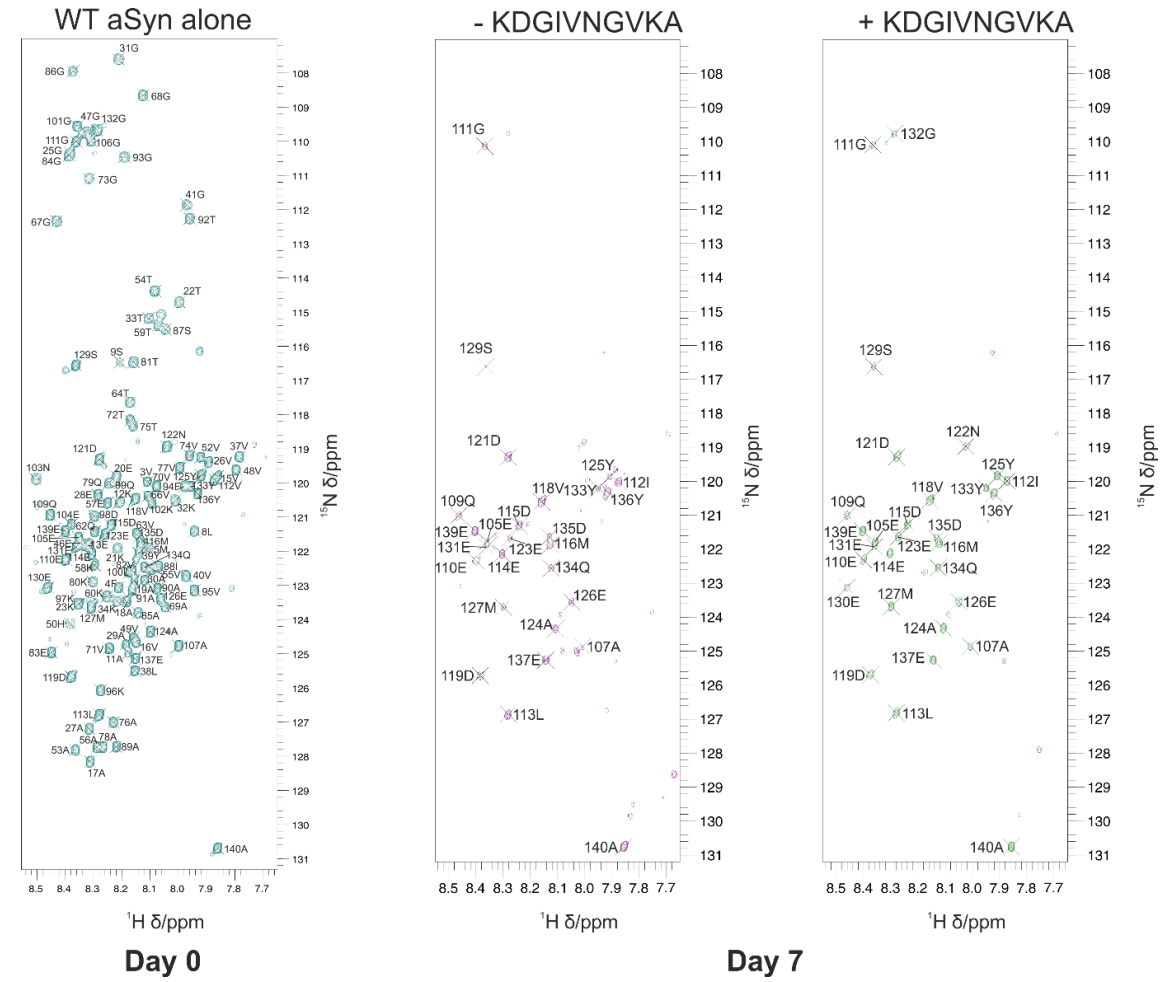

Figure 4-3 - HSQCs of WT aSyn before incubation and after incubation with and without KDGIVNGVKA for 7 days. *The incubation of WT aSyn for 7 days at 37°C results in a significant loss of peaks. This is the case for the samples with and without an equimolar concentration of KDGIVNGVKA peptide. The fact that this takes place for both samples suggests that the KDGIVNGVKA peptide does not bind to monomeric aSyn and does not impede the formation of aggregates of sufficient size as to be rendered invisible by NMR. Those peaks that remain are exclusively located with the CTD of aSyn, which are highly dynamic and likely have relaxation properties independent of the rest of the molecule.*

4.3.3 WaterLOGSY peptide-binding experiment

In order to investigate the hypothesis that KDGIVNGVKA is binding to higher-order aSyn species a more peptide-centric approach was utilized. Rather than trying to follow changes in protein signals the aim was to spot changes in the peptide and a loss of peptide signal upon binding. In light of this, WaterLOGSY experiments, in conjunction with 1D proton experiments, were used. Samples were prepared of protein plus peptide – alongside appropriate controls (peptide alone, protein alone) – and 1D proton and WaterLOGSY spectra were collected every day for one week. As seen in Figure 4-2 there was no evidence of binding between monomeric aSyn and KDGIVNGVKA

(the equivalent of day 0), but there were observable changes in signal intensity at later timepoints. This can be seen in Figure 4-4 which shows the raw 1D and WaterLOGSY spectra at day 0 and day 6, and the peptide signal intensity is reduced in the sample of KDGIVNGVKA plus aSyn relative to the sample of KDGIVNGVKA alone. This was plotted in Figure 4-4 C&F where the difference in area under the peaks between the peptide alone and peptide plus protein samples is shown. These show a clear increase in difference over time. The apparent time-dependence suggests that aSyn has begun to form larger aggregates, and it supports the data from Figure 4-2 and Figure 4-3 and the hypothesis that KDGIVNGVKA does not interact with monomeric aSyn but that it may do so with oligomeric or fibrillar aSyn.

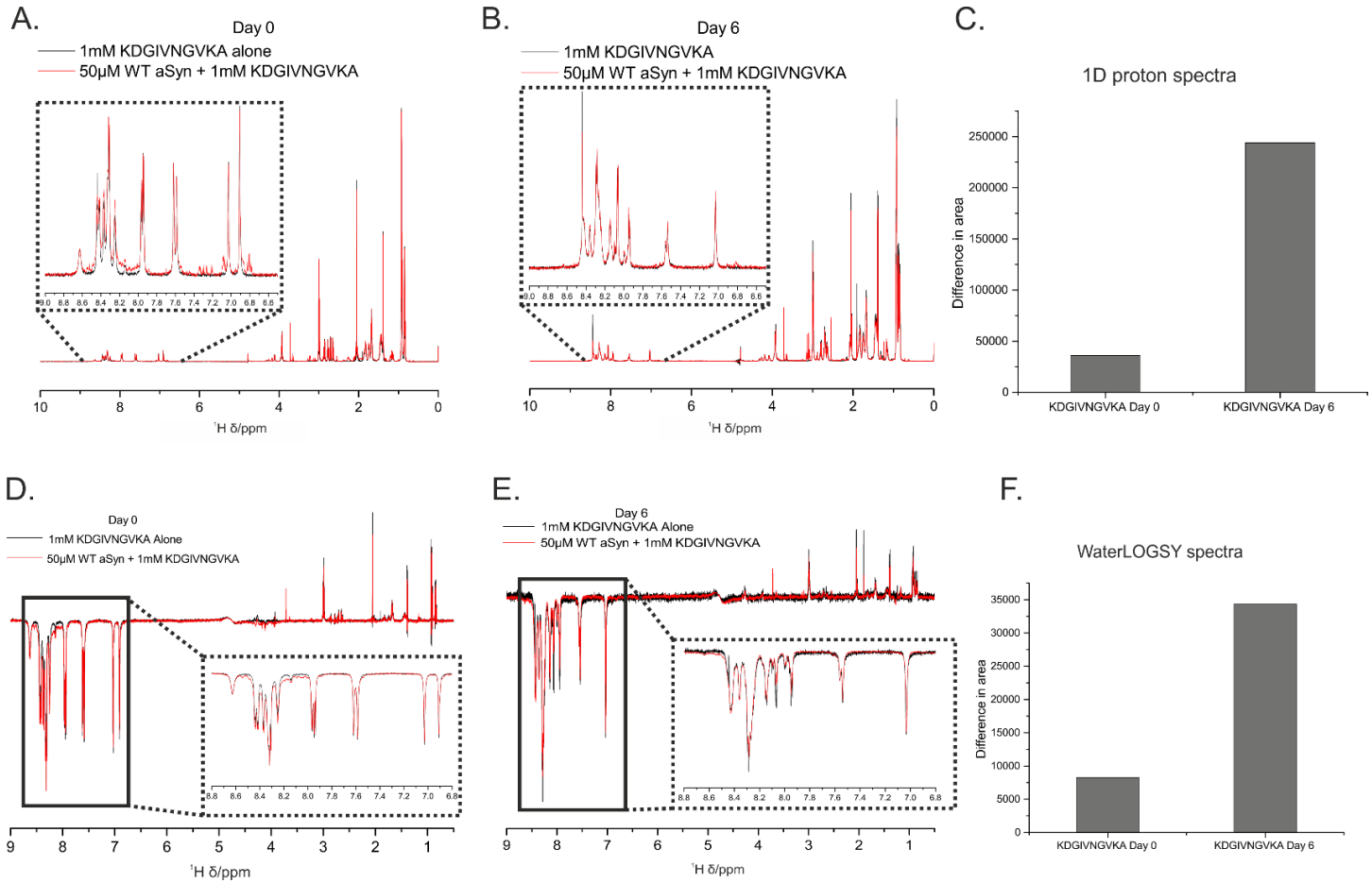

Figure 4-4 - 1D and WaterLOGSY timecourse experiments indicating the binding of KDGIVNGVKA to WT aSyn. *Raw 1D spectra of 1mM KDGIVNGVKA alone and 1mM KDGIVNGVKA plus 50μM WT aSyn that have been incubated for 0 (A) and 6 days (B) respectively at 37°C. There is a loss of intensity of some key peptide signals in the spectra of peptide plus protein compared to in the spectra of peptide alone. These differences are greater at the later timepoints, and are plotted on a bar chart (C). Raw WaterLOGSY spectra of 1mM KDGIVNGVKA alone and 1mM KDGIVNGVKA plus 50μM WT aSyn that have been incubated for 0 (D) and 6 (E) days respectively at 37°C. Similarly to in the 1D spectra there is a loss of intensity of some peptide signals in the spectra of the sample that contains WT aSyn versus that of the peptide alone. These losses of peptide signal, which increase over time, are likely due to the binding of KDGIVNGVKA to WT aSyn aggregates. The population of these aggregates will increase over time, and their size exceeds the size-limit of NMR rendering them "invisible". The binding of KDGIVNGVKA to these species would, in turn, render them invisible and result in a loss-of-signal.*

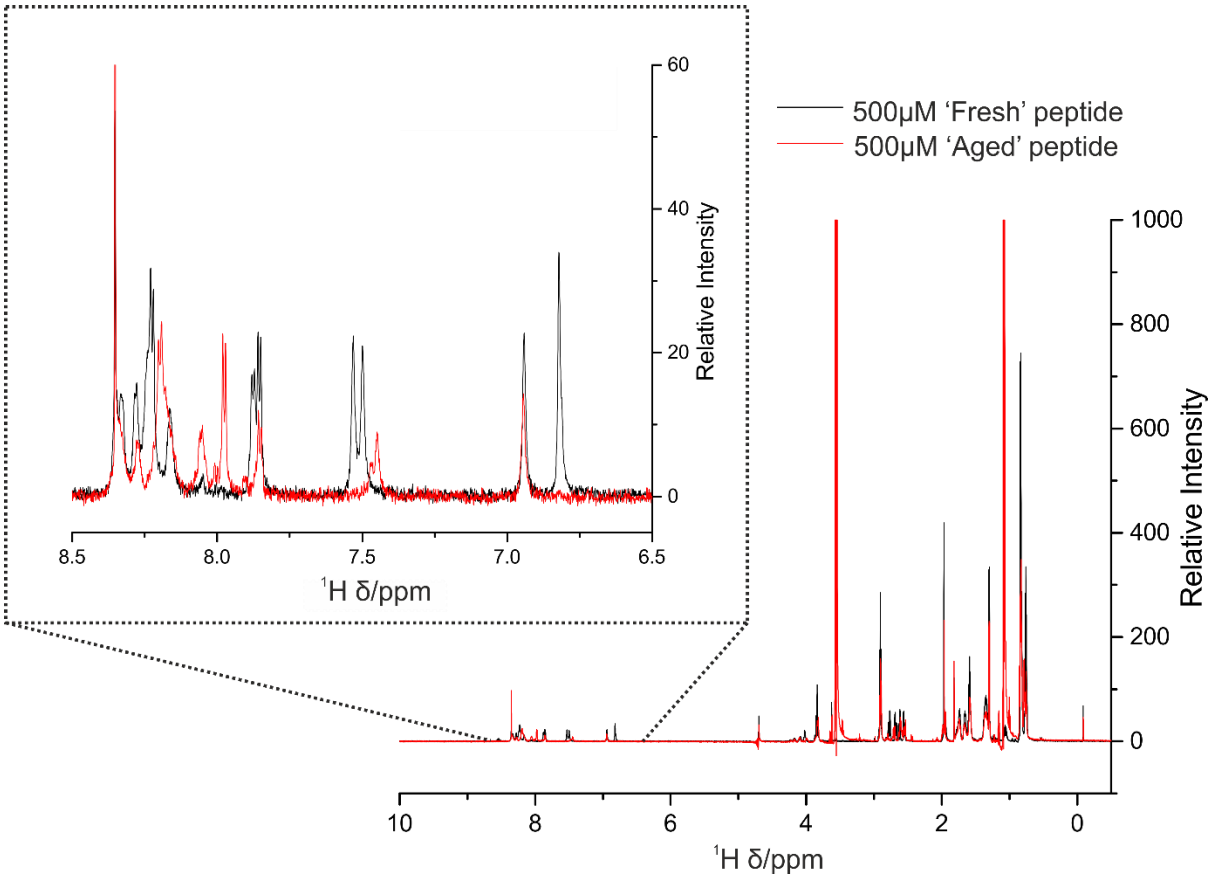

Figure 4-5 - 1D proton NMR spectra of "fresh" and "aged" KDGIVNGVKA. *Further samples were prepared using a different batch of peptide at 500µM in PBS pH 7.4 to ensure the changes over time were reproducible. Freshly prepared samples appear to contain two populations of peptide. After 7 days of incubation at 37°C with agitation the "aged" peptide appears to consist entirely of the modified peptide.*

It was also clear from the 1D and WaterLOGSY spectra of KDGIVNGVKA alone and of KDGIVNGVKA in the presence of aSyn that the peptide was changing over the timeframe of the experiments. These modifications and their potential relevance to aSyn interaction was investigated further by NMR and MS.

4.3.4 Probing changes in KDGIVNGVKA over time

To probe the changes seen during the timecourse of the WaterLOGSY peptide-binding experiments in more detail further NMR experiments on the peptide alone were carried out. To ensure that this was a batch independent phenomenon an alternative batch of KDGIVNGVKA was

used. A 500µM sample of KDGIVNGVKA alone was prepared in PBS pH 7.4. This sample was termed "fresh" and a 1D proton spectrum was collected. This sample was reanalysed 1 week later after being incubated at 37°C with. This was termed the "aged" peptide. The spectra of both are shown overlaid in Figure 4-5. The same changes that observed during the course of the WaterLOGSY experiments are apparent; the most obvious changes are in the amide region (6.5 – 8.5ppm) of spectrum. There is notably a peak present in the fresh sample at 6.8ppm that is not seen in the aged sample. This is likely the peak corresponding to the amide group in the sole asparagine residue of KDGIVNGVKA, which may become deamidated over time. This process occurs more rapidly at elevated temperatures (e.g. during incubation at 37°C) and when the residue is followed by a flexible residue – like glycine (121). A set of natural abundance ^{1}H-^{13}C HSQCs on the fresh and the aged peptide samples were also conducted (Figure 4-6). ^{13}C is naturally present as 1% of the total carbon on Earth, making these experiments possible with unlabelled peptide so long as a high peptide concentration was used (1mM).

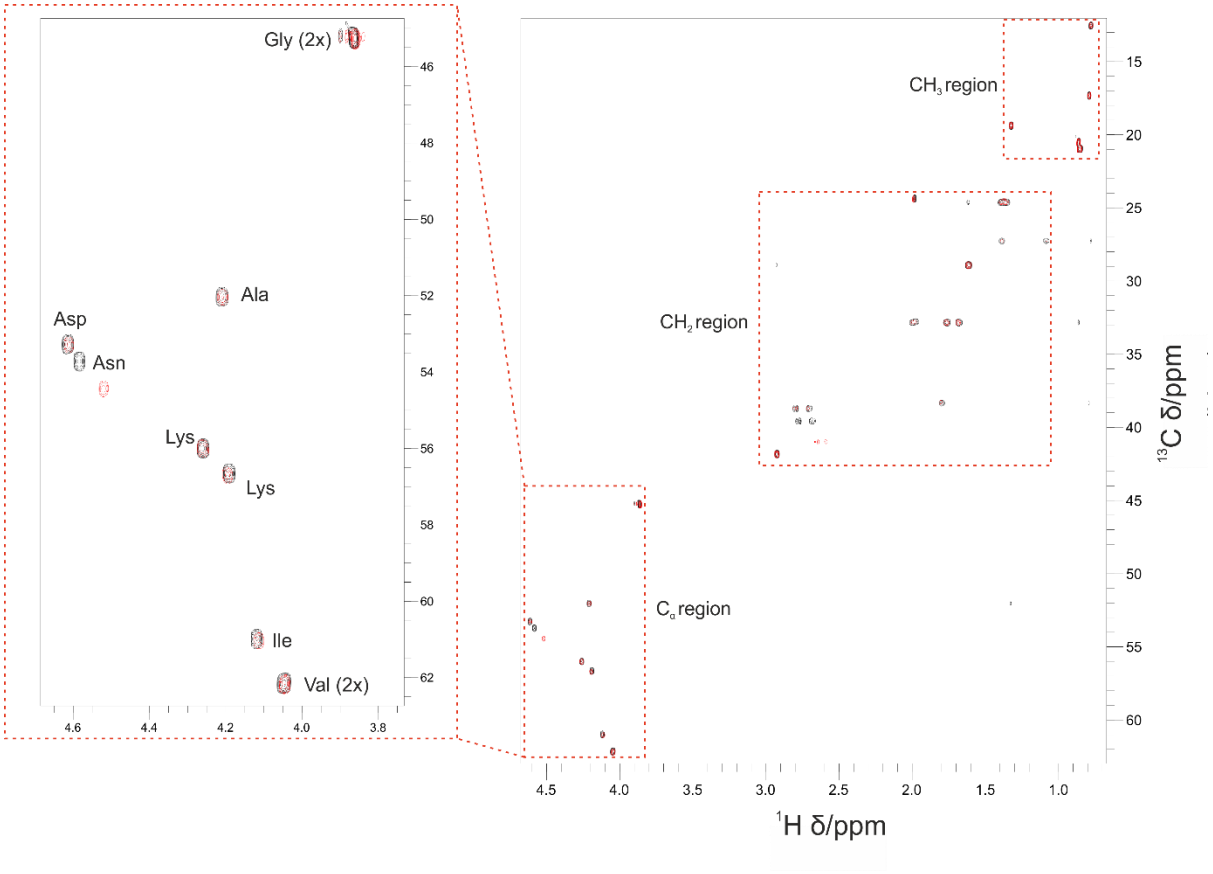

Figure 4-6 - Natural abundance 1H-13C HSQC spectrum of fresh and aged KDGIVNGVKA. *The black spectrum is fresh peptide whilst the red is the aged form. Note the shift in the asparagine C_α peak, which would suggest that the residue is deamidating over time. Concomitant shifts are also seen in the CH_2 peaks for asparagine.*

The spectra revealed clear shifts in the position of the C_α and C_β peaks likely corresponding to the asparagine residue (Figure 4-6). This was compelling evidence in favour of deamidation, but given the close proximity between the Asn and Asp peaks MS was used for confirmation. The deamidation of Asn results in a mass shift of 1Da, which is detectable by MS (122).

Fresh and aged KDGIVNGVKA, prepared under identical conditions to those used in the NMR experiments, was analysed by MS through direct infusion revealing a primary ion with the m/z value 521.3078 (Figure 4-7). The theoretical value is 521.3062, so the measured accuracy was to within 3ppm. In the fresh peptide sample the predominant peak has a value of 521.3078, with less abundant peaks at 521.8045 and 522.3008 which reflect those ions containing ^{13}C. In the aged sample the distribution of these peaks is different, with the predominant peak being the middle

peak (521.8045). This suggests that partial deamidation of the sample has occurred, and the first ^{13}C peak of the unmodified peptide now overlaps with that of the deamidated peptide. By looking at the ratio in the relative abundances of each peak in the two samples it was possible to determine the proportion of the peptide that had been deamidated; this was about 51%. With HCD MS-MS the location of this deamidation was determined (see Figure 4-8). Unlike in Figure 4-7 in which m/z values of the whole peptide were recorded, using HCD MS-MS ion fragments of the peptide were generated. As can be seen in Figure 4-8, the distribution of peaks mimics that seen for the whole peptide until Asn is removed. The loss of the preceding peak indicates that Asn is responsible for the dual population (with a difference in mass of 1Da). This corresponds to the mass change induced by deamidation and confirms that Asn6 in the ten-residue peptide is the site of deamidation.

This confirms that partial deamidation of the Asn residue is taking place within a similar timeframe to the aggregation of aSyn *in vitro*. This holds relevance from the point of view of therapeutic development, as this may modulate the affinity of interaction between aSyn aggregates and KDGIVNGVKA, and may also affect the concentration of peptide that needs to be utilized in order to obtain maximum inhibition.

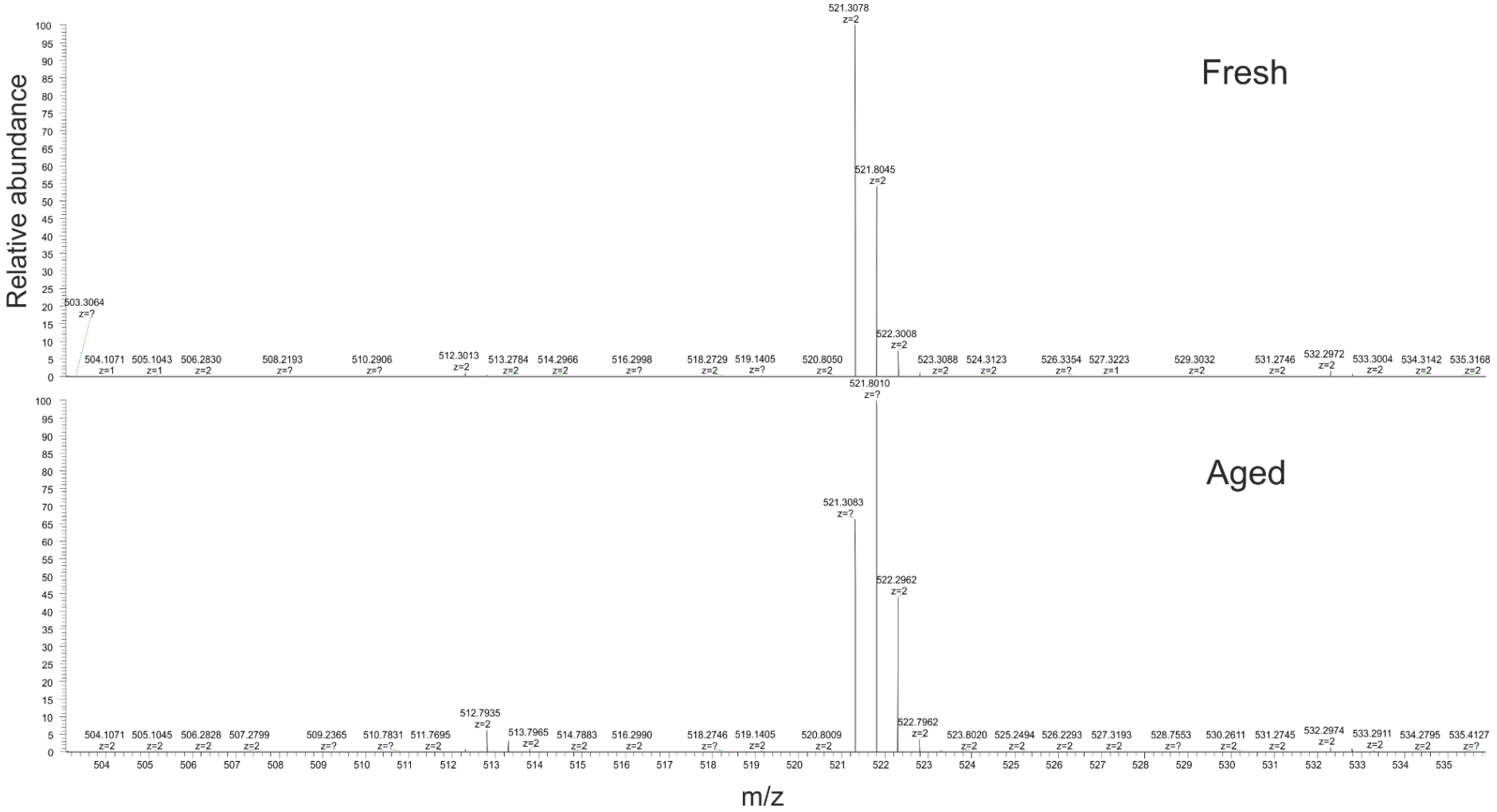

Figure 4-7 - Mass spectra of fresh and aged KDGIVNGVKA. *Samples of fresh and aged KDGIVNGVKA were prepared at 1pmol/µL and infused at 5µL/min on the ESI source of an Orbitrap Fusion. Mass difference of 1Da is indicative of deamidation. In the aged sample the deamidated peptide peak overlaps with the ^{13}C peak.*

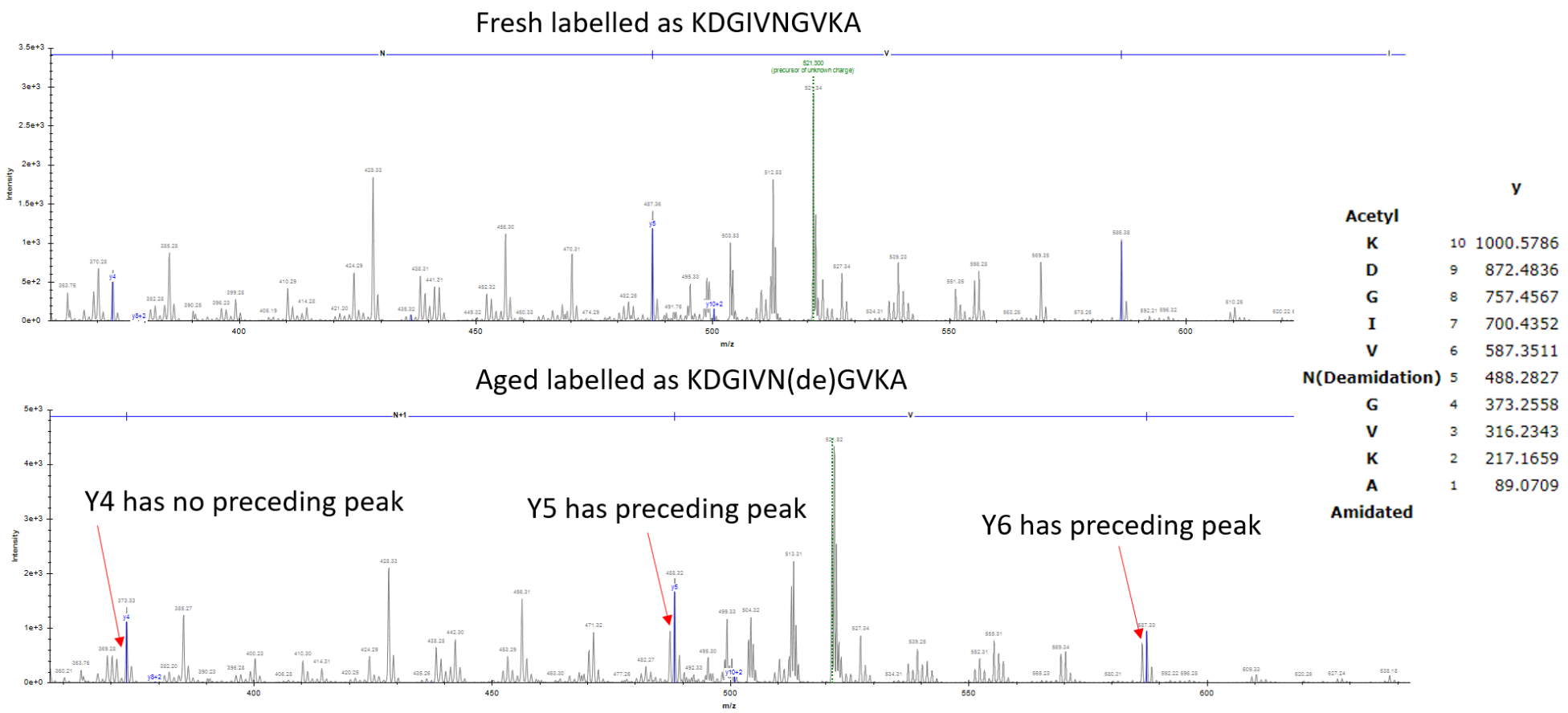

Figure 4-8 - HCD MS-MS spectra showing evidence for deamidation at position N6 in KDGIVNGVKA. *The top spectrum shows the spectrum of fresh KDGIVNGVKA, whilst the bottom shows that of KDGIVNGVKA that has been allowed to 'age' and thus deamidate. The Y6 and Y5 ions have preceding peaks, as shown by red arrows, whilst Y4 does not. This is indicative of the deamidation taking place at the Asn residue at position 6.*

It is worth highlighting that Asn and Asp are both present in the peptide and both are capable of undergoing modification under similar conditions, with Asp forming iso-Asp (Figure 4-9) (123). It is possible to infer iso-Asp formation using the AspN protease, which specifically cleaves the peptide bond N-terminal to Asp residues but is incapable of doing so with iso-Asp (124).

To investigate whether the formation of iso-Asp was also taking place further MS experiments were carried out on fresh and aged KDGIVAGVKA (Figure 4-10). KDGIVAGVKA was chosen due to its lack of Asn, which would otherwise complicate the analysis as it deamidates. The proportion of the total peptide containing iso-Asp rather than regular Asp is increased in the sample of aged peptide. This is indicated by the ratio of the peptides with the m/z values 414.7 and 499.8, which correspond to the +2 ions of DGIVNGVKA-Amid and Ac-KDGIVNGVKA-Amid respectively. After incubation with the AspN protease the ratio only increased marginally in the aged sample, even after 24 hours, whilst there was a much greater degree of cleavage in the fresh sample. This is demonstrated in Figure 4-10 B where the ratio of the 414.7 ion to the 499.8 increases much more substantially over time for the fresh KDGIVNGVKA peptide compared to the aged sample.

In summary, both deamidation of Asn and isomerization of Asp both take place within KDGIVNGVKA during the experimental timeframe. It seems that deamidation of Asn is a more prevalent modification in KDGIVNGKVA than iso-Asp formation. This is indicated by the shift in the Asn peak in the natural abundance HSQCs, whilst Asp remains static (Figure 4-6). Clearly any modifications to this residue don't occur in a sufficient proportion of the peptide population in the sample to be reflected in the NMR spectrum. The binding of KDGIVNGKVA to aSyn appears to increase over time, as suggested by the 1D and WaterLOGSY NMR experiments (Figure 4-4), but it remains to be seen whether deamidation is a help or a hindrance. Further experiments utilizing alanine variants of the KDGIVNGVKA peptide at the sites of the Asp and Asn residues will clarify the effect the modifications have in respect to binding.

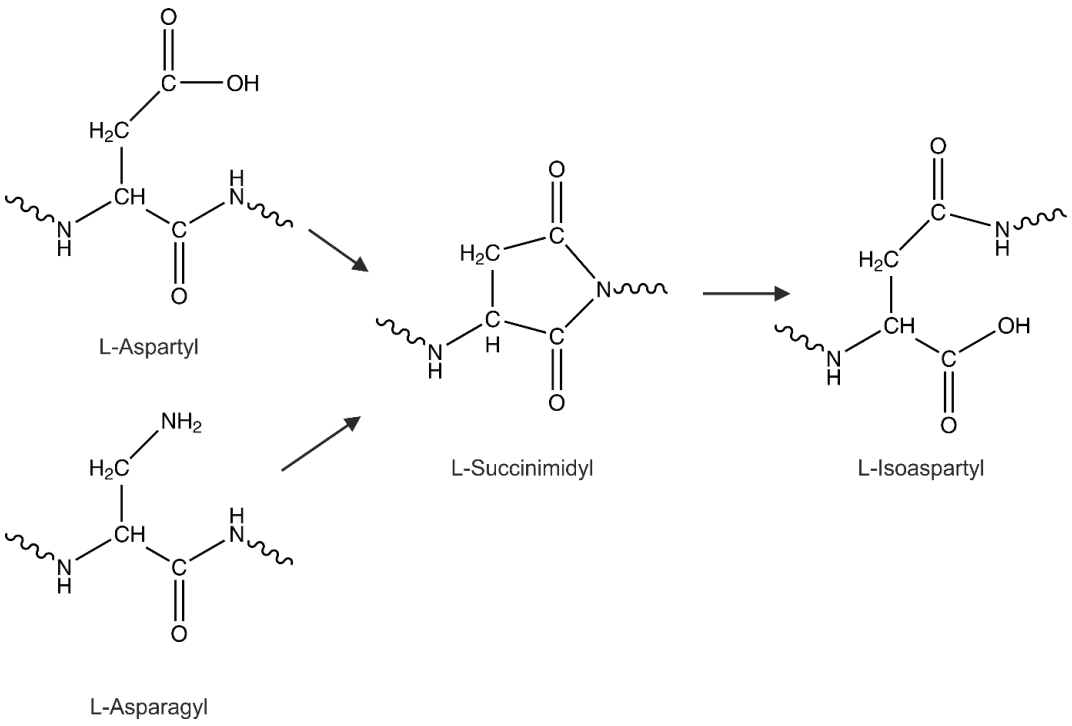

Figure 4-9 - Schematic showing the mechanism of isoaspartate formation from asparagine and aspartic acid sidechains via a succinimide intermediate.

A.

Ac-KDGIVAGVKA-Amid —AspN→ DGIVAGVKA-Amid

MH^{+1} (mono) = 998.5993 MH^{+1} (mono) = 828.4938

MH^{+2} (mono) = 499.8033 MH^{+2} (mono) = 414.7505

	Fresh			Aged		
Time	414.7	499.8	ratio	414.7	499.8	ratio
0	2.47E+05	2.53E+08	9.76E-04	2.42E+05	2.42E+08	1.00E-03
1	6.75E+06	2.35E+08	2.87E-02	3.37E+06	1.82E+08	1.85E-02
3.5	1.33E+07	1.48E+08	8.99E-02	1.15E+07	2.18E+08	5.28E-02
6	2.02E+07	1.68E+08	1.20E-01	1.39E+07	2.01E+08	6.92E-02
overnight	6.54E+07	5.91E+07	1.11E+00	4.29E+07	1.25E+08	3.43E-01

B.

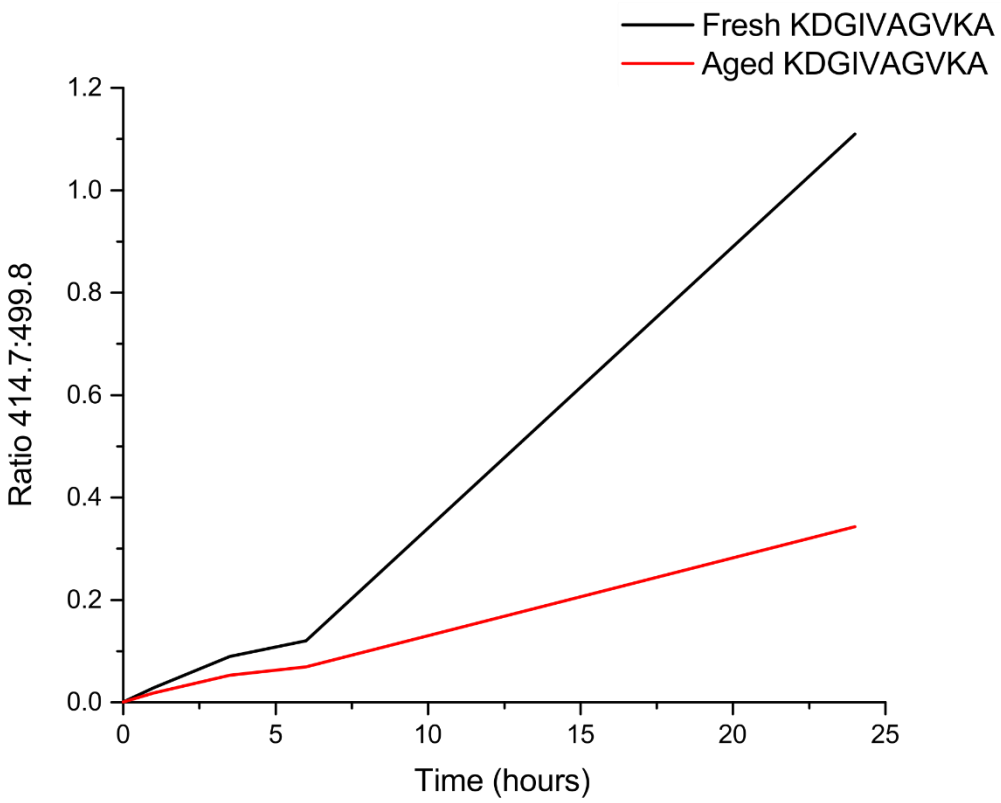

Figure 4-10 - Use of MS to determine isoaspartyl formation. *The peptide KDGIVAGVKA was used so that changes as a result of asparagine modification were not seen. The AspN enzyme cleaves after Asp residues (A) but not iso-Asp, thus the ratio of KDGIVAGVKA:DGIVAGVKA indirectly reports on the level of isoaspartate formation. Ac-KDGIVAGVKA-Amid has a +1 ion (998.5993) and a +2 ion (499.8033), as does DGIVAGVKA-Amid (+1 = 828.4938, +2 = 414.7505). The relative abundances of the +2 ions of both are plotted in the table. The ratio of these values have been plotted at different timepoints (B). This data infers an increase in the level of isoaspartate in the sample of aged KDGIVAGVKA compared to the fresh sample.*

4.3.5 ThT & TEM analysis of α-synuclein incubated with KDGIVNGVKA

In their publication, *Cheruvara et al* showed that incubating WT aSyn with equimolar amounts of KDGIVNGVKA resulted in an absolute abrogation of fibril formation; this was visible by AFM images and from their ThT data (108). In order to validate their work and check that the peptide was functional WT aSyn was incubated at 37°C with agitation for one week, with and without an equimolar concentration of KDGIVNGVKA.

Due to the observations in Figure 4-5 and Figure 4-6 that changes – deamidation – were taking place in KDGIVNGVKA ThT and TEM experiments were performed to compare the effects of fresh and aged forms of KDGIVNGVKA on fibril formation. Additionally, due to the fact that the peptide was intended to target the 45-54 region of aSyn its effects were also tested on the six PD-linked mutants.

4.3.5.1 Wild-type

WT aSyn alone forms long, straight fibrils as can be seen by TEM (Figure 4-11 A). Incubation with either fresh or aged KDGIVNGVKA appears to result in the formation of much shorter fibrils rather than the total abrogation reported by *Cheruvara et al* (Figure 4-11 B&C) (108). Generally, those formed in the presence of equimolar amounts of KDGIVNGVKA appeared as shorter versions of the “normal” fibrils averaging 50-100nm in length (Figure 4-11 D&E). These shorter fibrils don’t form the large, dense “nests” of fibrils common with the protein alone. Those formed in the presence of the aged peptide appear to be similarly affected. The differences in length between fibrils formed by WT aSyn alone and the two peptide conditions were found to be statistically significant (Figure 4-11 E). There are three plausible explanations for this data:

- The deamidation of the Asn residue of KDGIVNGVKA has no significant impact on its inhibitory activity and binding to aSyn, and thus similar effects are seen in the presence of both the fresh and aged peptide.
- The deamidated peptide is inactive and lacks the capability to bind to aSyn or impede its aggregation, yet a sufficient proportion of the unmodified "fresh" peptide remains and this plays an active role in inhibiting protein aggregation.
- Alternatively, the deamidated KDGIVNGVKA is the active inhibitory species that binds to aSyn. As KDGIVNGVKA deamidates over the timeframe of the experiment, both the fresh and aged samples contain a sufficient proportion of deamidated peptide to mediate the observed impact on aSyn aggregation.

The ThT data (Figure 4-11 F) shows that fluorescence increases over time in all three conditions as more β-rich species are formed. The samples of WT alone and WT plus fresh KDGIVNGVKA appear to be quite similar in their ThT profile, whilst those with the aged KDGIVNGVKA exhibit lower overall fluorescence. This is supported in the statistical analysis of the ThT data (Table 4-1). Using ANOVA with the Bonferroni means comparison test it was evident that the samples with aged KDGIVNGVKA are significantly different from the samples of WT aSyn alone and WT aSyn with fresh KDGIVNGVKA at day 1 and all later timepoints. These differences may be the result of two possibilities: that incubation with aged KDGIVNGVKA results in fewer overall fibrils; or that the incubation with aged KDGIVNGVKA results in the fibrils exhibiting an alternative morphology that is less able to bind ThT. The TEM images would suggest that there is not a reduced number of fibrils, and it is likely that the shortened fibrils formed in the presence of aged KDGIVNGVKA are less able to bind ThT.

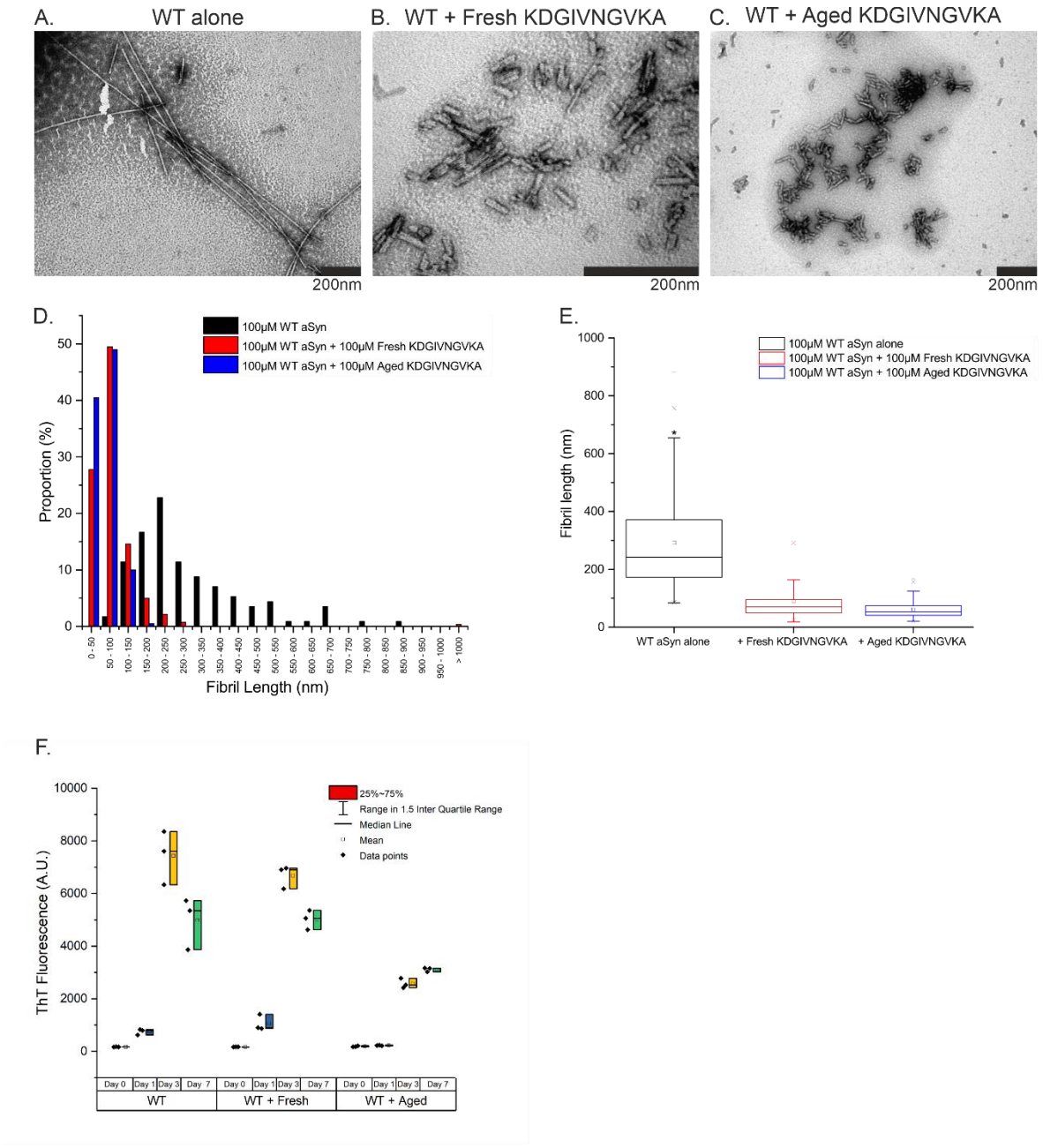

Figure 4-11 – TEM fibril lengths analysis and corresponding ThT endpoint data of WT aSyn incubated with/without fresh or aged KDGIVNGVKA. *100μM WT aSyn alone (A), with 100μM fresh KDGIVNGVKA peptide (B), or with 100μM aged KDGIVNGVKA (C) was incubated at 37°C for 1 week with agitation and analysed by TEM. Lengths analysis of the size of the fibrils formed (D) was performed and revealed that the incubation of WT aSyn with fresh or aged KDGIVNGVKA drastically reduces the average fibril size to <100nm. The fibril lengths data is also shown in box-and-whisker plot format (E). The upper and lower limits of the boxes indicate the 25th and 75th percentiles of the data, whilst the horizontal line and small square indicate the median and mean respectively. The "whiskers" indicate the 5th and 95th percentile range of the data. The number of length measurements taken for each condition were as follows: WT alone (114), plus fresh KDGIVNGVKA (281), and plus aged KDGIVNGVKA (200). Statistical significance was assessed by ANOVA with the Bonferroni post hoc test. * denotes significant differences to the 0.05 level with all other samples, † denotes significantly different to the 0.05 level from the fresh KDGIVNGVKA sample, and ‡ denotes significantly different to the 0.05 level from the aged KDGIVNGVKA sample. Corresponding ThT measurements (F) were performed – in triplicate – on sample aliquots taken at day 0, 1, 3, and 7. Three experimental plates were prepared, but due to saturation only data from one is shown.*

Table 4-1 - Table showing the statistical significance of the differences in the ThT data between WT aSyn alone, with fresh KDGIVNGVKA, or with aged KDGIVNGVKA. *ThT measurements were conducted in triplicate on 100μM WT aSyn alone, or with an equimolar concentration of fresh or aged KDGIVNGVKA peptide. The statistical significance was assessed by ANOVA with the Bonferroni test. Significant differences were those with p-values <0.05.*

	Day 0		Day 1		Day 3		Day 7	
	Significant Difference?	p-Value	Significant Difference?	p-Value	Significant Difference?	p-Value	Significant Difference?	p-Value
WT / WT + Fresh	No	1.0000	No	0.2623	No	0.6241	No	1.0000
WT / WT + Aged	No	0.5918	Yes	0.0407	Yes	0.0003	Yes	0.0283
WT + Fresh / WT + Aged	No	0.4878	Yes	0.0046	Yes	0.0007	Yes	0.0263

4.3.5.2 A30P

A30P aSyn will also form characteristic long amyloid fibrils by itself. These are long, straight and have a propensity to form huge clusters (Figure 4-12 A). In the presence of fresh or aged KDGIVNGVKA some short fibrils were present, but preferably formed less defined and more heterogeneous species (Figure 4-12 B&C). These were largely <150nm (Figure 4-12 D&E) and were more representative of oligomers or protofibrils. The differences between the lengths of the species formed in the two samples containing KDGIVNGVKA and the fibrils formed by A30P alone were found to be statistically significant (Figure 4-12 E). Judging by the ThT endpoint readings for these samples, however, there is little difference in ThT-binding and resultant fluorescence compared to A30P alone and this is reflected in the ANOVA statistical analysis carried out on the data (Figure 4-12 F & Table 4-2). Interestingly, the level of ThT-fluorescence appears to go down over time in all three conditions. This may reflect the emergence of a morphology early-on in the aggregation process common to all three conditions and to which ThT does not bind well. It is quite clear from the TEM data presented here that both fresh and aged KDGIVNGVKA have a potent impact on the

aggregation of A30P aSyn, apparently abrogating the protein's ability to form amyloid fibrils, and that this is not obvious when inspecting ThT-fluorescence data alone.

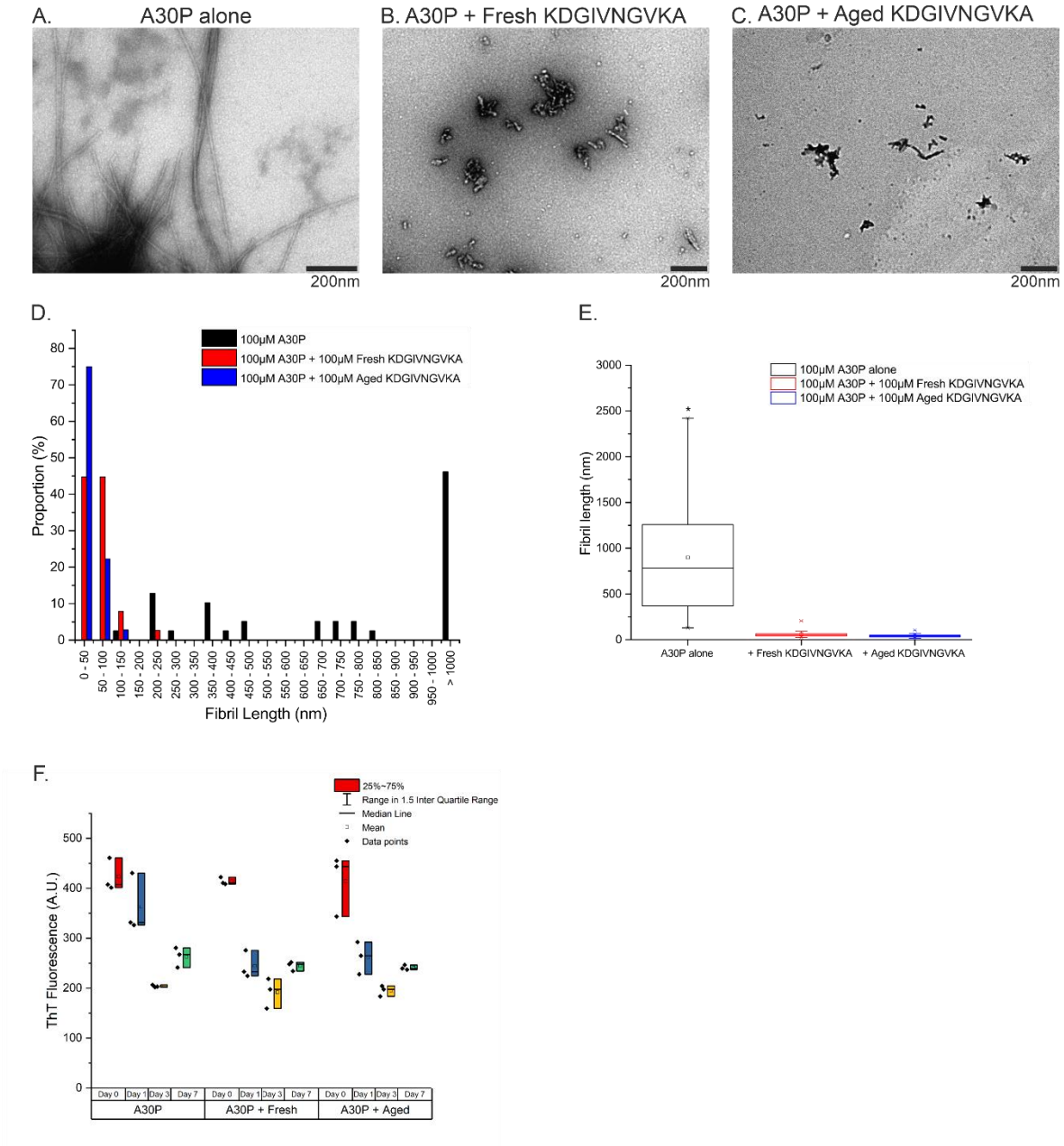

Figure 4-12 – TEM fibril lengths analysis and corresponding ThT endpoint data of A30P aSyn incubated with/without fresh or aged KDGIVNGVKA. *100μM A30P aSyn alone (A), with 100μM fresh KDGIVNGVKA peptide (B), or with 100μM aged KDGIVNGVKA (C) was incubated at 37°C for 1 week with agitation and analysed by TEM. Lengths analysis of the size of the fibrils formed (D) and summarized as box-and-whisker plots (E). The upper and lower limits of the boxes indicate the 25th and 75th percentiles of the data, whilst the horizontal line and small square indicate the median and mean respectively. The "whiskers" indicate the 5th and 95th percentile range of the data. The number of length measurements taken for each condition were as follows: A30P alone (39), plus fresh KDGIVNGVKA (38), and plus aged KDGIVNGVKA (36). Statistical significance was assessed by ANOVA with the Bonferroni post hoc test. * denotes significant differences to the 0.05 level with all other samples, † denotes significantly different to the 0.05 level from the fresh KDGIVNGVKA sample, and ‡ denotes significantly different to the 0.05 level from the aged KDGIVNGVKA sample. Corresponding ThT measurements (F) were performed – in triplicate – on sample aliquots taken at day 0, 1, 3, and 7. Three experimental plates were prepared, but due to saturation only data from one is shown.*

Table 4-2 - Table showing the statistical significance of the differences in the ThT data between A30P aSyn alone, with fresh KDGIVNGVKA, or with aged KDGIVNGVKA. *ThT measurements were conducted in triplicate on 100μM A30P aSyn alone, or with an equimolar concentration of either fresh or aged KDGIVNGVKA peptide. The statistical significance was assessed by ANOVA with the Bonferroni test. Significant differences were those with p-values <0.05.*

	Day 0		Day 1		Day 3		Day 7	
	Significant Difference?	p-Value	Significant Difference?	p-Value	Significant Difference?	p-Value	Significant Difference?	p-Value
A30P / A30P + Fresh	No	1.0000	Yes	0.0399	No	1.0000	No	0.4072
A30P / A30P + Aged	No	1.0000	No	0.0753	No	1.0000	No	0.2542
A30P + Fresh / A30P + Aged	No	1.0000	No	1.0000	No	1.0000	No	1.0000

4.3.5.3 E46K

E46K alone forms amyloid fibrils that are shorter than those formed by WT, and they also seem to have a weaker propensity to form the huge networks seen for WT and some of the other mutant aSyn forms (Figure 4-13 A). In the presence of the fresh KDGIVNGVKA the ability of E46K to form fibrils appears undiminished (Figure 4-13 B), however in the presence of the aged peptide it does seem that the fibrils are fewer and shorter in length when observed by TEM (Figure 4-13 C). The mean fibril length in the sample containing aged KDGIVNGVKA is approximately 100nm, whilst both E46K alone and in the presence of fresh KDGIVNGVKA form fibrils with a mean length of 300nm (Figure 4-13 E). These differences were statistically significant, as assessed by ANOVA with the Bonferroni *post hoc* test. This is especially interesting given that at day 1 and day 3 the ThT-fluorescence for the samples with aged KDGIVNGVKA is vastly greater than that for the samples of E46K alone or with the fresh peptide (Figure 4-13 F). This is reflected in the ANOVA statistical analysis shown in Table 4-3. By day 7 the statistically significant differences are no longer present. This suggests that E46K in the presence of the aged KDGIVNGVKA peptide aggregates via a different aggregation pathway to E46K alone or E46K plus fresh KDGIVNGKVA. This alternative aggregation

pathway initially results in the formation of highly ThT-reactive species but has shorter amyloid fibrils with lower ThT reactivity, more in line with the other sample conditions, as its endpoint.

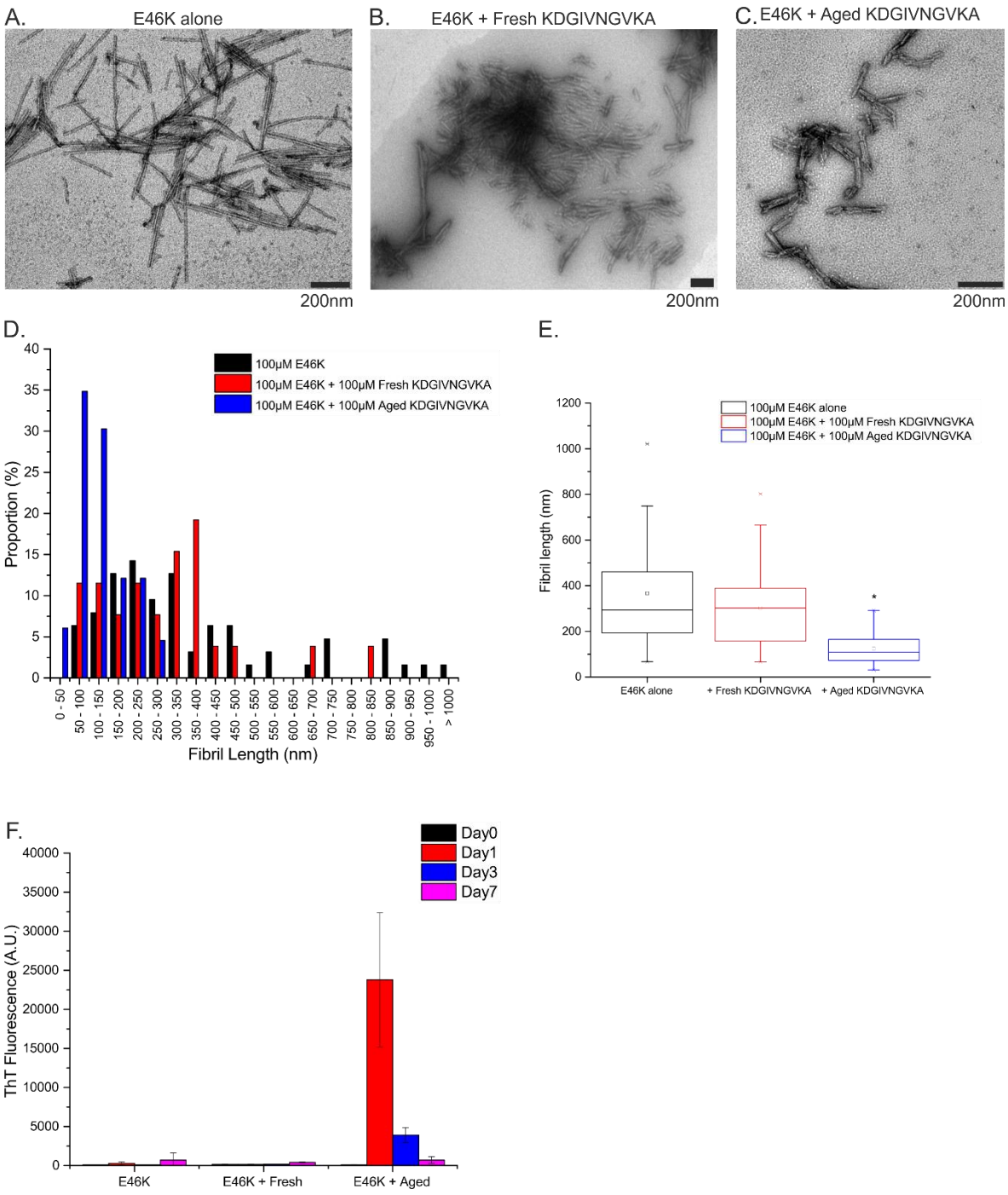

Figure 4-13 – TEM fibril lengths analysis and corresponding ThT endpoint data of E46K aSyn incubated with/without fresh or aged KDGIVNGVKA. *100µM E46K aSyn alone (A), with 100µM fresh KDGIVNGVKA peptide (B), or with 100µM aged KDGIVNGVKA (C) was incubated at 37°C for 1 week with agitation and analysed by TEM. Lengths analysis of the size of the fibrils formed (D) was performed and is also shown in box-and-whisker format (E). The upper and lower limits of the boxes indicate the 25th and 75th percentiles of the data, whilst the horizontal line and small square indicate the median and mean respectively. The "whiskers" indicate the 5th and 95th percentile range of the data. The number of length measurements taken for each condition were as follows: E46K alone (63), plus fresh KDGIVNGVKA (26), and plus aged KDGIVNGVKA (66). Statistical significance was assessed by ANOVA with the Bonferroni post hoc test. * denotes significant differences to the 0.05 level with all other samples, † denotes significantly different to the 0.05 level from the fresh KDGIVNGVKA sample, and ‡ denotes significantly different to the 0.05 level from the aged KDGIVNGVKA sample. Corresponding ThT measurements (F) were performed – in triplicate – on sample aliquots taken at day 0, 1, 3, and 7. Three experimental plates were prepared, but due to saturation only data from one is shown.*

Table 4-3 - Table showing the statistical significance of the differences in the ThT data between E46K aSyn alone, with fresh KDGIVNGVKA, or with aged KDGIVNGVKA. *ThT measurements were conducted in triplicate on 100μM E46K aSyn alone, or with an equimolar concentration of either fresh or aged KDGIVNGVKA peptide. Statistical significance was assessed by ANOVA with the Bonferroni test. Significant differences were those with a p-value of <0.05.*

	Day 0		Day 1		Day 3		Day 7	
	Significant Difference?	p-Value	Significant Difference?	p-Value	Significant Difference?	p-Value	Significant Difference?	p-Value
E46K / E46K + Fresh	No	1.0000	No	1.0000	No	1.0000	No	1.0000
E46K / E46K + Aged	No	1.0000	Yes	0.0034	Yes	0.0004	No	1.0000
E46K + Fresh / E46K + Aged	No	1.0000	Yes	0.0033	Yes	0.0005	No	1.0000

4.3.5.4 H50Q

H50Q alone forms relatively long fibrils (>150nm) (Figure 4-14 A&D), whilst in the presence of the fresh peptide it forms dense networks of very short fibrils (Figure 4-14 B). In the presence of aged KDGIVNGKVA fibrils are also seen and are of a similar length to those formed in the presence of fresh KDGIVNGVKA (Figure 4-14 C-E), but they appear more sparsely distributed and more heterogeneous. The ThT endpoint measurements (Figure 4-14 F) show that under all three conditions ThT fluorescence increases over time, and indicating an increase in cross-β character to which ThT will bind. Despite the differences in the samples as observed by TEM there are no statistically significant differences in the ThT data when compared by ANOVA, with the exception of the two samples containing KDGIVNGVKA at day 1 (Table 4-4). This may suggest that H50Q plus fresh KDGIVNGVKA initially embarks on a slightly different aggregation pathway to the other conditions, or that it reduces the initial rate of aggregation.

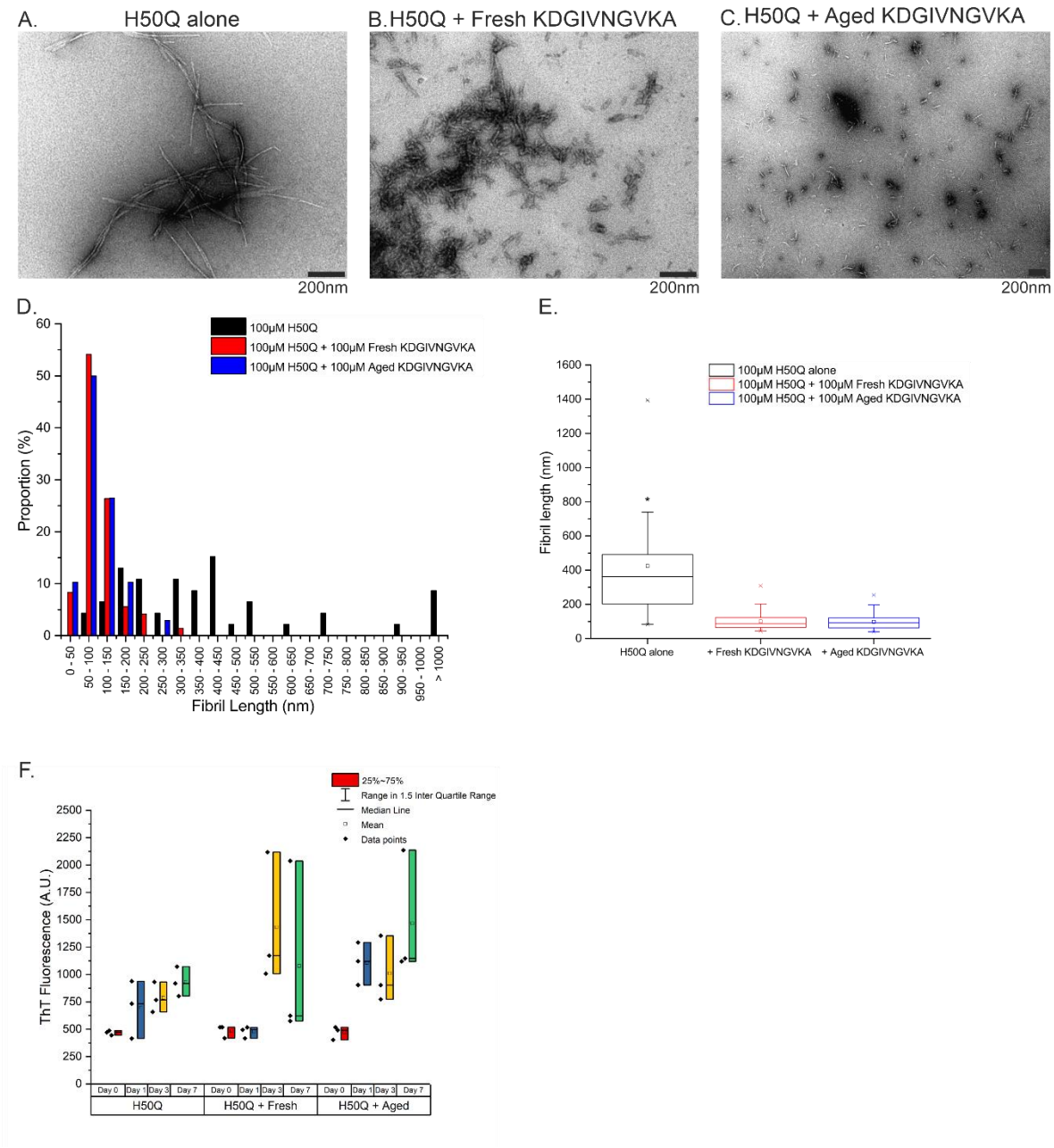

Figure 4-14 – TEM fibril lengths analysis and corresponding ThT endpoint data of H50Q aSyn incubated with/without fresh or aged KDGIVNGVKA. *100μM H50Q aSyn alone (A), with 100μM fresh KDGIVNGVKA peptide (B), or with 100μM aged KDGIVNGVKA (C) was incubated at 37°C for 1 week with agitation and analysed by TEM. Lengths analysis of the size of the fibrils formed was carried out (D). Both fresh and aged KDGIVNGVKA appear to result in shorter fibrils. The fibril lengths data is also shown in box-and-whisker plot format (E). The upper and lower limits of the boxes indicate the 25th and 75th percentiles of the data, whilst the horizontal line and small square indicate the median and mean respectively. The "whiskers" indicate the 5th and 95th percentile range of the data. The number of length measurements taken for each condition were as follows: H50Q alone (46), plus fresh KDGIVNGVKA (72), and plus aged KDGIVNGVKA (68). Statistical significance was assessed by ANOVA with the Bonferroni post hoc test. * denotes significant differences to the 0.05 level with all other samples, † denotes significantly different to the 0.05 level from the fresh KDGIVNGVKA sample, and ‡ denotes significantly different to the 0.05 level from the aged KDGIVNGVKA sample. Corresponding ThT measurements (F) were performed – in triplicate – on sample aliquots taken at day 0, 1, 3, and 7. Three experimental plates were prepared, but due to saturation only data from one is shown.*

Table 4-4 - Table showing the statistical significance of the differences in the ThT data between H50Q aSyn alone, with fresh KDGIVNGVKA, or with aged KDGIVNGVKA. *ThT measurements were conducted in triplicate on 100μM H50Q aSyn alone, or with an equimolar concentration of either fresh or aged KDGIVNGKVA peptide. Statistical significance was assessed by ANOVA with the Bonferroni test. Significant differences were those with a p-value of <0.05.*

	Day 0		Day 1		Day 3		Day 7	
	Significant Difference?	p-Value	Significant Difference?	p-Value	Significant Difference?	p-Value	Significant Difference?	p-Value
H50Q / H50Q + Fresh	No	1.0000	No	0.6279	No	0.2775	No	1.0000
H50Q / H50Q + Aged	No	1.0000	No	0.1180	No	1.0000	No	0.9246
H50Q + Fresh / H50Q + Aged	No	1.0000	Yes	0.0206	No	0.7185	No	1.0000

4.3.5.5 G51D

G51D is reported in the literature as persisting in the oligomeric state for longer than WT aSyn and as being more toxic (125). This was in evidence on the TEM grids of G51D alone (Figure 4-15 A) where only very few isolated patches of fibrils were seen. In the presence of the KDGIVNGVKA peptide – fresh or aged – fibrils were more prevalent (Figure 4-15 B&C). Similarly, approximately 50% of the fibrils in the sample of G51D alone were <100nm, whilst in the presence of the peptide there was generally a broader range in terms of fibril length seen (Figure 4-15 D&E). This suggests that the peptide pushes the G51D protein down a different aggregation pathway that favours the formation of amyloid fibrils. Therapeutically this may be beneficial rather than a bad thing as fibrils represent a more benign endpoint. All samples see an increase in ThT-fluorescence over time, indicating the formation of species with cross-β architecture (Figure 4-15 F). However, ANOVA reveals no statistically significant difference between the conditions (Table 4-5). The fact that there were comparatively few fibrils in the TEM sample of G51D alone, yet the ThT data is similar to the samples incubated in the presence of the peptide which formed many fibrils, could indicate that: the species formed by G51D alone have a different morphology that means they are

more ThT-reactive “pound-for-pound” than the species formed in the presence of the peptide, despite appearing fewer in number on the TEM grid; or that the fibrils formed by G51D alone did not adhere well to the TEM grid, and thus are underrepresented under the microscope.

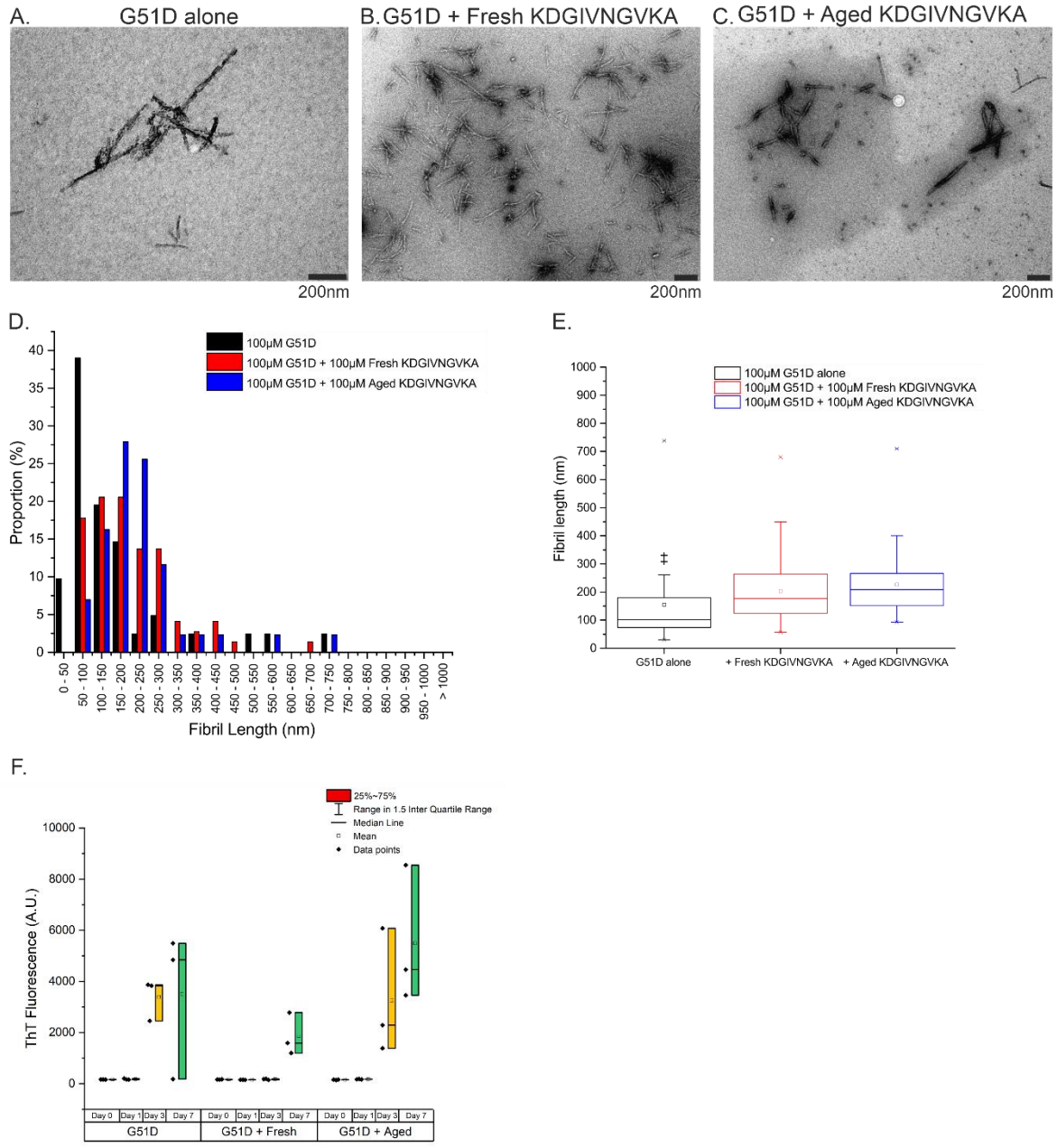

Figure 4-15 – TEM fibril lengths analysis and corresponding ThT endpoint data of G51D aSyn incubated with/without fresh or aged KDGIVNGVKA. *100µM G51D aSyn alone (A), with 100µM fresh KDGIVNGVKA peptide (B), or with 100µM aged KDGIVNGVKA (C) was incubated at 37°C for 1 week with agitation and analysed by TEM. Lengths analysis of the size of the fibrils formed (D) was carried out and suggests that the incubation of G51D with KDGIVNGVKA may result in the formation of longer fibrils than typically formed by G51D alone. The fibril lengths data is also shown in box-and-whisker plot format (E). The upper and lower limits of the boxes indicate the 25th and 75th percentiles of the data, whilst the horizontal line and small square indicate the median and mean respectively. The "whiskers" indicate the 5th and 95th percentile range of the data. The number of length measurements taken for each condition were as follows: G51D alone (41), plus fresh KDGIVNGVKA (73), and plus aged KDGIVNGVKA (43). Statistical significance was assessed by ANOVA with the Bonferroni post hoc test. * denotes significant differences to the 0.05 level with all other samples, † denotes significantly different to the 0.05 level from the fresh KDGIVNGVKA sample, and ‡ denotes significantly different to the 0.05 level from the aged KDGIVNGVKA sample. Corresponding ThT measurements (F) were performed – in triplicate – on sample aliquots taken at day 0, 1, 3, and 7. Three experimental plates were prepared, but due to saturation only data from one is shown.*

Table 4-5- Table showing the statistical significance of the differences in the ThT data between G51D aSyn alone, with fresh KDGIVNGVKA, or with aged KDGIVNGVKA. *ThT measurements were conducted in triplicate with 100μM G51D aSyn alone, or with an equimolar concentration of either fresh or aged KDGIVNGKVA. Statistical significance was assessed by ANOVA with the Bonferroni test. Significant differences were those with p-values <0.05.*

	Day 0		Day 1		Day 3		Day 7	
	Significant Difference?	p-Value	Significant Difference?	p-Value	Significant Difference?	p-Value	Significant Difference?	p-Value
G51D / G51D + Fresh	No	1.0000	No	0.3445	No	0.1214	No	1.0000
G51D / G51D + Aged	No	0.3602	No	1.0000	No	1.0000	No	1.0000
G51D + Fresh / G51D + Aged	No	0.3328	No	0.3421	No	0.1404	No	0.3153

4.3.5.6 A53T

A53T aSyn is reported to aggregate more rapidly than the WT protein and alone it readily forms numerous long, straight fibrils (Figure 4-16 A) (126). These morphologically look very similar to those formed by the WT protein alone (Figure 4-11 A). In the presence of equimolar fresh or aged KDGIVNGVKA peptide the fibrils are drastically reduced in length (Figure 4-16 B&C). A lengths analysis of the fibrils on the grid (Figure 4-16 D&E) shows that species present in the samples incubated with peptide generally range from 50-250nm in length, whilst for A53T alone there is a much broader distribution with over 10% >1μm. These differences in length are statistically significant, as determined by ANOVA. The samples incubated with fresh KDGIVNGVKA also seem to be more prone to twisting. The ThT fluorescence (Figure 4-16 F) increases over time, as the protein begins to aggregate. The statistical significance of these measurements has been assessed by ANOVA (Table 4-6). After 7 days there were no significant differences between the samples despite the clear differences observable by TEM. Given the largely similar appearance of the fibrils in the three conditions it seems likely that the 'end product' – the fibrils – are similarly able to bind ThT, whether long or short. It also suggests that there is a similar overall amount of fibril formed in the

three samples. The statistically significant differences between A53T alone and the samples with KDGIVNGVKA at day 1 may be an indication that the A53T alone aggregates faster, and that KDGIVNGVKA slows it down. After this time point, the other two samples have caught up.

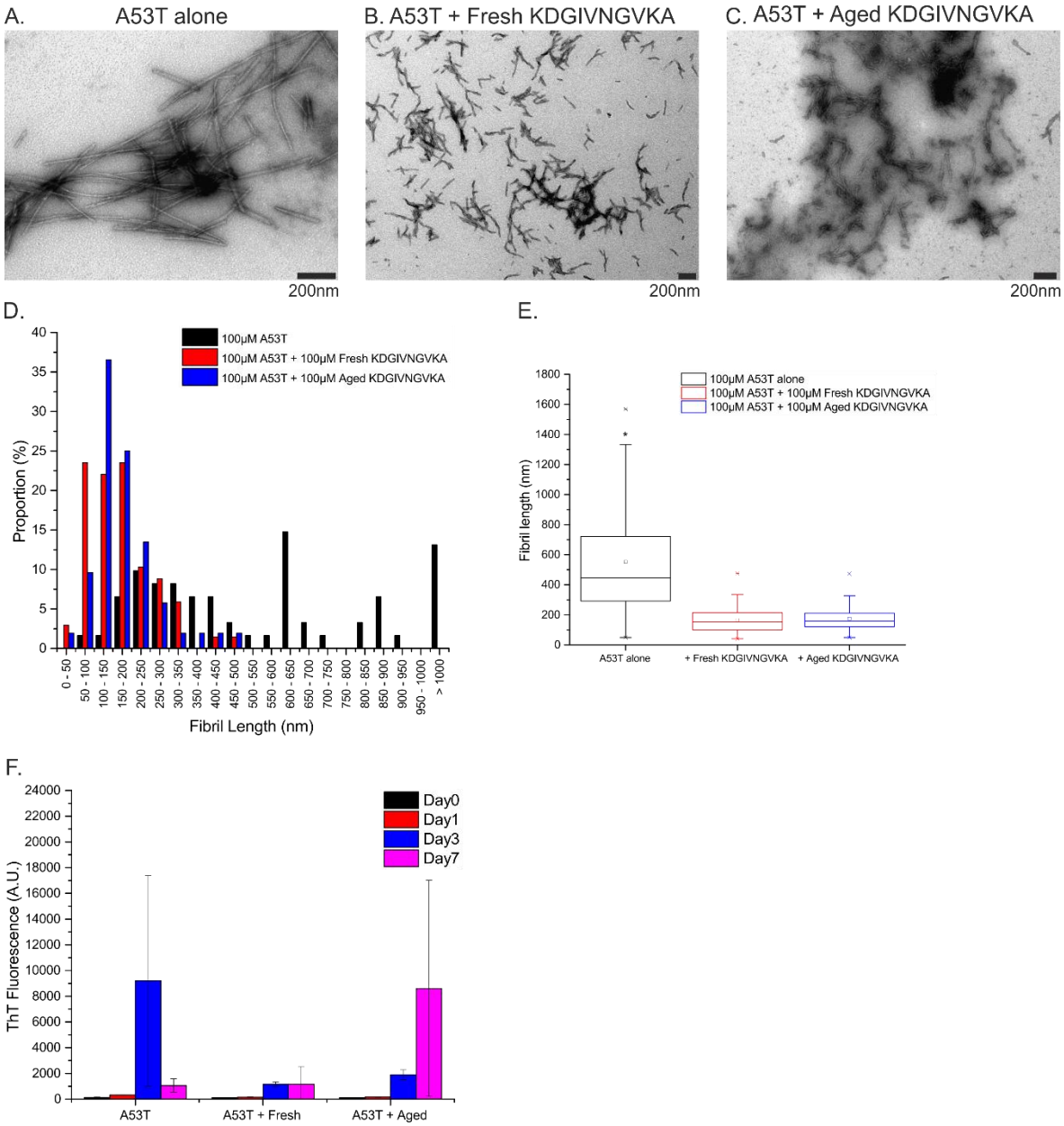

Figure 4-16 – TEM fibril lengths analysis and corresponding ThT endpoint data of A53T aSyn incubated with/without fresh or aged KDGIVNGVKA. *100µM A53T aSyn alone (A), with 100µM fresh KDGIVNGVKA peptide (B), or with 100µM aged KDGIVNGVKA (C) was incubated at 37°C for 1 week with agitation and analysed by TEM. Lengths analysis of the size of the fibrils formed (D) was performed and revealed that the incubation of A53T aSyn with fresh or aged KDGIVNGVKA reduces the size of most fibrils to below 200nm. The fibril lengths data is also shown in box-and-whisker plot format (E). The upper and lower limits of the boxes indicate the 25th and 75th percentiles of the data, whilst the horizontal line and small square indicate the median and mean respectively. The "whiskers" indicate the 5th and 95th percentile range of the data. The number of length measurements taken for each condition were as follows: A53T alone (62), plus fresh KDGIVNGVKA (68), and plus aged KDGIVNGVKA (52). Statistical significance was assessed by ANOVA with the Bonferroni post hoc test. * denotes significant differences to the 0.05 level with all other samples, † denotes significantly different to the 0.05 level from the fresh KDGIVNGVKA sample, and ‡ denotes significantly different to the 0.05 level from the aged KDGIVNGVKA sample. Corresponding ThT measurements (F) were performed – in triplicate – on sample aliquots taken at day 0, 1, 3, and 7. Three experimental plates were prepared, but due to saturation only data from one is shown.*

Table 4-6 - Table showing the statistical significance of the differences in the ThT data between A53T alone, with fresh KDGIVNGVKA, or with aged KDGIVNGVKA. *ThT measurements were conducted in triplicate with 100μM A53T aSyn, or with an equimolar concentration of fresh or aged KDGIVNGVKA peptide. Statistical significance was assessed by ANOVA with the Bonferroni test. Significant differences were those with p-values <0.05.*

	Day 0		Day 1		Day 3		Day 7	
	Significant Difference?	p-Value	Significant Difference?	p-Value	Significant Difference?	p-Value	Significant Difference?	p-Value
A53T / A53T + Fresh	No	0.6368	Yes	0.0002	No	0.2475	No	1.0000
A53T / A53T + Aged	No	0.6660	Yes	0.0002	No	0.3226	No	0.3278
A53T + Fresh / A53T + Aged	No	1.0000	No	1.0000	No	1.0000	No	0.3406

4.3.5.7 A53E

A53E is the most recently identified PD-linked point mutation in aSyn (77). It is thus the least characterized and little is known about its rate of aggregation and the fibrils that it forms. As can be seen by TEM, A53E by itself forms fibrils that are generally quite short and rarely exceed 300nm (Figure 4-17 A&D). This stands in contrast to many of the long fibrils formed by WT and the other aSyn mutants. The general fibril-forming propensity of the protein appears reduced in the presence of fresh KDGIVNGKVA as fewer fibrils were seen on the grids. Incubation with the fresh peptide also encouraged the formation of shorter amyloid fibrils, with over 50% observed being 50-100nm (Figure 4-17 B&D). The impact of aged KDGIVNGVKA on the length or number of fibrils was not quite so profound, and appeared quite similar to those formed by A53E alone (Figure 4-17 C). The ThT fluorescence of the samples increases over time, in line with the formation of β-rich species and fibrils (Figure 4-17 F). The statistical significance of the changes in ThT fluorescence was assessed by ANOVA, and significant differences were only measured at day 3 between the samples of A53E and the aged peptide compared to the samples of A53E alone or with the fresh peptide (Table 4-7). This may indicate that by the third day of incubation with the aged peptide that A53E

has proceeded down an aggregation pathway that is measurably different by ThT-assay and results in the differences seen by TEM – although by day 7 the differences in the ThT are no longer statistically significant. This would suggest that some oligomer or prefibrillar species in this alternative aggregation pathway binds to ThT more strongly than species formed in the other sample conditions and contains cross-β architecture.

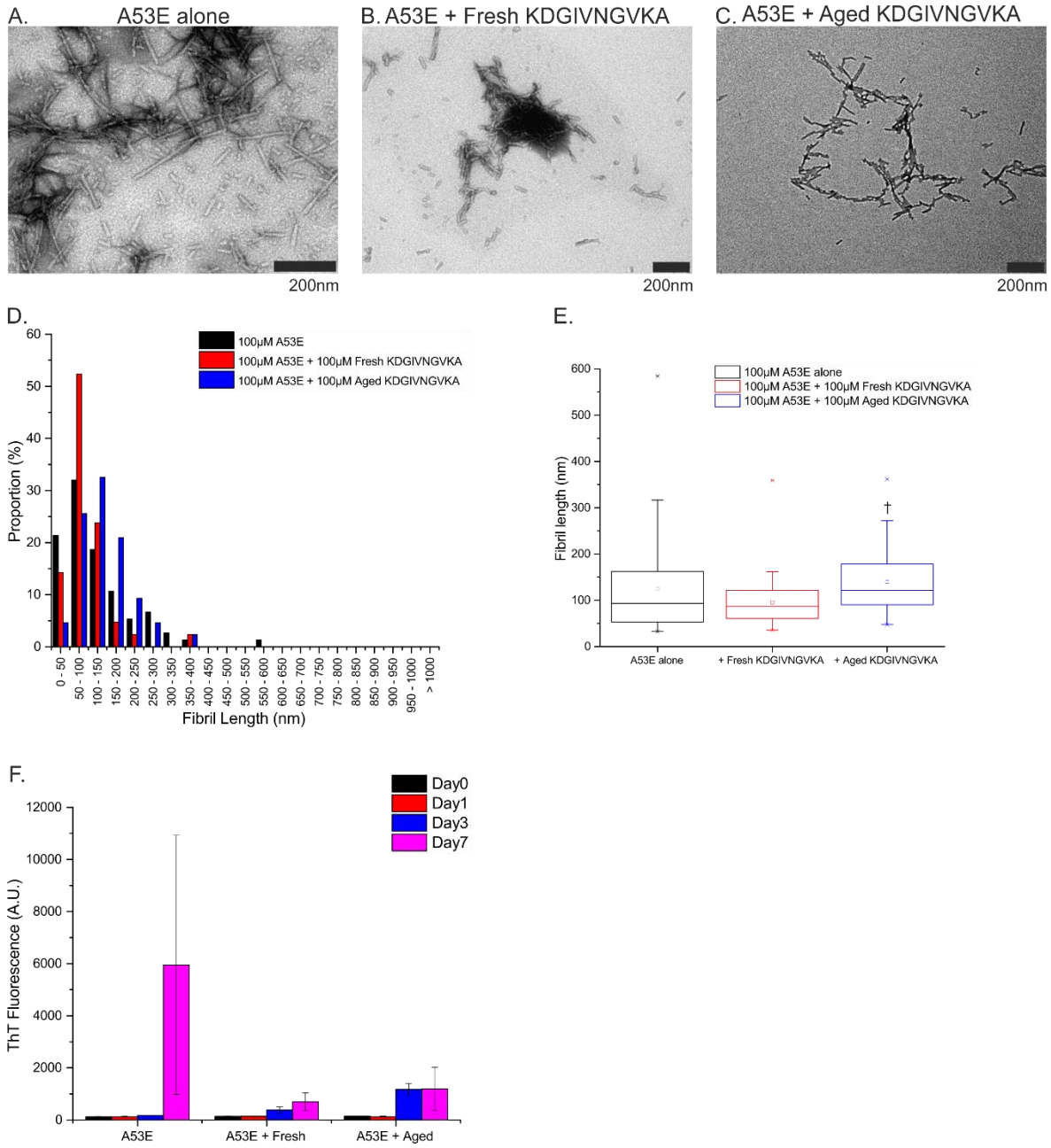

Figure 4-17 – TEM fibril lengths analysis and corresponding ThT endpoint data of A53E aSyn incubated with/without fresh or aged KDGIVNGVKA. *100µM A53E aSyn alone (A), with 100µM fresh KDGIVNGVKA peptide (B), or with 100µM aged KDGIVNGVKA (C) was incubated at 37°C for 1 week with agitation and analysed by TEM. Lengths analysis of the size of the fibrils formed (D) was performed. A53E alone forms lots of fibrils generally shorter than 300nm. The incubation of A53E with the aged peptide does not substantially change the distribution of lengths compared to the protein alone, but fresh KDGIVNGVKA does heighten the proportion of fibrils that are 50-100nm in length. The fibril lengths data is also shown in box-and-whisker plot format (E). The upper and lower limits of the boxes indicate the 25th and 75th percentiles of the data, whilst the horizontal line and small square indicate the median and mean respectively. The "whiskers" indicate the 5th and 95th percentile range of the data. The number of length measurements taken for each condition were as follows: A53E alone (75), plus fresh KDGIVNGVKA (42), and plus aged KDGIVNGVKA (43). Statistical significance was assessed by ANOVA with the Bonferroni post hoc test. * denotes significant differences to the 0.05 level with all other samples, † denotes significantly different to the 0.05 level from the fresh KDGIVNGVKA sample, and ‡ denotes significantly different to the 0.05 level from the aged KDGIVNGVKA sample. Corresponding ThT measurements (F) were performed – in triplicate – on sample aliquots taken at day 0, 1, 3, and 7. Three experimental plates were prepared, but due to saturation only data from one is shown.*

Table 4-7 - Table showing the statistical significance of the differences in the ThT data between A53E aSyn alone, with fresh KDGIVNGVKA, or with aged KDGIVNGVKA. *ThT measurements were conducted in triplicate with 100μM A53E aSyn, or with an equimolar concentration of fresh or aged KDGIVNGVKA peptide. Statistical significance was assessed by ANOVA with the Bonferroni test. Significant differences were those with p-values <0.05.*

	Day 0		Day 1		Day 3		Day 7	
	Significant Difference?	p-Value	Significant Difference?	p-Value	Significant Difference?	p-Value	Significant Difference?	p-Value
A53E / A53E + Fresh	No	0.9903	No	0.6639	No	0.4075	No	0.2087
A53E / A53E + Aged	No	0.2688	No	1.0000	Yes	0.0006	No	0.2788
A53E + Fresh / A53E + Aged	No	1.0000	No	0.7050	Yes	0.0022	No	1.0000

4.3.5.8 Summary of the effect of KDGIVNGVKA on α-synuclein fibril structure and aggregation propensity

The results of the TEM and ThT experiments on WT aSyn and the PD-linked point mutations are summarized (Table 4-8). KDGIVNGVKA generally has an effect on all of the proteins in one shape or form, and these effects are fairly consistent regardless of whether the peptide is fresh or aged – with some exceptions. In most cases KDGIVNGVKA results in the formation of shortened amyloid fibrils with a similar morphology to those formed by the protein itself, but there are exceptions. The mean length of G51D and A53E fibrils did not change/increased in the presence of the peptide (Figure 4-15 E and Figure 4-17 E) compared to protein alone whilst A30P in the presence of the peptide formed species more reminiscent of oligomers than fibrils (Figure 4-12 B-C). Comparisons of the ThT data are a little challenging due to error. Errors for data at the initial timepoints are low – indicating little in terms of systematic error – but at day 3/7 the errors for most samples are quite large. This is likely due to the aggregates physically impeding the passage of light in the samples; this is unavoidable. However ThT remains useful because samples that look similar by TEM can give quite different ThT measurements. This means that ThT can be used to provide indications

regarding the morphology or the quantity of fibrils. Ultimately, TEM and ThT must be used together to overcome the pitfalls of each and provide a holistic view of protein aggregation. The bearing the presence of fresh or aged KDGIVNGVKA has on the cell toxicity of aSyn has not been investigated here due to time constraints. However, this would be the next logical aspect to investigate.

Table 4-8 - Table summarizing the results of the TEM and ThT experiments for WT and PD-linked aSyn mutants. *Green = affirmative, red = negative.*

	+ Fresh KDGIVNGVKA			+ Aged KDGIVNGVKA		
	Shortens fibrils?	Changes fibril morphology?	ThT fluorescence at Day 7 compared to protein alone?	Shortens fibrils?	Changes fibril morphology?	ThT fluorescence at Day 7 compared to protein alone?
WT			—			↓
A30P			—			—
E46K			↓			—
H50Q			—			↑
G51D			↓			↑
A53T			—			↑
A53E			↓			↓

4.3.6 1D NMR & WaterLOGSY analysis of binding of KDGIVAGVKA and KAGIVNGVKA to α-synuclein

Alanine variants of the KDGIVNGVKA peptide, KDGIVAGVKA and KAGIVNGVKA, were used in repeats of the 1D and WaterLOGSY binding analysis experiments conducted in 4.3.3. These experiments were conducted in an effort to elucidate the role (if any) the Asp and Asn residues in KDGIVNGVKA have on binding to aSyn. This is particularly pertinent given the known modifications occurring at these sites in KDGIVNGVKA, as demonstrated in Figure 4-7 and Figure 4-8.

The 1D NMR experiments revealed a reduction in the intensity of the KAGIVNGVKA peaks in the samples of peptide plus aSyn in comparison to those controls of peptide alone (Figure 4-18 A-C). The difference in the intensity of these peaks increased over the course of the seven days of the

experiment. This was not observed in the case of the KDGIVAGVKA peptide, suggesting an inability of this peptide to bind to aSyn (Figure 4-19 A-C). These findings were also seen in the WaterLOGSY experiments on the two peptides (Figure 4-18 D-F & Figure 4-19 D-F).

This data supports the hypothesis in the case of the KDGIVNGVKA and KAGIVNGVKA peptides and that the peptide binds to aggregated forms of aSyn that form over the course of time. It also suggests that the Asn residue is of importance in the context of binding. In KDGIVAGVKA peptide lacking Asn, no decrease in the intensity of the peptide peaks was visible in the sample of peptide plus protein compared to the sample of peptide alone. A drop in the intensity of the peptide signals in samples of peptide plus protein compared to samples of peptide alone suggest that the peptide is interacting with large NMR-invisible species. The differences in the 1D with the KAGIVNGVKA are larger than those seen for the original KDGIVNGVKA peptide, which may suggest that it may be a better binder, although this is not seen in the WaterLOGSY data (Figure 4-18). It should be noted, however, that better binding does not necessarily equate to it being a better inhibitor of aSyn aggregation.

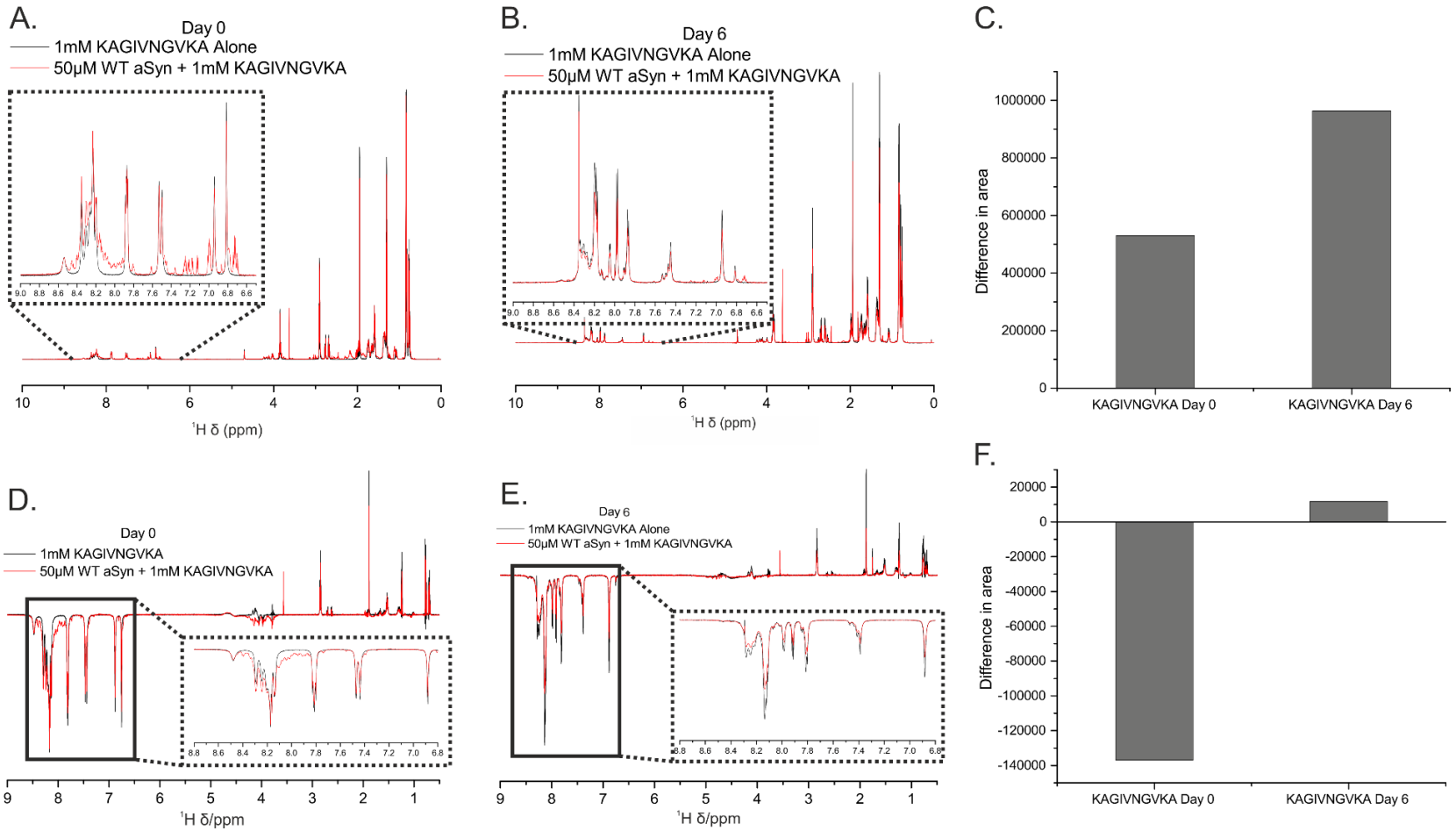

Figure 4-18 – 1D and WaterLOGSY spectra of KAGIVNGVKA peptide with and without WT aSyn at day 0 and day 6, and plots of differences in area under the peaks between spectra of KAGIVNGVKA alone and KAGIVNGVKA with WT aSyn. *1D spectra at day 0 (A) and day 6 (B) of 1mM KAGIVNGVKA alone (black) and with 50μM WT aSyn (red).The differences in the calculated area under the peaks of the spectra of peptide alone and in the presence of WT aSyn (C) are increased at day 6 than at day 0. WaterLOGSY spectra at day 0 (D) and day 6 (E) of these same samples are shown. The differences in area under the peak of these spectra are shown (F). These differences are also much increased at day 6 compared to day 0. These increases suggest a reduction in the peptide signals in those samples that contain WT aSyn compared to those of the peptide alone. The reduction in the peptide signal intensity is evidence in favour of a direct interaction between KAGIVNGVKA and large aSyn species (e.g. oligomers) that are "NMR-invisible".*

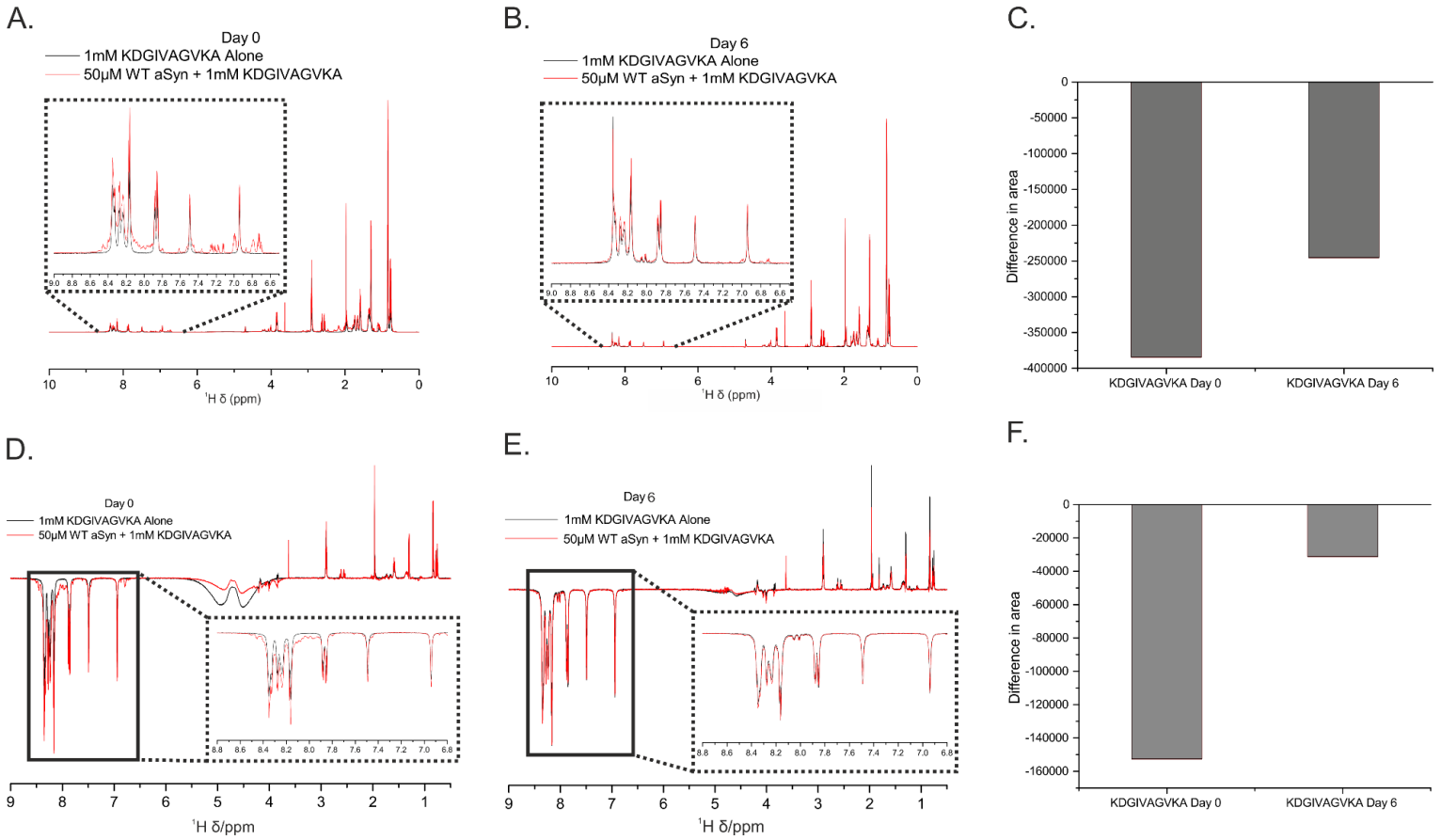

Figure 4-19 - 1D and WaterLOGSY spectra of KDGIVAGVKA peptide with and without WT aSyn at day 0 and day 6, and plots of differences in area under the peaks between spectra of KDGIVAGVKA alone and KDGIVAGVKA plus WT aSyn. *1D spectra at day 0 (A) and day 6 (B) of 1mM KDGIVAGVKA alone (black) and with 50μM WT aSyn (red).The differences in the calculated area under the peaks of the spectra of peptide alone and in the presence of WT aSyn (C) are reduced at day 6 than at day 0. WaterLOGSY spectra at day 0 (D) and day 6 (E) of these same samples are shown. The differences in area under the peak of these spectra are shown (F). These differences are also reduced at day 6 compared to day 0. The fact that the peptide signals in the sample of KDGIVAGVKA alone are not lower than those in the sample of KDGIVAGVKA plus WT aSyn would suggest that there is no binding to WT aSyn.*

4.3.7 ThT and TEM analysis of α-synuclein incubated with KDGIVAGVKA or KAGIVNGVKA

This is a repeat of the work carried out in 4.3.5.1 using the alanine variants of the peptide instead, KDGIVAGVKA and KAGIVNGVKA (Figure 4-20). It is clear from the TEM grids that neither fresh KDGIVAGVKA nor fresh KAGIVNGVKA do not abrogate the ability of aSyn to form amyloid fibrils (Figure 4-20 A&B). This is supported in the ThT data (Figure 4-20 C); both fresh peptide samples have the highest ThT-fluorescence at day 7, indicating the formation of amyloid fibrils (as seen in the TEM). However, it should be noted that the fluorescence of the samples incubated with the aged forms of these peptides have a comparable fluorescence to that of WT aSyn alone. There were also some fibrils visible by TEM, but not as prevalent as on the grids of WT aSyn alone. This may indicate either fewer fibrils, or that the fibrils have a lower affinity for ThT, or a combination of both of these factors. The fibrils formed in the presence of the aged KDGIVAGVKA also appear quite short in comparison to the fibrils formed by WT aSyn alone. Given the lack of Asn in this peptide and that the aged peptide has a different effect to the fresh form, it may be an indication that the formation of iso-Asp in this peptide is having more of an impact on fibril formation.

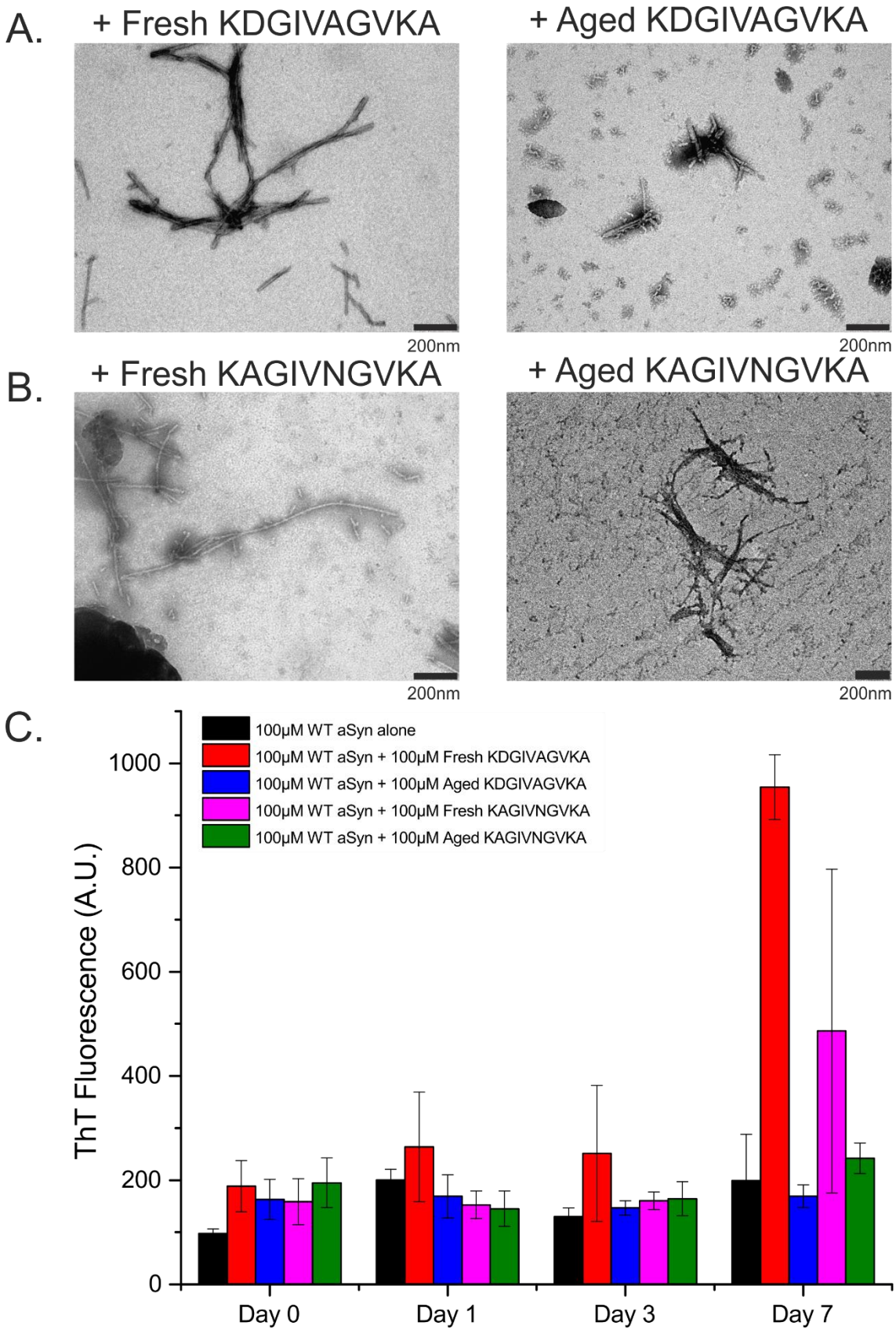

Figure 4-20 - TEM images and ThT endpoint reads of fresh and aged KDGIVAGVKA and KAGIVNGVKA with WT aSyn. *TEM images of 100μM WT aSyn with 100μM fresh or aged KDGIVAGVKA (A) and 100μM fresh or aged KAGIVNGVKA (B) were incubated at 37°C for 1week. Aliquots taken at different timepoints were used for ThT endpoint reads (C). All measurements were carried out in triplicate on the plate. n=1.*

4.3.8 WaterLOGSY NMR analysis of binding of alanine-scanning peptide variants to α-synuclein

Given the seeming abolition of binding to aSyn with the KDGIVAGVKA peptide, but not the KAGIVNGVKA peptide, further alanine-scanning variants of the peptide were prepared in an effort to identify those residues most essential for binding. These peptides were KDGAVNGVKA (A4), KDGIANGVKA (A5), KDGIVNAVKA (A7), and KDGIVNGAKA (A8). WaterLOGSY experiments identical to those conducted for the previous peptides were performed on these peptides. The results are not directly comparable due to an NMR system upgrade, however it is clear from the results of these experiments that the A7 and A8 peptides exhibit the same behaviour as seen for both KDGIVNGVKA and KAGIVNGVKA, in that the difference in peak intensity between the samples of peptide alone and peptide plus protein increases over time (Figure 4-21). This is indicative of their binding to aSyn aggregates. However, this was not seen for the A4 or A5 peptides. In conjunction with the data from the KDGIVAGVKA peptide this would suggest that the residues 4-6 (KDGIVNGVKA) are essential for binding to aSyn.

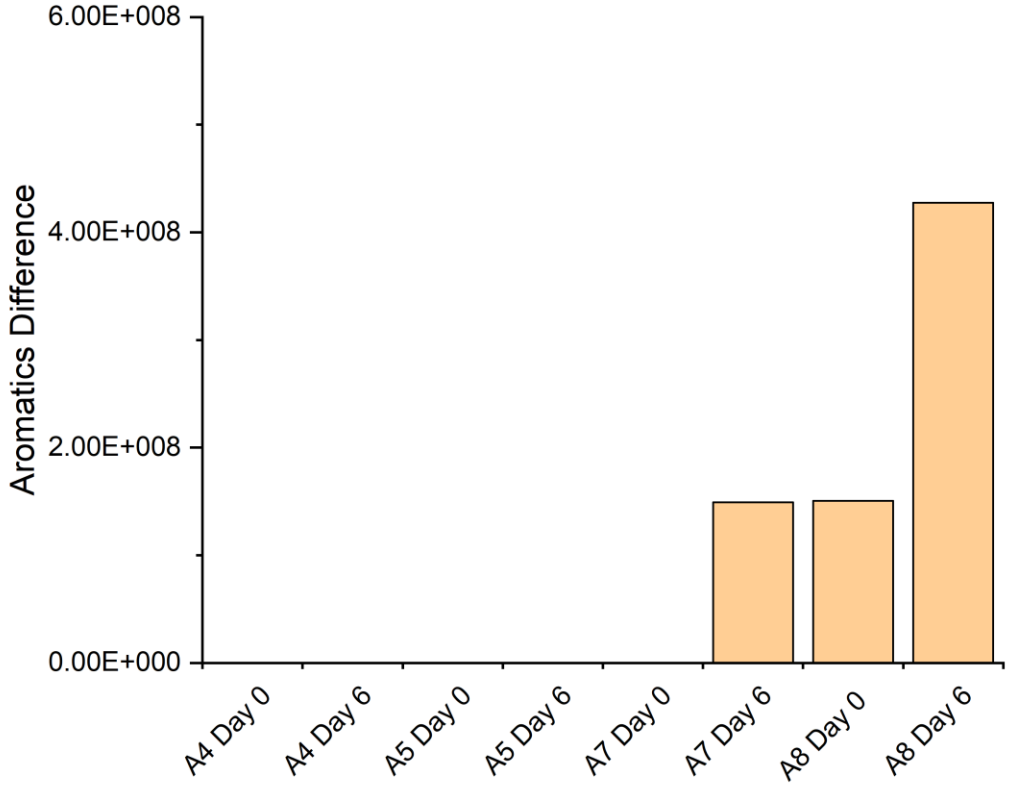

Figure 4-21 - Plot showing the difference in WaterLOGSY peak intensity over time for alanine-scanning variants of KDGIVNGVKA. *WaterLOGSY spectra were collected for each of 1mM KDGAVNGVKA (A4), KDGIANGVKA (A5), KDGIVNAVKA (A7), and KDGIVNGAKA (A8) alone and with 50µM WT aSyn. The difference in the area under the peptide peaks was calculated from the aromatic region (6-9ppm) of WaterLOGSY spectra collected at the initial timepoint (day 0) and a week later (day 6), following the incubation of the samples at 37°C with agitation. Negative differences are not shown. The positive differences seen for the A7 and A8 peptides are indicative of binding.*

4.4 Discussion

From the results of the experiments carried out in this chapter it seems that the ten-residue peptide KDGIVNGVKA is indeed binding to alpha-synuclein. The lack of peak shifts in the HSQC spectrum upon the addition of the peptide to aSyn suggest that it is not binding to the monomeric protein (Figure 4-2). The loss of peaks over time in the HSQC spectrum, in both the presence and absence of the KDGIVNGVKA peptide, suggests that the peptide does not prevent the aggregation of aSyn to the point where it reaches a size exceeding the size-limit of NMR (Figure 4-3). It is clearly apparent from TEM data that the peptide does impact aSyn aggregation, and it results in the formation of dramatically shortened fibrils (Figure 4-11). This may be through some form of 'capping' mechanism that prevents fibril elongation, and would explain the lack of observable peak shifts in the HSQC titration data. In an effort to probe this 1D and WaterLOGSY NMR experiments were used with the aim of focusing on the peptide itself, rather than trying to directly observe changes in the protein signals. Through this strategy depletions in the peptide signal were observed over a time period corresponding to that of aSyn aggregation; this was only seen for those samples containing both aSyn and KDGIVNGVKA, but not those of peptide alone (Figure 4-4). This provides an indication that as aSyn begins to aggregate to the point where it is no longer NMR-visible that the peptide binds to these species and its own signal is also lost. This hypothesis is supported by TEM data which shows that aSyn incubated in the presence of the peptide still forms fibrils, but of a much shorter length as if their elongation has been perturbed (Figure 4-11).

Interestingly, whilst probing this interaction through NMR it became evident that the KDGIVNGVKA peptide was subjected to modification over the timeframe of the experiment (Figure 4-5). Through the use of natural abundance HSQC experiments and MS this was determined to be a deamidation modification taking place at the Asn residue (Figure 4-6, Figure 4-7, and Figure 4-8). The precise impact of this modification on the binding of the peptide to aSyn is unclear. It cannot be ruled out from the results generated in this chapter that the deamidation has a) no impact; b)

improves the binding to aSyn; or c) impedes binding to aSyn. However, repeating the experiments with alanine-scanning variants of KDGIVNGVKA it became clear that the indications of binding seen in the 1D and WaterLOGSY data for KDGIVNGVKA were not seen if any of the three-residue stretch IVN were modified (Figure 4-21). This suggests that the IVN motif is necessary for binding, and this may imply that the deamidation of the Asn would be counter-productive with regards to binding.

The apparently successful identification of the region on the peptide responsible for binding is a step in the right direction, however the region of aSyn to which it binds could not be elucidated. The KDGIVNGVKA peptide was initially developed with the aim of targeting the 45-54 region of aSyn (108). However, it should also be noted that despite this the peptide seemed to remain effective against most of the PD-linked mutants, despite all-bar-one of these mutations occurring in this region (Table 4-8). Additionally, the initial experiment was aimed at targeting the monomeric form of aSyn, and yet the evidence here points to KDGIVNGVKA binding to aggregated forms of aSyn. There may be several possible explanations for these apparent dichotomies. It's possible that within the cells (in which the peptide library was initially screened) that aSyn began to aggregate and the peptides were better able to bind to this than the monomeric protein. The library screening technique described by *Cheruvara et al* also bears resemblance to the well-known yeast two-hybrid assay (108). This is an assay that is notorious for generating false positives (127). It is possible that the KDGIVNGVKA is one such false positive; but unusually, despite being a false positive in terms of monomeric aSyn, is able to bind to aggregated aSyn.

Studying this system has proved enormously challenging for a host of reasons. Chief amongst these is the nature of aSyn as a dynamic system. This dynamism makes it impossible to study aSyn by X-ray crystallography, and the utility of NMR rapidly fades as aSyn begins to aggregate and line-broadening becomes prohibitive. These circumstances led to the use of NMR in attempt to observe changes in the peptide induced by binding, rather than by looking directly at aSyn. This was complicated by the discovery that the peptide was changing over time, which made it difficult to

compare data at different time-points. Additionally, the 1kDa 10-residue peptide is in an unusual half-way house between being a very small protein and a substantially large small-molecule. This makes the utilization of many of the NMR experiments designed to probe ligand binding (including WaterLOGSYs) more challenging. The characteristic sign-inversions seen in WaterLOGSY experiments using small-molecules are not seen with a 1kDa peptide, and thus changes in peak intensity were measured here instead. This is not ideal, however it was the best strategy available and has provided insight into the binding between aSyn and KDGIVNGVKA. Other strategies for studying the peptide-protein interactions here, such as ITC and FRET, were ruled out due to the heat changes resulting from aSyn aggregation and the need for bulky fluorescent tags respectively.

The utility of using peptides to prevent the aggregation of amyloidogenic proteins, like aSyn, is open to debate. Peptides have a number of advantages over smaller molecules, particularly that they are generally more specific and thus less prone to off-target effects. However, they also have a number of disadvantages that have historically ruled them out of being considered 'serious' therapeutic molecules (97). These are namely that they are prone to proteolytic cleavage, modification (e.g. deamidation), and difficulties may be encountered in getting them to the desired target. Some of these issues have started to be overcome, however. For example, to protect them from cleavage/degradation peptides may be altered with modifications, such as acetylation or amidation. Additionally, some of the issues surrounding targeting/penetrance can be overcome through the addition of specific localization sequences or by packaging the peptide into lipid vesicles (97,128). Targeting the brain is especially difficult given the BBB. This may possibly be overcome by allowing the peptide to 'piggyback' across with another molecule for which there is a specific transporter at the BBB (e.g. glutathione) (129).

There are several other pitfalls that may be associated with the use of KDGIVNGVKA as a therapeutic for PD. Firstly, assuming that it was beneficial to inhibit the aggregation of aSyn as a treatment for targeting PD, it would likely require very early diagnosis. KDGIVNGVKA does not

exhibit any capacity for disaggregation of pre-exisiting fibrils, and is only preventative. Therefore, it would necessitate the identification of biomarkers that could be used to target those individuals going to develop PD before the manifestation of the hallmark clinical symptoms. Secondly, whether the inhibition of aSyn fibril elongation is beneficial is an open question. It is now widely considered that oligomers, rather than the fibrils themselves, that are species responsible for mediating toxicity (130). If this is the case then it may be that disrupting the kinetics of fibril formation could result in an increase in the supply of toxic oligomers, and thus the peptide may enhance neurodegeneration rather than abate it.

It is clear much future work is required if this peptide is going to progress further. Obvious steps include the systematic study of the alanine-scanning variants of KDGIVNGVKA and compare and contrast the TEM/ThT data; this is currently being undertaken by collaborators at the University of Bath. Also useful would be to carry out *in vivo* studies of the effects of the peptide on a PD-model organism. Models of PD in *C.elegans* may be an option. These systems are relatively easy and cheap to maintain, and they can exhibit visible signs of PD (e.g. rigidity and impaired movement) (131). The administration of the peptide would also be possible by packaging it into lipid vesicles. Depending upon the outcome of such experiments further downstream work could be considered. Despite these numerous hurdles, this is a promising area of research that should be pursued in the future.

5 NMR metabolomics study of peptide mode-of-action

5.1 Introduction

5.1.1 What is metabolomics?

Metabolomics is a nascent field of study and one of the newest members of the 'omics family, which also includes genomics, proteomics, and transcriptomics. The 'omics fields each aim to characterize a different layer of biological activity, with each having its own advantages and associated pitfalls. It is a holy grail of modern biology/biochemistry to integrate all of the data output by these studies to compile a holistic 'phenome'. The metabolome – the profile of the metabolites (small molecules) in a cell or entity at a given time – represents the most direct observation of the state of the cell/tissue/sample at a given point in time.

Metabolomics studies are generally conducted using either NMR or MS, again with each having their own advantages and limitations (132). NMR metabolomics is useful because it provides a highly-reproducible picture of small molecules within the sample; there is no separation step beforehand. It is also non-destructive meaning that samples may be re-analysed. However, in comparison to MS it is insensitive and requires a larger sample volume. Additionally, MS instrumentation is much more widely available and is very likely present in most research laboratories and clinical labs. NMR equipment – and by extension expertise in NMR metabolomics – is far less common, and this can prove to be a significant hurdle to a metabolomics study.

5.1.2 Why conduct NMR metabolomics experiments?

NMR metabolomics experiments are an extremely powerful way of reporting on the actual effects of different conditions or variables on a system. This is because the vast majority of metabolites contain ^{1}H and thus possess an intrinsic NMR signature without the need for chemical modification. NMR is also a solution-based technique and thus samples can typically be studied

directly. Disease impacts the metabolic profile of cells and this is probeable by NMR metabolomics. This can be exploited for the identification of novel biomarkers and the development of new therapeutics (133). For example, NMR metabolomics has been used to investigate the differential effects of incubation of monomers, oligomers and fibrils of aSyn and Aβ on SH-SY5Y neuroblastoma cells (109). This work saw significant differences in levels of metabolites associated with neurotoxicity and inflammation, including taurine, creatine, and glutamine. This presented a model system to probe the effects of KDGIVNGVKA on aSyn aggregation in more detail, as NMR metabolomics could be used to monitor the relative levels of these same metabolites in cells challenged to aSyn in the presence and absence of the peptide.

5.1.3 Outline of statistical methods used in NMR metabolomics

NMR metabolomics, like the other 'omics disciplines, generates huge quantities of data that are difficult to directly interpret and therefore statistical analysis is essential. Some of the more commonly used methods and techniques to interpret NMR metabolomics data are outlined here.

5.1.3.1 Normalization and scaling of data

Normalization is a procedure applied across data, in this case across different NMR spectra, in order to account for unwanted biases (e.g. differences in the number of cells or dilution effects) (134–136). This then enables the comparison of these spectra for downstream statistical analysis. For example, if peaks associated with one metabolite differ across two samples it needs to be known that is not simply the result of one sample being derived from a larger or smaller number of cells. Normalization achieves this and means that samples can be assessed in terms of variables of interest. The metabolomics data analysis in this chapter was conducted through the MetaboAnalyst web server, which allows for the use of multiple different types of normalization, including: normalization by sum, normalization by median, and quantile normalization (137,138). Normalization by sum means that all of the features across each spectrum are added together and

used to produce a normalization factor. This basic type of normalization assumes that the total concentration of metabolites in each sample is consistent, and it also means that highly abundant metabolites contribute more than less abundant metabolites. This means that the normalization factor is very sensitive to changes in the concentration of highly abundant metabolites, which could be disadvantageous. Normalization by median on the other hand operates by calculating the fold change in the intensity of every bucket/metabolite in one spectrum against a target spectrum. The median fold-change is then used to generate a normalization factor, which is unaffected by changes in just a few metabolites. Quantile normalization operates by calculating a normalization factor based upon spectra presenting exactly the same distribution of peak intensities (134,136).

Scaling of data is a related process but is applied to peaks within an individual spectrum to allow their comparison (135,136). In a spectrum there will be metabolites with a high abundance and there will be those at a lower abundance. Big differences in metabolites of low abundance may be of greater importance than smaller differences in metabolites with a higher abundance, but the methods used to display the data, such as principal component analysis (PCA) and principal least squares discriminant analysis (PLS-DA), do so in such a way to show the maximum variance. Thus, they would favour those metabolites that are highly abundant over those at lower abundance. Scaling is the method by which this is overcome and makes the differences between high abundance and low abundance metabolites within a spectrum more comparable. There are multiple types of scaling, and MetaboAnalyst allows for: mean centering, auto-scaling, Pareto scaling, and range scaling (139). The auto-scaling, Pareto scaling methods and range scaling methods also incorporate mean centering. Mean centering is the subtraction of the mean of all the peaks from each peak, enabling variables to be reported as higher than (positive) or lower than (negative) the mean. This does little to prevent one or two highly abundant metabolites from completely dominating the dataset, and so scaling is required (136). In auto-scaling the data is mean centered, and then subsequently the standard deviation of all the peaks is subtracted from all of the peaks (136). In Pareto scaling the peaks are mean centered, and then subsequently the peaks

are divided by the square-root of the standard deviation of the mean centered data (136). This is a trade-off between just applying mean centering, which maintains bias in favour of highly abundant metabolites, and auto-scaling which can go so far in providing a level playing-field between highly abundant and less abundant metabolites that it can bias in favour of noise and irrelevant features (136). Range scaling is another alternative, in which the mean centered data is divided by the range (the difference between the largest and smallest values). Whilst it can be a useful method it should be treated with caution as it can give undue influence to extremes in the data (136).

5.1.3.2 Univariate analysis

Univariate methods of statistical analysis, such as T-tests and one-way ANOVA, only consider one variable at a time (140). Univariate analysis is useful because it is easy to interpret, although it does not explore correlations between variables (metabolites) and requires adjustment to counteract compounding errors associated with performing multiple tests (for each metabolite peak). For more complicated datasets multivariate analyses may be preferable as they can enhance understanding of the effects in multiple metabolites and avoid the need for conservative adjustments to account for compounded error. Physical characteristics and how they relate to disease (height, age, body-mass index, etc.) are a good example. A univariate analysis can only consider one characteristic at a time whilst a multivariate analysis has the power to explore which characteristics (if any) are most indicative of a disease state.

5.1.3.2.1 Welch's T-test

The Welch's T-test is a univariate statistical method for determining whether samples adhere to the normal distribution (a bell or Gaussian distribution of values) (Figure 5-1A). Under the null hypothesis – an assumption that there is no divergence from this normal distribution – measurements should all fall within the normal distribution (Figure 5-1B). Failure to do this suggests that there is a deviation between the two conditions or that the sample collected in on the extreme

of the normal distribution (Figure 5-1C). The T-test calculates how "common" the measured data would be assuming it adhered to the normal distribution. This is where the p-value is introduced, and is why when the p-value is below a set threshold (e.g. 0.05) the null hypothesis is rejected.

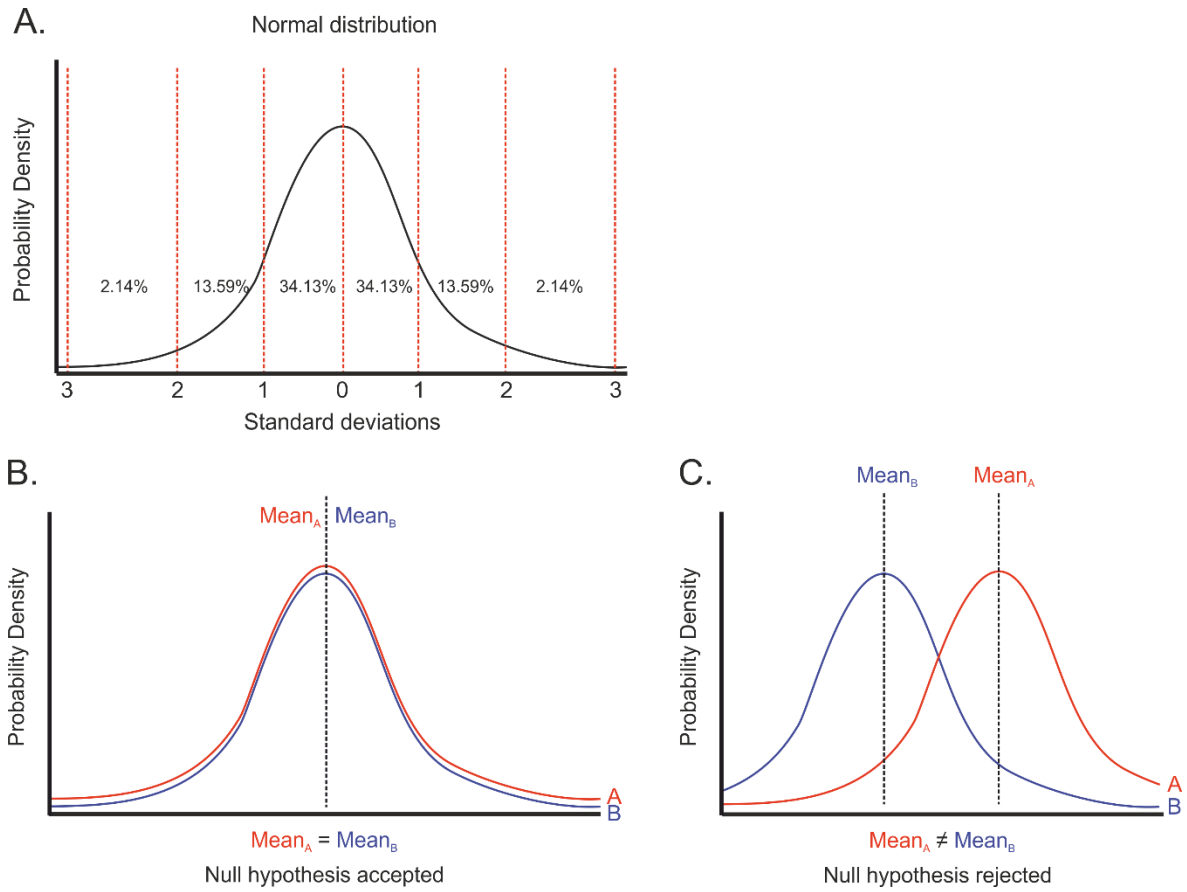

Figure 5-1 - The normal distribution and whether to accept or reject the null hypothesis. *The normal distribution is shown (A) with the proportion of the data shown according to the distance from the mean in terms of standard deviation. The null hypothesis assumes that the populations adhere to the normal distribution and that they have the same means (B). If this is not the case then the null hypothesis is rejected (C).*

5.1.3.2.2 Analysis of variance

The one-way ANOVA is a univariate statistical technique akin to the T-test that is useful when comparing multiple groups. The one-way ANOVA is used when only one independent variable is considered, however two-way ANOVAs that consider two independent variables are also available. These were not used in this study given the number of variables to consider. The use of multiple independent univariate tests when comparing multiple groups is considered sub-optimal as it increases the likelihood of a type I error (141). This occurs when the null hypothesis is rejected,

but it is true (a false positive). This can be accounted for in the one-way ANOVA using the Benjamin-Hochberg false-discovery rate (FDR) correction (142). The one-way ANOVA will, however, only report that there is a significant difference between groups; it does not give any information as to which groups these are. Consequently, there is a need for *post-hoc* tests to provide this information. In MetaboAnalyst Fisher's least significant difference (LSD) method was used as the *post hoc* test in this study (137,138).

5.1.3.3 Multivariate analysis

Multivariate methods of analysis, such as PCA and PLS-DA, are mathematical procedures that differ from univariate methods in that these take into account multiple different variables in the data at the same time (140). This is useful in the context of biological experiments because the results are often multi-factorial. For example, the rate of growth of bacteria may be affected by cell line, richness of growth medium, the temperature, aeration etc; this is a multivariate system for which a multivariate analysis must be conducted to allow proper interpretation.

5.1.3.3.1 Principal components analysis

PCA is a multivariate data transformation technique that strives to condense the dimensionality of variance within a sample by condensing multiple variables into so-called principal components (143). In a dataset there are some variables that are responsible for more variance than others, and some that may correlate/covariate. The principal components are new variables containing combinations of the original variables (as identified by the algorithm), and the first principal component presents the largest possible amount of "explained" variance in the data (143). The second principal component then explains the next largest, and so on. In doing this, the most important information is retained and the dataset can be explained in terms of a few principal components instead of a larger number of variables.

PCA is an unsupervised technique, meaning that it is given no prior information about the sample groups. For example, if bacterial growth was monitored under different conditions the PCA would not "know" that groups may be the different cell lines. It will simply project the data to show the maximum amount of variance possible. Principal components can be projected as a scores plot (Figure 5-2A). The "scores" refer to the degree to which the different principal components contribute to the variance of each of the samples. The principal components are then used as axes, and the data can be plotted in these terms. The loadings plot is similar to the scores plot in that its axes can be any of the principal components, but instead of plotting the different samples the factors contributing to the variance in the principal components are plotted instead – in this case it is the metabolite signals (Figure 5-2B). Also useful in the interpretation of PCA data is the biplot which is a combination of the scores plot and loadings plot (Figure 5-2C). Mean-centred data enables the axes to bisect 0, and thus points on these points further from 0 are more varied than those closer to 0 on any axis.

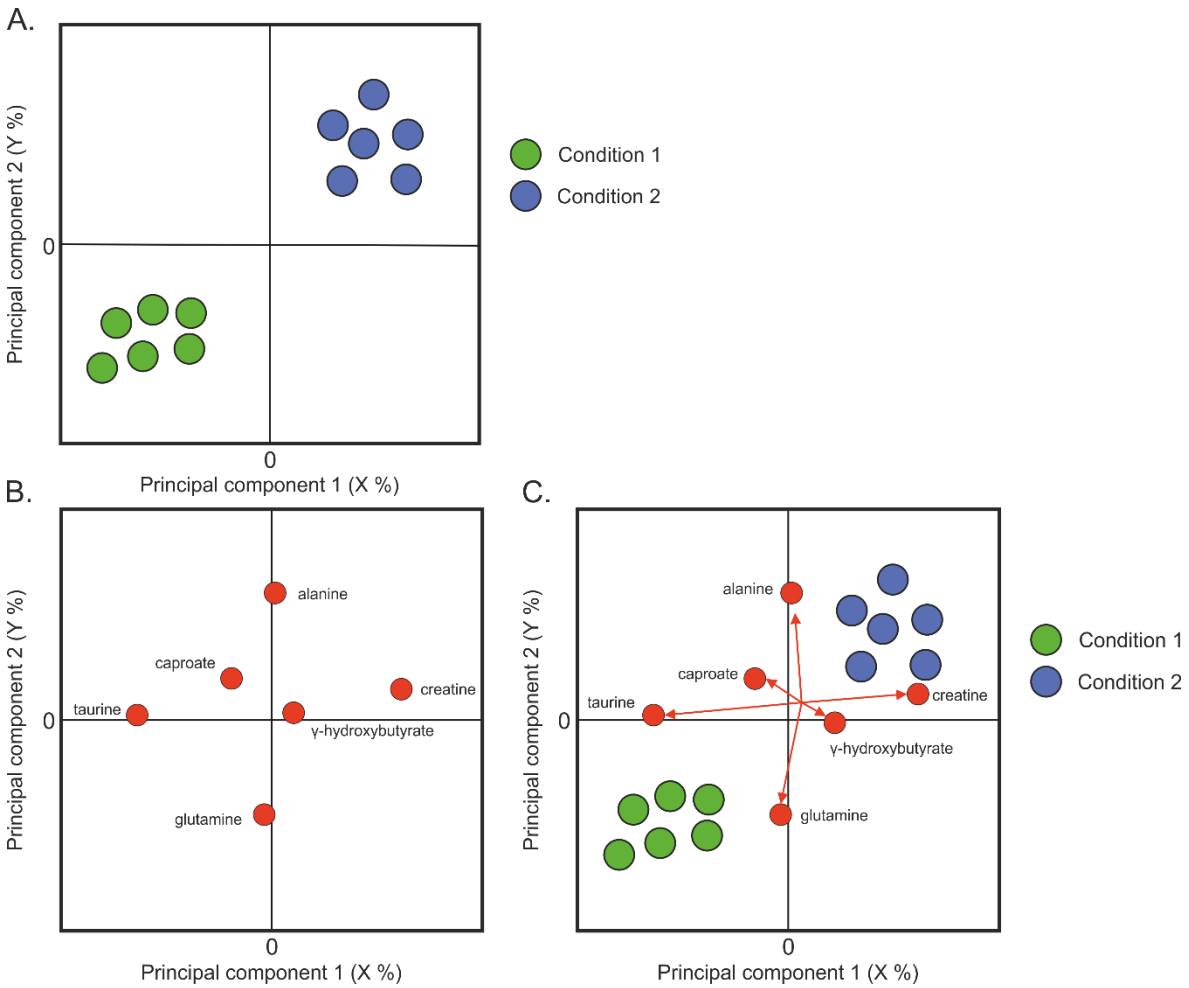

Figure 5-2 - Methods of representing PCA data. *A scores plot (A) is shown, and the samples from two conditions have been plotted according to their variance in terms of the two principal components. A loadings plot (B) shows which characteristics – in this case metabolites – contribute the most to the variance in the two principal components. Here, taurine and creatine contribute strongly to the variance in the first principal component, whilst alanine and glutamine are most important in the second principal component. The biplot (C) combines the scores plot (A) and the loadings plot (B) to show the samples and those metabolites contributing to the most variance.*

5.1.3.3.2 Partial least squares-discriminant analysis

PLS-DA is a multivariate data transformation technique, or more formally a linear regression model (144). Like PCA, PLS-DA converts variables into new principal components and aims to increase separation between groups whilst minimizing the variance within groups. Unlike PCA, however, which is an unsupervised method, PLS-DA is a discriminant analysis or supervised method (145). This reflects that PLS-DA is given information about the class-labels whilst PCA is not. For example, if looking at bacterial growth under different conditions different cell lines PLS-DA will

perform a linear regression to establish the separation between these groups. An unsupervised PCA on the other hand would plot the data to show the greatest separation between samples, irrespective of their label. This supervised method can be useful to enhance separation, but can introduce bias and overfitting is easily achieved using this technique. This makes cross-validation of PLS-DA output essential before drawing any conclusions. The advantages and limitations of this method have been described in great detail elsewhere (146).

Many of the plots used to display PLS-DA data are similar to those used for PCA (Figure 5-2). However, in addition to this variable importance in projection (VIP) plots are also used. VIP scores are calculated for each of the metabolites and are weighted sum of squares of the PLS loadings, taking into account the amount of explained Y-variation in each dimension. Essentially, the VIP plot shows those metabolites responsible for the most variance between the classes and their relative levels across them (e.g. creatine may be responsible for most variance and is elevated in condition 1 in comparison to condition 2).

5.1.3.4 Cross-validation

Cross-validation is essential when analysing mathematical models, especially with supervised methods such as PLS-DA. These methods are often associated with overfitting, which means that the model is being fit to the noise. In the work conducted here the leave-one-out cross validation (LOOCV) method is utilized. The metrics Q^2 and R^2 may be used to assess the quality of the PLS-DA model as reported by the MetaboAnalyst server (138). Calculation of Q^2 and R^2 operates on the basis of a small subset of data being set-aside from the dataset and not used in the generation of a model. Following the generation of a model this small subset (the reference set) of data is then used to see how well the model fits. R^2 and Q^2 are percentages indicating how close the data are to the fitted regression, so a higher number indicates a closer fit. The R^2 is the value

for the dataset as a whole, whilst the Q^2 is the value when the model is applied to the reference set of data (147).

5.1.4 Aims

In the study by *Phelan et al* it was shown that the exposure of SH-SY5Y cells to aSyn (and Aβ) resulted in changes in the level of various metabolites (including taurine and creatine) that were associated with inflammation and neurotoxicity (109). These effects were distinct, however depending on whether the cells were exposed to monomeric, oligomeric or fibrillar protein. From this study a library of the metabolites in SH-SY5Y cells was available. Using this library the aim was to use NMR metabolomics analysis to assist in investigating the effects of the KDGIVNGVKA peptide on aSyn toxicity. The hypothesis going into the study was that the incubation of KDGIVNGVKA peptide with aSyn reduced its toxicity, as seen by *Cheruvara et al* (108), and that this would be reflected in the metabolic profile of the cells when compared with those exposed to aggregated aSyn. On top of this NMR metabolomics would give detail into the mechanisms and pathways through which toxicity was mediated, and how the peptide mitigated this. NMR metabolomics studies necessitate precise control of experimental conditions and numerous control samples (see Table 5-1). In light of this it was possible to test multiple additional hypotheses. These included:

- Exposure of cells to aSyn fibrils results in an increased level of metabolites associated with cell stress and death, when compared to monomeric aSyn.
- That the exposure of cells to fresh or aged KDGIVNGVKA peptide alone results in no significant change in the metabolic profile of cells when compared to cells alone.
- That exposure of cells to aSyn fibrils and independently incubated KDGIVNGVKA exhibits no difference in metabolic profile when compared to those exposed to aSyn fibrils alone, whilst differences are apparent when compared to aSyn fibrils formed in the presence of KDGIVNGVKA.

Table 5-1 - The different conditions to which the SH-SY5Y cells were exposed for NMR metabolomics experiments.

Abbreviation	Condition
C	PBS Blank
P	Fresh KDGIVNGVKA alone
PA	Aged KDGIVNGVKA alone
M	Monomeric WT aSyn alone
MP	Monomeric WT aSyn + Fresh KDGIVNGVKA (1:1)
MPA	Monomeric WT aSyn + Aged KDGIVNGVKA (1:1)
F	WT aSyn fibrils alone
FPAT	WT aSyn fibrils formed in the presence of KDGIVNGVKA peptide (1:1)
FPAS	WT aSyn fibrils + Aged KDGIVNGVKA (formed separately)
FP	WT aSyn fibrils + Fresh KDGIVNGVKA

5.2 Methods

5.2.1 Cell viability experiments

Each condition (Table 5-1) was prepared to an equivalent monomer concentration of 55µM in PBS pH 7.4. Those peptide challenge conditions that did not require incubation over time (i.e. fresh) were snap frozen in LN_2 before storage at -80°C. SH-SY5Y neuroblastoma cells were grown up in F-12 Ham's media supplemented with 1x minimal essential medium (MEM), 10% fetal bovine serum (FBS) and 1% penicillin-streptomycin (Pen-Strep). 5,000 cells were added to each well used in a 96-well plate and incubated at 37°C 5% CO_2. After 24 hours 10µL of the challenge condition was added per well, with each condition having 6 repeats. PBS alone and 1% triton X-100 prepared in PBS pH 7.4 were used as "live" and "dead" cell controls, respectively. The cells were left for 24 hours before 10µL of CCK-8 reagent (Dojindo) was added to each well. After this, the absorbance at 450nm was measured per hour for 4 hours on a FlexStation 3 (Molecular devices). Data was processed and analyzed using OriginLab.

5.2.2 Cell culture of NMR metabolomics samples

Each condition (Table 5-1) was prepared as a 1.5mL 'stock' of 50µM protein and/or peptide in PBS pH 7.4. The PBS used in the experiment was all from a single batch prepared using a PBS tablet (Sigma). Those peptide challenge conditions that did not require incubation over time (i.e. fibrillation or ageing) were snap frozen in LN_2 before storage at -80°C. Concomitantly, mycoplasma-free SH-SY5Y neuroblastoma cells were cultured using Ham's F12 nutrient mixture supplemented with 10% FBS, 1% Pen-Strep and 1x MEM non-essential amino acids (all Sigma) in a 37°C incubator with 5% CO_2. Each peptide challenge condition was to be added to a T25 flask at 60 – 70% confluency at a final concentration of 5µM. Three clonal replicates (three flasks containing cells from the same batch) were required for each peptide challenge condition and thus the total number of T25's required was 30. All cells were from the same batch and were of the same passage number (passage number = 21). As the samples had been prepared at 50µM in 1.5mL they were diluted in complete cell growth medium to 15mL to provide a final concentration of 5µM. The old cell medium was decanted from each flask and replaced with 5mL of the medium containing the peptide challenge conditions (three replicates x 5mL per flask = 15mL sample). The cells were incubated with the samples for a further 24 hours before harvesting. The "post-incubation" cell medium containing the protein/peptide was poured off and collected in 15mL Falcon tubes and frozen on dry-ice in case needed for later analysis. The cells were washed with PBS pH 7.4 to remove excess media and any dead cells. The cells were trypsinized using 1x trypsin-versene (Gibco). The trypsin was neutralized using complete cell medium and the cells transferred to pre-weighed Universal tubes. The cells were then spun down at 500g 4°C for 5mins. All supernatant was pipetted off and the mass of the tube was recorded (to 3 decimal places) to allow the determination of the total cell mass. The cell pellets were resuspended in 6mL of PBS and spun back down at 500g 4°C for 5mins. The PBS was pipetted off and the cell pellet carefully resuspended in 3mL of PBS. The 3mL of resuspended cells was split into 3x 1mL aliquots in Eppendorf tubes to serve as the three extraction

replicates. In total there were 90 Eppendorfs (10 conditions x three clonal replicates x three extraction replicates). The 1mL aliquots were spun down at 500g for 5mins at 4°C. The PBS supernatant was discarded and the pellets were snap frozen in LN_2 and stored at -80°C for later extraction and analysis of polar metabolomics samples.

5.2.3 Extraction of polar metabolites

All steps were carried out on ice. The pellets were resuspended in 500µL of ice-cold 50% methanol, 50% double-distilled water (ddH_2O). The samples were sonicated with an exponential micro-tip sonicator in an ice-batch at 23 kHz and an amplitude of 10µm for three 30s cycles with 30s rest intervals. The samples were then vortexed for 30s before being centrifuged at 21,500g for 5mins at 4°C. The supernatant was snap frozen in LN_2 and lyophilized overnight. The pellets were snap frozen in LN_2 and stored at -80°C for potential subsequent lipid extraction.

5.2.4 Preparation of NMR metabolomics samples

The lyophilized samples were resuspended in 200µL of 100mM sodium phosphate pH 7.4, with 100µM trimethylsilylpropanoic acid (TSP) (all prepared in ^2H_2O). The samples were vortexed and then centrifuged for 5mins at 21,500g at 4°C. Being careful not to dislodge any pelleted material the supernatant was loaded into clean 3mm (outer diameter) NMR tubes and placed in a 96-tube rack.

5.2.5 NMR metabolomics data collection

1D ^1H NMR spectra were collected using pulse sequences based upon 1D NOE and Carr-Purcell-Meiboom-Gill (CPMG) experiments. NMR spectra were acquired using a Bruker AVANCE IIIHD 700MHz spectrometer equipped with an automated SampleJet sample changer and a TCI gradient CryoProbe (Bruker). All spectra were collected at 298K with the temperature having been

calibrated using a 98% deuterated standard methanol sample and the methanol thermometer method of *Amman et al* (148). 1D ^{1}H NOE spectra were collected with 32 scans, 4 dummy scans, an acquisition time of 2.726s, and a spectral width of 25.7491ppm. 1D ^{1}H CPMG spectra were collected with 512 scans, 4 dummy scans, an acquisition time of 3.067s, and a sweep width of 17.1661ppm. TopSpin 3.5 pl 7 and IconNMR 4.6.7 (Bruker) were used for data acquisition and processing with standard processing routine comprising the line-broadening window function (0.3Hz), Fourier transformation, phasing, and referencing to TSP.

5.2.6 NMR spectra quality control

The quality of the NMR spectra were verified prior to any statistical analysis. This quality control entailed the analysis of the half-height line-width of the TSP peak, which should ideally be ~1Hz, that the water suppression was successful and that the baseline peak was not distorted (149,150). Those samples that failed this initial quality control check were excluded and re-run on the spectrometer. Samples were also excluded if their signal:noise fell below the average total intensity of all spectra minus the standard deviation of the total intensity, which was 58,106,308,602 AU.

5.2.7 Annotation of NMR spectra and identification of metabolites

AMIX (Bruker) was used to prepare bucket tables for submission to MetaboAnalyst (138), whilst TAME NMR (https://github.com/PGB-LIV/tameNMR) was used to optimize bucket size/positioning. Previous work by *Phelan et al* (MetaboLights ID: MTBLS455) meant that a preliminary metabolic profile of SH-SY5Y cells was available and that metabolites were already assigned for each bucket (109).

5.2.8 Statistical analysis of NMR metabolomics data

All statistical analysis was carried out using the MetaboAnalyst server (138). Quantile normalization, mean-centering and Pareto scaling was applied (136). Welch's T-test, ANOVA, PCA and PLS-DA analysis were all used to determine the separation between the groups. All statistical graphs and charts were produced by MetaboAnalyst.

5.3 Results

5.3.1 Cell viability experiment

Cell viability experiments, complementary to the metabolomics study, were conducted as a more direct measure of the toxicity to cells and to ensure comparable cell numbers in the metabolomics study (backed up by the measured mass of cell pellets). The challenge conditions are listed in Table 5-1. The data showed consistent viability across all conditions as can be seen (Figure 5-3). This is perhaps not entirely surprising as the cells were only challenged for 24 hours prior to measurement. This timeframe may be sufficient for differences to emerge in the metabolic profile of the cells but not sufficient to result in cell death. So long as the cells are metabolically active, formazan dye will be formed from the CCK-8 reagent and therefore the A_{450} will increase. Consequently this assay gives a binary assessment of whether the cells are alive or dead, and provides no information on the relative "health" of the cells. A one-way ANOVA was carried out to try and determine if any of the minor differences between the conditions were statistically relevant. Using the Bonferroni means comparison test no statistically significant differences were observed.

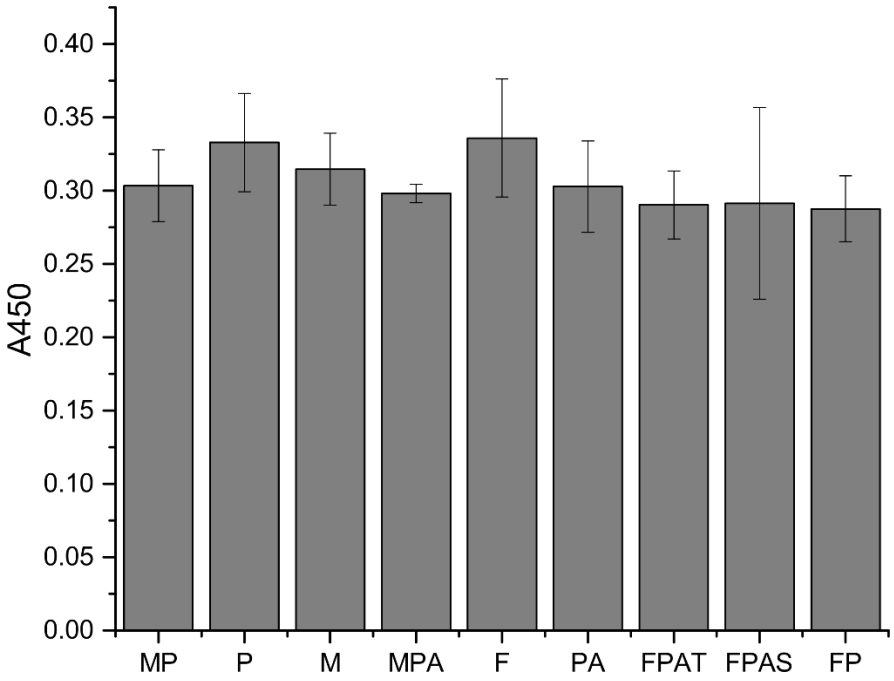

Figure 5-3 - Cell viability of cells exposed to the same conditions as used in the NMR metabolomics experiments. *Cell viability was assessed using the CCK-8 reagent and measuring the absorbance at 450nm (A). Cell were challenged with identical conditions to those used in the NMR metabolomics experiments for 24 hours prior to measurement. Six wells were prepared for each condition. N=1. Viability was consistent across all conditions and no statistically significant differences were determined by one-way ANOVA with the Bonferroni means comparison test.*

5.3.2 Initial spectral and statistical analysis

In total there were ten different sample conditions (Table 5-1), and for each of these there were a further three clonal replicates and three extraction replicates generating a total of ninety samples. For each sample 1D ^{1}H CPMG spectra were collected. These are widely used in NMR metabolomics as they can attenuate certain peaks according to their T_2 and thus are used to remove the contribution from large molecules (e.g. proteins, polysaccharides) and improve the visibility of small molecules (151,152). Following on from the stringent quality control steps eighty of the original ninety collected spectra were useable (see Table 5-2).

Table 5-2 - Table showing the number of useable spectra per condition following quality control.

Abbreviation	Condition	Number (after quality control)
C	PBS blank	8
P	Fresh KDGIVNGVKA alone	9
PA	Aged KDGIVNGVKA alone	8
M	Monomeric WT aSyn alone	8
MP	Monomeric WT aSyn + Fresh KDGIVNGVKA (1:1)	8
MPA	Monomeric WT aSyn + Aged KDGIVNGVKA (1:1)	9
F	WT aSyn fibrils alone	8
FPAT	WT aSyn fibrils formed in the presence of KDGIVNGVKA (1:1)	7
FPAS	WT aSyn fibrils + Aged KDGIVNGVKA (formed separately) (1:1)	6
FP	WT aSyn fibrils + Fresh KDGIVNGVKA (1:1)	7

Representative CPMG spectra following quality control are shown (Figure 5-4). The spectra were bucketed using the pattern file and library by *Phelan et al* as a template (109). "Bucketing" refers to the process by which the spectrum is split up into lots of sections or "buckets" that may cover a single peak or a group of peaks that are associated with a metabolite. The buckets were slightly edited to reflect minor differences in buffer composition and spectrometer frequency causing slight peak shifts compared to those in the published study. Following curation the spectra were split up into 245 buckets, for which 78 metabolites were associated with individual peaks or groups of peaks (see Figure 5-5 and Appendix Table 10-1).

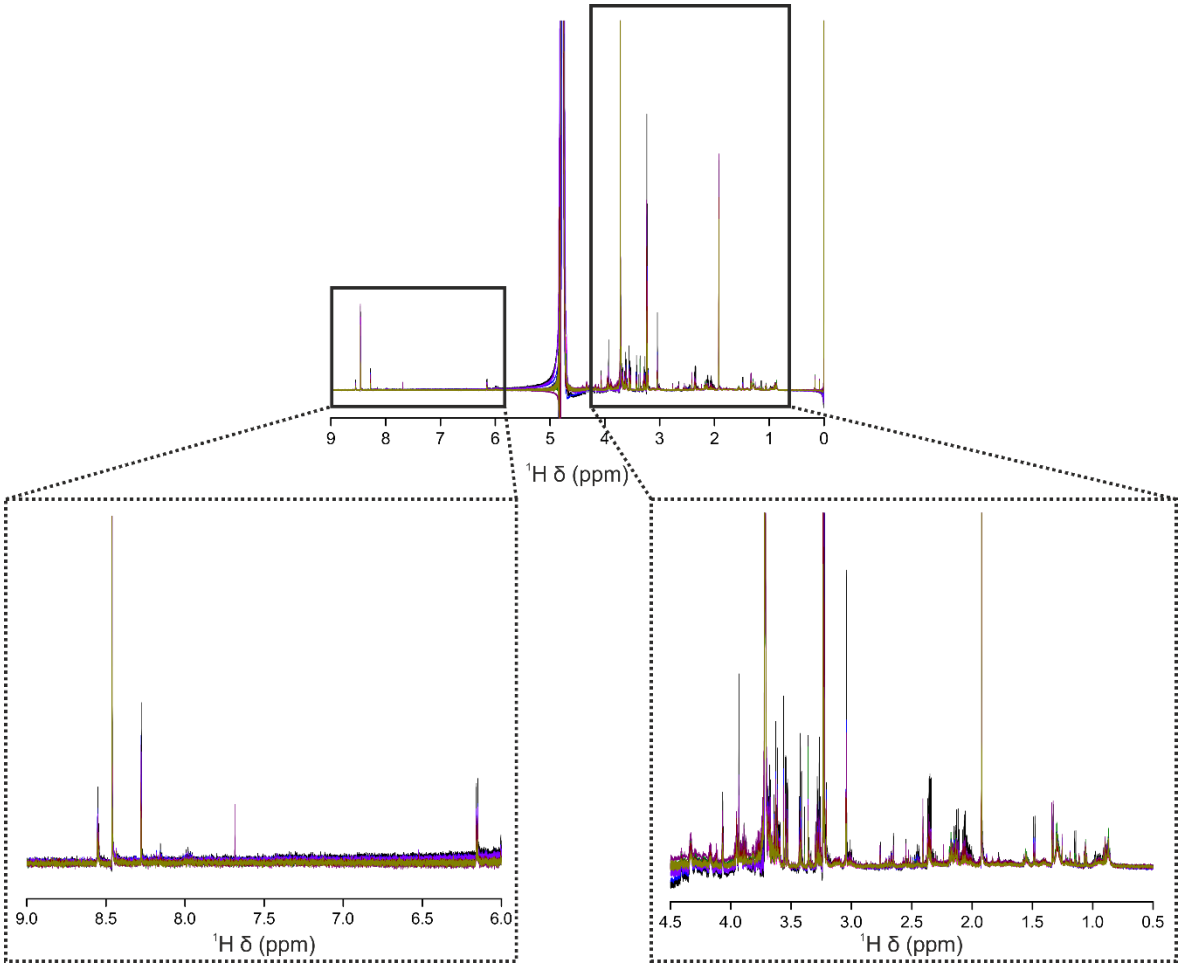

Figure 5-4 – Ten representative 1D ^{1}H CPMG spectra of samples from the dataset, having undergone quality control. *Note, the large residual water peak at ~4.7ppm is purposely avoided during spectral analysis. Inset below are zoomed in images of the aliphatic and aromatic regions.*

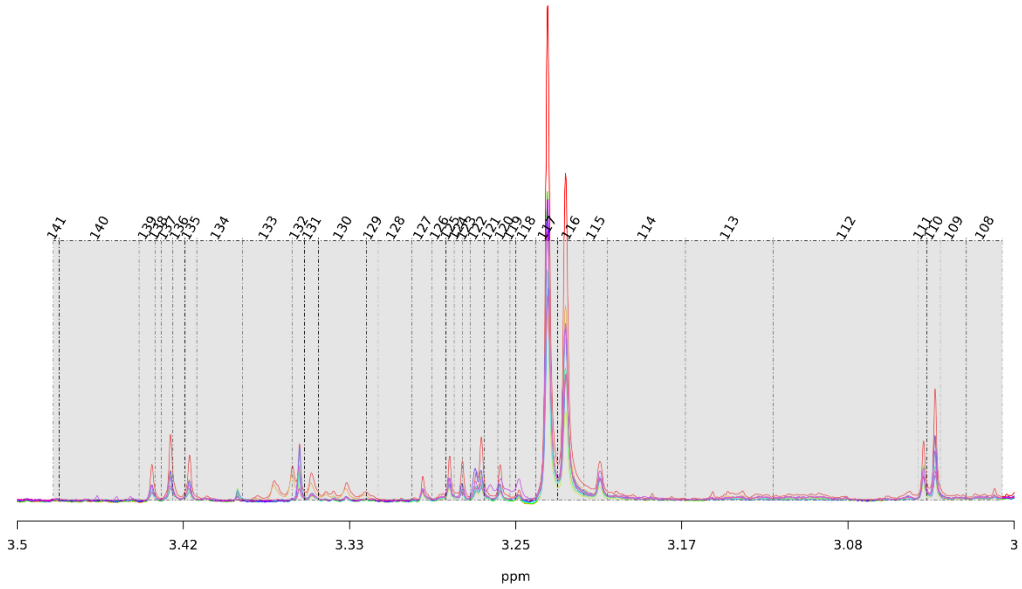

Figure 5-5 – ^{1}H CPMG spectra overlaid with buckets. *TameNMR was used to visualize the buckets and optimize their position/width. Here is shown the buckets 108-141. The buckets cover either single peaks, or groups of peaks that vary together.*

5.3.2.1 Peptide toxicity

The first question addressed using this dataset was whether SH-SY5Y cells exposed to KDGIVNGVKA in its fresh (P) or aged (PA) forms exhibited metabolic changes compared to cells exposed to the PBS control (C). The study by *Cheruvara et al* did not suggest that the KDGIVNGVKA peptide was toxic, but it was important for this study to determine that the peptide alone in either its fresh or aged (deamidated) forms did not impact the cell metabolome (108).

By inputting the spectra into MetaboAnalyst statistical analyses were carried out to assess whether any significant differences were apparent. By ANOVA no significant differences were seen in the levels of any metabolites between the control samples and those exposed to the peptides (Figure 5-6). PCA was used to further inspect the data, as being an unsupervised multivariate technique it can consider multiple variables at once. Nevertheless, the groups did not separate especially well (Figure 10-1). This means that further analysis can continue on the assumption that the peptide itself is not directly affecting the metabolome of the cells.

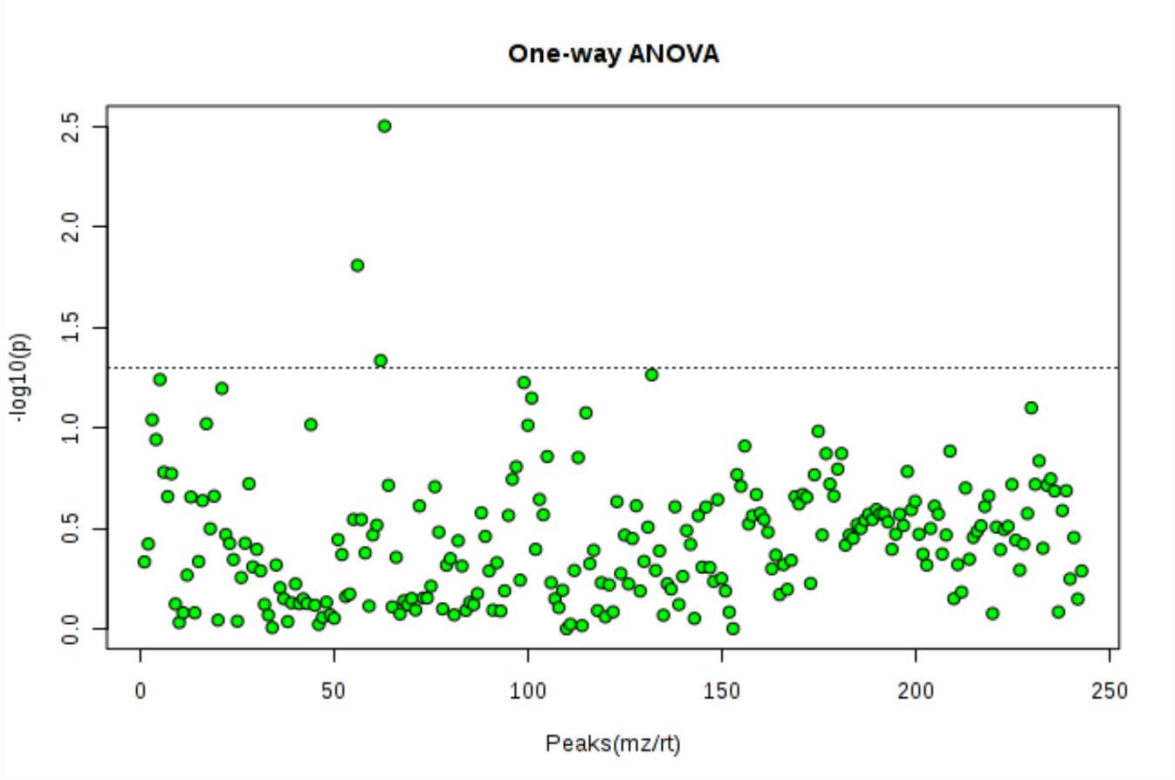

Figure 5-6 - ANOVA of the effect of KDGIVNGVKA on SH-SY5Y cells. *A one-way ANOVA (A) comparing the NMR peak intensities of SH-SY5Y cells challenged with fresh KDGIVNGVKA, aged KDGIVNGVKA, or a PBS control did not reveal any statistically significant differences to the FDR-adjusted 0.05 level. The dotted line reveals the raw (not FDR-adjusted) threshold.*

5.3.2.2 Fibril toxicity

Prior to further studies the effect of aSyn fibrils (F) on the metabolome of SH-SY5Y cells, compared to that of monomeric aSyn (M) or a PBS control (C) was assessed. It is increasingly accepted that amyloid fibrils are not the toxic species responsible for neurodegeneration, and rather it is oligomers that are the truly toxic species (20). It is clear from previous studies that fibrils, oligomers and monomeric aSyn have differential effects on cells that is visible in their metabolic profile (109). It was necessary to investigate these changes here, especially given that the KDGIVNGVKA peptide inhibitor may alter the delicate equilibrium existing between these three states.

The metabolic profile of SH-SY5Y cells exposed to three different conditions – PBS control, monomeric aSyn, and aSyn fibrils – were compared to address this question. An initial comparison

was made by one-way ANOVA (Figure 5-7 A). Eight buckets corresponding to five metabolites were found to be significantly different (to the FDR-adjusted 0.05 level) between the samples. These metabolites were: 3,4-dihydrobenzoic acid, homoserine, glutamine, taurine, and creatine. The normalized fluctuations in concentrations of each are shown, with all exhibiting a reduction in concentration compared to the control cells (Figure 5-7 B). To analyse these changes in greater detail the multivariate analytical techniques PCA and PLS-DA were used (Appendix Figure 10-2 and Figure 5-8).

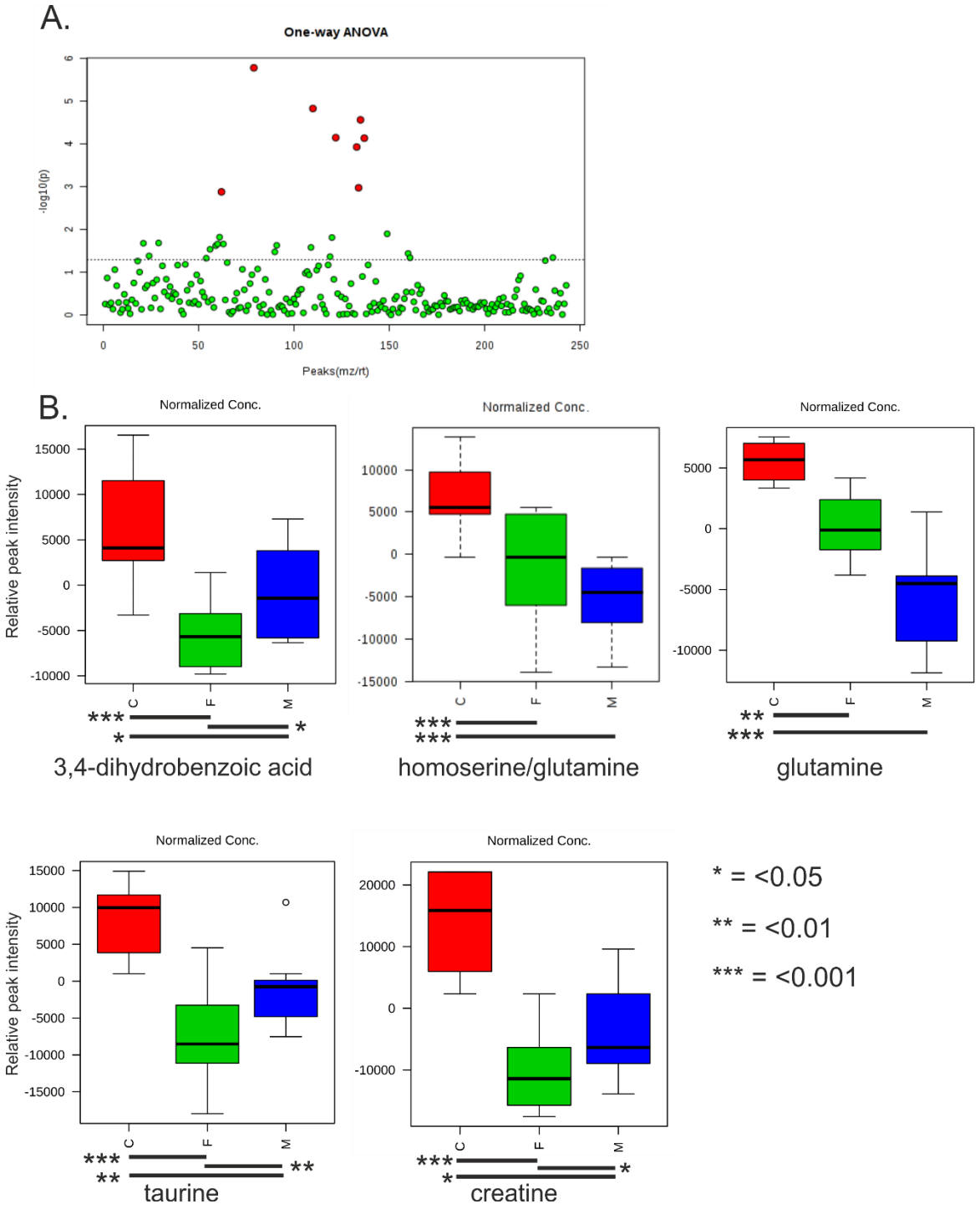

Figure 5-7 - ANOVA of the differential effects of aSyn monomers and fibrils on SH-SY5Y cells. *A one-way ANOVA (A) comparing the peak intensities of different metabolites in SH-SY5Y cells exposed to PBS alone, monomeric aSyn, and aSyn fibrils. Eight peaks corresponding to five different metabolites (dihydrobenzoic acid, homoserine, glutamine, taurine, and creatine) were found to be significantly different to the FDR-adjusted 0.05 significance level (red). The raw threshold is indicated by the dotted line. Box-and-whisker plots (B) are shown for the different metabolites and reflect the difference in concentration of each under the different conditions. Black lines and asterisks underneath each indicate significant differences between the conditions as determined by Fisher's LSD means comparison (* = <0.05, ** = <0.01, *** = <0.001).*

PLS-DA was carried out on the three conditions together, but pairwise comparisons were also made in a bid to identify key sources of variability. The PLS-DA of all three conditions was able to separate out the control samples from those exposed to aSyn, but struggled in distinguishing between those that had been exposed to monomeric aSyn or aSyn fibrils (Figure 5-8 A). The list of the forty metabolites contributing most to this variation are shown and those metabolites identified by ANOVA were also highlighted here, especially creatine (Figure 5-8 B). PLS-DA of just two samples at a time was better able to separate out the groups (Figure 5-8 C&E) and similarly highlighted 3,4-dihydrobenzoic acid, homoserine, glutamine, taurine, and creatine as metabolites of interest (Figure 5-8 D&F).

The findings here show that the exposure of the cells to the aSyn fibrils resulted in a reduction in the level of creatine. This is interesting given that creatine has reported neuroprotective properties, and may reflect that aSyn fibrils induce some level of bioenergetic stress (153,154). Taurine, which was also found at lower levels in those samples challenged with aSyn fibrils, is also neuroprotective and has been reported to lower neurotoxicity from Aβ (155). The reported gain in myoinositol (Figure 5-8 B,D,F) in the samples exposed to fibrils also fits with the available literature. An increase in myoinositol has been associated with AD and reported to precede amyloid pathology (156,157). Many of the metabolites observed to change here were also seen to change in the paper by *Phelan et al,* in which cells were challenged with aSyn or Aβ in different aggregation states (109). The fact that the same metabolites are reported here gives an indication that these differences are reproducible and serves as an extra layer of verification.

A.

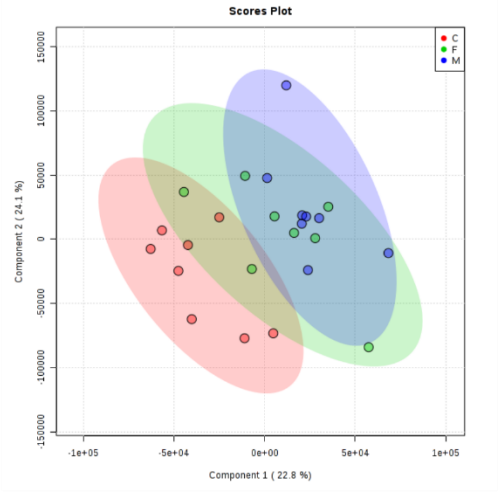
Scores Plot
C
F
M
Component 2 (24.1 %)
Component 1 (22.8 %)
-1e+05
-5e+04
0e+00
5e+04
1e+05
150000
100000
50000
0
-50000
-100000
-150000

B.

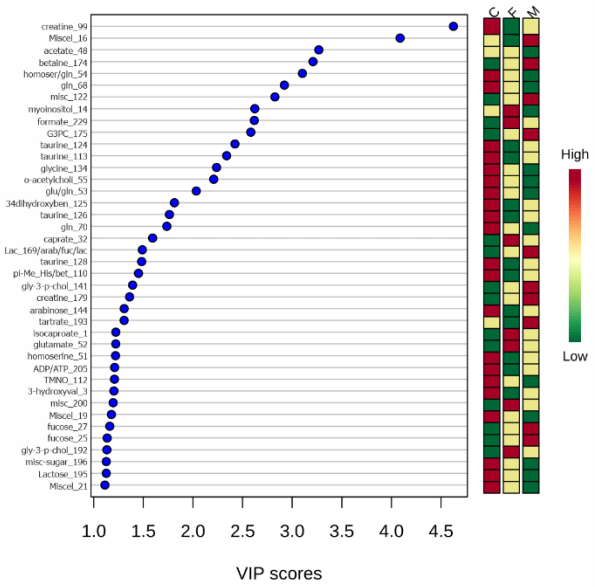
creatine_99
Miscel_16
acetate_48
betaine_174
homoser/gln_54
gln_68
misc_122
myoinositol_14
formate_229
G3PC_175
taurine_124
taurine_113
glycine_134
o-acetylcholi_55
glu/gln_53
34dlhydroxyben_125
taurine_126
gln_70
caprate_32
Lac_169/arab/fuc/lac
taurine_128
pi-Me_His/bet_110
gly-3-p-chol_141
creatine_179
arabinose_144
tartrate_193
isocaproate_1
glutamate_52
homoserine_51
ADP/ATP_205
TMNO_112
3-hydroxyval_3
misc_200
Miscel_19
fucose_27
fucose_25
gly-3-p-chol_192
misc-sugar_196
Lactose_195
Miscel_21
C
F
M
High
Low
1.0
1.5
2.0
2.5
3.0
3.5
4.0
4.5
VIP scores

C.

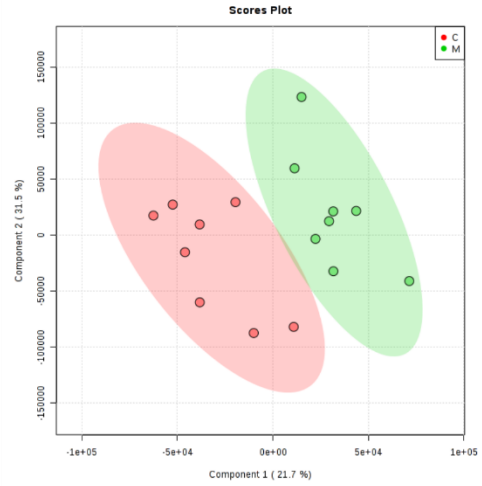
Scores Plot
C
M
Component 2 (31.5 %)
Component 1 (21.7 %)
-1e+05
-5e+04
0e+00
5e+04
1e+05
150000
100000
50000
0
-50000
-100000
-150000

D.

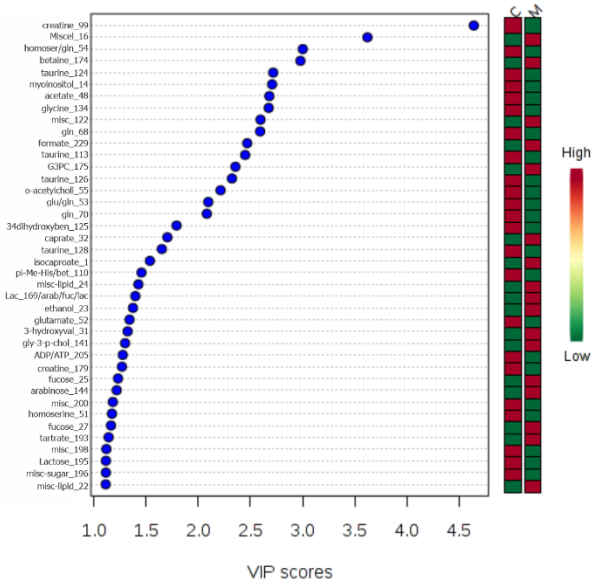
creatine_99
Miscel_16
homoser/gln_54
betaine_174
taurine_124
myoinositol_14
acetate_48
glycine_134
misc_122
gln_68
formate_229
taurine_113
G3PC_175
taurine_126
o-acetylcholi_55
glu/gln_53
gln_70
34dlhydroxyben_125
caprate_32
taurine_128
isocaproate_1
pi-Me-His/bet_110
misc-lipid_24
Lac_169/arab/fuc/lac
ethanol_23
glutamate_52
3-hydroxyval_31
gly-3-p-chol_141
ADP/ATP_205
creatine_179
fucose_25
arabinose_144
misc_200
homoserine_51
fucose_27
tartrate_193
misc_198
Lactose_195
misc-sugar_196
misc-lipid_22
C
M
High
Low
1.0
1.5
2.0
2.5
3.0
3.5
4.0
4.5
VIP scores

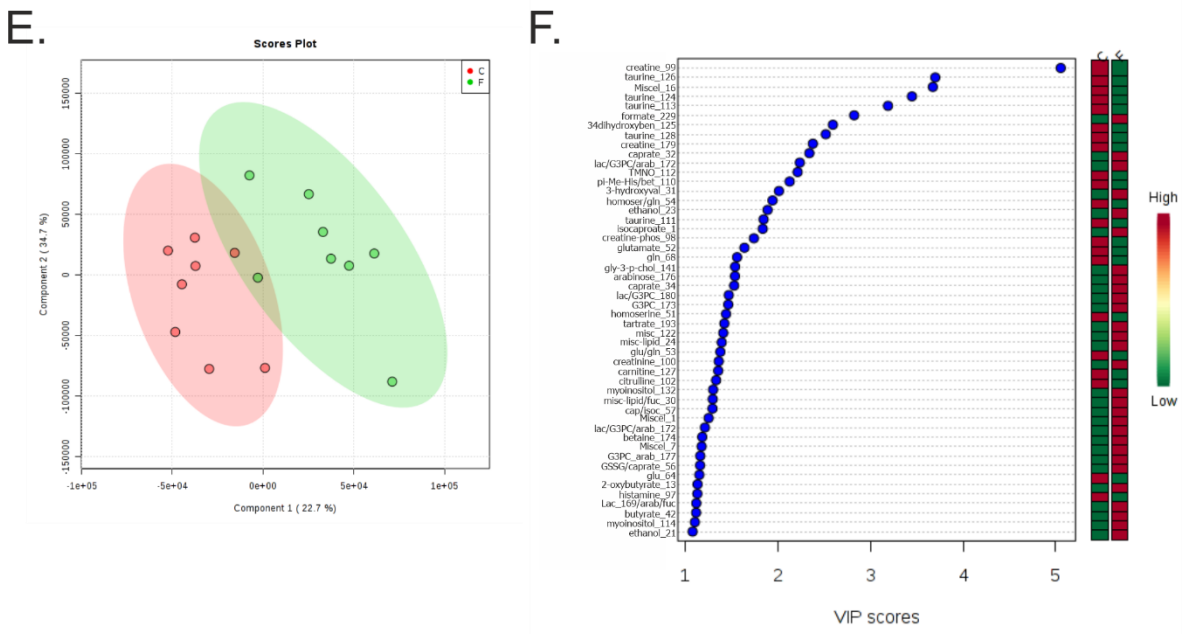

Figure 5-8 - PLS-DA of the differential effects of aSyn monomers and fibrils on SH-SY5Y cells. *The conditions of PBS alone (C), aSyn monomer alone (M), and aSyn fibrils alone (F) were compared. Scores plots of C compared to F and M (A), C compared to M (C), and C compared to F (E) are shown. Corresponding VIP tables are shown in (B), (D), and (F) respectively. These list the 40 metabolites that vary most across the conditions. Cross-validation was carried out for each. The R^2 and Q^2 scores for each are as follows: C vs F vs M (R^2 = 0.9058, Q^2= 0.6013 with 4 components), C vs M (R^2 = 0.9927, Q^2= 0.7082 with 5 components), and C vs F (R^2 = 0.9952, Q^2= 0.6327 with 5 components). F vs M was also carried out but is not shown here due to cross-validation suggesting that the results are the result of overfitting (R^2 = 0.9743, Q^2= 0.0236 with 5 components).*

5.3.2.3 The effect of KDGIVNGVKA on fibril toxicity

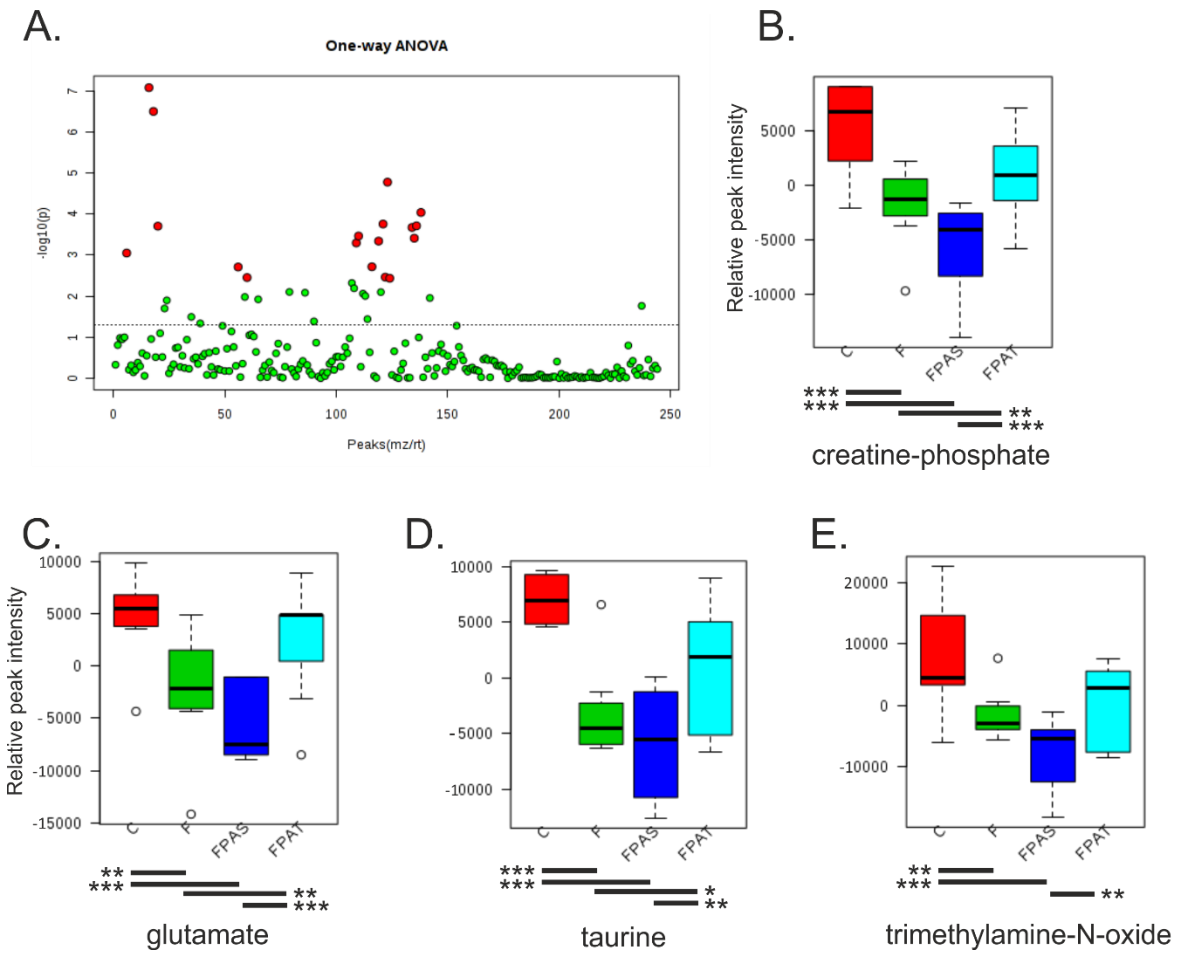

Figure 5-9 - ANOVA of the differential effects of aSyn fibrils on SH-SY5Y cells in the presence and absence of KDGIVNGVKA. *A one way ANOVA (A) in the peak intensities of different metabolites extracted from SH-SY5Y cells that had been exposed to PBS alone (C), fibrils alone (F), fibrils plus aged KDGIVNGVKA (formed together) (FPAT), and fibrils plus aged KDGIVNGVKA (formed separately) (FPAS). Multiple buckets were found to be significantly different across the conditions to the FDR-adjusted 0.05 cut-off (red). These buckets represent the metabolites creatine-phosphate, glumate, taurine, and trimethylamine-N-oxide. The dotted line represents the raw cut-off. Box-and-whisker plots are shown for the changes in concentration of creatine-phosphate (B), glutamate (C), taurine (D) and trimethylamine-N-oxide (E) in the four conditions. Black lines and asterisks underneath each indicate significant differences between the conditions as determined by Fisher's LSD means comparison (* = <0.05, ** = <0.01, *** = <0.001).*

The primary focus of the metabolomics study was whether the shortening of the amyloid fibrils as a result of the incubation of aSyn in the presence of the KDGIVNGVKA peptide significantly changed the metabolic profile of exposed SH-SY5Y cells relative to those exposed to fibrils alone. In the analyses conducted previously (4.3.5) the shortening of fibrils was seen in those samples of peptide and protein incubated together. However, it needed to be verified that any observed changes in the cellular metabolome were as a result of this shortening, and not as a result of the

cells simply being exposed to aged KDGIVNGVKA and fibrils at the same time. Thus, the metabolic profile of SH-SY5Y cells was compared for those which had been exposed to PBS alone (C), WT aSyn fibrils alone (F), WT aSyn fibrils that had been formed in the presence of KDGIVNGVKA (FPAT), and WT aSyn fibrils to which aged KDGIVNGVKA (FPAS) had been added.

A one-way ANOVA revealed significant differences in multiple bucket groups (down to the FDR-adjusted 0.05 level) between the conditions (Figure 5-9 A). These buckets corresponded to the metabolites creatine-phosphate, glutamate, taurine, and trimethylamine-N-oxide (Figure 5-9 B-E). To try and observe more subtle effects in the data PCA and PLS-DA were used. Unsupervised PCA did not show good clustering of the data (Appendix Figure 10-3), whilst through the supervised technique PLS-DA to compare pairs of sample conditions it was possible to achieve good separation and identify those metabolites varying the most across the conditions (Figure 5-10). Creatine and taurine were highlighted again here, and it is interesting that their levels are generally higher in the control samples and the FPAT samples than in the others. This suggests that the metabolome of the SH-SY5Y cells exposed to the shortened fibrils formed by aSyn in the presence of the KDGIVNGVKA peptide is more similar to the metabolome of the cells exposed to the PBS control and thus the peptide is mitigating the effects of aSyn. This is further backed up by the fact that the PLS-DA was able to separate C and FPAS (Figure 5-10 A) and FPAS and FPAT well (Figure 5-10 E), but was less successful with C and FPAT (Figure 5-10 C).

A.

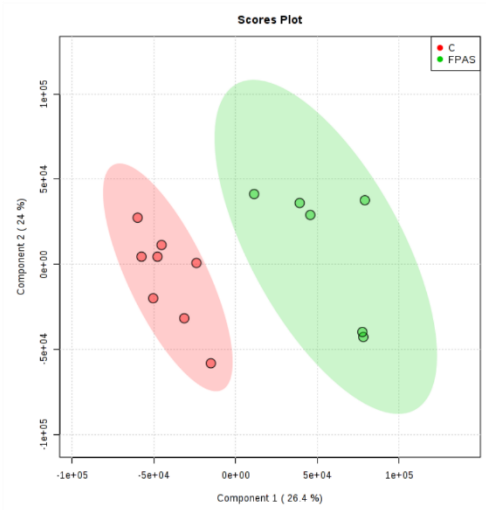
Scores Plot
C
FPAS
Component 2 (24 %)
Component 1 (26.4 %)

B.

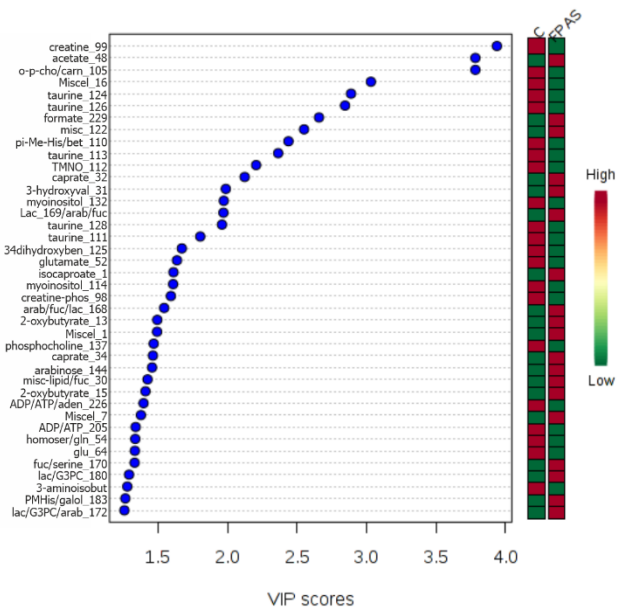
creatine_99
acetate_48
o-p-cho/carn_105
Miscel_16
taurine_124
taurine_126
formate_229
misc_122
pi-Me-His/bet_110
taurine_113
TMNO_112
caprate_32
3-hydroxyval_31
myoinositol_132
Lac_169/arab/fuc
taurine_128
taurine_111
34dihydroxyben_125
glutamate_52
isocaproate_1
myoinositol_114
creatine-phos_98
arab/fuc/lac_168
2-oxybutyrate_13
Miscel_1
phosphocholine_137
caprate_34
arabinose_144
misc-lipid/fuc_30
2-oxybutyrate_15
ADP/ATP/aden_226
Miscel_7
ADP/ATP_205
homoser/gln_54
glu_64
fuc/serine_170
lac/G3PC_180
3-aminoisobut
PMHis/galol_183
lac/G3PC/arab_172
C
FPAS
High
Low
VIP scores

C.

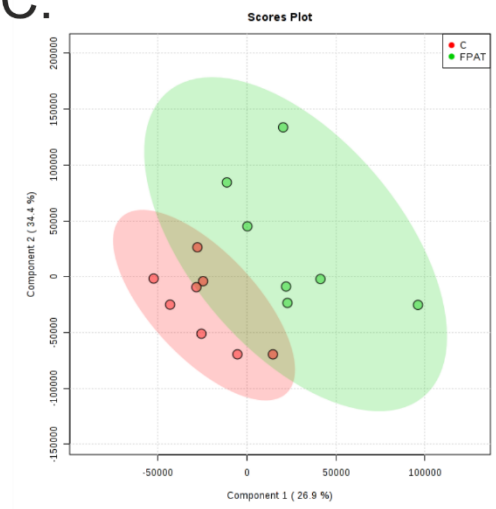
Scores Plot
C
FPAT
Component 2 (34.4 %)
Component 1 (26.9 %)

D.

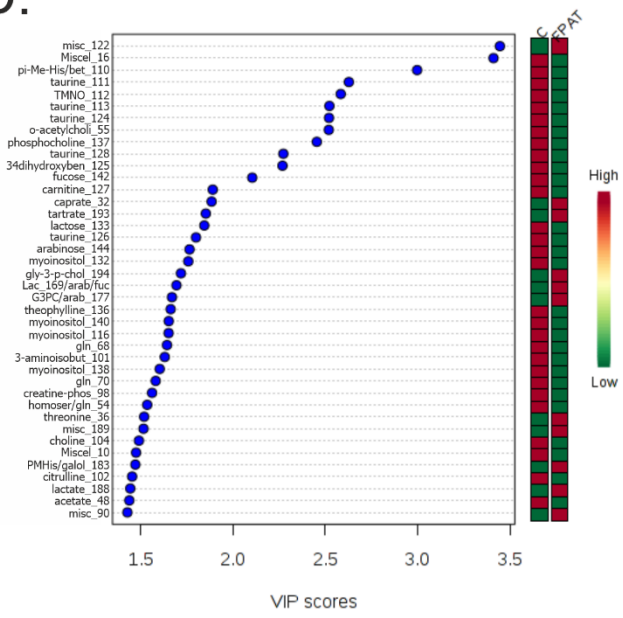
misc_122
Miscel_16
pi-Me-His/bet_110
taurine_111
TMNO_112
taurine_113
taurine_124
o-acetylcholi_55
phosphocholine_137
taurine_128
34dihydroxyben_125
fucose_142
carnitine_127
caprate_32
tartrate_193
lactose_133
taurine_126
arabinose_144
myoinositol_132
gly-3-p-chol_194
Lac_169/arab/fuc
G3PC/arab_177
theophylline_136
myoinositol_140
myoinositol_116
gln_68
3-aminoisobut_101
myoinositol_138
gln_70
creatine-phos_98
homoser/gln_54
threonine_36
misc_189
choline_104
Miscel_10
PMHis/galol_183
citrulline_102
lactate_188
acetate_48
misc_90
C
FPAT
High
Low
VIP scores

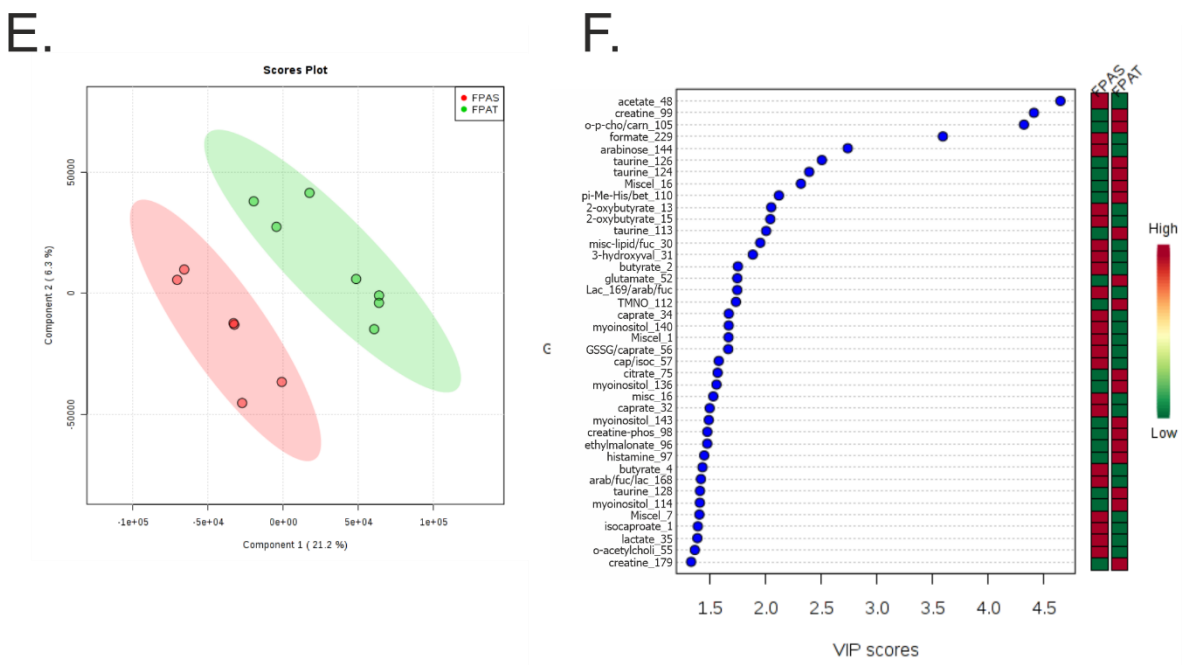

Figure 5-10 - PLS-DA of the differential effects of aSyn fibrils on SH-SY5Y cells in the presence and absence of KDGIVNGVKA. *PLS-DA was carried out on the following sample conditions: PBS alone (C), aSyn fibrils alone (F), aSyn fibrils that had been formed in the presence of the KDGIVNGVKA peptide (FPAT), and aSyn fibrils to which aged KDGIVNGVKA peptide had been added (FPAS). Scores plots of C compared to FPAS (A), C compared to FPAT (C), and FPAS compared to FPAT (E) are shown. VIP plots show the 40 metabolites that vary most in these conditions (B, D, and F). Cross-validation was carried out for each. The R^2 and Q^2 values for each are as follows: C vs FPAS (R^2 = 0.9696, Q^2 = 0.8523 with 3 components), C vs FPAT (R^2 = 0.9779, Q^2 = 0.5473 with 4 components)), and FPAS vs FPAT (R^2 = 0.9960, Q^2 = 0.6193 with 5 components).*

5.4 Discussion

In this chapter is described the results of the analysis of the data generated through NMR metabolomics experiments, conducted with the aim of shedding light on the mechanism(s) of action of the KDGIVNGVKA peptide inhibitor of aSyn aggregation. In their initial publication *Cheruvara et al* conducted cell viability assays suggesting that the KDGIVNGVKA peptide operated to reduce aSyn-mediated toxicity (108). Cell viability assays are relatively binary and so NMR metabolomics experiments were attempted here with the aim of trying to identify pathway-specific information and gain a greater understanding of how the peptide enacted its protective effects. Ten challenge conditions (see Table 5-2) were prepared based upon information gained in Chapter 4, such as fresh and aged KDGIVNGVKA peptide, and fibrils formed in the presence of the peptide which should thus be shortened compared to standard aSyn fibrils. Cell viability experiments using

these sample challenge conditions showed no loss in viability over a 24-hour window, meaning that any apparent differences across the samples were as a result of metabolic changes induced by the conditions and not due to cell death (Figure 5-3).

Previously our group has taken advantage of NMR metabolomics to observe differences in the metabolic profiles of SH-SY5Y cells that had been challenged with monomeric, oligomeric, or fibrillar aSyn (109). In this work it was seen that metabolites associated with oxidative stress and neurotoxicity exhibited changes. This study also meant that there was easy access to a pre-existing metabolite library and associated pattern file for SH-SY5Y cells. Changes in some of the metabolites seen in the paper by *Phelan et al* were similarly found here. In the conditions of F, FPAT, and FPAS differences in taurine, creatine, and trimethylamine-N-oxide were seen relative to the control (Figure 5-9). This is of interest as these metabolites have all been linked to neurodegeneration. Taurine has been reported to be neuroprotective, which is thought to be mediated through the activation of GABA receptors (155). Creatine has been seen to block the appearance of aSyn aggregates in MPTP models of PD and has been used in clinical trials (154,158). Trimethylamine-N-oxide has been reported by *Jamal et al* to promote compactness in peptides of aSyn which may be less aggregation-prone, and thus may be neuroprotective (159). In F and FPAS these metabolites were seen at lower levels compared to the control, whilst in the FPAT samples they were at levels more in-line with those in the control samples (Figure 5-9). This may be indicative of the KDGIVNGVKA peptide having a protective role, as in the FPAT samples cells have been challenged with the shortened fibrils that form in the presence of the peptide. By comparing those samples challenged with the peptide alone versus the control samples (P, PA vs C) it was ruled out that these observed differences were the direct result of the peptide and were instead the result of its effects on aSyn itself (Figure 5-6 & Appendix Figure 10-1).

There are, however, numerous drawbacks to this study that should be mentioned. Firstly, the model is not perfect. The addition of aSyn to cells is not a truly physiologically-relevant system

and any differences in the cellular metabolome of these samples may reflect more of a difference in the internalization of aSyn rather than a change in toxicity. Thus, although the FPAT samples are apparently more like the control samples this may merely reflect that the aSyn species are less able to enter the cells to cause damage. This seems unlikely, however, given that the aSyn species present in the FPAT samples should be smaller than in the F and FPAS samples, and thus if anything are probably better internalized than the others. Secondly, pathway-level detail of metabolites could not be obtained and this makes it challenging to draw concrete conclusions from the results of the experiment. It may have been the case that greater differences, and thus more information, could have been obtained had the cells been challenged with the sample conditions for a longer period of time. In this experiment the cells were challenged for just 24 hours, but 48 hours may have been more appropriate. Additionally, the data analysis was at times not straightforward. Part of this difficulty may have arisen as a result of the comparatively poor signal:noise seen for the samples as a result of the sample extraction procedure utilizing 50% methanol rather than acetonitrile, as used in the study by *Phelan et al* (109). The switch to methanol was carried out to allow the isolation of lipidic metabolites subsequent to the extraction of the polar molecules. This lipidomics analysis was ultimately not carried out due to time constraints. It's possible that the use of acetonitrile would have led to improved signal:noise to the point that more interesting features in the data were observable. It is also possible that had the lipidomics work been undertaken that this would have complemented the polar metabolomics and revealed other interesting findings. Both of these are possibilities for any wishing to work on this project in the future.

6 The effect of pathogenic mutations and post-translational modifications on α-synuclein aggregation and lipid-interactions

6.1 Introduction

6.1.1 Point mutations in α-synuclein

As stated earlier in 1.7.1.2 there are six point mutations in the aSyn protein sequence which have been identified as causing hereditary forms of PD (Table 6-1). The different mutations, despite their close proximity (Figure 6-1), can have quite radically different effects on pathology (e.g. early-onset vs late-onset). The effects of these mutations have been characterized to varying extents, and thus one of the aims of this chapter has been to carry out experiments on each under identical conditions and at the same time. This is to both tread new ground and to perhaps help resolve some of the controversies that currently exist in the literature regarding these mutants.

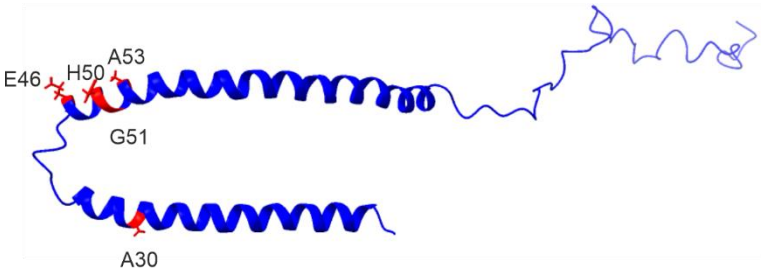

Figure 6-1 - Micelle-bound aSyn with highlighted PD-linked mutation sites. *Solution NMR structure of WT aSyn bound to a sodium dodecyl sulfate (SDS) micelle (PDB: 1XQ8)* (30)*. The broken α-helix lies across the surface of the micelle and is made up of residues (3-37 and 45-92), meaning much of the NTD (1-60) and the NAC region (61-95) are involved. The residues highlighted in red mark the sites of the PD-linked point mutations in aSyn studied in this chapter (A30P, E46K, H50Q, G51D, A53T, and A53E).*

Table 6-1 - List of PD-linked point mutations in aSyn and their features. *Listed include the year of discovery, the apparent time at which PD is diagnosed, the reported effect (if any) on the ability of aSyn to bind to lipid membranes, and the effect of the mutations on the rate of aSyn's aggregation.*

Mutation	Discovered	Time of onset (visibly)	Effect on membrane binding	Effect on aggregation
A30P	1998 (75)	Early-onset. Observed as early as 56 years of age (75).	Perturbs membrane interactions. Exhibits disrupted N-terminal helix formation (160).	Reported to accelerate aggregation compared to WT (78).
E46K	2004 (76)	Early-onset. Observed as early as 50 years of age (76).	Reportedly results in stronger affinity for membranes and the extension of the helix-forming region of the N-terminal (160,161).	Reported to accelerate aggregation compared to WT (161).
H50Q	2013 (49,162)	Late-onset (49,162).	No impact (163).	Increased rate of aggregation compared to WT (163,164).
G51D	2013 (50)	Early-onset. Observed as early as 19 years of age (50,165).	Exhibits impaired membrane association (79,125).	Reduced rate of aggregation. Persists in an oligomeric state for a longer period (125,166).
A53T	1997 (58)	Early-onset (58).	No impact (160).	Accelerated rate of aggregation compared to WT (78,167).
A53E	2014 (77)	Early-onset. Onset at 36 years-old has been reported (77).	Not reported.	Reduces rate of aggregation (168).

6.1.2 Post-translational modifications and α-synuclein

Post-translational modifications (PTMs) to proteins are a major component of biochemistry and molecular biology. They can be the result of controlled processes, or aberrant indicators of disease. These modifications can be essential for the functioning of a protein, or they may play a

role in the mediation of cell signalling pathways. With respect to aSyn multiple PTMs are known to play roles in its physiology and pathophysiology. These include phosphorylation, nitration, ubiquitination, and acetylation (53,55,169,170). This chapter is aimed at investigating the role of tyrosine nitration in aSyn aggregation and its effect on the lipid-binding properties of the protein. This PTM was of interest partially because of its poor characterization with respect to aSyn, and especially its effect on PD-linked mutants.

6.1.2.1 Tyrosine nitration

The nitration of L-tyrosine to form 3-nitro-L-tyrosine is one of many PTMs that can take place within the body (Figure 6-2). It is particularly associated with neurodegenerative disease because of the close link between neurodegeneration and oxidative stress (171,172); nitration itself is carried out by peroxynitrite ($ONOO^-$) which is formed from the reaction of superoxide ($O_2^{\bullet -}$) and nitric oxide ($NO^\bullet$), both of which are indicative of cellular oxidative/nitrative stress. It is of interest to me in this study because nitrated aSyn is present at elevated levels in Lewy bodies (53). It has also been reported that the nitration/oxidation of aSyn through exposure to peroxynitrite can lead to the cross-linking of tyrosine residues to form dityrosine, and that this results in the formation of stable higher-order aSyn species (173). Additionally, it has been shown that nitration can impede aSyn's ability to associate with lipid membranes – presumably through nitration of Y39 which is the only tyrosine found within the lipid-binding region – but this has not been covered in any substantial detail for the PD-linked mutations described in 6.1.1 (174).

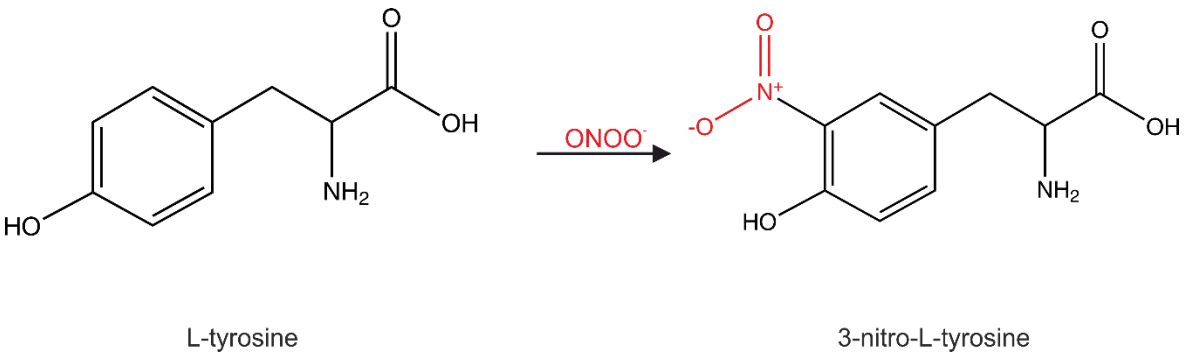

Figure 6-2 - Schematic showing the formation of 3-nitro-L-tyrosine. *3-nitro-L-tyrosine is formed from L-tyrosine by peroxynitrite ($ONOO^-$), which is a powerful oxidizing agent formed under conditions of oxidative stress.*

6.1.3 Lipid-binding and α-synuclein

As discussed in 1.5.1 and 1.5.2 aSyn binds to lipid-membranes via its NTD. In doing so the NTD forms an amphipathic helix that lies across the surface of the membrane (or membrane-mimetic) (Figure 6-3) (30). The precise role of this interaction in the native function of aSyn remains elusive, but appears closely linked to the maintenance of the "reserve-pool" of synaptic vesicles, and also in the promotion of SNARE-complex formation that facilitates the docking and fusion of synaptic vesicles to the presynaptic membrane (26,47). Synaptic vesicles are small, tightly-rounded and contain negatively-charged lipid headgroups, such as phosphatidylserine (175). This is thought to be why the NTD of aSyn contains such a high proportion of residues with positively-charged sidechains. More recently, *Fusco et al* have shown the involvement of two other regions in aSyn's lipid-binding behaviour (36). They showed by NMR that residues 1-25 form a helix that serves as a lipid-anchor, whilst residues 26-97 interact with the membrane more transiently to serve as a lipid sensor. They also showed weak interactions from the highly dynamic CTD of aSyn. Together they report that the regions allow aSyn to bind to multiple synaptic vesicles and promote synaptic vesicle clustering (36,37).

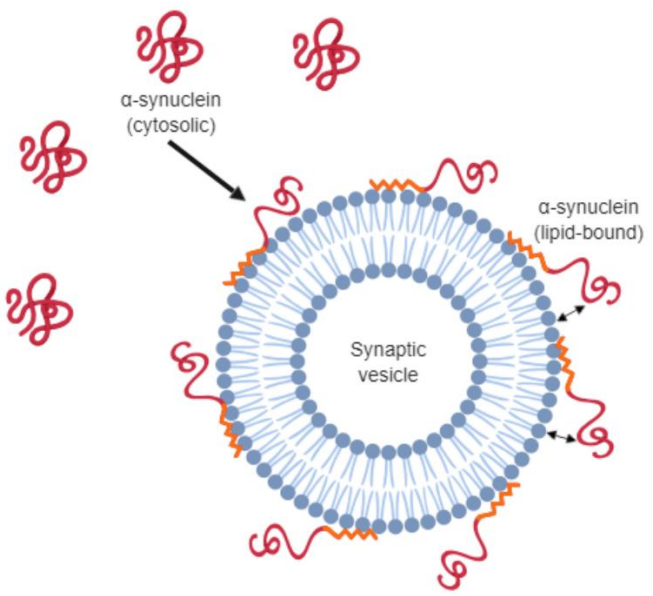

Figure 6-3 - Schematic showing the binding of aSyn to synaptic vesicles. *Cytosolic aSyn protein exists as a disordered monomer, but has an affinity for tigtly-curved lipid bilayers containing negatively-charged lipid headgroups; properties exhibited by synaptic vesicles. In the presence of the vesicles the N-terminal portion of the protein forms a helix that lies across the surface of the bilayer, whilst the CTD remains disordered and only weakly interacts with the membrane* (36).

The relationship between aSyn aggregation and lipid-interactions is unclear. It has been shown that the association of aSyn and lipid bilayers promote primary nucleation, which is the ultimate rate-limiting step in amyloid formation (176). This is likely due to the reduced dimensionality and conformational space available when the protein is attached to the membrane. However, a reduced affinity for lipid bilayers – caused by mutations or PTMs – would presumably result in an increased supply of cytosolic aSyn (177). This, too, could encourage or prevent protein aggregation. The influence of lipids on the aggregation of aSyn is dependent on a number of factors, including the size, curvature and composition of the lipid membranes in question, and on the total amount of aSyn in the cell and the proportion of this which is lipid-bound (178).

6.1.4 Aims

In the body of work encompassing this chapter the differential effects of the PD-linked mutants and tyrosine nitration on membrane-affinity and the rate of aggregation of aSyn are explored using a combination of CD spectroscopy, TEM, and ThT fluorescence. The pathological relevance of these modifications is well known, but has not been explored in a systematic manner

and thus many gaps exist in the literature (53,166,167). Large quantities of each of the PD-linked mutants were expressed and purified for use in these studies, and tyrosine nitration was performed using peroxynitrite produced in-house. This allowed for a comprehensive and systematic study of the properties of each of the mutants under identical conditions at the same time.

6.2 Methods

6.2.1 Preparation of peroxynitrite

Peroxynitrite was prepared using the procedure first described by Hughes and Nicklin (179). To a 50mL ice-cold and stirring mixture of 50mM sodium nitrite and 50mM hydrogen peroxide 25mL of 1M HCl was added. Immediately thereafter, 25mL of 1.5M NaOH was added to the mixture to stabilize the formed peroxynitrite.

6.2.2 Nitration of α-synuclein by peroxynitrite

Lyophilized aSyn was reconstituted in nitration buffer (100mM potassium phosphate pH 7.4, 25mM $NaHCO_3$, 0.1mM diethylenetriaminepentaacetic acid (DEPA)) to facilitate the nitration of the protein by peroxynitrite. Freshly prepared peroxynitrite was added to the protein samples at approximately a 100-fold excess. Confirmation of the success of nitration was inferred by dot blot and by measuring the absorbance at 430nm. The protein solution also takes on a yellow tinge.

6.2.3 Confirmation of nitration by dot blot

Nitrated WT and mutant (A30P, E46K, H50Q, G51D, A53T and A53E) forms of aSyn were prepared to a final concentration of 100µM as determined by A_{280} in nitration buffer. 5µL of each was pipetted as a small spot onto a strip of nitrocellulose membrane. The spots were allowed to air-dry and then a further 5µL of sample was pipetted on top. This was then also allowed to air-dry. The membrane was blocked through incubation for 1hr in 5% bovine serum albumin (BSA) in

phosphate buffered saline with Tween 20 (PBS/T) at room temperature (RT). The membrane was then incubated with an anti-3-nitrotyrosine primary antibody produced in mice (Sigma) at a 1 in 2,000 dilution for 1hr at room temperature. The membrane was then washed for 3x 10mins in PBS/T. The membrane was then incubated with the goat anti-mouse secondary antibody conjugated to alkaline phosphatase at a 1 in 10,000 dilution for 30mins. The membranes were then washed with PBS/T for 3x 10mins. Dots were visualized using SIGMAFAST™ Fast Red TR/Naphthol AS-MX tablet kit according to the manufacturer's instructions.

6.2.4 Confirmation of nitration by measuring A_{430}

2µL of sample was loaded onto a NanoDrop 2000 spectrophotometer (Thermo Scientific) that had been pre-blanked with buffer. The absorbance of the sample at 430nm was recorded.

6.2.5 Native-PAGE of nitrated and non-nitrated α-synuclein

Nitrated and non-nitrated aSyn (WT, A30P, E46K, H50Q, G51D, A53T and A53E) was prepared as previously described, and buffer exchanged into ddH_2O and lyophilized. This was then resuspended in PBS pH 7.4 to a final concentration of 100µM. Native PAGE gels, loading and running buffer were prepared as described here (180). 12µL of sample was loaded per well and the gels were run at 100V at 4°C for 4 hours. Bands were visualized using Coomassie blue.

6.2.6 Cell viability experiments with nitrated and non-nitrated α-synuclein

Both nitrated and non-nitrated forms of aSyn (WT, A30P, E46K, H50Q, G51D, A53T and A53E) were prepared as previously described. 100µM samples were prepared in PBS pH 7.4 and. 100µL aliquots were taken and snap frozen in LN_2 at different time points: day 0, day 3 and day 7. SH-SY5Y neuroblastoma cells were grown up in F-12 Ham's media supplemented with 1x MEM, 10% FBS and 1% Pen-Strep. 5,000 cells in 100µL were added to each well used in a 96-well plate. After

24 hours 5µL of protein aliquot was added per well, with each condition having 6 repeats. PBS alone and 1% triton X-100 prepared in PBS pH 7.4 were used as “live” and “dead” cell controls, respectively. The cells were left for 24 hours before 10µL of CCK-8 reagent (Dojindo) was added to each well. After this, the absorbance at 450nm was measured per hour for 4 hours on a FlexStation 3 (Molecular devices). Data was processed and analyzed using OriginLab.

6.2.7 Preparation of small unilamellar vesicles

Small unilamellar vesicles (SUVs) containing 1,2-dioleoyl-sn-glycero-3-phosphoethanolamine (DOPE), 1,2-dioleoyl-sn-glycero-3-phospho-L-serine (DOPS), and 1,2-dioleoyl-sn-glycero-3-phosphocholine (DOPC) were prepared using Coagulation Reagent I at a 5:3:2 ratio of DOPE:DOPS:DOPC (Avanti Lipids, USA). The chloroform solvent was evaporated away under a stream of nitrogen and the lipid residue was resuspended in nitration buffer to 10mg/mL. The SUVs were formed through sonication on ice with a fine probe head using three cycles of 1 minute “on, 1 minute “off”.

6.2.8 Circular dichroism analysis of secondary structure

CD measurements were performed using a Jasco J-1100 spectrometer. The cell used was a Quartz SUPRASIL cell (Hellma) with a 0.2mm path length. Measurements were collected between 260 and 180nm at a temperature of 25°C with 3 accumulations. The DIT was set to 1s, the scan speed to 50nm/min and the data pitch to 1nm. 60µL samples were pipetted between the plates of the cell with care taken to avoid large bubbles. Nitrated and non-nitrated forms of aSyn (WT, A30P, E46K, H50Q, G51D, A53T and A53E) were freshly prepared as previously described in nitration buffer. For the experiments with SDS micelles the protein was diluted in buffer to achieve a final concentration of 50µM. 10mM SDS micelles were prepared by dissolving SDS powder in 1mL of nitration buffer to prepare a 0.25M stock solution. Prior to use this stock was warmed to 40°C to ensure the SDS was fully solubilized and this was added directly to the protein sample, such that

the final concentration of SDS and protein was 10mM and 50μM respectively. For the experiments with the lipid SUVs the final protein concentration used was 10μM (0.14mg/mL). The SUVs (prepared as described in 6.2.7), were added to the sample such that the lipid concentration was 1.4mg/mL. Data were processed using Microsoft Excel and OriginLab. The baseline contribution from the buffer or buffer plus SDS micelles/lipid SUVs was subtracted and the 260nm region adjusted to zero. Secondary structure content predictions were made using the BeStSel prediction server (181,182). The secondary structure content predictions were based upon the 190-250nm portion of the CD spectrum. The 180-190nm portion was not used for secondary structure deconvolution due to the high-tension (HT) often rising above 500V and leading to excessive noise in this region of the CD spectra.

6.2.9 ThT analysis of the aggregation of Parkinson's-linked α-synuclein mutants

Unless otherwise explicitly stated, samples of 500μL aSyn (WT, A30P, E46K, H50Q, G51D, A53T and A53E) were prepared in PBS pH 7.4 at a concentration of 100μM. Each of these tubes was incubated at 37°C with agitation for 1 week. Samples were taken and used for endpoint fluorescence measurements on a Flexstation 3 microplate reader (Molecular Devices). Samples were measured in triplicate and the final volume in each well was 50μL. The 50μL was made up using 25μL of sample and 25μL of buffer with 2μM ThT. λ_{ex} = 440nm and λ_{em} = 490nm. Data was processed and analysed using OriginLab. Lag times were estimated from the time at which fluorescence began to climb as signal saturation prevented the use of sigmoidal fitting functions to determine the halfway point.

6.2.10 TEM analysis of the aggregation of Parkinson's-linked α-synuclein mutants

5µL of each sample as used for the ThT assay was mounted onto a carbon-coated copper grid for 2mins. The grid was then gently blotted onto a piece of filter paper to remove excess liquid before applying 4% (w/v) uranyl acetate for 30s. Uranyl acetate was removed and the grid dried by blotting onto a piece of filter paper. Images were collected on a 120kV Tecnai G2 Spirit BioTWIN electron microscope (FEI) with a SIS Megaview III camera. Image and fibril length analysis was carried out using ImageJ and OriginLab (183).

6.2.11 ThT analysis of the aggregation of nitrated α-synuclein

Nitrated and non-nitrated WT aSyn were prepared as previously described and both were lyophilized. The lyophilized protein was resuspended in PBS pH 7.4 to a concentration of 345µM. The nitrated and non-nitrated protein were loaded into wells on a 96-well plate. Each well contained a final volume of 100µL with 2µM ThT. The plate was incubated at 37°C with agitation. λ_{ex} = 440nm and λ_{em} = 490nm. The protein concentration was chosen at the time because I was trialling conditions for another experiment (small-angle X-ray scattering) that ultimately was not possible.

6.3 Results

6.3.1 TEM analysis of the aggregation of α-synuclein Parkinson's-linked mutants

The ability to successfully express and purify each of these forms of aSyn has already been confirmed in section 3.3.1. The PD-linked aSyn mutants have been discovered over the course of the past 20 years, and thus this represents a hitherto unseen systematic study of the mutants under identical conditions. By TEM WT and each of the recombinantly-produced forms of aSyn associated with PD are seen to be fully capable of forming amyloid fibrils *in vitro* (Figure 6-4A-G). The distribution of the lengths of fibrils formed is shown in Figure 6-5. Broadly, the TEM data shows that the synucleins can be split into two groups: those that generally form long (>300nm), straight fibrils,

and those that are more inclined to form shorter and more heterogenous fibrils (Figure 6-5H). The latter group consists of G51D and A53E, whilst the former group is all of the others. Intriguingly, these are the most recently discovered of the PD-mutants and thus least characterized. G51D is thought to persist in an oligomeric state for longer (125), which may explain the presence of fewer fibrils, whilst A53E forms lots of fibrils, but many of these are sub-200nm. A30P is exceptional in that although it typically forms long, straight fibrils those >1000nm in length constitute nearly half of all those measured, with very few fibrils under 200nm seen at all (Figure 6-5 B).

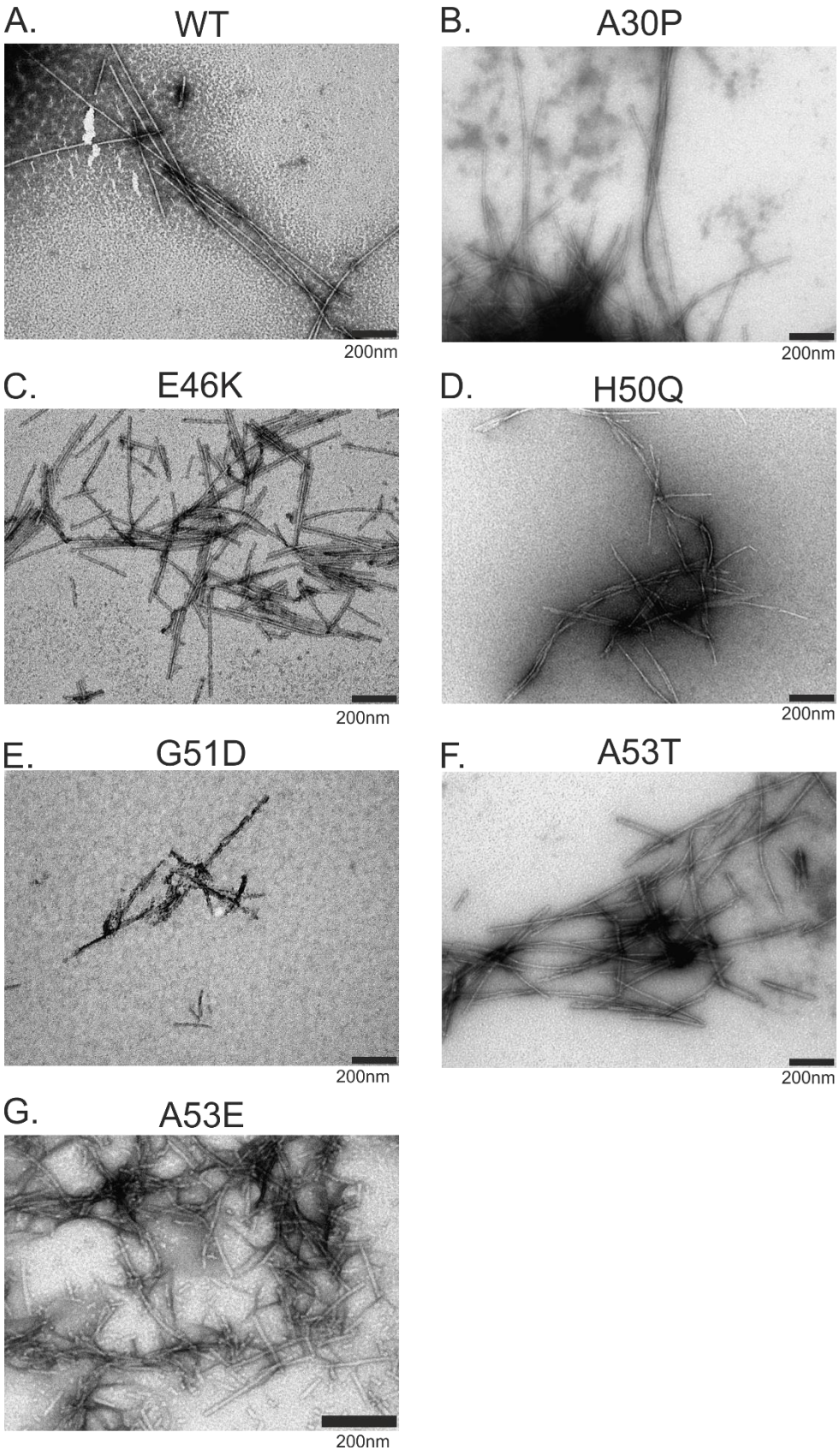

Figure 6-4 - TEM images of WT aSyn and each of the PD-linked mutants. *Each protein was prepared to 100μM in PBS pH 7.4 and incubated at 37°C with agitation for 1 week. The samples (WT (A), A30P (B), E46K (C), H50Q (D), G51D (E), A53T (F) and A53E (G)) were negatively stained with 4% uranyl acetate. Scale bars are 200nm in length.*

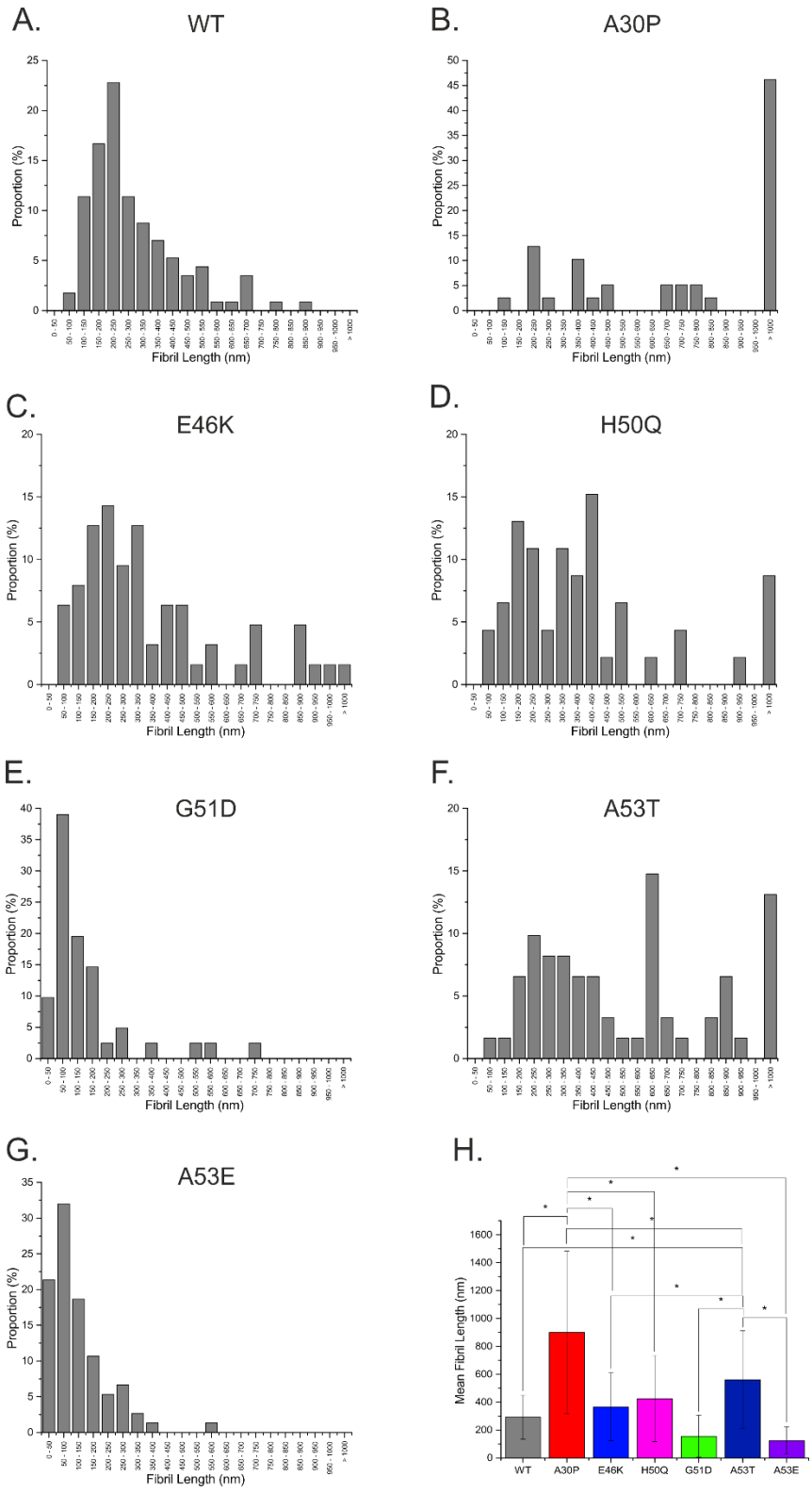

Figure 6-5 - Fibril lengths analysis of the fibrils formed by WT aSyn and each of the PD-linked mutants. *Each protein was prepared to 100µM in PBS pH 7.4 and incubated at 37°C with agitation for 1 week. Images were collected of the fibrils mounted on carbon-coated copper grids and negatively-stained using 4% uranyl acetate. The fibril lengths distributions are shown for: WT (A), A30P (B), E46K (C), H50Q (D), G51D (E), A53T (F) and A53E (G). The lengths were measured using ImageJ* (183)*. The mean fibril lengths for each are shown (H) and the statistical significance of the differences were determined by ANOVA with Bonferroni post-hoc analysis. Asterisks indicate the p-value <0.05. The number of measurements used for each lengths analysis is as follows: WT (114), A30P (39), E46K (63), H50Q (46), G51D (41), A53T (61), and A53E (75).*

6.3.2 ThT analysis of the aggregation of α-synuclein Parkinson's-linked mutants

To analyse the effect of the point mutations on the aggregation propensity of aSyn, ThT fluorescence assays were carried out. The assay was poorly reproducible, despite setting up wells in triplicate and running the experiment multiple times on several plates with different batches of protein and freshly prepared stocks of ThT. As a consequence of this poor reproducibility the errors are quite large and the n-number is different for some of the proteins (Figure 6-6). Some measurements were not included in the analysis due to their being clearly anomalous (either not aggregating at all or appearing saturated). Additionally, it was not possible to determine the lag times by fitting the curves to the Boltzmann function – as would be done under ideal circumstances – because the top of the curves for many of the measurements was not reached before the detector reached saturation. This is probably a result of the relatively high (100µM) protein concentration used, yet a high concentration of protein must be used to ensure that the protein is capable of aggregating within a reasonable timeframe. Thus, the lag time was estimated manually as the point at which the ThT fluorescence rose above the baseline for each sample. The data is summarized in Figure 6-6. It is noteworthy that A53T appears to have the shortest lag time of all the mutants, whilst A30P appeared to have the longest lag time. This is unsurprising given the previously reported rapid aggregation of A53T, but the A30P result is more unexpected (167). This is doubly interesting given its seeming propensity to form the longest fibrils (Figure 6-5 B). All of the other aSyn variants are within the same general range of ~20hours.

The results are extremely variable, and this is likely because the rate of aggregation can be dramatically affected by the presence of any seeds (oligomers). Given that these species exist in equilibrium with monomeric protein it is impossible to remove them, and thus obtaining truly homogenous stating samples is not feasible despite treatment with HFIP. It is worth highlighting that Figure 6-6B shows that despite the variation there are clear clusters for many of the variants.

This presumably reflects batch-to-batch variation in the number of seeds/oligomers present at the start of the experiment or slight variations in concentration .The introduction of a set starting quantity of seeds was not desirable as this would eliminate any effort to probe the propensity of the aSyn variants to seed their own aggregation.

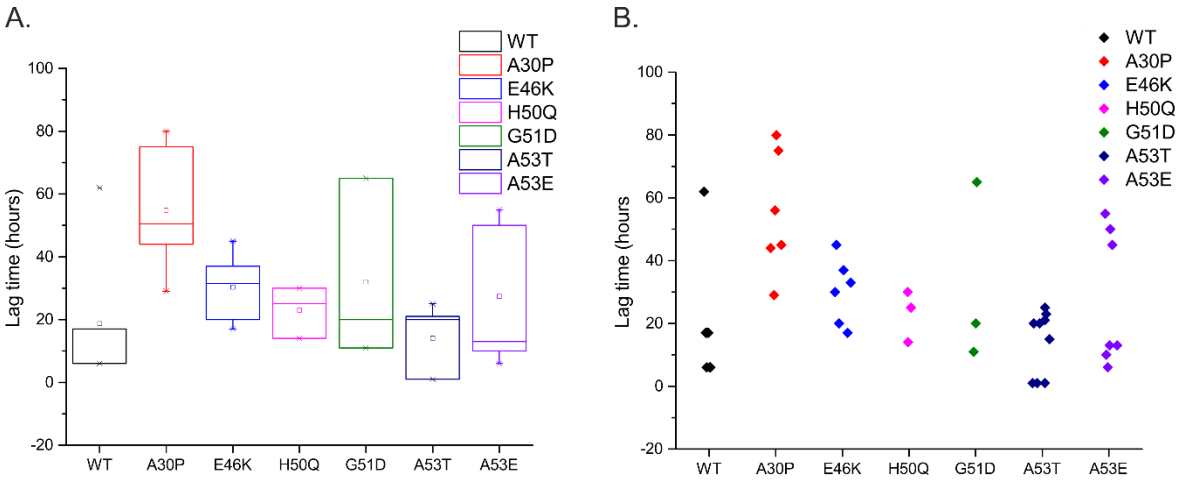

Figure 6-6 – Aggregation lag times for WT and PD-linked aSyn variants, as measured by ThT fluorescence. *A box-and-whisker plot (A) shows the variation in the data. The upper and lower limits of the boxes indicate the 25th and 75th percentiles of the data, whilst the horizontal line and small square indicate the median and mean respectively. The "whiskers" indicate the 5th and 95th percentile range of the data. A column scatter plot (B) shows the individual lag time datapoints. The data is variable overall, but seems prone to clustering around particular timepoints. This may reflect batch-to-batch variation or errors associated with a particular experiment. The samples consisted of 100μM protein in PBS pH 7.4. The plates were incubated at 37°C for 1 week with agitation and the fluorescence measurements recorded every five minutes (λ_{ex} = 440nm, λ_{em} = 490nm). Wells were set up in triplicate, and the experiment was run on three occasions (n=3). The number of data points for each are as follows: WT (7), A30P (6), E46K (6), H50Q (3), G51D (3), A53T (9), and A53E (7).*

6.3.3 Circular dichroism analysis of the variation in lipid-affinity between α-synuclein mutants

CD spectroscopy is a powerful "soft" biophysical technique used to probe protein secondary structure. As mentioned previously and shown in Figure 6-3, aSyn forms a helix in the presence of a membrane (or membrane mimetic), which enables the use of CD spectra to effectively report on the structural changes occurring upon membrane binding (30). Measurements were carried out on protein alone, protein plus SDS micelles, and protein plus SUVs (DOPE:DOPS:DOPE 5:3:2). SDS micelles were used as a membrane-mimetic and because these had been used in solving

the NMR solution structure (PDB: 1XQ8) (30). The SUVs of DOPE:DOPS:DOPE were used as a mimic of synaptic vesicles as has been established elsewhere in the literature (36). The experimental conditions for the measurements using the SDS micelles and the SUVs were slightly different; this was a reflection of physical necessity. The critical micelle concentration (CMC) of SDS is 6-8mM at 25°C, and thus in order to form the SDS micelles needed for this experiment the concentration of SDS must be above 8mM. The SUVs were utilized at a concentration of 1.4mg/mL in the presence of just 10μM (0.14mg/mL) protein. This was a compromise to minimize light scattering from the SUVs that would render the spectra noisy, whilst also providing a sufficient excess of lipid to protein. It is a consequence of the light scattering from the SUVs, and to a lesser extent the SDS micelles, that the normalized root mean square deviation (NRMSD) – a measure of the "goodness of fit" between the experimental data and the calculated spectrum – is greater for those samples. This means that there is greater error associated with those samples than for the samples of protein alone. Lower NRMSD values are therefore more desirable, however a perfect fit is unlikely to ever be reached and thus the calculated values for secondary structure content in CD are rarely completely accurate. Due to the possibility of noise and the fact that the secondary structure deconvolution software operates by looking for 'key' indicative features (e.g. negative peak at 222nm for α-helices), the percentage secondary structure values should be taken with a pinch of salt and an awareness that the spectra can be over-interpreted by the software. This is especially true for β-sheet elements, which exhibit a large degree of heterogeneity from structure-to-structure. BeStSel, the software used in this analysis, shows greater care with β-structural elements and takes this heterogeneity into account, however no approach is likely to be perfect

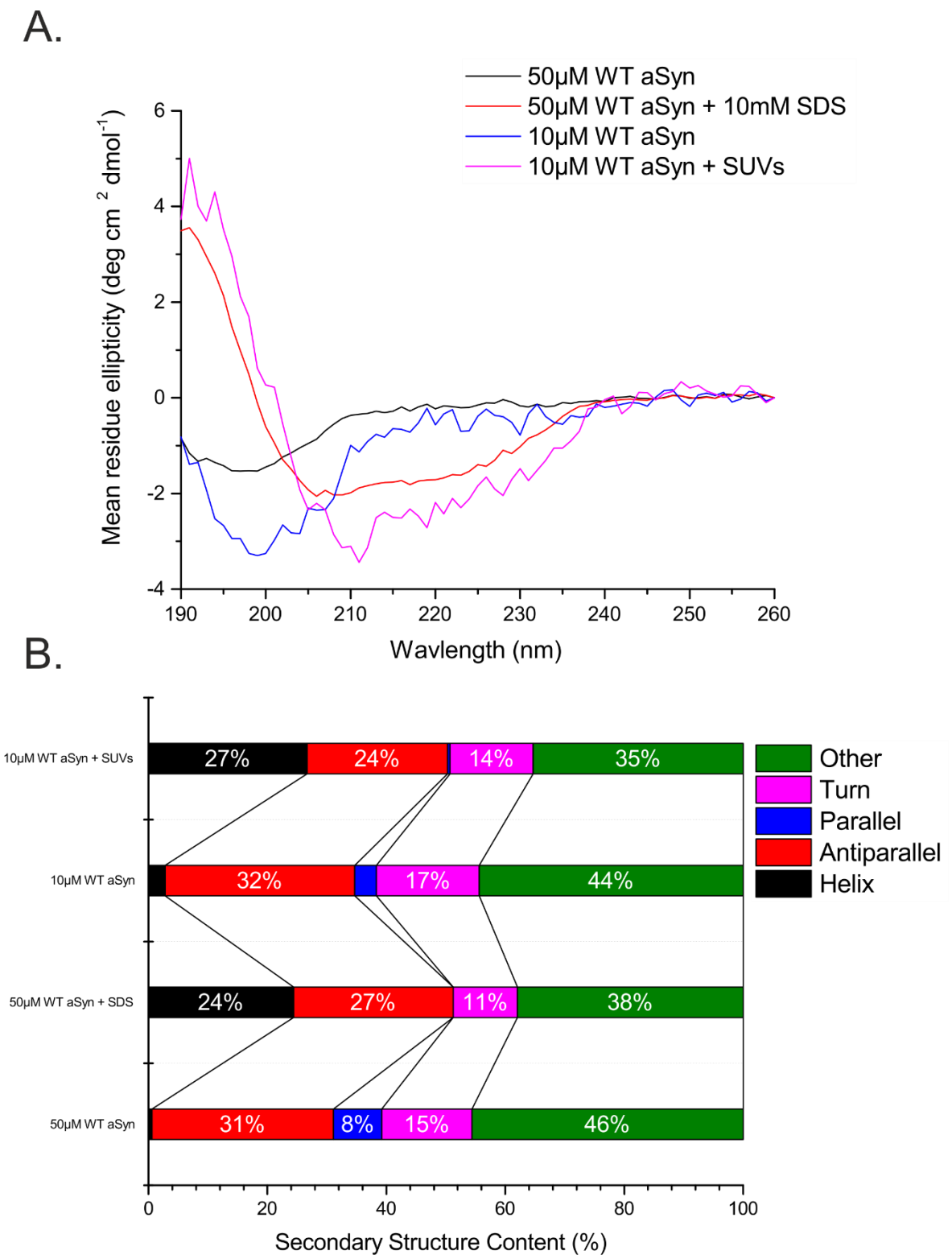

Figure 6-7 - CD spectra and estimations of secondary structural content of WT aSyn alone, in the presence of SDS micelles, and in the presence of SUVs. *CD spectra (A) of 50μM WT aSyn alone, of 50μM WT aSyn with 10mM SDS, of 10μM WT aSyn, and of 10μM WT aSyn with 1.4mg/mL SUVs (DOPE:DOPS:DOPC 5:3:2). Secondary structural content estimations (B) were carried out using BeStSel* (181,182). *As expected WT aSyn alone exhibits little helical content, but this rises significantly in the presence of SDS micelles or SUVs. This comes at the expense of the proportion in random coil ("other") conformation. The normalized root mean square deviation (NRMSD) values are 0.03314, 0.00771, 0.04622, and 0.02811 for the samples of 50μM WT alone, with SDS, 10μM WT aSyn alone and with SUVs respectively.*

Representative CD data (for the WT protein) is shown (Figure 6-7). Note, the helicity increases (as expected) in the presence of both SDS micelles and lipid SUVs. This comes largely at the expense of the proportion of random coil. In both conditions the level of helicity is similar, suggesting comparable affinity (Figure 6-7 B). It is noteworthy that the spectrum of 10µM WT aSyn alone is more intense than that of 50µM WT aSyn alone (Figure 6-7 A). This is surprising given that the molar residue ellipticity normalizes the spectra on the basis of the protein concentration (as seen for all of the other samples/conditions), and so this case likely reflects an inaccurate concentration determination for this sample. However, it should be noted that this does not affect the estimation of the secondary structural content by BeStSel, as it is the spectral features rather than their intensity which are important.

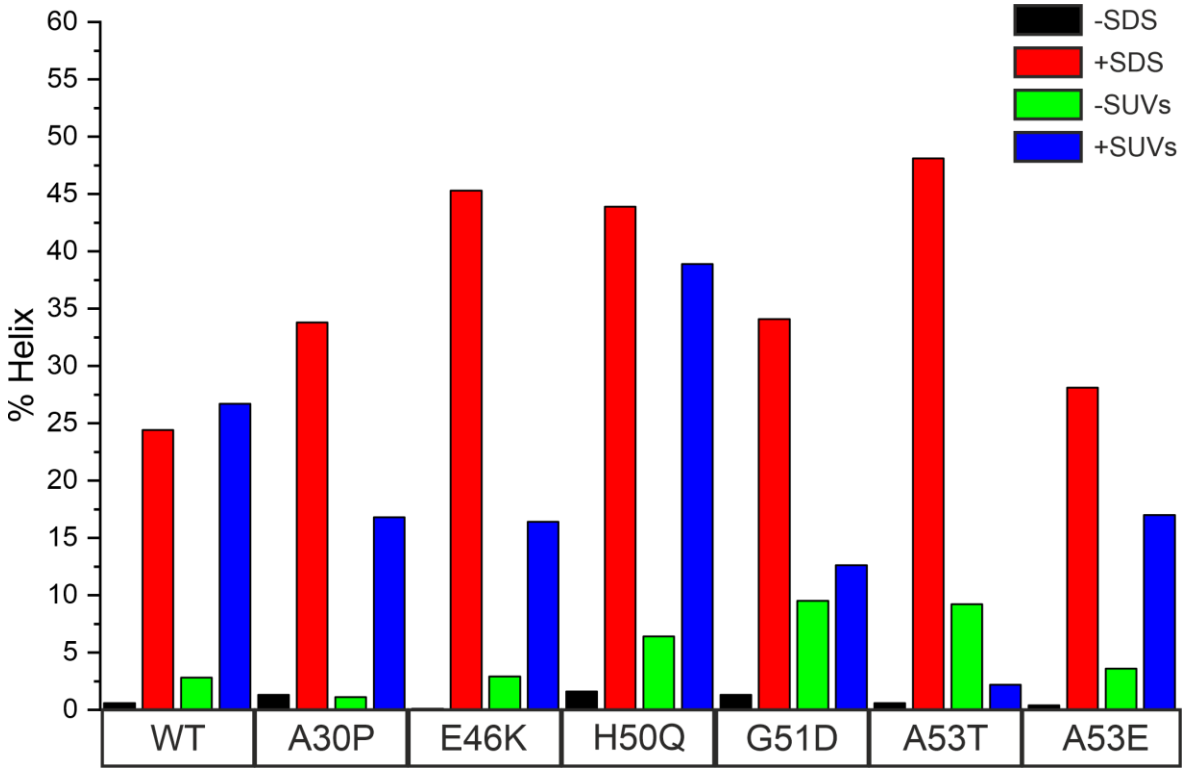

Figure 6-8 - Helical content of aSyn alone, in the presence of a membrane mimetic, and in the presence of SUVs. *The amount of helix as a proportion of the total secondary structure of aSyn (WT and PD-linked mutants) was calculated from CD spectra using the secondary structure prediction server BeStSel* (182). *Helical content increases in the presence of SDS micelles, a membrane mimetic, and SUVs composed of 5:3:2 DOPE:DOPS:DOPC, used as a more physiological mimic of synaptic vesicles. Measurements of protein alone (black) and protein plus SDS micelles (red) were conducted with 50µM protein (and 10mM SDS). Measurements of protein alone (green) and protein plus SUVs (blue) were conducted with 10µM protein (and 1.4mg/mL SUVs) so as to minimize light scattering.*

This experiment was repeated for each of the PD-linked mutants, for which the full spectra and their corresponding secondary structure calculations are found in Appendix 10.3. The general trend of the CD data is that the samples of protein alone are mainly composed of "other" secondary structure elements, as defined by BeStSel (181,182). "Other" encompasses random coil/disordered protein, as well as very rare and uncommon elements such as poly-proline helices. Given that aSyn is considered to be an IDP this is likely to just be random coil content (44). The samples of protein alone also contain a significant level of β-content, mainly antiparallel strands but also β-turns and a small level of parallel strands. This may reflect the fact that aSyn exists in an equilibrium with early aggregates (e.g. oligomers), and thus there is likely always a low level of β-containing aggregates present. The samples in the presence of SDS micelles and lipid SUVs typically exhibited increased helical content, which can be inferred to mean the protein is associated with membranes (Figure 6-8). The only exception to this was A53T which did not form helices in the presence of SUVs. Generally, the helicity of the samples is greater in the presence of the SDS micelles than with the lipid SUVs, although the WT protein is seemingly an exception to this. SDS micelles are quite small in diameter (~1.75nm), tightly curved, and strongly negatively charged (184). By contrast the DOPE:DOPS:DOPC SUVs are larger in diameter, SUVs are on the order of tens of nanometres to 100nm, are less strongly charged, and not as tightly curved as the SDS micelles. It may be the case that this combination of features of SDS micelles make them particularly attractive to aSyn, especially given that the helix forming NTD region has a net-positive charge, but this data is less physiologically relevant compared to that with the SUVs. This increase in helicity comes largely at the expense of the other/random coil secondary structural content, but also somewhat at the expense of β-content. Whilst it has been established in the literature that membrane-binding can induce the aggregation of aSyn (and thus result in β-sheet formation) it has also been shown that helix formation can extend into the NAC region and can thus also be protective from aggregation (160,185). A53T is especially notable as exhibits the highest-level of helicity of all the samples in the presence of SDS, but has exceedingly low (<5%) helicity in the presence of the SUVs (Figure 6-8 and

Appendix Figure 10-8). However, in the presence of the SUVs 55% of A53T is either antiparallel or parallel β-strand, or β-turn. This may indicate that in the presence of the lipid SUVs A53T forms aggregates, whilst it binds to SDS-micelles and remains helical. Interestingly, in a publication by *Bodner et* al A53T was reported as having a similar lipid-affinity to WT, whilst E46K was reported as having enhanced lipid-affinty and A30P as having a lower affinity (160). Here, E46K and A30P exhibit similar helicity under all conditions. This may reflect a problem with the indirect nature of these experiments, however more direct means of probing aSyn-lipid interactions (e.g. surface plasmon resonance (SPR) and isothermal titration calorimetry (ITC)) proved unfeasible with this system.

The degree of helicity, and the inferred lipid-affinity, of the aSyn variants is quite varied. It is possible that these differences may reflect difference in toxicity and disease pathology. Reduced affinity for membranes may increase the cytosolic supply of protein, whilst increased affinity may provide additional nucleation points for aggregation. Alternatively helix formation involving residues required for β-sheet formation can be inhibitory of aggregation (160). The physical basis of the differences in interaction between the mutants, however, are more difficult to explain. The PD-linked mutations are all in a similar region (the NTD), of which three result in a change in the charge. That may be enough in this critical membrane-associating region to cause significant alterations in their lipid-affinity. The only two mutants described as forming helices of differing lengths, A30P and E46K (160), here show similar helicity (Figure 6-8). This may suggest that the mutations have an allosteric effect that affects lipid-binding in some other manner or perhaps that they alter binding to different types of lipid to different extents.

6.3.4 Nitration of α-synuclein by peroxynitrite

The success of the nitration of aSyn by peroxynitrite was confirmed through an increase in absorbance at 430nm compared to a control of WT aSyn that was not exposed to peroxynitrite (Figure 6-9A). 3-nitrotyrosine absorbs at 430nm and causes the sample to exhibit a characteristic

yellow colour. Independent confirmation was obtained by Dot blot through the use of an anti-nitrotyrosine antibody derived from mice. With the exception of the negative control, all samples showed spots with the spot intensity appearing to match up well with the A_{430} values (Figure 6-9B). The slight variation may be due to either minor differences in protein concentration or non-uniform modification of tyrosine residues. Nevertheless, this demonstrates that nitrated aSyn can be prepared for downstream studies.

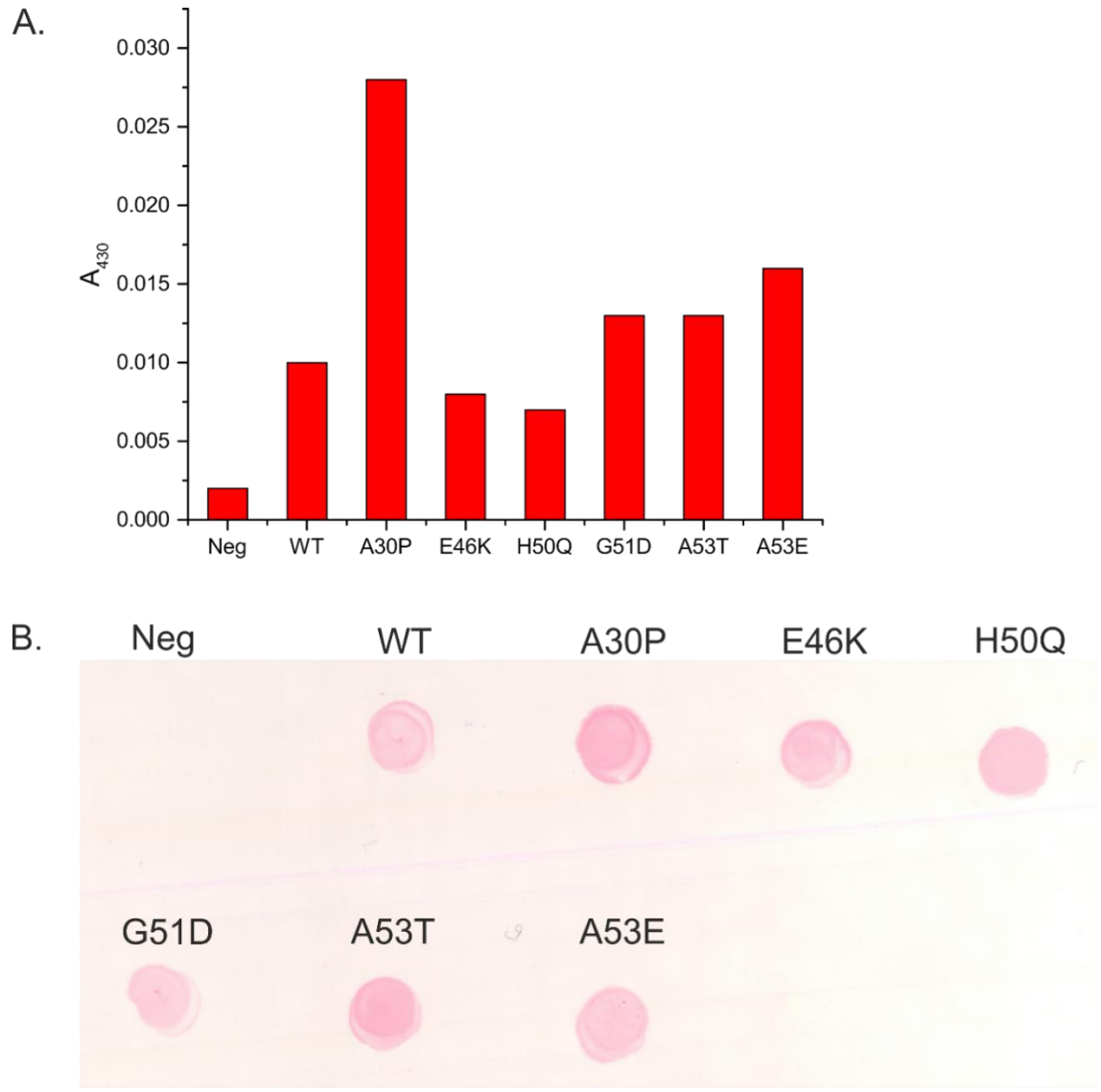

Figure 6-9 - A plot of absorbance values and a Dot blot of WT aSyn, exposed to peroxynitrite, confirming nitrotyrosine formation. *The bar chart (A) shows the A_{430} values for aSyn exposed to peroxynitrite and a negative control sample (WT aSyn not exposed to peroxynitrite). The A_{430} value corresponds to the absorbance of 3-nitrotyrosine. Dot blot of 5µL of each sample at 100µM (B). The primary antibody was an anti-nitrotyrosine antibody isolated from mice. An anti-mouse antibody conjugated to alkaline phosphatase was used as a secondary, and spots were visualized using a SIGMAFAST Fast Red kit.*

6.3.5 Native-PAGE analysis of the effect of tyrosine nitration on the oligomerization state of WT α-synuclein

A Native-PAGE of the nitrated and non-nitrated forms of WT aSyn was run to compare the oligomerization state of the proteins. In the non-nitrated sample the protein exists predominantly as a single strong band – the monomer – whilst there are also some other bands which are presumably less prevalent oligomeric species, such as dimers and tetramers, which would ordinarily be denatured, and thus not apparent, on an SDS-PAGE gel (Figure 6-10). The nitrated sample presents as a streak, which is indicative of a wide range of different protein sizes and conformations; this suggests that the protein is aggregating. However, given that the sample is able to enter the gel at all they are probably not fibrils and are more likely to be oligomers. This is supported by material in the literature suggesting that exposure to peroxynitrite results in the formation of cross-linked tyrosine and stable aggregates (173).

The samples loaded onto the gel were freshly prepared and not incubated for any significant length of time prior to loading. The oligomer formation induced by tyrosine nitration appear to occur rapidly and spontaneously without much encouragement. Contrastingly, the aggregation of WT aSyn *in vitro* requires prolonged incubation (~1 week) at 37°C with agitation to form fibrils.

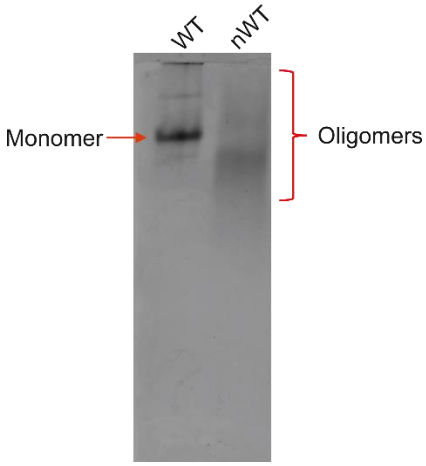

Figure 6-10 - Native-PAGE gel of nitrated and non-nitrated WT aSyn. *Approximately 8.5µg protein was loaded per well. Non-nitrated WT aSyn appeared predominantly monomeric, with some other minor species present; presumably dimers*

and higher-order species. Nitrated WT aSyn appeared as a streak, indicating significant sample heterogeneity e.g. dimers, tetramers and higher-order oligomers.

6.3.6 ThT and TEM analysis on the effect of tyrosine nitration on the rate of aggregation of WT α-synuclein

ThT fluorescence experiments were used to probe the effect of tyrosine nitration in WT aSyn on its rate of aggregation. It is clear from Figure 6-11 that non-nitrated WT aSyn aggregates as expected, yet the nitrated form of the protein does not result in a gain of ThT fluorescence. This suggests that no fibrils are being formed, and that the oligomers implied by the Native-PAGE gel in Figure 6-10 are likely amorphous or unable to bind ThT. This corroborates data obtained by *Hodara et al* who also found that nitrated aSyn did not form fibrils by itself, but that it could be incorporated into pre-existing fibrils of unmodified protein (174). Lengths analysis of aggregates or fibrils was not possible due to the sheer paucity of any measurable species formed.

It was the initial aim of this body of work to use nitrated WT aSyn (and H50Q and G51D) to carry out small-angle X-ray scattering (SAXS) experiments to monitor the aggregation process of aSyn as described by *Herranz-Trillo et al* (45). SAXS experiments would necessitate a high protein concentration (≥5mg/mL) in order to obtain the necessary signal:noise. Sadly, due to unforeseen circumstances it was not possible to carry out these planned experiments in collaboration with Bente Vestergaard at the University of Copenhagen. It is for this reason, however, that the protein concentration used in this ThT experiment was 345µM (5mg/mL) rather than 100µM as used elsewhere in this thesis.

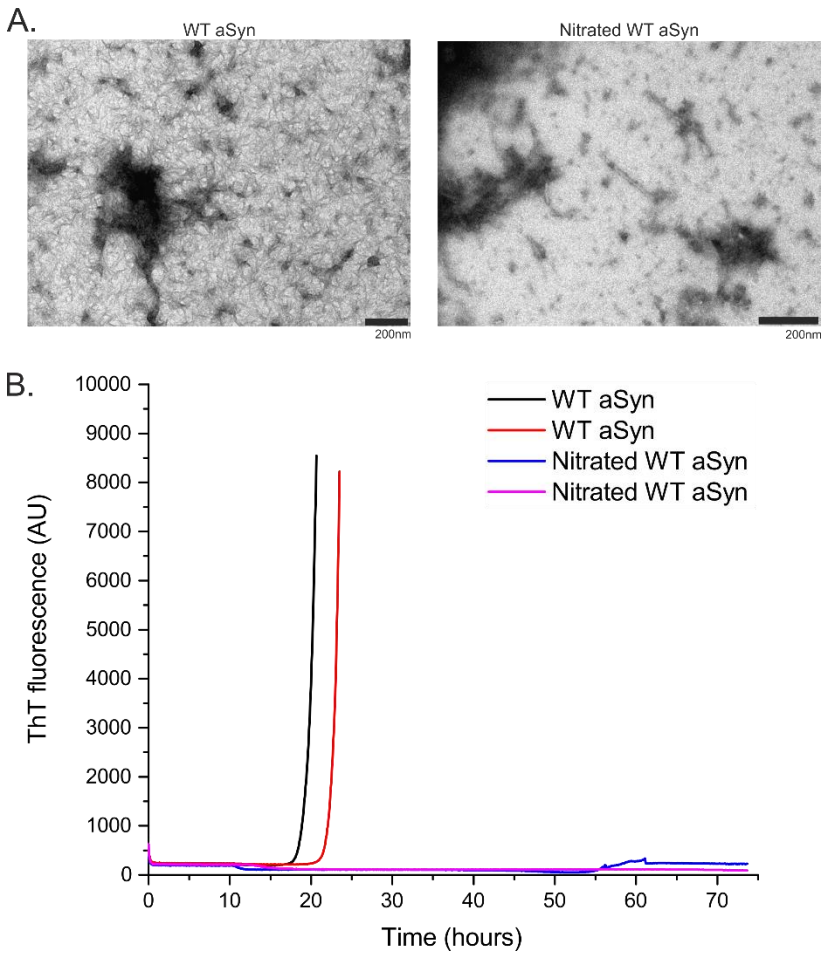

Figure 6-11 - TEM and ThT analysis of the aggregation of nitrated WT aSyn. *Negative-stain TEM images (A) of WT aSyn and of nitrated WT aSyn. The samples had both been incubated at 37°C with agitation in in PBS pH 7.4 at a concentration of 345µM (5mg/mL) for 1 week. WT aSyn forms huge numbers of fibrils at this concentration making it difficult to see individual fibrils. Nitrated WT aSyn does not really form fibrils, with there only being a few isolated strands. This is corroborated by the ThT fluorescence data (B) which shows a rapid increase in the fluorescence for the sample of the non-nitrated protein whilst the nitrated WT aSyn remains flat, suggesting little or no fibril formation.*

6.3.7 Native-PAGE analysis of the effect of tyrosine nitration on the oligomerization state of the α-synuclein Parkinson's-linked mutants

Having confirmed the nitration of WT aSyn results in the rapid formation of oligomeric species, it was of interest to see if the same effect could be replicated for the PD-linked mutants (A30P, E46K, H50Q, G51D, A53T, and A53E). By Native-PAGE a similar effect to that seen with the WT protein was also seen for the mutants (Figure 6-12). The nitrated proteins, unlike the non-nitrated proteins, do not migrate as discrete bands but rather as smeary streaks suggesting a large

number of different species. This suggests that the nitrated samples are inclined to rapid oligomerization. This may lead to increased cytotoxicity.

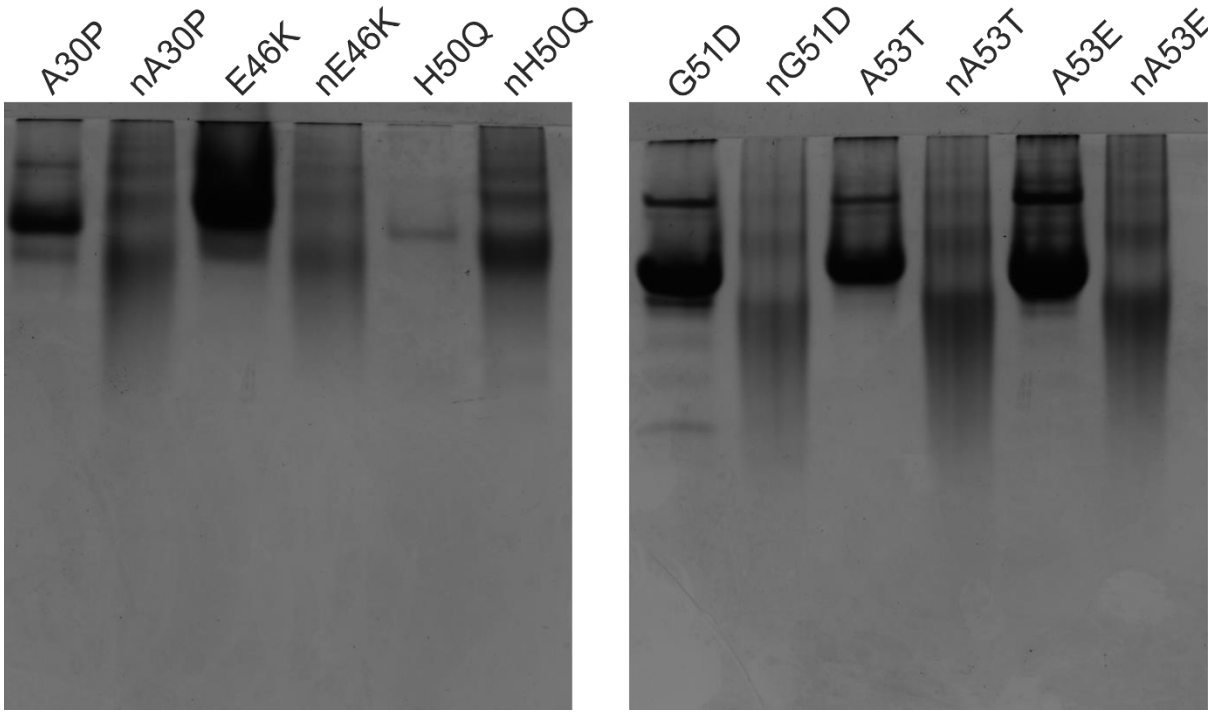

Figure 6-12 - Native-PAGE gel of nitrated and non-nitrated aSyn mutants. *Approximately 8.5µg protein was loaded per well. Non-nitrated aSyn – for each mutant – appeared predominantly as a monomeric band although some, particularly E46K and A53E, were quite streaked suggesting a significant level of oligomer formation. However, as with the WT protein, the streaking was far more pronounced for the samples of nitrated protein.*

6.3.8 Effect of tyrosine nitration on α-synuclein toxicity

Given that tyrosine nitration induces the rapid oligomerization of aSyn, and that oligomers are now widely considered to be the species associated with toxicity (20), cell viability assays were carried out on samples of nitrated and non-nitrated aSyn – WT and the PD-linked point mutants. SH-SY5Y neuroblastoma cells were challenged for 24 hours with a final concentration of 5µM nitrated and non-nitrated forms of aSyn that had been incubated for different lengths of time. The percent viability of the cells was calculated relative to Live (PBS alone) and Dead (1% Triton X-100) controls. The viability of the cells exposed to the proteins that had been freshly prepared (day 0) and that had been incubated for three days is shown (Figure 6-13 A&B). The general trend at the initial timepoint (day 0) is that the nitrated samples are more toxic than the non-nitrated samples

(Figure 6-13 A). This fits with the previous findings in Figure 6-12 that nitrated samples form oligomeric species and with information in the literature that oligomers are the main toxic species (20). Nitrated H50Q is particularly toxic at the first timepoint and this is a statistically significant difference from the other conditions (Figure 6-13 A&C). After the protein samples had been incubated for three days, however, the picture is less clear. After this period of time most non-nitrated protein will have begun to form toxic oligomers, and indeed many of the non-nitrated samples exhibit similar or greater toxicity than their nitrated counterparts after three days (Figure 6-13B). The exceptions to this are nitrated H50Q and G51D, which both reduce the viability of the cells to about 60%. This is reflected in the statistical analyses (Figure 6-13 D). It has been suggested that tyrosine nitration in aSyn can have allosteric effects (186), far removed from the modification sites, and this may result in H50Q and G51D adopting a conformation that is particularly toxic comparative to the other aSyn mutants. The immediacy of the toxicity of nitrated H50Q is surprising given the association of H50Q with late-onset PD, in contrast to G51D which is associated with early-onset disease (166). An interesting question posed by this data is whether nitration pushes aSyn down alternative aggregation pathways to the non-nitrated protein, which results in the formation of more toxic species, or whether it simply accelerates the “normal” aggregation process and it is the presence of oligomers that is accountable for the observed results in Figure 6-13. Given that the non-nitrated samples do “catch-up” with the nitrated samples after incubation (with the sole exception of G51D) it would suggest that the latter is true, however the former option cannot be ruled out.

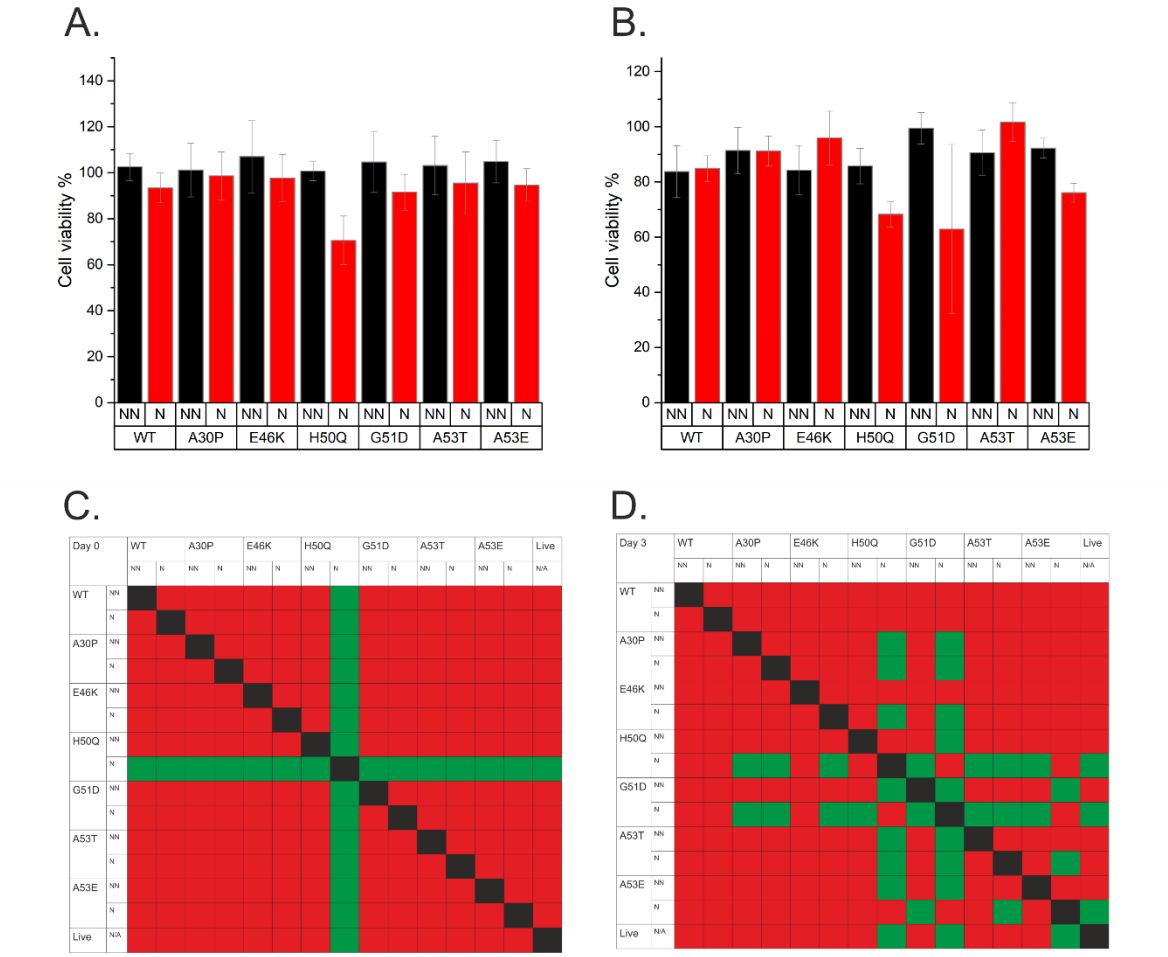

Figure 6-13 - Bar charts comparing the viability of cells exposed to nitrated and non-nitrated aSyn at different timepoints, and tables showing the statistical significance of these differences. *Nitrated and non-nitrated forms of aSyn were prepared at 100μM and incubated with agitation at 37°C. Aliquots were taken at day 0 and day 3 and were added to wells of SH-SY5Y cells at a final concentration of 5μM. The absorbance of the formazan dye CCK-8 at 450nm was used to assess viability at day 0 (A) and day 3 (B), and all data were normalized relative to live and dead controls. Nitrated (N) samples were more toxic than non-nitrated (NN) samples at day 0, likely due to a higher prevalence of oligomers, but results were more mixed for the samples incubated for 3 days. This is likely due to the non-nitrated samples having had more time to form toxic oligomers. ANOVA with Bonferroni post-hoc analysis was carried out to assess the statistical significance of the differences at day 0 (C) and day 3 (D). Squares coloured green indicate p-value < 0.05, whilst red indicates p-value >0.05. Six wells were prepared for each condition. N=2.*

6.3.9 Effect of tyrosine nitration on the lipid-association of α-synuclein

It has been suggested that tyrosine nitration of aSyn can result in an impairment of the protein's ability to associate with lipid membranes (186,187). Tyr39, as the only tyrosine residue within the helix-forming region of the protein, is thought to be key in this, and the reduced affinity is thought to be as a result of electrostatic repulsion due to the introduction of a negatively charged

NO_2^- group. Interestingly, the same study revealed that nitration of just the C-terminal tyrosine residues within aSyn also reduced membrane affinity, suggesting some form of allostery (186). Here, the aim was to see if this same effect was seen in the PD-linked mutants of aSyn as well as the WT protein, and if this is reflected for the physiologically relevant SUVs as well as the membrane mimetic SDS.

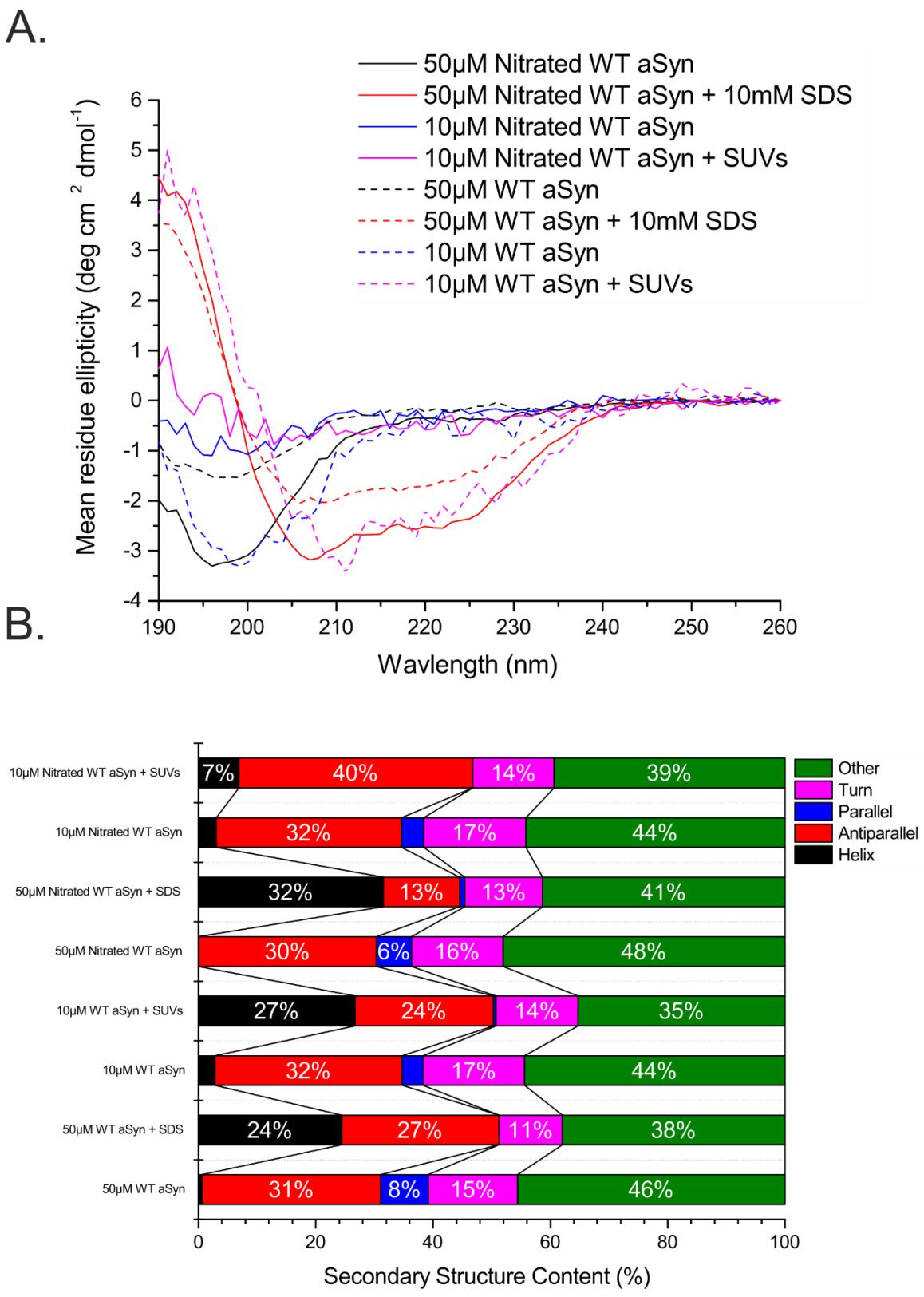

Figure 6-14 - CD spectra and estimations of secondary structural content for nitrated WT aSyn in comparison to non-nitrated protein. *CD spectra (A) for nitrated (solid line) and non-nitrated (dashed-line) 50μM WT aSyn alone or with SDS micelles, and 10μM WT aSyn alone or with lipid SUVs composed of DOPE:DOPS:DOPC (5:3:2) are shown. Secondary structure estimations from the CD spectra as calculated by the BeStSel server are shown (B)* (181,182). *The NMRSD values are as follows: 50μM WT aSyn alone (0.03314) or with SDS (0.00771), 10μM WT aSyn alone (0.04622) or with SUVs (0.02811), 50μM nitrated WT aSyn alone (0.01935) or with SDS (0.00719), and 10μM nitrated WT aSyn alone (0.04619) or with SUVs (0.08725).*

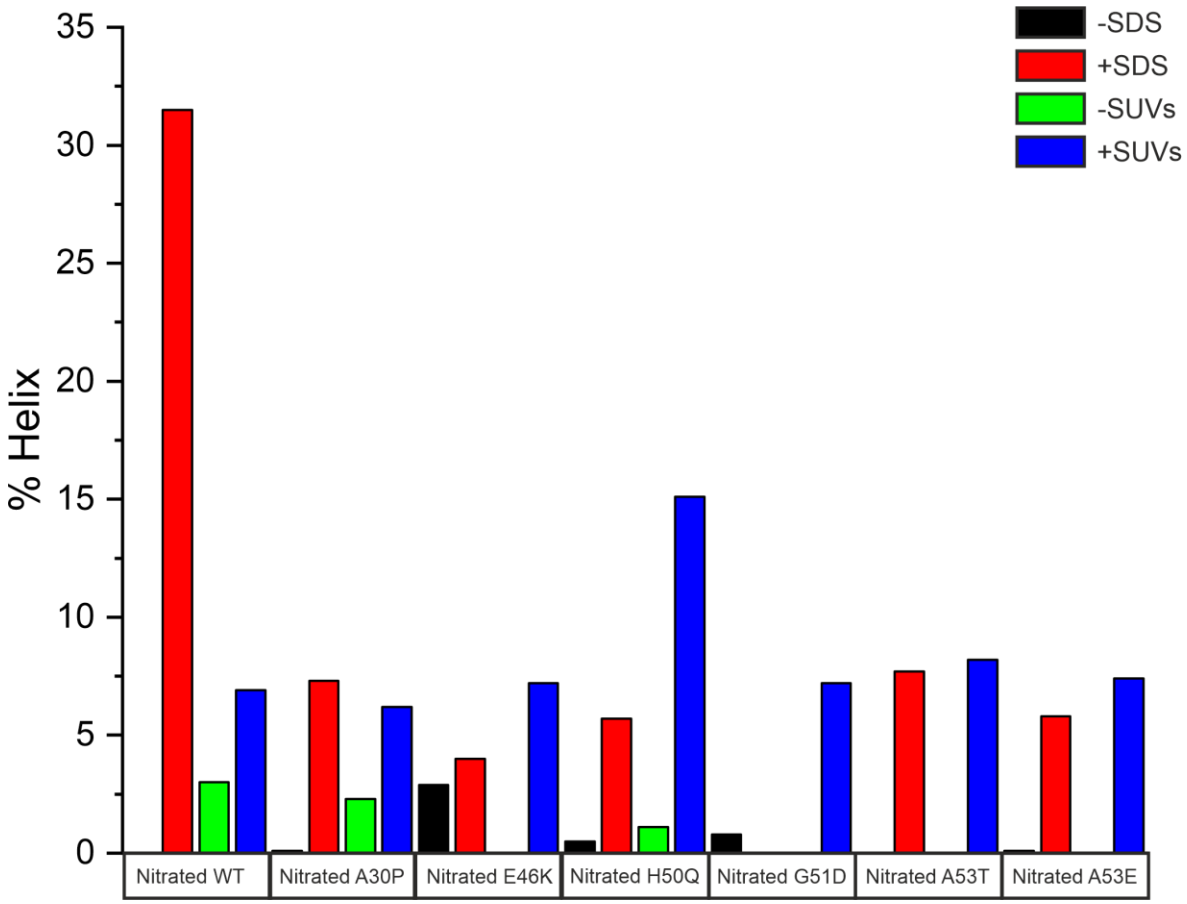

Figure 6-15 - Helical content of nitrated aSyn alone, in the presence of a membrane mimetic, and in the presence of SUVs. *The amount of helix as a proportion of the total secondary structure of aSyn (WT and PD-linked mutants) was calculated from CD spectra using the secondary structure prediction server BeStSel* (182)*. Helical content increases in the presence of SDS micelles, a membrane mimetic, and SUVs composed of 5:3:2 DOPE:DOPS:DOPC, used as a more physiological mimic of synaptic vesicles. Measurements of protein alone (black) and protein plus SDS micelles (red) were conducted with 50μM protein (and 10mM SDS). Those of protein alone (green) and protein plus SUVs (blue) were conducted with 10μM protein (and 1.4mg/mL lipid) so as to minimize light scattering.*

CD spectra were collected for nitrated protein alone, in the presence of SDS micelles, and in the presence of the SUVs (DOPE:DOPS:DOPC 5:3:2) designed to mimic synaptic vesicles. A representative dataset of CD spectra for nitrated WT (superimposed over the spectra of the non-nitrated samples) is shown (Figure 6-14). The CD data, including the secondary structure estimations and associated NRMSDs, for each of the other nitrated aSyn variants is located in the Appendix 10.4. The helical content of nitrated protein alone, in the presence of SDS-micelles, and in the presence of the lipid SUVs, is given (Figure 6-15). The nitrated forms of the aSyn variants alone exhibit little or no helicity, as expected. The data suggest that the majority of their secondary structure is instead random coil, but with also a large proportion of antiparallel β-structure. Despite

the Native-PAGE data (Figure 6-12) suggesting that the nitrated forms of aSyn are more oligomeric than the non-nitrated forms, there is little difference in the secondary structure profiles of nitrated and non-nitrated protein alone (see Appendix 10.4). The general trend, as seen with non-nitrated aSyn, is that in the presence of SDS micelles or lipid SUVs the helicity in the samples increases. Noteworthy examples include nitrated WT, which exhibits high helicity (>30%) in the presence of SDS, and nitrated H50Q which has the most helix (>15%) of any of the proteins in the presence of SUVs (Figure 6-15). It should be highlighted, however, that the proportion of helix formed is generally much lower in the nitrated samples as compared to the non-nitrated, which corroborates the findings of *Sevcsik et al* (186). This is probably due to the introduction of a negative charge on Tyr39 (located in the lipid-associating NTD of aSyn) and the consequent electrostatic repulsion with the negatively charged lipid headgroups.

It is difficult to draw hard-and-fast "rules" from this data, as there are clear exceptions. For example, nitrated G51D exhibits helicity in the presence of lipid SUVs but none with SDS micelles (Figure 6-15). These variations likely reflect intrinsic properties about the different proteins that result in their preference for membranes of different composition, size, charge, and curvature.

6.4 Discussion

The work presented in this chapter has focused on multiple different aspects on aSyn biochemistry, with the aim of shedding light on its physiology and pathophysiology. This includes its affinity for lipid membranes, its rate of aggregation, fibril length and morphology, and cell toxicity. These parameters have been investigated in previous studies, but these analyses frequently suffer from batch-to-batch variation and different conditions (pH, ionic strength, seed concentration) making it difficult to cross-compare and draw concrete conclusions. The work conducted in this chapter stands apart from these previous studies in that the experiments were conducted as far as possible under identical conditions in the same lab, with the aim of providing a more robust analysis. Additionally, the six PD-linked point mutations in aSyn and the effects of tyrosine nitration have also been investigated

here. The six mutations are associated with familial forms of PD yet can have quite distinct disease profiles, despite their relative proximity within the NTD (75–77,125,162,188). Tyrosine nitration, on the other hand, is a PTM of pathological relevance that has been identified within LBs (53). The elucidation of the effects of each of these modifications and mutations is important if the complex nature of PD and the synucleinopathies is to be disentangled.

It is known that the PD-linked mutants exhibit differences in their affinity for lipid bilayers, their rate of aggregation, and their fibril morphologies (31,166). Differences in the lipid affinity were probed through CD spectroscopy, which reported on the level of helicity in the samples; an occurrence in aSyn upon binding to lipids (33). This ability to bind to lipid bilayers is thought to be part of aSyn's native physiological function, which appears to be closely linked to the regulation/replenishment of the synaptic vehicle pool and in the formation of SNARE complexes that promote synaptic vehicle docking at the presynaptic terminal (39,47). It has long been considered that these differences may be relevant to the disease process, too. However, the findings on whether lipid-binding enhances or impedes protein aggregation have been contradictory (189,190). This question has been at the periphery of research into aSyn for some time, but has newfound prominence given the discovery by *Shahmoradian et al* that LBs contain far more in terms of lipid membranes than previously realized (191). The rate of protein aggregation is also of great interest, but is equally enigmatic given the recent doubt thrown onto the historic assumption that it is the fibrils that mediate cell toxicity (20). For example, A53T is widely considered to have the fastest rate of aggregation of the PD-linked mutants, and the recently discovered early-onset mutation G51D is known to have a much reduced aggregation rate (125,167). Interestingly, this suggests that G51D persists in an oligomeric state for longer, and these oligomers are now widely considered to be the main species responsible for mediating toxicity (20). This may go some way to rationalizing why G51D results in an early-onset form of PD and highlights the need to understand the protein aggregation process in detail.

The work conducted within this chapter makes several important and novel contributions to the field. CD experiments revealed that tyrosine nitration – induced via peroxynitrite, a highly-reactive compound formed as a consequence of oxidative stress – impedes the ability of each of the PD-linked mutants of aSyn to associate with lipid membranes, a phenomenon previously only shown for the WT protein (Figure 6-8 & Figure 6-15). Additionally, nitrotyrosine formation also results in the formation of oligomeric or polymeric aSyn species for each of the PD-linked mutants, as inferred from Native-PAGE (Figure 6-10 and Figure 6-12). These oligomeric species are resistant to downstream aggregation and amyloid formation (Figure 6-11). Cell toxicity assays of nitrated versus non-nitrated protein here suggest that, at least at early timepoints, nitrated aSyn is more toxic to cells than non-nitrated (Figure 6-13). These cell toxicity assays are imperfect, however, as the cells are challenged with aSyn species applied externally and thus the assays are possibly also reflecting differences in internalization of the protein.

Given the findings of *Shahmoradian et al* it is clear that a greater investigation of the effects of nitrotyrosine formation is needed *in vivo* (191). Impaired lipid-affinity as a direct result of tyrosine nitration may result in an increased cytosolic supply of aSyn. If the oligomers formed in the presence of peroxynitrite are truly resistant to amyloid formation this may be a beneficial modification. However, whilst nitrated aSyn alone may itself not form amyloid fibrils it may be able to attach to pre-existing fibrils and participate in amyloid formation in this way. In this case, peroxynitrite and oxidizing conditions may result in a swelling of the cytosolic aSyn concentration and result in aggregation and increased cell toxicity. The links between neurodegenerative disease and oxidative stress are established and well-known, and thus it seems unlikely that nitrotyrosine formation is beneficial in the context of aSyn (192).

In the course of this study it was also discovered through TEM that aSyn and its mutants can be broadly separated into three groups in terms of fibrils. G51D and A53E typically form numerous, short (~50nm) fibrils, whilst the others generally form fibrils >300nm (Figure 6-5). A30P rests in a group of

its own as it alone formed a majority of fibrils >1000nm in length. Different lengths/numbers of fibrils present a varying number of fibril ends to serve as elongation points and fibril surface which can facilitate secondary nucleation processes, thus altering aggregation kinetics. It is also possible that different morphologies may differentially facilitate seeding which may affect cell-cell transmission of aSyn pathology (100). Recent breakthroughs in cryo-EM have made it possible to solve the structures of amyloid fibrils, and even distinguish between polymorphic species in near-atomic detail (46). Such a detailed analysis of multiple species of aSyn fibril was beyond the scope of this project, but it would be interesting to see the effect of these different point mutations on the final fibril structure given that these residues are likely involved in the preNAC steric zipper in the 'rod' polymorph.

There are a number of drawbacks and caveats that need to be considered regarding the work in this chapter. CD spectroscopy has been used as a measure of the affinity of aSyn and its variants for SDS-micelles and lipid SUVs. This is legitimate given that aSyn is known to form helices that lie across the surface of membranes, which is observable using CD. However, this is an indirect measure of lipid-binding and in an ideal world supplementary evidence from a more direct and complementary technique would be welcome. Efforts to obtain such supporting evidence using SPR were unsuccessful, as both aSyn and the SUVs proved too sticky to the chip to get interpretable data. ITC, on the other hand, was also not viable as numerous competing processes (aggregation, lipid association etc) would make interpretation of the data extremely difficult. Consequently, CD alone has been used to probe aSyn-lipid interactions. Also, the most information-rich portion of the far-UV (260-180nm) region of the CD spectrum is in the 180-190nm range. Unfortunately, this is the region that suffers most from light-scattering caused by the detergent micelles and SUVs. In light of this the secondary structure estimations using the BeStSel prediction server only took into account the spectrum to 190nm. The calculated spectra were fitted as close as possible to the experimental spectrum, but the individual spectra should be considered as well as the determined secondary structural values to ensure that the values make sense given the possibility of noise.

ThT measurements of aSyn aggregation were also inconsistent and suffered from batch-to-batch variation. Attempts to control this were made by using freshly-prepared ThT stock solutions and only using HFIP-treated aSyn prepared from the same batch. These steps did not fully ameliorate these consistency issues, and so the data presented here should be considered with caution. This is seemingly a widespread issue in the analysis of amyloid rates of aggregation and may be reflective of different starting quantities of seeds in the samples.

Future work should aim at trying to tie together these different aspects of aSyn biochemistry in a more *in vivo* context and establishing their relationship with each other. The toxicity of the different mutants could be investigated in an animal model; *C.elegans* would be a good starting point given its comparative simplicity, the availability of PD models, and low cost. Antibodies and fluorescent tags could be used to assess the presence of oligomers and fibrils, investigate co-localization with membranes, and the extent to which nitrotyrosine is found in these systems.

7 The association between α-synuclein, cyclophilin-D, and the mitochondria

7.1 Introduction

The work within this chapter was initially formatted and compiled for a publication, which was sent to Scientific Reports. Subsequently to receiving and addressing the reviewers' comments it was decided that this work was to be put towards a patent application. This is currently underway, and thus the contents of this chapter are to remain under embargo. The NMR and ITC experiments in this chapter were conducted by Prof Lu-Yun Lian. Cyclophilin-D was expressed and purified by Dr Amy Wood and given to me on behalf of Prof Lu-Yun Lian. I expressed and purified all full-length aSyn (including ^{15}N-labelled form), conducted the ThT assays, TEM, and the cell viability experiments.

7.1.1 Cyclophilin name controversy

There is controversy and inconsistency in the literature regarding the correct nomenclature of cyclophilins/peptidyl-prolyl isomerases and their corresponding gene names. All of the following experiments have been conducted on cyclophilin-D (CypD) (Uniprot ID: P30405), a peptidyl prolyl isomerase encoded by the gene *PPIF*.

7.1.2 Neurodegenerative disease, mitochondrial dysfunction, and oxidative stress

Neurodegenerative disease has been the subject of intense research for many years. However, many of the most basic questions surrounding this conglomerate of diseases remain unanswered. One such question is: why do the neurons die? A common element in neurodegenerative disease is mitochondrial dysfunction and oxidative stress (192,193). As stated in 1.7.1.1 there are a number of environmental factors implicated in PD-onset, including the

exposure to the compounds rotenone and paraquat which have been used as pesticides (73). These compounds operate by binding to the complexes of the electron transport chain within the mitochondria, resulting in an increase in the levels of reactive oxygen species (ROS) and impeding ATP synthesis (194). Indeed, rotenone exposure has been used to induce Parkinsonian symptoms in some mouse models of PD (74). Alongside this are the number of genes implicated in familial forms of PD, such as those encoding DJ-1 (redox sensor/protein deglycase), PINK1 (serine/threonine protein kinase), and parkin (E3 ubiquitin ligase), which seem to play roles in maintaining mitochondrial integrity (195–197). These different features overlap to start painting a picture of PD not just as a disease of the brain, but as a disease of the mitochondria. Greater understanding of this relationship between protein aggregation, oxidative stress and mitochondrial dysfunction is clearly needed in the 21st century if we are to design successful therapeutic agents.

7.1.3 The mitochondria and α-synuclein

Recently, there has been a growing body of evidence that aSyn can localize to the mitochondria and that this may be associated with disease (Figure 7-1) (198–202). For example, it has been shown that aSyn can interact with the phospholipid cardiolipin when it is exposed on the outer mitochondrial membrane, and that this leads to mitochondrial fragmentation and mitophagy (199). It has also been shown that oligomeric or post-translationally modified aSyn can bind to TOM20 and prevent the import of proteins into the mitochondria (203). This, too, results in impaired mitochondrial function and oxidative stress. Of special interest have been the reports that oligomers of aSyn can bind to the β-subunit of ATP synthase and induce the opening of the mPTP (198). Our group has generated data showing that aSyn is able to interact with CypD, a component/regulator of the mPTP. Given the key role of the mPTP and, by extension, CypD to both necrotic and apoptotic cell death this is an interaction that is quite clearly worth investigating further (204).

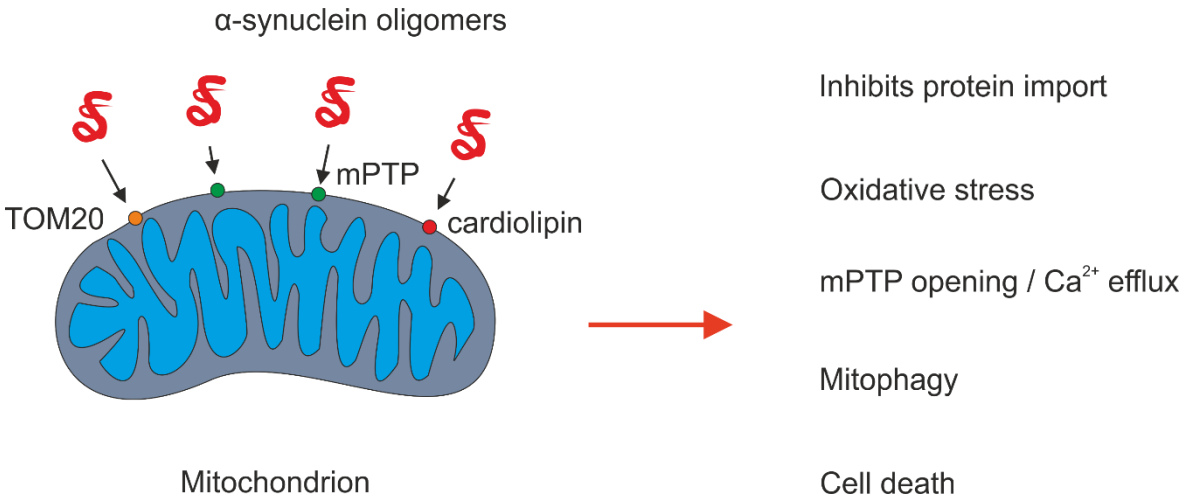

Figure 7-1 - Schematic showing the effects of aSyn localization to the mitochondria. *The localization of aSyn to the mitochondria has been implicated in mitochondrial dysfunction. Notably, aSyn appears to impair mitochondrial function resulting in oxidative stress, associate with cardiolipin (red circle) which modulates its aggregation behaviour, bind TOM20 (orange circle) to inhibit the translocation of proteins into the mitochondria, and aSyn oligomers promote the opening of the mPTP (green circle) and promote* Ca^{2+} *efflux, and by extension cell death* (198,199,203,205).

7.1.4 Cyclophilin-D and the mitochondrial permeability transition pore

Human CypD is a mitochondrial protein that is synthesised as a 22kDa protein that is subsequently processed into a 17.8kDa protein following the removal of the mitochondrial localization sequence (Figure 7-2). It is a peptidyl-prolyl isomerase meaning that it catalyzes the interconversion between the *cis* and *trans* states of proline, and this functionality is thought to be involved in assisting the correct folding of proteins (206,207). The protein was found, through knockout studies in mice, to be a key regulator of the mPTP (110).

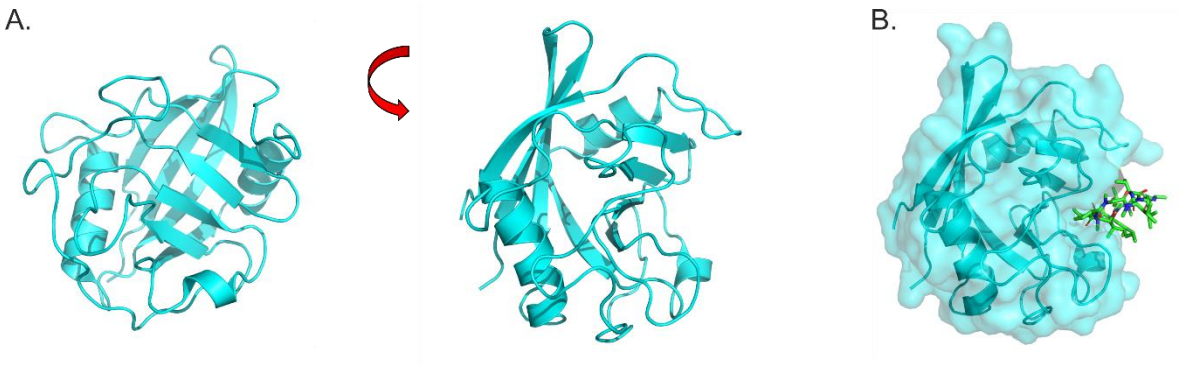

Figure 7-2 - Crystal structure of human WT CypD (PPIF). *The crystal structure (PDB: 2Z6W) was solved to 0.96Å resolution to reveal a mixed α/β protein (A)* (208)*. The structure shown is that of the processed 17.8kDa fragment, which has the mitochondrial localization sequence removed. The structure of the protein was solved with the potent inhibitor cyclosporin A (CsA) bound (B). The protein is shown in cyan, whilst the inhibitor of its activity, the 11-residue cyclic peptide CsA, is in shown in green.*

The mitochondrial permeability transition is a strange phenomenon of the mitochondria. It refers to a process by which the exposure of the mitochondria to high levels of Ca^{2+} results in swelling of the mitochondria and the sudden non-specific permeabilization of the inner mitochondrial membrane to molecules under 1.5kDa (209,210). This appears to be the result of the opening of a pore termed the mPTP. The opening of the mPTP results in the degeneration of the proton-motive force required to drive ATP synthesis, and instead ATP begins to be hydrolysed by the mitochondria. This leads to an energy crisis within the cell and necrotic cell death (204). The rupturing of the mitochondrial membranes may also occur, leading to the release of pro-apoptotic factors such as cytochrome c. However, apoptosis will generally only be initiated if the closure of the pore is achieved before necrotic cell death takes hold (211).

The opening of the mPTP, and the damage associated with it, can be inhibited through the use of the cyclic peptide cyclosporine A (CsA) (Figure 7-2) (212). This peptide operates by binding CypD and preventing the opening of the mPTP (213). In this way the administration of CsA has been posed as a strategy to reduce damage to cardiac tissue during myocardial reperfusion (211).

7.1.5 Aims

Given the strong evidence in the literature of an overlap between CypD, mPTP opening, and aSyn aggregation the aim of this chapter was to shed more light on this area and elucidate what was happening with respect to aSyn at the mitochondria. The first step was to identify whether there was any form of interaction between aSyn and CypD, and if so to characterize it, primarily through the use of NMR spectroscopy and ITC. Following on from this the aim was to characterize the effect of the interaction on the aggregation of aSyn and the ramifications this had on its toxicity to cells. This was carried out primarily using TEM, ThT fluorescence assays, and cell viability experiments.

7.2 Methods

7.2.1 Peptides of α-synuclein

ASynM peptide (residues 50-65, GVATVAEKTKEQVTN) and aSynC peptide (residues 119-140, DPDNEAYEMPSEEGYQDYEPE140A) were synthesized by Gemini Biosciences at 98% purity. A control aSyn peptide (residues 74-95, VTAVAQKTVEGAGSIAAATGFV) was synthesized by Protein Peptide Research at 98% purity.

7.2.2 Expression and purification of cyclophilin-D (WT, R55K, R82K)

The 17.8kDa “mature” form of WT CypD, and the mutants R55K and R82K, were expressed and purified by Dr Amy Wood. The expression and purification procedure was as described previously (208).

7.2.3 NMR experiments

All NMR measurements were conducted on a Bruker Avance III 800MHz spectrometer equipped with a TCI CryoProbe (Bruker) at either 298K or 283K. All samples were prepared in 20mM phosphate pH 6.5, 20mM NaCl containing 5% D_2O. The backbone resonances of CypD were assigned using 3D HNCA, HN(CO)CA, HNCO, HN(CA)CO, CBCA(CO)NH, and CBCANH experiments, whilst the

assignment of full-length WT aSyn was described in 3.2.7. Chemical shift perturbations were expressed as:

$$\Delta\delta = \{(\Delta H)^2 + (0.15\Delta N)^2\}^{1/2}$$

Δδ values greater than 0.07 were considered significant. All data was processed in TopSpin (Bruker) and analysed in CCPN Analysis.

7.2.3.1 NMR study of the interactions between cyclophilin-D and α-synuclein peptides

ASyn peptides were prepared to a final concentration of 1mM and resonance assignments of the peptides were obtained using 2D TOCSY and NOESY experiments utilizing mixing times of 60ms and 350ms respectively. To investigate the binding of aSynC to CypD, $^{13}C/^{15}N$ – labelled CypD was utilized. The $^{13}C/^{15}N$ CypD was used in conjunction with the aSynC peptide at a 20:1 peptide:protein ratio and the binding site of aSynC on CypD was identified using ^{1}H-^{15}N HSQC experiments. The assignment of the bound form of aSynC was enabled by collecting $^{13}C/^{15}N$-filtered 1D, 2D TOCSY and 2D NOESY experiments (350ms mixing time).

7.2.3.2 NMR study of the interactions between cyclophilin-D and full-length α-synuclein (wild-type & A53T)

The binding between WT CypD and WT or A53T aSyn was also probed. 1D proton and ^{1}H-^{15}N HSQC experiments were collected at 283K on samples containing 1mM unlabelled WT CypD and 100µM ^{15}N-labelled WT or A53T aSyn.

7.2.3.3 NMR study of the interactions between cyclophilin-D and full-length α-synuclein fibrils

Experiments investigating the interaction between CypD and aSyn fibrils utilized ^{15}N-labelled full-length recombinant WT aSyn (prepared as described in 3.2.3) and were conducted at

288K. $^{2}H/^{15}N$-labelled CypD was utilized to optimize the shift perturbations when in complex with the fibrils.

7.2.4 ITC analysis of the interaction between α-synuclein peptides and cyclophilin-D

ITC measurements were conducted on a MicroCal iTC200 instrument (Malvern Panalytical) at 25°C. All samples were prepared in 20mM phosphate pH 6.5, 20mM NaCl and this buffer was used to wash/equilibrate the cell. The experiments consisted of an initial injection of 0.5µL and then subsequently by fifteen 2.39µL injections, and a final injection of 1.89µL. Control experiments consisted of injecting buffer into buffer, and buffer into CypD. All experiments were carried out in duplicate, however for some titrations data from two runs was concatenated to achieve a saturating isotherm. The cell contained 50-100µM CypD whilst the syringe contained 500-2000µM aSyn peptides. All data was analysed using OriginLab.

7.2.5 ThT fluorescence analysis of the effect of cyclophilin-D on α-synuclein aggregation

The following samples were prepared in PBS pH 7.4: 50µM WT aSyn fibrils alone, 150µM (WT, R55K, or R82K) CypD alone, 150µM WT CypD:CsA, 50µM WT aSyn plus 150µM (WT, R55K or R82K) CypD, and 50µM WT aSyn plus 150µM WT CypD:CsA. Samples of 50µM WT aSyn plus 25, 50, 100, and 150µM WT CypD were also prepared. All samples contained ThT to a final concentration of 2µM. The samples were plated out in triplicate onto a 96-well black, clear-bottomed plate with 100µL per well and incubated at 37°C with agitation for 7 days. Measurements were recorded using a Flexstation 3 microplate reader at wavelengths λ_{ex} = 440nm and λ_{em} = 490nm. Data was processed and analysed using OriginLab.

7.2.6 TEM analysis of the effect of cyclophilin-D on α-synuclein disaggregation

The samples were 50µM WT aSyn fibrils alone, 150µM (WT, R55K or R82K) CypD alone, and 50µM WT aSyn plus 25, 50, 100 or 150µM WT CypD which had been incubated at 37°C for 7 days. 5µL of sample was mounted on a carbon-coated copper grid for 2mins, before blotting off and negative staining using 4% uranyl acetate. Excess uranyl acetate was blotted off on filter paper and the grids left to dry. Grids were observed by TEM using a 120kV Tecnai G2 Spirit BioTWIN electron microscope (FEI) with a SIS Megaview III camera. Image and fibril length analysis was carried out using ImageJ and OriginLab.

7.2.7 Cell viability experiments of SH-SY5Y cells exposed to α-synuclein fibrils pre-treated with cyclophilin-D

To test the toxicity of fibrils that had been pre-treated with CypD SH-SY5Y neuroblastoma cells were grown in T25 flasks in F-12 Ham's growth medium supplemented with: 10% fetal bovine serum, 1% Pen-Strep, and 1x MEM essential amino acids. Cells were grown incubated at 37°C with 5% CO_2 until 90% confluency. At this point cell growth medium was decanted and the cells washed with PBS pH 7.4. The PBS was discarded and the cells trypsinized. Trypsinized cells were resuspended in the complete growth medium and plated out onto a 96-well clear-bottom plate, with 5000 cells/well in a volume of 100µL. The plate was incubated for 24 hours, after which 10µL of sample was added per well. Samples were as follows: live control (PBS alone), dead control (1% Triton X-100), 50µM WT aSyn fibrils alone, 150µM WT CypD alone, and 50µM WT aSyn fibrils plus 150µM WT CypD. All samples had been pre-incubated quiescently at 37°C for 3 days prior to use. After the addition of samples the plate was incubated for a further 24 hours. 10µL of cell counting kit-8 (CCK-8) reagent (Dojindo) was added per well. The plate was incubated at 37°C for a further 4 hours with absorbance measurements at 450nm being recorded every hour using a Flexstation 3 microplate reader (Molecular Devices). The percentage cell viability was calculated by using the absorbance relative to the live and dead controls, which represented 100% and 0% viability respectively. For all sample conditions n=6.

7.3 Results

7.3.1 The binding of α-synuclein by cyclophilin-D

The question of whether there is an interaction between aSyn and CypD is of interest due to the reports in the literature of the linkages between aSyn, mPTP opening, and mitochondrial dysfunction (198,214). This question was probed by NMR due to our access to our previously obtained backbone assignments of both WT aSyn (see 3.2.7 and 3.3.2) and CypD (determined previously by Prof Lu-Yun Lian), and due to the technique's utility in the study of IDPs and PPIs. To get a complete picture of the interaction HSQCs were collected for ^{15}N-labelled WT aSyn in the presence of unlabelled CypD, and for ^{15}N-labelled CypD in the presence of unlabelled aSyn.

The addition of unlabelled CypD to the labelled aSyn resulted in peak shifts that were clearly evident on the HSQC spectrum (Figure 7-3A). Peak shifts corresponded largely to residues located within the C-terminus, but none of these shifts were >0.06 (Figure 7-3B). Peaks also exhibited substantial line-broadening, which is also commonly used to map sites of interaction and occurs as a result of intermediate exchange between the free and complexed states. Two main regions in aSyn were affected: H50, A53-A58, and E110, D119-Y125 (Figure 7-3B). Other peaks also exhibited line-broadening, but due to peak overlap their interpretation is extremely difficult. The majority of aSyn peaks remained visible after 48 hours, suggesting that the protein is not aggregating over this timeframe (Figure 7-3C). Interestingly, most of the line-broadening effects, like the chemical shift perturbations, were seen around the C-terminal portion of the protein suggesting that this is the site with which CypD interacts.

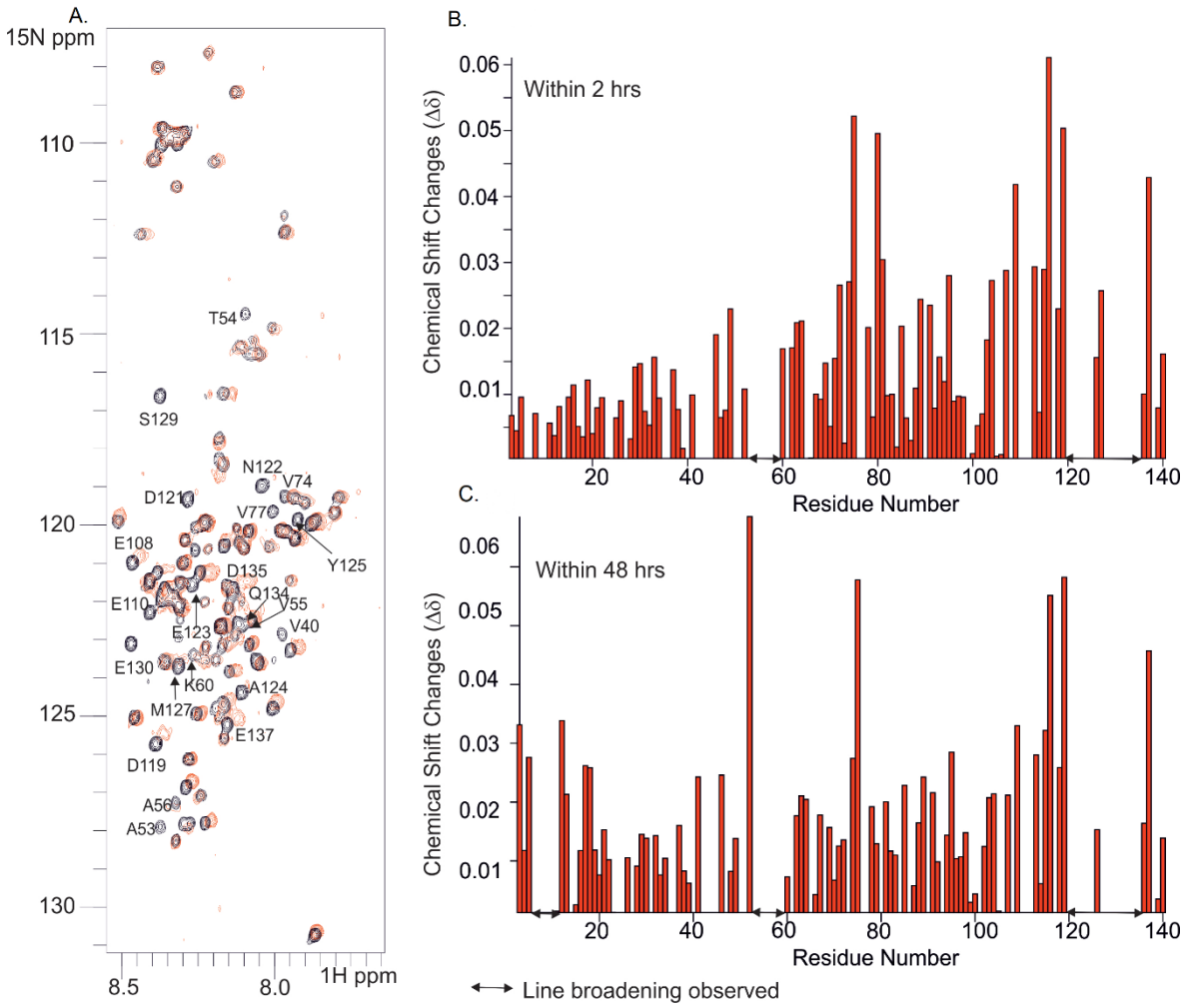

Figure 7-3 – HSQC spectra revealing the site on aSyn with which CypD interacts, and the corresponding chemical shift perturbations. *^{1}H-^{15}N HSQC spectra (A) show 100μM ^{15}N-labelled WT aSyn alone (black) and in the presence of 1mM CypD (red) collected in 20mM phosphate pH 6.5, 20mM NaCl at 298K. Chemical shift perturbations are plotted for within 2 hours (B) and within 48 hours (C). Some chemical shifts are evident at both timepoints, predominantly in the C-terminal region of aSyn. Numerous gaps are apparent due to the loss of the peaks entirely as a result of line-broadening (indicated by double arrows). Both shift perturbations and line-broadening suggest PPIs. The data after 48 hours also suggests that the protein has not begun to aggregate.*

The addition of unlabelled aSyn to ^{15}N-labelled CypD similarly resulted in chemical shift perturbations and substantial line-broadening of peaks also suggestive of binding (Figure 7-4A). It was thought from the results of the HSQCs of ^{15}N-labelled aSyn that the main residues with which CypD interacted were in the C-terminus of aSyn. To confirm this HSQC experiments were conducted between ^{15}N-labelled CypD and the aSynC peptide (residues 119-140) as well as the full-length aSyn protein (Figure 7-4B). Similar effects were seen here as with the full-length protein, confirming that CypD interacts with the C-terminal portion of aSyn. Those residues of CypD identified as being

involved are Gln63, Ser77, Phe83, Ala101, Asn102, Ala103, Gln111, Ser110, Phe112, Phe113, and Trp121. These residues are all located in or around the putative ligand-binding site of CypD (Figure 7-4C). Given that the CTD of aSyn contains five proline residues and CypD catalyses the isomerization of these residues this is perhaps unsurprising. It may suggest that the interaction between the two proteins is in the capacity of CypD acting as a molecular chaperone, rather than as a key regulator of the mPTP.

Identical experiments carried out using ^{15}N-labelled CypD and an aSyn control peptide (residues 74-95) showed no signs of interaction, whilst with aSynM (residues 50-65) only showed very slightly shifted resonances and minimal line-broadening. To further probe the binding location within aSyn the A53T mutant was used. Similar peak shifts to those observed in Figure 7-3A with WT aSyn are also observed with A53T aSyn (Figure 7-5). If this were the binding site this mutation would be expected to perturb the aSyn-CypD interaction. Taken together this very strongly suggests that the region to which CypD binds is located away from the H50, A53-A58 region and is likely specific to the C-terminal region of the protein.

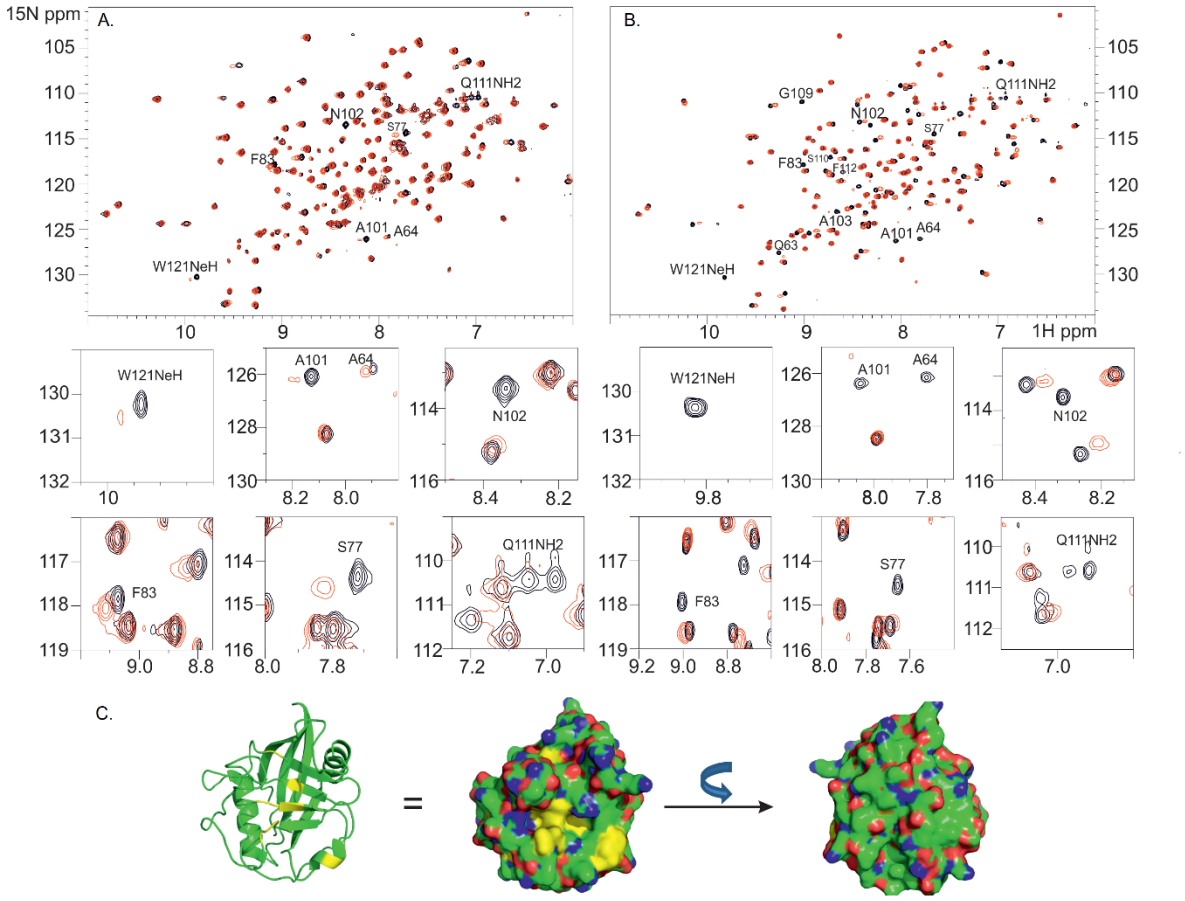

Figure 7-4 - HSQC spectra showing the binding site of aSyn on CypD. *^{1}H-^{15}N HSQC spectra (A) collected at 298K of 100μM ^{15}N-labelled CypD alone (black) and in the presence of 1mM aSyn (red). Underneath the spectra are zoomed-in images of peaks associated with chemical shift perturbation and line-broadening. ^{1}H-^{15}N HSQC spectra (B) collected at 283K of 50μM ^{15}N-labelled CypD alone (black) and in the presence of 1mM aSynC peptide. The lower temperature was utilized to minimize exchange and increase the affinity of the peptide for CypD. Underneath the spectra are zoomed-in images of those peaks that shift or broaden extensively following the addition of the aSynC peptide. The crystal structure of CypD (PDB:2BIT)* (215) *is shown (C) with those residues that exhibit substantial chemical shift perturbations or line-broadening coloured in yellow. These residues are located within or around the putative ligand-binding pocket of CypD.*

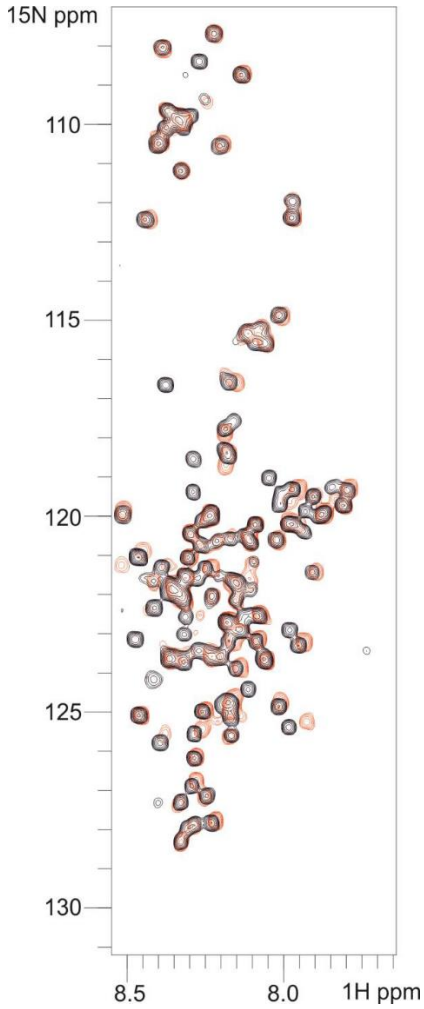

Figure 7-5 - HSQC spectra showing the association between WT CypD and A53T aSyn. *^{1}H-^{15}N HSQC spectra of 100µM ^{15}N-labelled A53T aSyn alone (black) and in the presence of 1mM unlabelled WT CypD. The samples were prepared in 20mM phosphate pH 6.5, 20mM NaCl and collected at 283K. Clear chemical shift pertubations are visible, indicating that WT CypD is capable of binding to A53T. This indicates that the binding site is likely located away from this region.*

To confirm that CypD was acting in its capacity as an isomerase more detailed NMR analyses were undertaken. The 1D spectrum of aSynC peptide alone shows both major and minor conformations, and this is particularly evident for the residues E137 and E139 (Figure 7-6B). Given the preponderance of proline residues in this region of aSyn this is likely due to *cis*-*trans* proline isomers. Integration of the major and minor peaks suggests that the *trans* conformation is about nine times more prevalent than the *cis* conformation. Filtered 1D experiments show that upon the addition of 50µM ^{13}C/^{15}N-labelled CypD there is substantial line-broadening of aSynC signals, especially those of the minor conformations of E137 and E139, and of E123, E130, Y133, D135, and

Y136 (Figure 7-6A). To confirm that CypD is having an impact on the *cis-trans* isomerization of the aSynC NOESY and $^{13}C/^{15}N$-filtered NOESY spectra were collected on 1mM aSynC alone, and in the presence of 50µM $^{13}C/^{15}N$-labelled CypD respectively (Figure 7-6 C&D). The addition of CypD to the aSynC peptide revealed the emergence of crosspeaks between the major and minor conformations of E137 and E139 that were not present in the spectrum of aSynC alone. This suggests that CypD is indeed fulfilling its role as a peptidyl-prolyl isomerase with respect to aSyn and that it is increasing the rate of isomerization between the *cis* and *trans* conformations. Given that the isomerization of CypD is potently inhibited by the cyclopeptide CsA we added it to a final concentration of 100µM in the sample containing 1mM aSynC and 50µM $^{13}C/^{15}N$-labelled CypD to see if this resulted in the abolition of the new crosspeaks. This was indeed the case (Figure 7-6 E) and fully confirmed our hypothesis that CypD binds at the C-terminal region of aSyn via its isomerase domain whereby it proceeds to facilitate *cis-trans* isomerization of aSyn in its most proline-rich region.

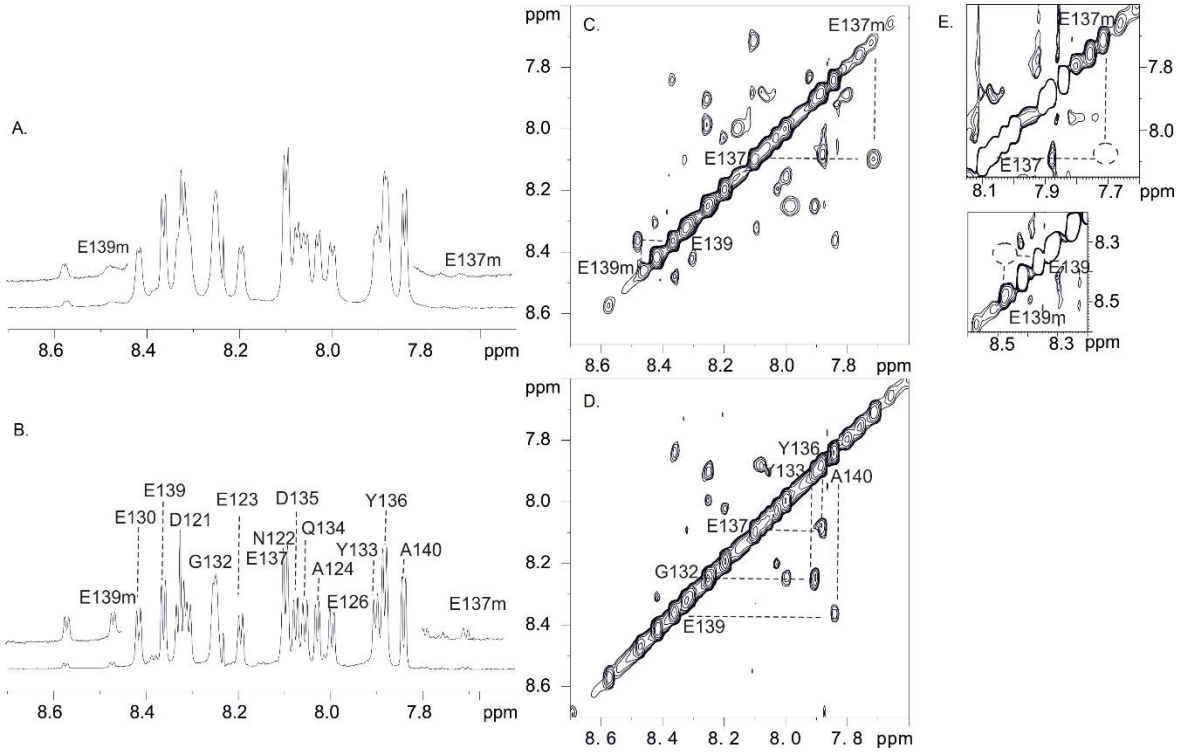

Figure 7-6 - NMR analysis of the isomerization of aSynC peptide by CypD. *The $^{13}C/^{15}N$-filtered proton spectrum (A) of 1mM aSynC in the presence of 50µM $^{13}C/^{15}N$-labelled CypD, collected at 283K. The proton spectrum (B) of 1mM aSynC collected at 283K. The minor conformation peaks of E139 and E137 (E139m and E137m) are shown via zoomed-in peaks. These are likely the result of cis-trans peptidyl-prolyl isomers. Many of the aSynC peaks, especially those of E139m and E137m appear substantially broadened in (A) in comparison to in (B). This suggests an interaction between aSynC and CypD. A $^{13}C/^{15}N$-filtered NOESY spectrum (C) of 1mM aSynC with 50µM of $^{13}C/^{15}N$-labelled CypD shows crosspeaks between the major and minor conformation peaks of E137 and E139 which are not seen in the control NOESY spectrum (D) of 1mM aSynC alone collected at 283K. A NOESY spectrum (E) showing the abolition of these same crosspeaks following the addition of the potent CypD inhibitor, CsA, at 100µM.*

7.3.2 ITC analysis of the interaction between α-synuclein and cyclophilin-D

In light of the NMR data showing that CypD binds to the C-terminal region of aSyn the next objective was to characterize the strength of this interaction by ITC. The experimental set-up consisted of CypD in the cell and aSynC/aSynM peptides in the syringe at high concentration. As expected following on from the NMR experiments, the injection of aSynC peptide resulted in heat pulses suggestive of tight binding to CypD (Figure 7-7A). This data was then fit to a single-site binding model, which output a K_d = 150µM. A repeat of this experiment with the aSynM peptide did not yield data suggestive of tight binding, which is supportive of the findings from the NMR

experiments (Figure 7-7B). The data from the aSynM could not be fit easily as any binding was considerably weaker and the calculated K_d >500µM.

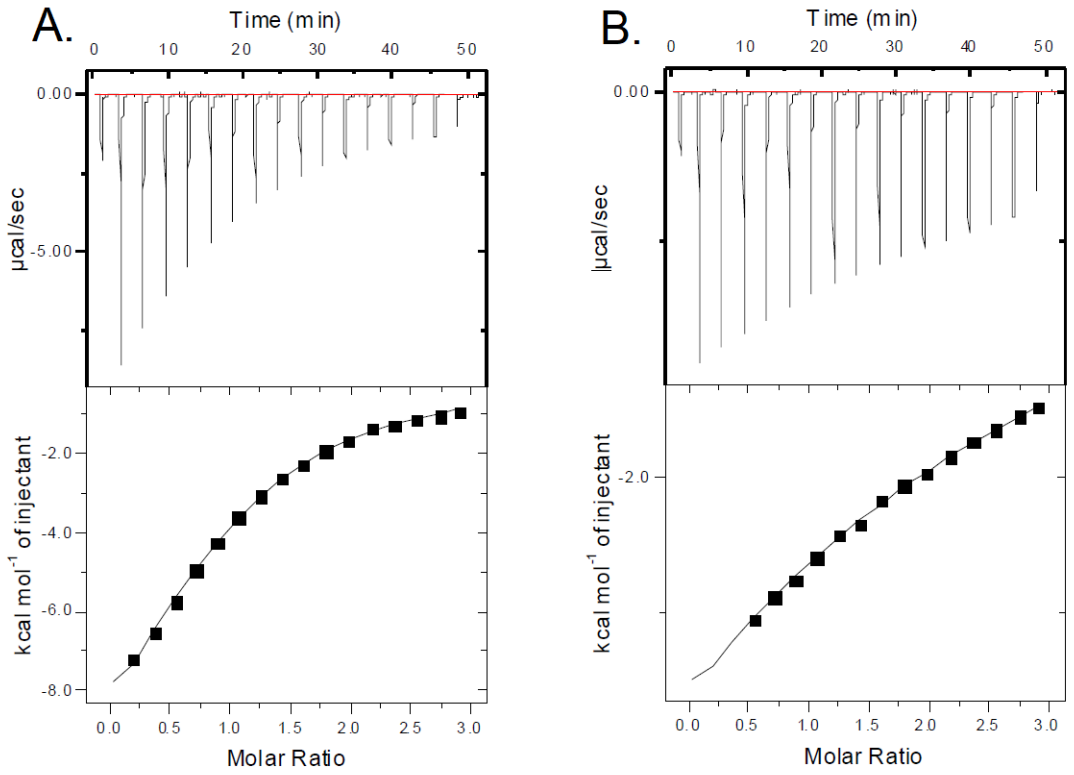

Figure 7-7 - ITC binding curves between CypD and the peptides aSynC and aSynM. *The ITC data for CypD binding to aSynC (A) and aSynM (B) is shown. The top panel for each is the raw calorimetric data output. The bottom panels show the plots of integrated heat signal as a function of the molar ratio of ligand to protein. The data was fit to a one-site binding model to output the K_d, ΔH, and ΔS of the interaction. The K_d for aSynC was determined to be 150µM, whilst the K_d for aSynM could not be determined due to the binding being too weak. This made it impossible to output a reliable binding isotherm.*

7.3.3 ThT and TEM analysis of the effect of cyclophilin-D on α-synuclein aggregation and disaggregation

A recent publication by *Baker et* al showed that cyclophilin-40, a peptidyl-prolyl isomerase like CypD, is capable of dissolving amyloid fibrils formed by aSyn and tau (106). In light of this and our NMR data showing the binding of CypD to the CTD of aSyn, which lies outside the core amyloid fibril and remains disordered in the ssNMR and cryo-EM structures of aSyn fibrils, we investigated whether CypD had an impact on aSyn fibril formation or if it could even disaggregate pre-formed fibrils. A ThT fluorescence assay was carried out to assess the effect on aSyn aggregation using

50µM WT aSyn alone, 150µM WT CypD alone, 50µM WT aSyn plus 150µM WT, R55K or R82K CypD, and 50µM WT aSyn plus 150µM WT CypD:CsA. Each of these samples were incubated with agitation at 37°C for 7 days and endpoint ThT fluorescence measurements were recorded (Figure 7-8A). Control samples of relevant CypD alone and CypD:CsA were also collected and used for subtraction. The samples of aSyn that had been incubated with CypD exhibited ThT fluorescence that was significantly lower ($P < 0.001$) than those of aSyn alone, whilst the addition of the potent CypD-inhibitor, CsA, abolished this effect. This suggests that CypD is indeed preventing aSyn aggregation and fibril formation. Intriguingly this was observed for the R55K catalytically compromised mutant of CypD but not R82K. This may suggest that R82K as well as being catalytically-inactive is also unable to bind CypD, and that it is the binding rather than the isomerase activity that is responsible for the prevention of aggregation. It could thus also be inferred that CsA prevents aSyn binding.

To explore whether this preventative effect was concentration dependent an additional ThT fluorescence assay was conducted, using CypD at concentrations ranging from 25µM to 150µM (Figure 7-9). It was evident from this data that at below a 1:1 CypD:aSyn ratio that aggregation was not prevented. However, at 1:1 and above there was no rise in ThT fluorescence, which is indicative of no fibril formation.

The effects of CypD on pre-existing aSyn fibrils were assessed by TEM. Clear differences were observed (Figure 7-8B) and a lengths analysis of the fibrils formed by aSyn alone shows quite a broad distribution, with the average at ~450nm (Figure 7-8 C&D). However, when fibrils were incubated with WT CypD a vast number of much smaller fibrils is observed (Figure 7-8 B). This is reflected in the reduced size distribution of the fibrils, and the mean length is just ~50nm (Figure 7-8 C&D). Interestingly, the data also suggests that this shortening of the fibrils is a result of the isomerase activity of CypD, as the same effect is not exhibited by the catalytically compromised mutants, R55K and R82K (Figure 7-8 B-D).

The ability of WT CypD to disaggregate pre-formed aSyn fibrils was tested at a range of concentrations (Figure 7-10). Samples of fibrils of WT aSyn alone (prepared to 50µM monomer equivalent) and in the presence of 25-150µM WT CypD were incubated at 37°C for 7 days. Representative TEM images of WT aSyn fibrils alone, and in the presence of 50µM and 100µM WT CypD are shown (Figure 7-10 A-C). An analysis of the lengths of the fibrils on the grids was performed (Figure 7-10 D). This revealed that the mean length of fibrils decreases very sharply upon the addition of CypD (from ~450nm to <200nm). The addition of CypD also results in a narrower distribution in the lengths of the fibrils. The mean length of aSyn fibrils drops consistently as the concentration of CypD present increases, up until 150µM CypD. This is likely due to the increased concentration of CypD resulting in itself aggregating, as a significant quantity of precipitated protein was observed in this sample.

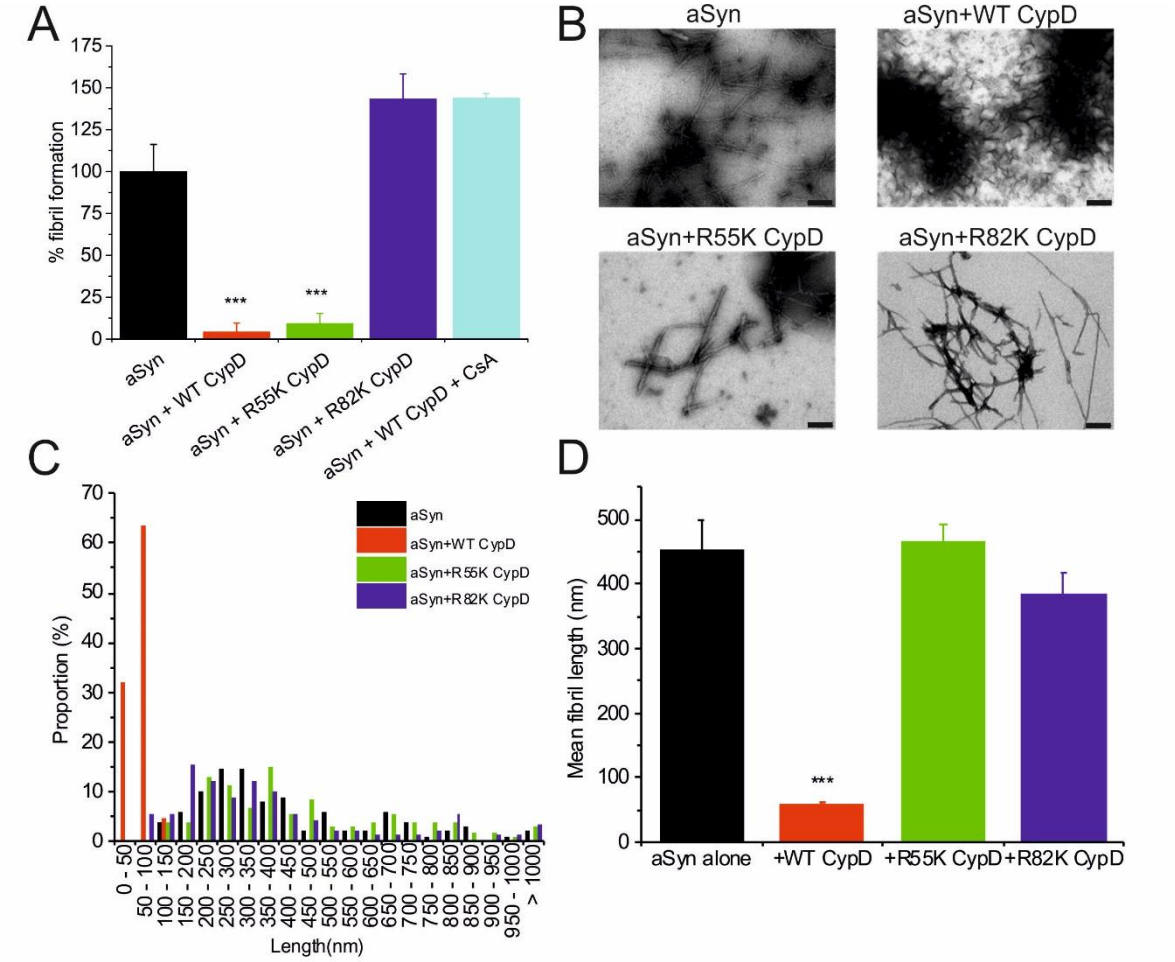

Figure 7-8 - ThT fluorescence data and TEM images showing the effect of CypD on aSyn aggregation and disaggregation. *ThT fluorescence endpoint reads (A) of 50μM WT aSyn, 50μM WT aSyn plus 150μM WT, R55K or R82K CypD, and of 50μM WT aSyn plus 150μM WT CypD:CsA are shown. All samples were incubated at 37°C for 7 days with agitation prior to measurement. Control samples of CypD(:CsA) alone were also collected, and these values were subtracted from the reads containing aSyn and CypD(:CsA). The ThT fluorescence of aSyn is reduced in those samples that were incubated with CypD, suggesting that CypD may prevent or impede aSyn aggregation. All ThT samples were plated in triplicate. N=2. The ability of CypD to disaggregate pre-formed aSyn fibrils was probed by TEM (B). Samples of 50μM aSyn fibrils, and of 50μM fibrils with 150μM CypD (WT, R55K or R82K) were incubated for 7 days at 37°C. The images suggest CypD may exhibit disaggregation behaviour as samples that had been incubated with WT CypD formed dense networks of much shorter fibrils compared to those in the sample of aSyn alone. The catalytically impaired CypD mutants, R55K and R82K, did not exhibit this same fibril shortening behaviour. Scale bars are 200nm. Fibril lengths analyses (C & D) show how the incubation of aSyn with WT CypD reduces the mean fibril length and that this is statistically significant. *** P <0.001 as determined by ANOVA with the Tukey range test. The number of measurements used for the lengths analysis are as follows: WT aSyn alone (103), with 150μM WT CypD (107), with 150μM R55K CypD (108), with 150μM R82K CypD (91).*

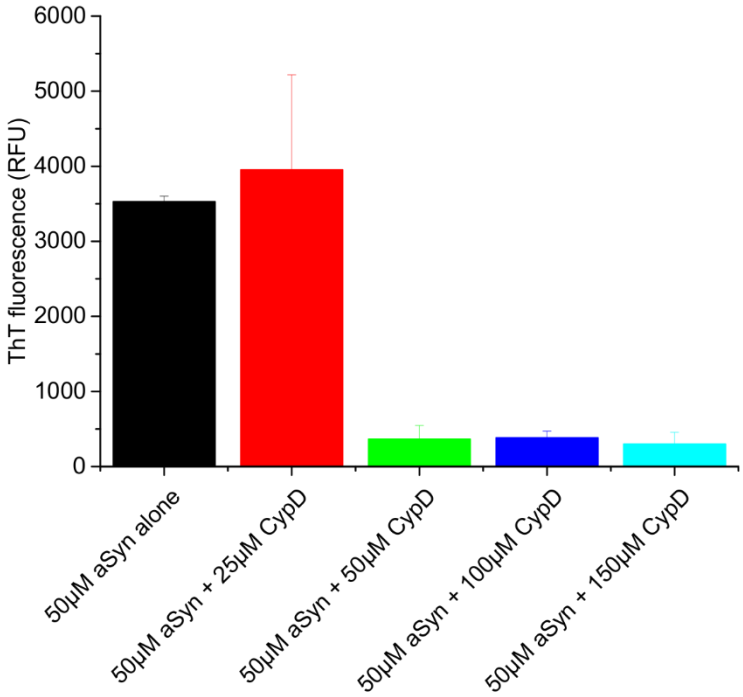

Figure 7-9 - ThT fluorescence data showing the effect of varying CypD concentration on aSyn aggregation. *Samples of 50μM aSyn alone, and containing 25, 50, 100, and 150μM WT CypD were prepared in PBS pH 7.4. These samples were incubated for 7 days at 37°C with agitation prior to measurement. All samples were measured in triplicate. Relevant control samples were also prepared and subtracted. N=1.*

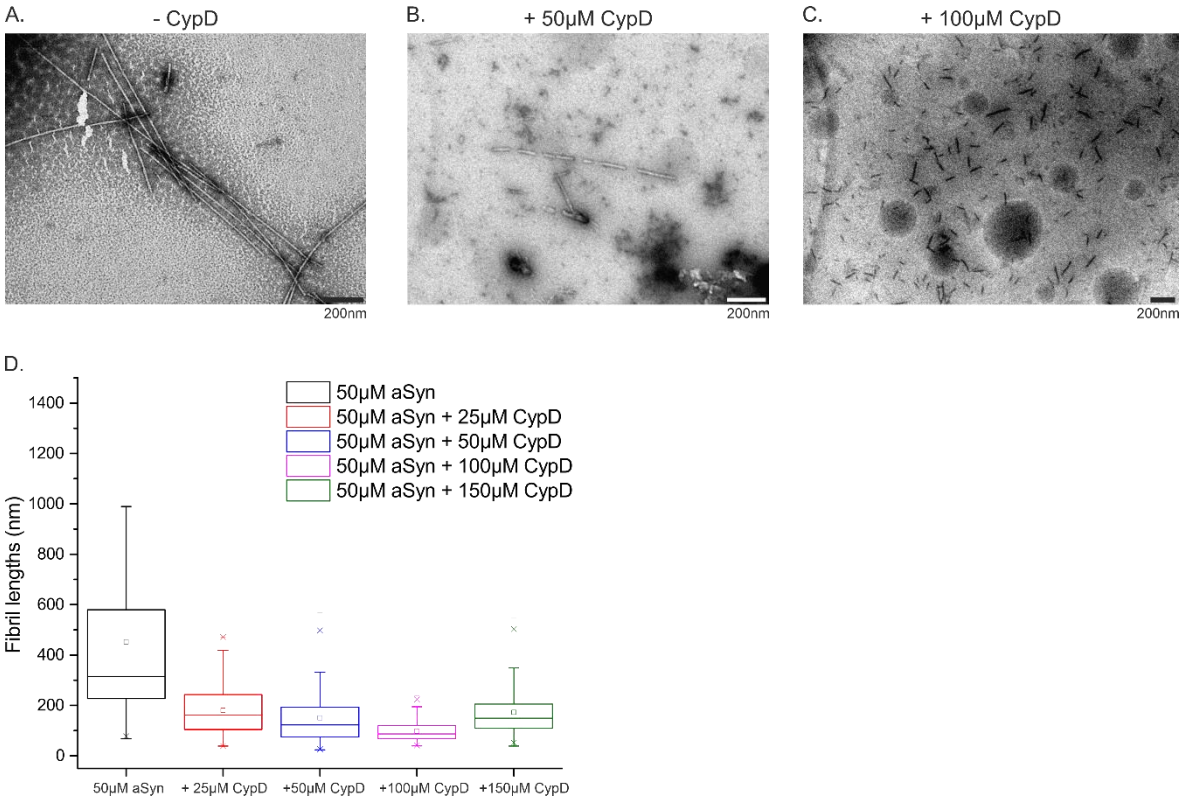

Figure 7-10 - TEM images and fibril lengths analysis showing the effect of concentration on the ability of WT CypD to disaggregate aSyn fibrils. *TEM images of 50μM WT aSyn alone (A), 50μM WT aSyn plus 50μM WT CypD (B), and 50μM WT aSyn plus 100μM WT CypD (C). The fibrils were formed by incubation of 100μM WT aSyn for 7 days with agitation at 37°C. The fibrils alone or with WT CypD were incubated for a further 7 days without agitation at 37°C. All images were collected on carbon-coated copper grids and visualized by negatively-staining with 4% uranyl acetate. A box-and-whisker plot showing the fibril lengths data of WT aSyn alone and with 25-150μM WT CypD (D). The upper and lower limits of the boxes indicate the 25th and 75th percentiles of the data, whilst the horizontal line and small square indicate the median and mean respectively. The "whiskers" indicate the 5th and 95th percentile range of the data. The number of measurements used for the lengths analysis are as follows: WT aSyn alone (103), plus 25μM WT CypD (52), 50μM WT CypD (116), 100μM WT CypD (145), and 150μM WT CypD (156).*

7.3.4 NMR analysis of the disaggregation of α-synuclein fibrils by cyclophilin-D

Following on from the TEM data suggesting that WT CypD was actively shortening aSyn fibrils we wanted to probe this process by NMR. As aSyn begins to aggregate and oligomerize its molecular weight rapidly exceeds the "size-limit" of NMR. This is generally ~35kDa without the use of non-uniform labelling or other techniques (216). Above this size-limit excessive line-broadening, caused by the slow tumbling rate of the molecules, causes the peaks to disappear. This could be seen in the HSQC of aSyn fibrils, whereby the only remaining residue peaks visible were generally

within the highly dynamic CTD which tumbles/relaxes independently of the rest of the fibril (Figure 7-11A). However, over time in the presence of WT CypD many of these peaks reappeared and became more intense (Figure 7-11B-D). This suggests that the fibrils were being disaggregated by CypD and the monomer population of aSyn progressively restored. This would fit with the TEM data shown in Figure 7-8. The catalytic activity of CypD is passive in that the hydrolysis of neither ATP nor GTP is required to drive the process. This stands in contrast to the activity of some other chaperones (e.g. the Hsp70 disaggregase) that have been reported to disaggregate pre-existing aSyn fibrils, but in a process that is dependent on ATP hydrolysis (105).

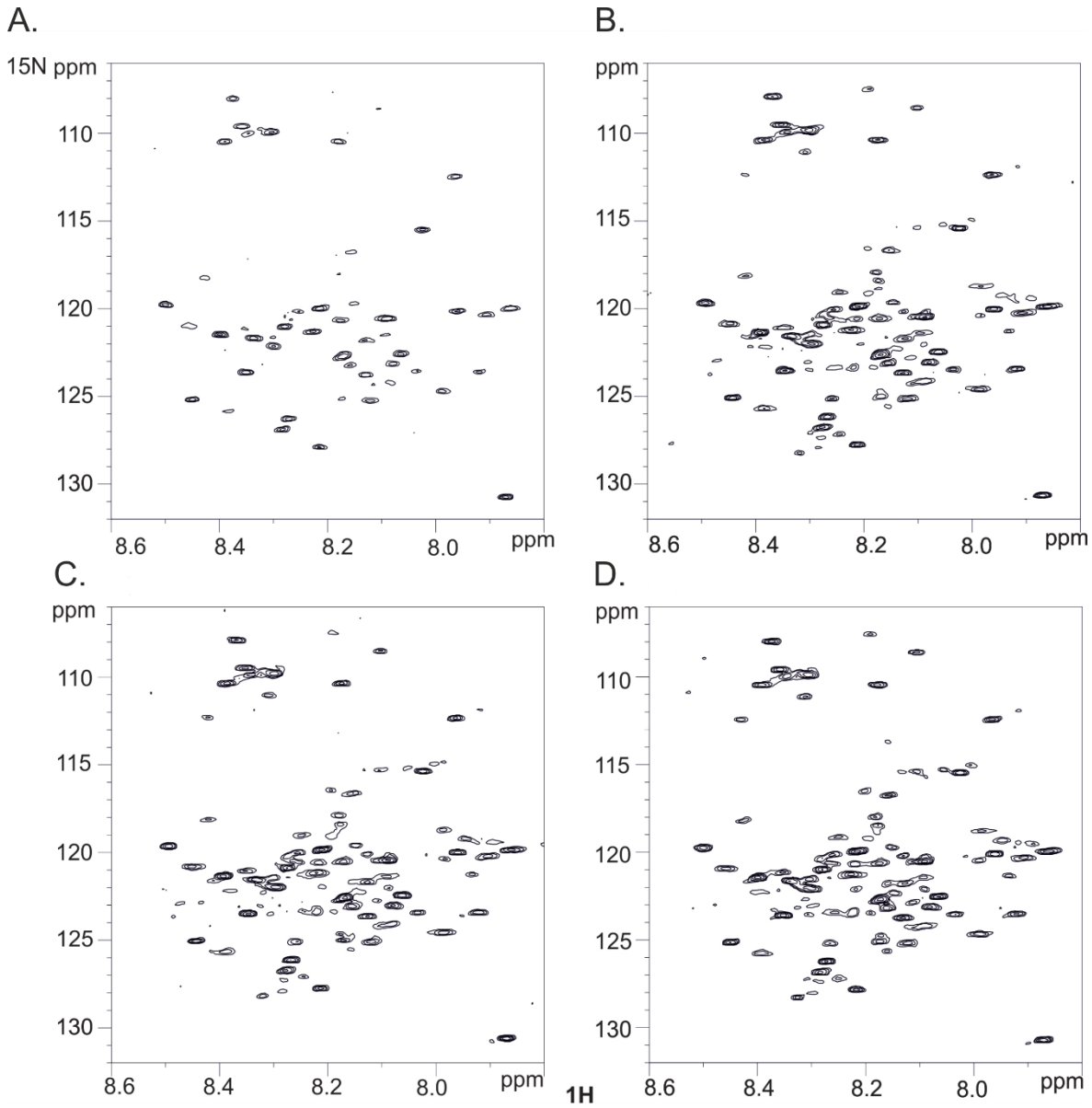

Figure 7-11 - HSQCs showing the disaggregation of aSyn fibrils by CypD. *^{1}H-^{15}N HSQC spectra were taken of 100µM ^{15}N-labelled WT aSyn fibrils in the presence of 300µM WT CypD at 298K. All samples were prepared in 20mM phosphate pH 6.5, 20mM NaCl. Spectra were collected at 0 hours (A), 8 hours (B), 12 hours (C), and 36 hours (D). As aSyn aggregates peaks are lost due to significant line-broadening. However, in the presence of WT CypD peaks are recovered over time. This restoration of peaks suggests that CypD is disaggregating the aSyn fibrils over time.*

7.3.5 Cell viability experiments of SH-SY5Y cells exposed to α-synuclein fibrils pre-treated with cyclophilin-D

Given that the incubation of aSyn fibrils with CypD results in their apparent shortening and disaggregation it became a question as to whether this resulted in a change of toxicity. Whilst fibrils are no longer considered to be the main toxic species any rise in the level of oligomers as a

consequence of fibril shortening/disaggregation could result in an increase in toxicity. Here, SH-SY5Y neuroblastoma cells were exposed to WT aSyn fibrils alone, WT CypD alone, and WT aSyn fibrils that had been pre-incubated with WT CypD. All the samples had been incubated at 37°C for 3 days prior to exposure to the cells, which were challenged for 24 hours. PBS pH 7.4 and 1% Triton X-100 were used as live and dead controls, respectively. As expected, neither the WT aSyn fibrils alone nor WT CypD alone were toxic to the cells, as indicated by the intensity at 450nm (Figure 7-12). Additionally, the fibrils that had been pre-treated with CypD also exhibited no cell toxicity. This suggests that the action of CypD does not result in an increased population of oligomers, and thus a similar mechanism of action could be a viable strategy in targeting amyloid fibrils.

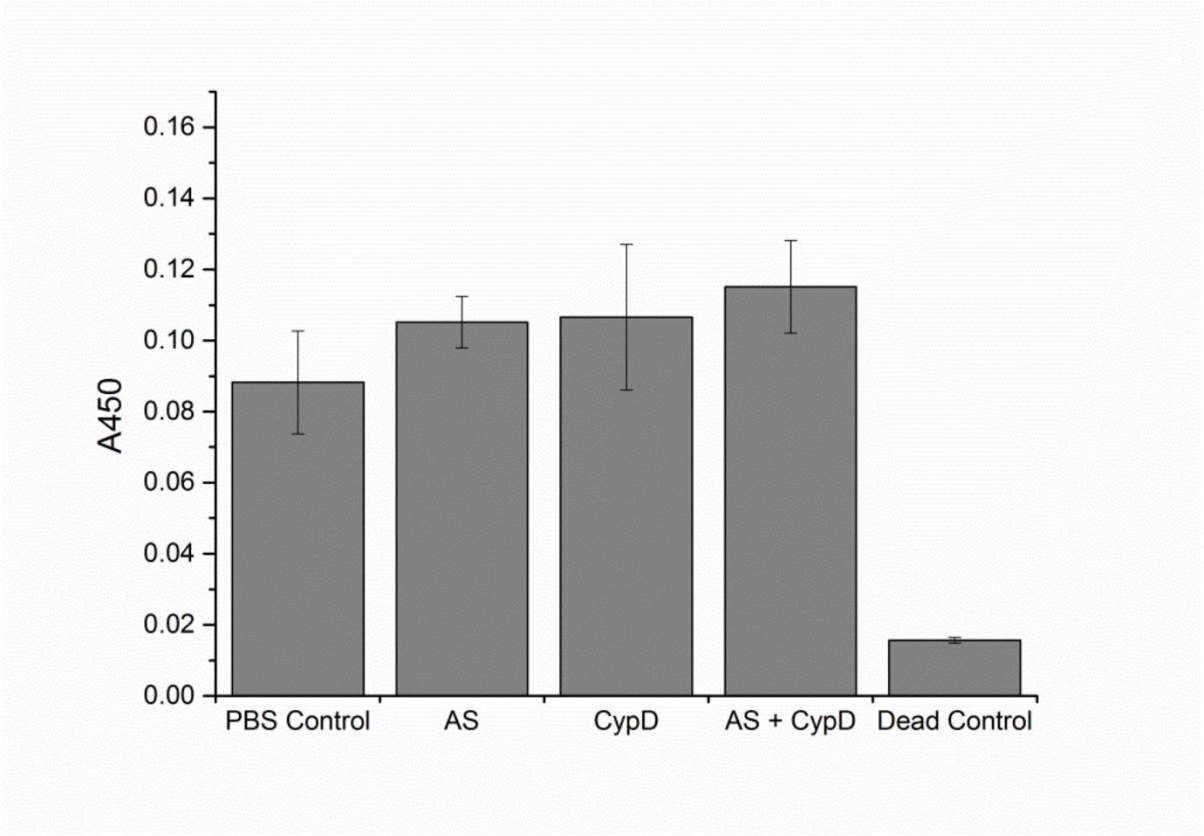

Figure 7-12 - Cell viability assay of SH-SY5Y cells exposed to WT aSyn fibrils, WT CypD, and WT aSyn fibrils pre-treated with WT CypD using CCK-8. *The cells were exposed to the following conditions for 24hours: PBS pH 7.4 alone (live control), 5µM WT aSyn fibrils, 15µM WT CypD, 5µM WT aSyn fibrils pre-incubated with a three-fold molar excess of WT CypD, and 1% Triton X-100 (dead control). The data shows that the pre-treatment of aSyn fibrils with CypD does not result in an increase in toxicity. Six wells were prepared per condition. N=1.*

7.4 Discussion

In this chapter is described a hitherto unknown and uncharacterized interaction between aSyn and the mitochondrial protein CypD. This work was initially conducted in response to reports that aSyn oligomers travelled to the mitochondria in neurodegenerative disease and initiated mPTP opening; a process regulated by CypD (112). The question of what triggers neuronal cell death is an open one and, given the known links between neurodegeneration, oxidative stress, and mitochondrial dysfunction, it seemed plausible that aSyn aggregates initiated Ca^{2+}-mediated cell death via an interaction with CypD and subsequent mPTP opening (193). Lending a measure of credence to this hypothesis is the knowledge that many of the genes identified in familial cases of PD (e.g. parkin, PINK1) are also involved in mitochondrial quality control (69). The initial results of the experiments described in this chapter were extremely encouraging. HSQC titrations showed peak shifts and line-broadening in both aSyn and CypD when they were titrated against each other, which is strongly indicative of binding (Figure 7-3 & Figure 7-4). These shifts were in peaks associated with amino acids in the C-terminal portion of aSyn and those residues that make up the catalytic site of CypD. This data was backed-up by evidence from ITC experiments involving CypD and peptides of aSyn (Figure 7-7). It was seen that CypD and the aSynC peptide exhibited binding with a K_d = 150μM, whilst no binding was observed with the aSynM peptide. It has been shown previously that the CTD portion of aSyn transiently 'wraps around' to interact with the NTD and in this way protect the NAC domain from aggregation (38). In light of the NMR and ITC data obtained showing that CypD binds to the CTD of aSyn it was thought that this interaction would potentiate and encourage aSyn aggregation. In this vein ThT assays were conducted to follow aSyn aggregation over a period of 7 days, alone and in the presence of CypD. In stark contrast to initial expectations it was clear that CypD prevented the aggregation of aSyn in a concentration-dependent manner (Figure 7-8 & Figure 7-9). Not only was no ThT fluorescence apparent, but neither were any fibrils/aggregates seen by TEM. Interestingly, the addition of the potent CypD inhibitor, CsA,

abolished this effect as did the R82K mutation (Figure 7-8A). The catalytically-compromised mutant, R55K, exhibited the same effect as the WT CypD protein. This suggests that the prevention of aSyn aggregation is not as a result of the catalytic activity of CypD, but rather due to binding alone. It was around this time that *Baker et al* published a paper detailing how Cyp40 could unravel pre-existing amyloid fibrils of tau and aSyn (106). In light of this the effect of CypD on pre-formed aSyn fibrils was tested. ASyn alone forms fibrils with a quite broad distribution of lengths, with the mean ~450nm. However, when incubated in the presence of CypD a vast number of shorter amyloid fibrils were seen, with the mean length being ~50nm (Figure 7-8 & Figure 7-10). This was not, however, seen in the presence of CsA or with the catalytically compromised mutants R55K and R82K. This indicates that, unlike the preventative activity, the ability of CypD to disaggregate pre-existing fibrils does rely on its catalytic peptidyl-prolyl isomerization activity. These TEM data were supported by NMR data in which ^{15}N-labelled aSyn had been incubated with agitation so as to form fibrils. The ^{15}N-labelled fibrils were then incubated in the NMR tube in the presence of WT CypD and HSQC spectra were recorded every 12 hours for three days. HSQC spectra of aggregated aSyn tend to display only the peaks corresponding to the CTD of the protein, as the aggregates exceed the size-limit of NMR and thus their NMR spectra are subjected to prohibitive line-broadening. The highly dynamic nature of the C-terminus of aSyn means that these peaks are often visible, however. Over the course of time the other peaks were restored and this is supportive of aSyn fibrils being broken up by CypD and an increase in the population of monomeric aSyn (Figure 7-11). It is also noteworthy that the NMR spectra of the aSynC peptide in the presence of CypD revealed numerous minor conformation peaks that were not present in the spectra of aSynC alone. These were likely the result of *cis-trans* proline isomerization catalysed by CypD, further supporting the TEM data.

Given the recent reports that oligomers, rather than fibrils, are the aSyn species most associated with toxicity it was also important to assess whether this disaggregation process catalysed by CypD resulted in a gain of toxicity (20). In my hands this was not the case, and SH-SY5Y cells challenged with aSyn fibrils treated with CypD did not exhibit a gain of toxicity compared to

the non-disaggregated fibrils (Figure 7-12). This makes the approach interesting from a therapeutic point-of-view and consequently the results of these experiments are being used as the basis of a patent application.

This approach is therapeutically interesting for a number of reasons. Firstly, it can act against pre-existing aggregates. This is extremely useful given that PD only becomes outwardly visible, and ergo diagnosable, in Braak stage 3 (61). Strategies that solely impede the aggregation process also by extension require supplementary research into biomarkers that may accurately predict PD onset. This means that this approach could potentially prevent the pathology getting worse, and hopefully go some way to reversing pre-existing problems. This statement should be tempered with the understanding that neuronal loss is irreversible and thus actual brain damage that has taken place during disease progression is likely to remain permanent. It may be possible to rescue neurons in the throes of Lewy pathology, though. Secondly, the ability of CypD to disaggregate aSyn fibrils is an ATP-independent process. This is quite remarkable given the stability of amyloid fibrils, and is in stark contrast to the ATP-driven disaggregation process observed by *Gao et al* using the Hsp70 disaggregase (105). It is my hypothesis that the disaggregation of aSyn by CypD instead works through CypD shifting the monomer-oligomer-fibril equilibrium back towards the monomeric state. This more passive approach could prove highly favourable given that bio-energetic stress is a feature of neurodegenerative disease, and thus placing an additional energetic burden on diseased neurons could be counter-productive.

Despite these positives there are likely to be a number of other factors that need to be taken into consideration. If the preventative/disaggregase activity of CypD with respect to aSyn were to be harnessed therapeutically, in what form would this take? There is the possibility of administering CypD to patients, in which case there are questions as to how this would best reach the brain and enter the neurons. It would likely need to be packaged or modified in some way to allow its crossing of the blood-brain barrier and subsequent entry into neurons. If this were

successful how much CypD would be needed to mediate its disaggregase activity successfully? In the results reported in this chapter it was found that CypD reduced fibril length in a concentration-dependent manner (Figure 7-10). This may mean that substantial quantities of CypD would be required to reach the brain. Surmounting these challenges may prove to be a herculean task. It should also be noted that CypD itself is a protein of key therapeutic interest and its role in the mitochondria and the permeability transition is incompletely understood. In light of this, any therapeutic administration of the protein or effort to modulate the activity of the protein should be approached with caution.

The reality is, as also necessitated by the patent application, that substantial *in vivo* work is required to take this project to the next level. This is to test the efficacy of the approach in a more physiological environment, to observe any unintended side-effects, and also to get a feeling for how any hurdles that may present themselves (e.g. delivery) may be circumvented. I believe that in the first instance it may be useful to assess the viability of the approach in cell models or in *C.elegans* before later moving onto more challenging systems (e.g. mice). This is an exciting chapter in the story of aSyn and it certainly warrants further investigation.

8 Concluding Statement and Future Directions

Despite decades of intensive study the physiology and pathophysiology of aSyn remain poorly understood. This lack of understanding extends more broadly into the disease processes underlying neurodegeneration as a whole, and thus exists a total absence of non-symptomatic therapeutics. Research into tackling neurodegenerative diseases, especially AD, has been rocked by recent high-profile failures at late-stages of clinical trials and the resultant withdrawal of several pharmaceutical giants from the field as a whole. It is in this uncertain and myopic climate that the field of neurodegenerative research now rests. It is a time for the field to return back to basics, for researchers to learn to walk before they can run, and for previously established dogmatic truths to come under renewed scrutiny. This has recently been exemplified with respect to PD and the discovery, by *Shahmoradian et al*, that LBs are not as jam-packed with aSyn fibrils as previously thought, but also consist of vast quantities of organelles and lipid membranes (191). This finding alone in my view is paradigm-shifting. It forces a re-evaluation of the place of aSyn fibril formation at the centre of PD pathology and of the role that aSyn-lipid interactions play in the disease process. It also brings the role of mitochondrial dysfunction and oxidative stress more firmly back into the picture, as the mitochondria were found to 'ring' the LBs, and perhaps will encourage more effort into establishing the role of the other genes associated with familial PD (e.g. parkin, LRRK2) which are clearly of pathological relevance yet have been previously considered to be peripheral to the main story (60).

In light of all of this I feel that my PhD thesis represents a valuable contribution to the amyloid field. I have shown two approaches with future potential in being utilized as therapeutics. One of these is the KDGIVNGVKA peptide inhibitor of aSyn aggregation and the other is the use of CypD to both prevent aSyn aggregation and actively disaggregate pre-existing fibrils, for which a patent application is currently being compiled. Numerous challenges are likely to arise in the utilization of any peptide inhibitor of aSyn aggregation (stability, penetrance etc) and thus the

insight gained here – that it is the IVN motif that is necessary for aSyn binding – will be valuable in the development of any further peptide inhibitors without abrogating aSyn binding. The biophysics of the aSyn-CypD interactions have been well-characterized here, although greater insight into how precisely proline cis-trans isomerization mediates the observed effects would be welcome, as this could provide a link to using a similar strategy with other amyloids. Both of these approaches need further exploration *in vivo*, however. My efforts through NMR metabolomics and cell viability assays to assess their physiological effects provided encouraging results, suggesting that shortened fibrils and the disaggregation of fibrils do not increase cell toxicity, but are not alone sufficient to give insight as to how these approaches would fare in a more physiologically-relevant environment. This is the next step in carrying this work forward and is essential for the patent application process.

The studies of aSyn-lipid interactions described in this thesis also have enhanced relevance in light of the recent advances in the literature. These lipid interactions are modulated by a variety of factors including charge and conformational state; nitration results in impaired lipid-interactions through seemingly a combination of electrostatic repulsion and tyrosine cross-linking to form non-amyloidogenic oligomers/polymers. Slight changes in these variables, as exhibited by the different PD-linked aSyn mutants, result in differences in lipid affinity that may have profound downstream consequences. This is an aspect of aSyn pathology that remains a mystery and is of great interest; the question of why different point mutations in aSyn only one or two residues apart result in such great differences in the onset of PD. In this work I have attempted to answer this question by studying rates of aggregation, lipid affinity, fibril structure and morphology, and toxicity to cells. Differences were clearly evident across the different point mutants in both their nitrated/non-nitrated forms and it seems likely that the answer is some combination of all of these features. However, the complete answer may only become evident with a greater understanding of the other processes at play in the development of PD. For example, recent work has shown the importance of prion-like seeding in spreading aSyn pathology. It is possible that different fibril structures will have different seeding capacities, and the formation of these different structures may be

dependent on a variety of factors including rate of aggregation, lipid-binding, and the local chemical environment.

In conclusion, I am proud of the contribution I have made to the field as part of this PhD thesis and see it as a foundation on which future work can build. I am also optimistic for the future of the field. Despite large setbacks it seems that research and development is heading in the right direction, and hopefully this will lead to the emergence of new disease-modifying therapeutics.

9 References

1. Sipe JD, Benson MD, Buxbaum JN, Ikeda SI, Merlini G, Saraiva MJM, et al. Amyloid fibril proteins and amyloidosis: chemical identification and clinical classification International Society of Amyloidosis 2016 Nomenclature Guidelines. Amyloid. 2016;23(4):209–13.

2. Romero D, Aguilar C, Losick R, Kolter R. Amyloid fibers provide structural integrity to Bacillus subtilis biofilms. Proc Natl Acad Sci. 2010 Feb 2;107(5):2230–4.

3. Masters CL, Simms G, Weinman NA, Multhaup G, McDonald BL, Beyreuther K. Amyloid plaque core protein in Alzheimer disease and Down syndrome. Proc Natl Acad Sci. 1985;82(12):4245–9.

4. Westermark P, Andersson A, Westermark GT. Islet Amyloid Polypeptide, Islet Amyloid, and Diabetes Mellitus. Physiol Rev. 2011 Jul;91(3):795–826.

5. Esch FS, Keim PS, Beattie EC, Blacher RW, Culwell AR, Oltersdorf T, et al. Cleavage of amyloid β peptide during constitutive processing of its precursor. Science (80-). 1990 Jun 1;248(4959):1122–4.

6. Vassar R, Bennett BD, Babu-Khan S, Kahn S, Mendiaz EA, Denis P, et al. β-Secretase cleavage of Alzheimer's amyloid precursor protein by the transmembrane aspartic protease BACE. Science (80-). 1999 Oct 22;286(5440):735–41.

7. Zhang Z, Nadeau P, Song W, Donoviel D, Yuan M, Bernstein A, et al. Presenilins are required for γ-secretase cleavage of β-APP and transmembrane cleavage of Notch-1. Nat Cell Biol. 2000 Jul 1;2(7):463–5.

8. Lashuel HA, Petre BM, Wall J, Simon M, Nowak RJ, Walz T, et al. α-Synuclein, Especially the Parkinson's Disease-associated Mutants, Forms Pore-like Annular and Tubular Protofibrils. J Mol Biol. 2002 Oct;322(5):1089–102.

9. Chen SW, Drakulic S, Deas E, Ouberai M, Aprile FA, Arranz R, et al. Structural characterization of toxic oligomers that are kinetically trapped during α-synuclein fibril formation. Proc Natl Acad Sci. 2015;112(16):E1994–2003.

10. Tuttle MD, Comellas G, Nieuwkoop AJ, Covell DJ, Berthold DA, Kloepper KD, et al. Solid-state NMR structure of a pathogenic fibril of full-length human α-synuclein. Nat Struct Mol Biol. 2016 Mar 28;23(5):409–15.

11. Chiti F, Dobson CM. Protein misfolding, functional amyloid, and human disease. Annu Rev Biochem. 2006 Jan 6;75:333–66.

12. Jahn TR, Makin OS, Morris KL, Marshall KE, Tian P, Sikorski P, et al. The Common Architecture of Cross-β Amyloid. J Mol Biol. 2010 Jan 29;395(4):717–27.

13. Bousset L, Pieri L, Ruiz-Arlandis G, Gath J, Jensen PH, Habenstein B, et al. Structural and functional characterization of two alpha-synuclein strains. Nat Commun. 2013 Jan;4:2575.

14. Guo JL, Covell DJ, Daniels JP, Iba M, Stieber A, Zhang B, et al. Distinct α-synuclein strains differentially promote tau inclusions in neurons. Cell. 2013 Jul 3;154(1):103–17.

15. DiFiglia M, Sapp E, Chase KO, Davies SW, Bates GP, Vonsattel JP, et al. Aggregation of huntingtin in neuronal intranuclear inclusions and dystrophic neurites in brain. Science (80-). 1997 Sep 26;277(5334):1990–3.

16. Goedert M, Spillantini MG, Jakes R, Rutherford D, Crowther RA. Multiple isoforms of human microtubule-associated protein tau: sequences and localization in neurofibrillary tangles of Alzheimer's disease. Neuron. 1989 Oct 1;3(4):519–26.

17. Spillantini MG, Schmidt ML, Lee VM-Y, Trojanowski JQ, Jakes R, Goedert M. α-Synuclein in Lewy bodies. Nature. 1997 Aug 28;388(6645):839–40.

18. Milanesi L, Sheynis T, Xue W-F, Orlova E V, Hellewell AL, Jelinek R, et al. Direct three-

dimensional visualization of membrane disruption by amyloid fibrils. Proc Natl Acad Sci U S A. 2012 Dec 11;109(50):20455–60.

19. Holmes C, Boche D, Wilkinson D, Yadegarfar G, Hopkins V, Bayer A, et al. Long-term effects of Aβ42 immunisation in Alzheimer's disease: follow-up of a randomised, placebo-controlled phase I trial. Lancet. 2008 Jul 19;372(9634):216–23.

20. Winner B, Jappelli R, Maji SK, Desplats PA, Boyer L, Aigner S, et al. In vivo demonstration that α-synuclein oligomers are toxic. Proc Natl Acad Sci. 2011 Mar 8;108(10):4194–9.

21. Kayed R, Sokolov Y, Edmonds B, McIntire TM, Milton SC, Hall JE, et al. Permeabilization of lipid bilayers is a common conformation-dependent activity of soluble amyloid oligomers in protein misfolding diseases. J Biol Chem. 2004 Nov 5;279(45):46363–6.

22. Dunker AK, Silman I, Uversky VN, Sussman JL. Function and structure of inherently disordered proteins. Curr Opin Struct Biol. 2008 Dec;18(6):756–64.

23. Uversky VN, Gillespie JR, Fink AL. Why are "natively unfolded" proteins unstructured under physiologic conditions? Proteins Struct Funct Genet. 2000 Nov 15;41(3):415–27.

24. Van Der Lee R, Buljan M, Lang B, Weatheritt RJ, Daughdrill GW, Dunker AK, et al. Classification of intrinsically disordered regions and proteins [Internet]. Vol. 114, Chemical Reviews. American Chemical Society; 2014. p. 6589–631.

25. Iwai A, Masliah E, Yoshimoto M, Ge N, Flanagan L, Rohan de Silva H., et al. The precursor protein of non-Aβ component of Alzheimer's disease amyloid is a presynaptic protein of the central nervous system. Neuron. 1995;14(2):467–75.

26. Burré J, Sharma M, Südhof TC. α-Synuclein assembles into higher-order multimers upon membrane binding to promote SNARE complex formation. Proc Natl Acad Sci U S A. 2014 Oct 7;111(40):E4274-83.

27. Nakajo S, Shioda S, Nakai Y, Nakaya K. Localization of phosphoneuroprotein 14 (PNP 14) and its mRNA expression in rat brain determined by immunocytochemistry and in situ hybridization. Mol Brain Res. 1994 Nov;27(1):81–6.

28. Buchman VL, Hunter HJA, Pinon LGP, Thompson J, Privalova EM, Ninkina NN, et al. Persyn, a Member of the Synuclein Family, Has a Distinct Pattern of Expression in the Developing Nervous System. J Neurosci. 1998 Nov 15;18(22):9335–41.

29. Waterhouse AM, Procter JB, Martin DMA, Clamp M, Barton GJ. Jalview Version 2--a multiple sequence alignment editor and analysis workbench. Bioinformatics. 2009 May 1;25(9):1189–91.

30. Ulmer TS, Bax A, Cole NB, Nussbaum RL. Structure and dynamics of micelle-bound human α-synuclein. J Biol Chem. 2005 Mar 11;280(10):9595–603.

31. Bodner CR, Dobson CM, Bax A. Multiple Tight Phospholipid-Binding Modes of α-Synuclein Revealed by Solution NMR Spectroscopy. J Mol Biol. 2009 Jul 24;390(4):775–90.

32. Bartels T, Ahlstrom LS, Leftin A, Kamp F, Haass C, Brown MF, et al. The N-terminus of the intrinsically disordered protein α-synuclein triggers membrane binding and helix folding. Biophys J. 2010 Oct 6;99(7):2116–24.

33. Trexler AJ, Rhoades E. α-Synuclein binds large unilamellar vesicles as an extended helix. Biochemistry. 2009 Mar 24;48(11):2304–6.

34. Maltsev AS, Ying J, Bax A. Impact of N-terminal acetylation of α-synuclein on its random coil and lipid binding properties. Biochemistry. 2012 Jun 26;51(25):5004–13.

35. Han H, Weinreb PH, Lansbury PT. The core Alzheimer's peptide NAC forms amyloid fibrils which seed and are seeded by beta-amyloid: is NAC a common trigger or target in neurodegenerative disease? Chem Biol. 1995 Mar;2(3):163–9.

36. Fusco G, De Simone A, Gopinath T, Vostrikov V, Vendruscolo M, Dobson CM, et al. Direct observation of the three regions in α-synuclein that determine its membrane-bound behaviour. Nat Commun. 2014 May 29;5:671–8.

37. Fusco G, Pape T, Stephens AD, Mahou P, Costa AR, Kaminski CF, et al. Structural basis of synaptic vesicle assembly promoted by α-synuclein. Nat Commun. 2017;8:15667.

38. Bertoncini CW, Jung Y-S, Fernandez CO, Hoyer W, Griesinger C, Jovin TM, et al. Release of long-range tertiary interactions potentiates aggregation of natively unstructured α-synuclein. Proc Natl Acad Sci. 2005 Feb 1;102(5):1430–5.

39. Burré J, Sharma M, Tsetsenis T, Buchman V, Etherton MR, Südhof TC. α-Synuclein promotes SNARE-complex assembly in vivo and in vitro. Science (80-). 2010 Sep 24;329(5999):1663–7.

40. Li W, West N, Colla E, Pletnikova O, Troncoso JC, Marsh L, et al. Aggregation promoting C-terminal truncation of α-synuclein is a normal cellular process and is enhanced by the familial Parkinson's disease-linked mutations. Proc Natl Acad Sci U S A. 2005 Jan 31;102(6):2162–7.

41. Bartels T, Choi JG, Selkoe DJ. α-Synuclein occurs physiologically as a helically folded tetramer that resists aggregation. Nature. 2011 Sep 1;477(7362):107–10.

42. Binolfi A, Theillet F-X, Selenko P. Bacterial in-cell NMR of human α-synuclein: a disordered monomer by nature? Biochem Soc Trans. 2012 Oct;40(5):950–4.

43. Burré J, Vivona S, Diao J, Sharma M, Brunger AT, Südhof TC. Properties of native brain α-synuclein. Nature. 2013 Jun 13;498(7453):E4-6; discussion E6-7.

44. Theillet FX, Binolfi A, Bekei B, Martorana A, Rose HM, Stuiver M, et al. Structural disorder of monomeric α-synuclein persists in mammalian cells. Nature. 2016 Jan 25;530(7588):45–50.

45. Herranz-Trillo F, Groenning M, van Maarschalkerweerd A, Tauler R, Vestergaard B, Bernadó P. Structural Analysis of Multi-component Amyloid Systems by Chemometric SAXS Data Decomposition. Structure. 2017 Jan 3;25(1):5–15.

46. Li B, Ge P, Murray KA, Sheth P, Zhang M, Nair G, et al. Cryo-EM of full-length α-synuclein reveals fibril polymorphs with a common structural kernel. Nat Commun. 2018 Dec 6;9(1):3609.

47. Cabin DE, Shimazu K, Murphy D, Cole NB, Gottschalk W, McIlwain KL, et al. Synaptic vesicle depletion correlates with attenuated synaptic responses to prolonged repetitive stimulation in mice lacking alpha-synuclein. J Neurosci. 2002 Oct 15;22(20):8797–807.

48. Rivers RC, Kumita JR, Tartaglia GG, Dedmon MM, Pawar A, Vendruscolo M, et al. Molecular determinants of the aggregation behavior of α- and β-synuclein. [Internet]. Vol. 17, Protein science : a publication of the Protein Society. 2008. p. 887–98.

49. Appel-Cresswell S, Vilarino-Guell C, Encarnacion M, Sherman H, Yu I, Shah B, et al. Alpha-synuclein p.H50Q, a novel pathogenic mutation for Parkinson's disease. Mov Disord. 2013 Jun 1;28(6):811–3.

50. Dürr A, Honoré A, Verny C, Letournel F, Pieri L, Anheim M, et al. G51D α-synuclein mutation causes a novel Parkinsonian-pyramidal syndrome. Ann Neurol. 2013 Apr;73(4):459–71.

51. Spillantini MG, Crowther RA, Jakes R, Hasegawa M, Goedert M. α-Synuclein in filamentous inclusions of Lewy bodies from Parkinson's disease and dementia with Lewy bodies. Proc Natl Acad Sci. 1998 May 26;95(11):6469–73.

52. Anderson JP, Walker DE, Goldstein JM, De Laat R, Banducci K, Caccavello RJ, et al. Phosphorylation of Ser-129 is the dominant pathological modification of α-synuclein in familial and sporadic lewy body disease. J Biol Chem. 2006 Oct 6;281(40):29739–52.

53. Duda JE, Giasson BI, Chen Q, Gur TL, Hurtig HI, Stern MB, et al. Widespread nitration of

pathological inclusions in neurodegenerative synucleinopathies. Am J Pathol. 2000 Nov;157(5):1439–45.

54. Baba M, Nakajo S, Tu P, Tomita T, Nakaya K, Lee VM, et al. Aggregation of alpha-Synuclein in Lewy Bodies of Sporadic Parkinson's Disease and Dementia with Lewy Bodies. Am J Pathol. 1998 Apr;152(4):879–84.

55. Tofaris GK, Razzaq A, Ghetti B, Lilley KS, Spillantini MG. Ubiquitination of α-Synuclein in Lewy Bodies Is a Pathological Event Not Associated with Impairment of Proteasome Function. J Biol Chem. 2003 Nov 7;278(45):44405–11.

56. Tu PH, Galvin JE, Baba M, Giasson B, Tomita T, Leight S, et al. Glial cytoplasmic inclusions in white matter oligodendrocytes of multiple system atrophy brains contain insoluble α-synuclein. Ann Neurol. 1998 Sep;44(3):415–22.

57. Papp MI, Kahn JE, Lantos PL. Glial cytoplasmic inclusions in the CNS of patients with multiple system atrophy (striatonigral degeneration, olivopontocerebellar atrophy and Shy-Drager syndrome). Vol. 94, Journal of the Neurological Sciences. Elsevier; 1989. p. 79–100.

58. Polymeropoulos MH, Lavedan C, Leroy E, Ide SE, Dehejia A, Dutra A, et al. Mutation in the α-synuclein gene identified in families with Parkinson's disease. Science (80-). 1997 Jun 27;276(5321):2045–7.

59. Tysnes O-B, Storstein A. Epidemiology of Parkinson's disease. J Neural Transm. 2017 Aug 1;124(8):901–5.

60. Kalia L V, Lang AE. Parkinson's disease. Lancet. 2015;386(9996):896–912.

61. Braak H, Tredici K Del, Rüb U, de Vos RA., Jansen Steur EN., Braak E. Staging of brain pathology related to sporadic Parkinson's disease. Neurobiol Aging. 2003 Mar;24(2):197–211.

62. Cotzias GC, Papavasiliou PS, Gellene R. Modification of Parkinsonism — Chronic Treatment with L-Dopa. N Engl J Med. 1969 Feb 13;280(7):337–45.

63. Doty RL. Olfactory dysfunction in Parkinson disease. Nat Rev Neurol. 2012 Jun 15;8(6):329–39.

64. Klein C, Westenberger A. Genetics of Parkinson's Disease. Cold Spring Harb Perspect Med. 2012;363–9.

65. Thomas B, Beal MF. Parkinson's disease. Hum Mol Genet. 2007 Jul 31;16(R2):R183–94.

66. Healy DG, Falchi M, O'Sullivan SS, Bonifati V, Durr A, Bressman S, et al. Phenotype, genotype, and worldwide genetic penetrance of LRRK2-associated Parkinson's disease: a case-control study. Lancet Neurol. 2008 Jul;7(7):583–90.

67. Larsen CN, Krantz BA, Wilkinson KD. Substrate specificity of deubiquitinating enzymes: Ubiquitin C-terminal hydrolases. Biochemistry. 1998;37(10):3358–68.

68. Shimura H, Hattori N, Kubo S, Mizuno Y, Asakawa S, Minoshima S, et al. Familial Parkinson disease gene product, parkin, is a ubiquitin-protein ligase. Nat Genet. 2000 Jul 1;25(3):302–5.

69. Kane LA, Lazarou M, Fogel AI, Li Y, Yamano K, Sarraf SA, et al. PINK1 phosphorylates ubiquitin to activate Parkin E3 ubiquitin ligase activity. J Cell Biol. 2014 Apr 28;205(2):143–53.

70. Wang X, Yan MH, Fujioka H, Liu J, Wilson-delfosse A, Chen SG, et al. LRRK2 regulates mitochondrial dynamics and function through direct interaction with DLP1. Hum Mol Genet. 2012 May 1;21(9):1931–44.

71. Kong SMY, Chan BKK, Park J-S, Hill KJ, Aitken JB, Cottle L, et al. Parkinson's disease-linked human PARK9/ATP13A2 maintains zinc homeostasis and promotes α-Synuclein externalization via exosomes. Hum Mol Genet. 2014 Jun 1;23(11):2816–33.

72. Canet-Aviles RM, Wilson MA, Miller DW, Ahmad R, McLendon C, Bandyopadhyay S, et al. The Parkinson's disease protein DJ-1 is neuroprotective due to cysteine-sulfinic acid-driven mitochondrial localization. Proc Natl Acad Sci. 2004 Jun 15;101(24):9103–8.

73. Uversky VN, Li J, Fink AL. Pesticides directly accelerate the rate of α-synuclein fibril formation: a possible factor in Parkinson's disease. FEBS Lett. 2001 Jul;500(3):105–8.

74. Sherer TB, Kim J-H, Betarbet R, Greenamyre JT. Subcutaneous Rotenone Exposure Causes Highly Selective Dopaminergic Degeneration and α-Synuclein Aggregation. Exp Neurol. 2003;179(1):9–16.

75. Krüger R, Kuhn W, Müller T, Woitalla D, Graeber M, Kösel S, et al. Ala30Pro mutation in the gene encoding α-synuclein in Parkinson's disease. Nat Genet. 1998 Feb 1;18(2):106–8.

76. Zarranz JJ, Alegre J, Gómez-Esteban JC, Lezcano E, Ros R, Ampuero I, et al. The new mutation, E46K, of α-synuclein causes parkinson and Lewy body dementia. Ann Neurol. 2004 Feb 1;55(2):164–73.

77. Pasanen P, Myllykangas L, Siitonen M, Raunio A, Kaakkola S, Lyytinen J, et al. A novel α-synuclein mutation A53E associated with atypical multiple system atrophy and Parkinson's disease-type pathology. Neurobiol Aging. 2014 Sep;35(9):2180.e1-5.

78. Narhi L, Wood SJ, Steavenson S, Jiang Y, Wu GM, Anafi D, et al. Both familial Parkinson's disease mutations accelerate α-synuclein aggregation. J Biol Chem. 1999 Apr 2;274(14):9843–6.

79. Ysselstein D, Joshi M, Mishra V, Griggs AM, Asiago JM, McCabe GP, et al. Effects of impaired membrane interactions on α-synuclein aggregation and neurotoxicity. Neurobiol Dis. 2015 Jul;79:150–63.

80. Diagnosis of dementia with Lewy bodies | Alzheimer's Society (https://www.alzheimers.org.uk/about-dementia/types-dementia/dementia-with-lewy-

bodies-diagnosis#content-start). Accessed 26/10/2019.

81. Dementia | Parkinson's UK (https://www.parkinsons.org.uk/information-and-support/dementia). Accessed 26/10/2019.

82. Dementia with Lewy bodies: what is it and what causes it? | Alzheimer's Society (https://www.alzheimers.org.uk/about-dementia/types-dementia/dementia-with-lewy-bodies). Accessed 26/10/2019.

83. Hansen LA. The Lewy body variant of Alzheimer disease. J Neural Transm Suppl. 1997;51:83–93.

84. Brief Guide to MSA – Multiple System Atrophy Trust (https://www.msatrust.org.uk/what-is-msa/brief-guide-to-msa/). Accessed 26/10/2019.

85. Wenning GK, Shlomo Y Ben, Magalhaes M, Daniel SE, Quinn NP. Clinical features and natural history of multiple system atrophy An analysis of 100 cases [Internet]. Vol. 117, Brain. 1994.

86. Gilman S, Low P., Quinn N, Albanese A, Ben-Shlomo Y, Fowler C., et al. Consensus statement on the diagnosis of multiple system atrophy. J Neurol Sci. 1999 Feb 1;163(1):94–8.

87. Gilman S, Wenning FG, Low P, Brooks FD, Mathias FmC, Trojanowski FmJ, et al. Second consensus statement on the diagnosis of multiple system atrophy. Neurology. 2008;71(9).

88. Prusiner SB, Woerman AL, Mordes DA, Watts JC, Rampersaud R, Berry DB, et al. Evidence for α-synuclein prions causing multiple system atrophy in humans with parkinsonism. Proc Natl Acad Sci. 2015 Aug 31;112(38):201514475.

89. CARLSSON A, LINDQVIST M, MAGNUSSON T, WALDECK B. On the presence of 3-hydroxytyramine in brain. Science. 1958 Feb 28;127(3296):471.

90. Nagatsu T, Levitt M, Udenfriend S. The initial step in norepinephrine biosynthesis. J Biol Chem. 1964;239(S):2910–7.

91. Kageyama T, Nakamura M, Matsuo A, Yamasaki Y, Takakura Y, Hashida M, et al. The 4F2hc/LAT1 complex transports L-DOPA across the blood-brain barrier. Brain Res. 2000 Oct 6;879(1–2):115–21.

92. Shannon KM, Bennett JP, Friedman JH. Efficacy of pramipexole, a novel dopamine agonist, as monotherapy in mild to moderate Parkinson's disease. Neurology. 1997 May 1;49(3):724–8.

93. Mierau J, Schingnitz G. Biochemical and pharmacological studies on pramipexole, a potent and selective dopamine D2 receptor agonist. Eur J Pharmacol. 1992 May 14;215(2–3):161–70.

94. Mierau J, Schneider FJ, Ensinger HA, Chio CL, Lajiness ME, Huff RM. Pramipexole binding and activation of cloned and expressed dopamine D2, D3 and D4receptors. Eur J Pharmacol Mol Pharmacol. 1995 Jun 23;290(1):29–36.

95. Weintraub D, Siderowf AD, Potenza MN, Goveas J, Morales KH, Duda JE, et al. Association of dopamine agonist use with impulse control disorders in Parkinson disease. Arch Neurol. 2006 Jul 1;63(7):969–73.

96. Rabinak CA, Nirenberg MJ. Dopamine agonist withdrawal syndrome in parkinson disease. Arch Neurol. 2010 Jan 1;67(1):58–63.

97. Fosgerau K, Hoffmann T. Peptide therapeutics: Current status and future directions. Drug Discov Today. 2015 Jan 1;20(1):122–8.

98. Huggins KNL, Bisaglia M, Bubacco L, Tatarek-Nossol M, Kapurniotu A, Andersen NH. Designed Hairpin Peptides Interfere with Amyloidogenesis Pathways: Fibril Formation and Cytotoxicity Inhibition, Interception of the Preamyloid State. Biochemistry. 2011 Sep 27;50(38):8202–12.

99. Madine J, Doig AJ, Middleton DA. Design of an N-methylated peptide inhibitor of alpha-

synuclein aggregation guided by solid-state NMR. J Am Chem Soc. 2008 Jun 25;130(25):7873–81.

100. Luk KC, Kehm V, Carroll J, Zhang B, O'Brien P, Trojanowski JQ, et al. Pathological α-synuclein transmission initiates Parkinson-like neurodegeneration in nontransgenic mice. Science. 2012 Nov 16;338(6109):949–53.

101. Tran HT, Chung CH-Y, Iba M, Zhang B, Trojanowski JQ, Luk KC, et al. A-synuclein immunotherapy blocks uptake and templated propagation of misfolded α-synuclein and neurodegeneration. Cell Rep. 2014 Jun 26;7(6):2054–65.

102. Masliah E, Rockenstein E, Mante M, Crews L, Spencer B, Adame A, et al. Passive immunization reduces behavioral and neuropathological deficits in an alpha-synuclein transgenic model of lewy body disease. McAlonan GM, editor. PLoS One. 2011 Apr 29;6(4):e19338.

103. Jankovic J, Goodman I, Safirstein B, Marmon TK, Schenk DB, Koller M, et al. Safety and Tolerability of Multiple Ascending Doses of PRX002/RG7935, an Anti–α-Synuclein Monoclonal Antibody, in Patients With Parkinson Disease. JAMA Neurol. 2018 Oct 1;75(10):1206.

104. Muchowski PJ, Schaffar G, Sittler A, Wanker EE, Hayer-Hartl MK, Hartl FU. Hsp70 and Hsp40 chaperones can inhibit self-assembly of polyglutamine proteins into amyloid-like fibrils. Proc Natl Acad Sci. 2000;97(14):7841–6.

105. Gao X, Carroni M, Nussbaum-Krammer C, Mogk A, Nillegoda NB, Szlachcic A, et al. Human Hsp70 Disaggregase Reverses Parkinson's-Linked α-Synuclein Amyloid Fibrils. Mol Cell. 2015 Aug 19;59(5):781–93.

106. Baker JD, Shelton LB, Zheng D, Favretto F, Nordhues BA, Darling A, et al. Human cyclophilin 40 unravels neurotoxic amyloids. Bates G, editor. PLoS Biol. 2017 Jun 27;15(6):e2001336.

107. Salloway S, Sperling R, Fox NC, Blennow K, Klunk W, Raskind M, et al. Two Phase 3 Trials of Bapineuzumab in Mild-to-Moderate Alzheimer's Disease. N Engl J Med. 2014 Jan 23;370(4):322–33.

108. Cheruvara H, Allen-Baume VL, Kad NM, Mason JM. Intracellular screening of a peptide library to derive a potent peptide inhibitor of α-synuclein aggregation. J Biol Chem. 2015 Mar 20;290(12):jbc.M114.620484.

109. Phelan MM, Caamaño-Gutiérrez E, Gant MS, Grosman RX, Madine J. Using an NMR metabolomics approach to investigate the pathogenicity of amyloid-beta and alpha-synuclein. Metabolomics. 2017 Dec 29;13(12):151.

110. Baines CP, Kaiser RA, Purcell NH, Blair NS, Osinska H, Hambleton MA, et al. Loss of cyclophilin D reveals a critical role for mitochondrial permeability transition in cell death. Nature. 2005 Mar 31;434(7033):658–62.

111. Elrod JW, Molkentin JD. Physiologic Functions of Cyclophilin D and the Mitochondrial Permeability Transition Pore. Circ J. 2013;77(5):1111–22.

112. Ludtmann MHR, Angelova PR, Horrocks MH, Choi ML, Rodrigues M, Baev AY, et al. α-synuclein oligomers interact with ATP synthase and open the permeability transition pore in Parkinson's disease. Nat Commun. 2018 Dec 12;9(1):2293.

113. Keeler J. Understanding NMR Spectroscopy. 2nd ed. John Wiley & Sons, Ltd; 2010.

114. Antanasijevic A, Ramirez B, Caffrey M. Comparison of the sensitivities of WaterLOGSY and saturation transfer difference NMR experiments. J Biomol NMR. 2014 Sep 12;60(1):37–44.

115. Zuiderweg ERP. Mapping Protein-Protein Interactions in Solution by NMR Spectroscopy. Biochemistry. 2002;41.

116. O'Connell MR, Gamsjaeger R, Mackay JP. The structural analysis of protein-protein

interactions by NMR spectroscopy. Vol. 9, Proteomics. 2009. p. 5224–32.

117. Williamson MP. Using chemical shift perturbation to characterise ligand binding. Prog Nucl Magn Reson Spectrosc. 2013;73:1–16.

118. Prince M, Knapp M, Guerchet M, McCrone P, Prina M, Comas-Herrera A, Wittenberg R, Adelaja B, Hu B, King D, Rehill A SD. Dementia UK: Update. 2014.

119. Kim YS, Lim D, Kim JY, Kang SJ, Kim Y-H, Im H. β-Sheet-breaking peptides inhibit the fibrillation of human α-synuclein. Biochem Biophys Res Commun. 2009 Oct 2;387(4):682–7.

120. PepDraw (http://www.tulane.edu/~biochem/WW/PepDraw/index.html). Accessed 26/10/2019.

121. Tyler-Cross R, Schirch V. Effects of amino acid sequence, buffers, and ionic strength on the rate and mechanism of deamidation of asparagine residues in small peptides. J Biol Chem. 1991;266(33):22549–56.

122. Yang H, Zubarev RA. Mass spectrometric analysis of asparagine deamidation and aspartate isomerization in polypeptides. Vol. 31, Electrophoresis. John Wiley & Sons, Ltd; 2010. p. 1764–72.

123. Aswad DW, Paranandi M V, Schurter BT. Isoaspartate in peptides and proteins: Formation, significance, and analysis. J Pharm Biomed Anal. 2000 Jan 1;21(6):1129–36.

124. Ni W, Dai S, Karger BL, Zhou ZS. Analysis of isoaspartic acid by selective proteolysis with Asp-N and electron transfer dissociation mass spectrometry. Anal Chem. 2010 Sep 1;82(17):7485–91.

125. Fares M-B, Ait-Bouziad N, Dikiy I, Mbefo MK, Jovičić A, Kiely A, et al. The novel Parkinson's disease linked mutation G51D attenuates in vitro aggregation and membrane binding of α-synuclein, and enhances its secretion and nuclear localization in cells. Hum Mol Genet. 2014

Sep 1;23(17):4491–509.

126. Conway KA, Harper JD, Lansbury PT. Accelerated in vitro fibril formation by a mutant alpha-synuclein linked to early-onset Parkinson disease. Nat Med. 1998 Nov;4(11):1318–20.

127. Hengen PH. Methods and reagents: False positives from the yeast two-hybrid system. Trends Biochem Sci. 1997;22(1):33–4.

128. Baig MH, Ahmad K, Saeed M, Alharbi AM, Barreto GE, Ashraf GM, et al. Peptide based therapeutics and their use for the treatment of neurodegenerative and other diseases. Biomed Pharmacother. 2018 Jul 1;103:574–81.

129. Oller-Salvia B, Sánchez-Navarro M, Giralt E, Teixidó M. Blood–brain barrier shuttle peptides: an emerging paradigm for brain delivery. Chem Soc Rev. 2016;45(17):4690–707.

130. Winner B, Jappelli R, Maji SK, Desplats PA, Boyer L, Aigner S, et al. In vivo demonstration that α-synuclein oligomers are toxic. Proc Natl Acad Sci U S A. 2011 Mar 8;108(10):4194–9.

131. Schmidt E, Seifert M, Baumeister R. *Caenorhabditis elegans* as a Model System for Parkinson's Disease. Neurodegener Dis. 2007;4(2–3):199–217.

132. Emwas AHM. The strengths and weaknesses of NMR spectroscopy and mass spectrometry with particular focus on metabolomics research. Methods Mol Biol. 2015;1277:161–93.

133. Monteiro MS, Carvalho M, Bastos ML, Guedes de Pinho P. Metabolomics Analysis for Biomarker Discovery: Advances and Challenges. Curr Med Chem. 2013 Dec 1;20(2):257–71.

134. Kohl SM, Klein MS, Hochrein J, Oefner PJ, Spang R, Gronwald W. State-of-the art data normalization methods improve NMR-based metabolomic analysis. Metabolomics. 2012 Jun;8(1):146–60.

135. Craig A, Cloarec O, Holmes E, Nicholson JK, Lindon JC. Scaling and Normalization Effects in NMR Spectroscopic Metabonomic Data Sets. Anal Chem. 2006;78(7):2262–7.

136. Karaman I. Preprocessing and pretreatment of metabolomics data for statistical analysis. In: Advances in Experimental Medicine and Biology. Springer, Cham; 2017. p. 145–61.

137. Xia J, Psychogios N, Young N, Wishart DS. MetaboAnalyst: a web server for metabolomic data analysis and interpretation. Nucleic Acids Res. 2009 Jul 1;37:W652–60.

138. Li C, Soufan O, Chong J, Xia J, Bourque G, Li S, et al. MetaboAnalyst 4.0: towards more transparent and integrative metabolomics analysis. Nucleic Acids Res. 2018 Jul 2;46(W1):W486–94.

139. van den Berg RA, Hoefsloot HC, Westerhuis JA, Smilde AK, van der Werf MJ. Centering, scaling, and transformations: improving the biological information content of metabolomics data. BMC Genomics. 2006 Jun 8;7(1):142.

140. Saccenti E, Hoefsloot HCJ, Smilde AK, Westerhuis JA, Hendriks MMWB. Reflections on univariate and multivariate analysis of metabolomics data. Metabolomics. 2014 Jun;10(3):361–74.

141. Gardner M, Altman D. 5. Differences between means: type I and type II errors and power. (https://www.bmj.com/about-bmj/resources-readers/publications/statistics-square-one/5-differences-between-means-type-i-an). Accessed 26/10/2019.

142. Benjamini Y, Hochberg Y. Controlling the False Discovery Rate: A Practical and Powerful Approach to Multiple Testing. J R Stat Soc Ser B. 1995;57(1):289–300.

143. Abdi H, Williams LJ. Principal component analysis. Wiley Interdiscip Rev Comput Stat. 2010;2(4):433–59.

144. Barker M, Rayens W. Partial least squares for discrimination. J Chemom. 2003;17(3):166–73.

145. Perez DR, Narasimhan G. So you think you can PLS-DA? bioRxiv. 2018 Jan 15;207225.

146. Gromski PS, Muhamadali H, Ellis DI, Xu Y, Correa E, Turner ML, et al. A tutorial review:

Metabolomics and partial least squares-discriminant analysis – a marriage of convenience or a shotgun wedding. Anal Chim Acta. 2015 Jun 16;879:10–23.

147. Westerhuis JA, Hoefsloot HCJ, Smit S, Vis DJ, Smilde AK, van Velzen EJJ, et al. Assessment of PLSDA cross validation. Metabolomics. 2008 Mar;4(1):81–9.

148. Amman C, Meier P MA. A Simple Multinuclear NMR Thermometer sample. J Magn Reson. 1982;321:319–20.

149. Sumner LW, Amberg A, Barrett D, Beale MH, Beger R, Daykin CA, et al. Proposed minimum reporting standards for chemical analysis. Metabolomics. 2007 Sep 19;3(3):211–21.

150. Giraudeau P, Silvestre V, Akoka S. Optimizing water suppression for quantitative NMR-based metabolomics: a tutorial review. Metabolomics. 2015 Oct 15;11(5):1041–55.

151. Wishart DS. Quantitative metabolomics using NMR. TrAC Trends Anal Chem. 2008 Mar 1;27(3):228–37.

152. Tang H, Wang Y, Nicholson JK, Lindon JC. Use of relaxation-edited one-dimensional and two dimensional nuclear magnetic resonance spectroscopy to improve detection of small metabolites in blood plasma. Anal Biochem. 2004 Feb 15;325(2):260–72.

153. Beal MF. Neuroprotective effects of creatine. Amino Acids. 2011 May 30;40(5):1305–13.

154. Klopstock T, Elstner M, Bender A. Creatine in mouse models of neurodegeneration and aging. Amino Acids. 2011 May 10;40(5):1297–303.

155. LOUZADA PR, LIMA ACP, MENDONÇA-SILVA DL, NOËL F, DE MELLO FG, FERREIRA ST. Taurine prevents the neurotoxicity of β-amyloid and glutamate receptor agonists: activation of GABA receptors and possible implications for Alzheimer's disease and other neurological disorders. FASEB J. 2004 Mar 1;18(3):511–8.

156. Voevodskaya O, Sundgren PC, Strandberg O, Zetterberg H, Minthon L, Blennow K, et al. Myo-

inositol changes precede amyloid pathology and relate to APOE genotype in Alzheimer disease. Neurology. 2016 May 10;86(19):1754–61.

157. Miller BL, Moats RA, Shonk T, Ernst T, Woolley S, Ross BD. Alzheimer disease: depiction of increased cerebral myo-inositol with proton MR spectroscopy. Radiology. 1993 May 1;187(2):433–7.

158. Mo J-J, Liu L-Y, Peng W-B, Rao J, Liu Z, Cui L-L. The effectiveness of creatine treatment for Parkinson's disease: an updated meta-analysis of randomized controlled trials. BMC Neurol. 2017 Jun 2;17(1):105.

159. Jamal S, Kumari A, Singh A, Goyal S, Grover A. Conformational Ensembles of α-Synuclein Derived Peptide with Different Osmolytes from Temperature Replica Exchange Sampling. Front Neurosci. 2017;11:684.

160. Bodner CR, Maltsev AS, Dobson CM, Bax A. Differential Phospholipid Binding of α-Synuclein Variants Implicated in Parkinson's Disease Revealed by Solution NMR Spectroscopy. Biochemistry. 2010 Feb 9;49(5):862–71.

161. Choi W, Zibaee S, Jakes R, Serpell LC, Davletov B, Crowther RA, et al. Mutation E46K increases phospholipid binding and assembly into filaments of human α-synuclein. FEBS Lett. 2004 Oct 22;576(3):363–8.

162. Proukakis C, Dudzik CG, Brier T, MacKay DS, Cooper JM, Millhauser GL, et al. A novel α-synuclein missense mutation in Parkinson disease. Neurology. 2013 Mar 12;80(11):1062–4.

163. Khalaf O, Fauvet B, Oueslati A, Dikiy I, Mahul-Mellier A-L, Ruggeri FS, et al. The H50Q mutation enhances α-synuclein aggregation, secretion, and toxicity. J Biol Chem. 2014 Aug 8;289(32):21856–76.

164. Ghosh D, Mondal M, Mohite GM, Singh PK, Ranjan P, Anoop A, et al. The Parkinson's Disease-Associated H50Q Mutation Accelerates α-Synuclein Aggregation *in Vitro*. Biochemistry. 2013

Oct 8;52(40):6925–7.

165. Kiely AP, Ling H, Asi YT, Kara E, Proukakis C, Schapira AH, et al. Distinct clinical and neuropathological features of G51D SNCA mutation cases compared with SNCA duplication and H50Q mutation. Mol Neurodegener. 2015 Aug 27;10:41.

166. Rutherford NJ, Moore BD, Golde TE, Giasson BI. Divergent effects of the H50Q and G51D *SNCA* mutations on the aggregation of α-synuclein. J Neurochem. 2014 Dec;131(6):859–67.

167. Li J, Uversky VN, Fink AL. Effect of familial Parkinson's disease point mutations A30P and A53T on the structural properties, aggregation, and fibrillation of human α-synuclein. Biochemistry. 2001;40(38):11604–13.

168. Ghosh D, Sahay S, Ranjan P, Salot S, Mohite GM, Singh PK, et al. The Newly Discovered Parkinson's Disease Associated Finnish Mutation (A53E) Attenuates α-Synuclein Aggregation and Membrane Binding. Biochemistry. 2014 Oct 21;53(41):6419–21.

169. Anderson JP, Walker DE, Goldstein JM, de Laat R, Banducci K, Caccavello RJ, et al. Phosphorylation of Ser-129 is the dominant pathological modification of alpha-synuclein in familial and sporadic Lewy body disease. J Biol Chem. 2006 Oct 6;281(40):29739–52.

170. Maltsev AS, Ying J, Bax A. Impact of N-terminal acetylation of α-synuclein on its random coil and lipid binding properties. Biochemistry. 2012 Jun 26;51(25):5004–13.

171. Smith MA, Richey Harris PL, Sayre LM, Beckman JS, Perry G. Widespread Peroxynitrite-Mediated Damage in Alzheimer's Disease. J Neurosci. 1997 Apr 15;17(8):2653–7.

172. Good PF, Hsu A, Werner P, Perl DP, Warren Olanow C. Protein nitration in Parkinson's disease. J Neuropathol Exp Neurol. 1998 Apr 1;57(4):338–42.

173. Souza JM, Giasson BI, Chen Q, M-Y Lee V, Ischiropoulos H. Dityrosine Cross-linking Promotes Formation of Stable-Synuclein Polymers. J Biol Chem. 2000;275:18344–9.

174. Hodara R, Norris EH, Giasson BI, Mishizen-Eberz AJ, Lynch DR, Lee VMY, et al. Functional consequences of α-synuclein tyrosine nitration: Diminished binding to lipid vesicles and increased fibril formation. J Biol Chem. 2004 Nov 12;279(46):47746–53.

175. Takamori S, Holt M, Stenius K, Lemke EA, Grønborg M, Riedel D, et al. Molecular Anatomy of a Trafficking Organelle. Cell. 2006 Nov 17;127(4):831–46.

176. Galvagnion C, Buell AK, Meisl G, Michaels TCT, Vendruscolo M, Knowles TPJ, et al. Lipid vesicles trigger α-synuclein aggregation by stimulating primary nucleation. Nat Chem Biol. 2015 Mar 2;11(3):229–34.

177. Pineda A, Burré J. Modulating membrane binding of α-synuclein as a therapeutic strategy. Proc Natl Acad Sci U S A. 2017 Feb 7;114(6):1223–5.

178. Pfefferkorn CM, Jiang Z, Lee JC. Biophysics of α-synuclein membrane interactions. Biochim Biophys Acta. 2012 Feb;1818(2):162–71.

179. Hughes MN, Nicklin HG. The chemistry of peroxonitrites. Part II. Copper(II)-catalysed reaction between hydroxylamine and peroxonitrite in alkali. J Chem Soc A Inorganic, Phys Theor. 1970 Jan 1;0(0):925.

180. Assay-Protocol-NativePAGE (http://www.assay-protocol.com/molecular-biology/electrophoresis/native-page). Accessed 04/02/2019.

181. Micsonai A, Wien F, Bulyáki É, Kun J, Moussong É, Lee YH, et al. BeStSel: A web server for accurate protein secondary structure prediction and fold recognition from the circular dichroism spectra. Nucleic Acids Res. 2018 Jul 2;46(W1):W315–22.

182. Micsonai A, Wien F, Kernya L, Lee Y-H, Goto Y, Réfrégiers M, et al. Accurate secondary structure prediction and fold recognition for circular dichroism spectroscopy. Proc Natl Acad Sci U S A. 2015 Jun 16;112(24):E3095-103.

183. Schneider CA, Rasband WS, Eliceiri KW. NIH Image to ImageJ: 25 years of image analysis. Nat Methods. 2012 Jul 1;9(7):671–5.

184. Duplâtre G, Ferreira Marques MF, Da Graça Miguel M. Size of sodium dodecyl sulfate micelles in aqueous solutions as studied by positron annihilation lifetime spectroscopy. J Phys Chem. 1996;100(41):16608–12.

185. Lee HJ, Choi C, Lee SJ. Membrane-bound α-synuclein has a high aggregation propensity and the ability to seed the aggregation of the cytosolic form. J Biol Chem. 2002 Jan 4;277(1):671–8.

186. Sevcsik E, Trexler AJ, Dunn JM, Rhoades E. Allostery in a Disordered Protein: Oxidative Modifications to α-Synuclein Act Distally To Regulate Membrane Binding. J Am Chem Soc. 2011 May 11;133(18):7152–8.

187. Burai R, Ait-Bouziad N, Chiki A, Lashuel HA. Elucidating the Role of Site-Specific Nitration of α-Synuclein in the Pathogenesis of Parkinson's Disease via Protein Semisynthesis and Mutagenesis. J Am Chem Soc. 2015 Apr 22;137(15):5041–52.

188. Polymeropoulos MH. Mutation in the -Synuclein Gene Identified in Families with Parkinson's Disease. Science (80-). 1997 Jun 27;276(5321):2045–7.

189. Zhu M, Fink AL. Lipid binding inhibits α-synuclein fibril formation. J Biol Chem. 2003 May 9;278(19):16873–7.

190. Lee H-J, Choi C, Lee S-J. Membrane-bound α-synuclein has a high aggregation propensity and the ability to seed the aggregation of the cytosolic form. J Biol Chem. 2002 Jan 4;277(1):671–8.

191. Shahmoradian SH, Lewis AJ, Genoud C, Hench J, Moors TE, Navarro PP, et al. Lewy pathology in Parkinson's disease consists of crowded organelles and lipid membranes. Nat Neurosci. 2019;22(7):1099–109.

192. Andersen JK. Oxidative stress in neurodegeneration: cause or consequence? Nat Med. 2004 Jul;10 Suppl(July):S18-25.

193. Lin MT, Beal MF. Mitochondrial dysfunction and oxidative stress in neurodegenerative diseases. Vol. 443, Nature. 2006. p. 787–95.

194. Hollingworth RM, Ahammadsahib KI, Gadelhak G, McLaughlin JL. New inhibitors of Complex I of the mitochondrial electron transport chain with activity as pesticides. Biochem Soc Trans. 1994;22(1):230–3.

195. Bonifati V, Rizzu P, van Baren MJ, Schaap O, Breedveld GJ, Krieger E, et al. Mutations in the DJ-1 Gene Associated with Autosomal Recessive Early-Onset Parkinsonism. Science (80-). 2003 Jan 10;299(5604):256 LP – 259.

196. Valente EM, Abou-Sleiman PM, Caputo V, Muqit MMK, Harvey K, Gispert S, et al. Hereditary early-onset Parkinson's disease caused by mutations in PINK1. Science (80-). 2004 May 21;304(5674):1158–60.

197. Kitada T, Asakawa S, Hattori N, Matsumine H, Yamamura Y, Minoshima S, et al. Mutations in the parkin gene cause autosomal recessive juvenile parkinsonism. Nature. 1998 Apr 9;392(6676):605–8.

198. Ludtmann MHR, Angelova PR, Horrocks MH, Choi ML, Rodrigues M, Baev AY, et al. α-synuclein oligomers interact with ATP synthase and open the permeability transition pore in Parkinson's disease. Nat Commun. 2018 Dec 12;9(1):2293.

199. Ryan T, Bamm V V., Stykel MG, Coackley CL, Humphries KM, Jamieson-Williams R, et al. Cardiolipin exposure on the outer mitochondrial membrane modulates α-synuclein. Nat Commun. 2018 Dec 26;9(1):817.

200. Nakamura K, Nemani VM, Azarbal F, Skibinski G, Levy JM, Egami K, et al. Direct membrane association drives mitochondrial fission by the Parkinson disease-associated protein α-

synuclein. J Biol Chem. 2011 Jun 10;286(23):20710–26.

201. Chinta SJ, Mallajosyula JK, Rane A, Andersen JK. Mitochondrial alpha-synuclein accumulation impairs complex I function in dopaminergic neurons and results in increased mitophagy in vivo [Internet]. Vol. 486, Neuroscience Letters. 2010.

202. Vicario M, Cieri D, Brini M, Calì T. The Close Encounter Between Alpha-Synuclein and Mitochondria. Front Neurosci. 2018 Jun 7;12:388.

203. Di Maio R, Barrett PJ, Hoffman EK, Barrett CW, Zharikov A, Borah A, et al. α-synuclein binds to TOM20 and inhibits mitochondrial protein import in Parkinson's disease. Vol. 8, Science Translational Medicine. 2016.

204. Crompton M. The mitochondrial permeability transition pore and its role in cell death. Biochem J. 1999 Jul 15;341(2):233.

205. Parihar MS, Parihar A, Fujita M, Hashimoto M, Ghafourifar P. Alpha-synuclein overexpression and aggregation exacerbates impairment of mitochondrial functions by augmenting oxidative stress in human neuroblastoma cells. Int J Biochem Cell Biol. 2009 Oct;41(10):2015–24.

206. Fischer G, Wittmann-Liebold B, Lang K, Kiefhaber T, Schmid FX. Cyclophilin and peptidyl-prolyl cis-trans isomerase are probably identical proteins. Nature. 1989 Feb;337(6206):476–8.

207. Göthel SF, Marahiel MA. Peptidyl-prolyl cis-trans isomerases, a superfamily of ubiquitous folding catalysts. Vol. 55, Cellular and Molecular Life Sciences. Birkhäuser Verlag; 1999. p. 423–36.

208. Kajitani K, Fujihashi M, Kobayashi Y, Shimizu S, Tsujimoto Y, Miki K. Crystal structure of human cyclophilin D in complex with its inhibitor, cyclosporin A at 0.96-Å resolution. Proteins Struct Funct Genet. 2008 Dec 12;70(4):1635–9.

209. Hunter DR, Haworth RA. The Ca2+-induced membrane transition in mitochondria. III. Transitional Ca2+ release. Arch Biochem Biophys. 1979 Jul 1;195(2):468–77.

210. Halestrap AP. What is the mitochondrial permeability transition pore? J Mol Cell Cardiol. 2009 Jun 1;46(6):821–31.

211. Halestrap AP, Clarke SJ, Javadov SA. Mitochondrial permeability transition pore opening during myocardial reperfusion - A target for cardioprotection. Vol. 61, Cardiovascular Research. Oxford University Press; 2004. p. 372–85.

212. Crompton M, Ellinger H, Costi A. Inhibition by cyclosporin A of a Ca2+-dependent pore in heart mitochondria activated by inorganic phosphate and oxidative stress. Biochem J. 1988 Oct 1;255(1):357–60.

213. Friberg H, Ferrand-Drake M, Bengtsson F, Halestrap AP, Wieloch T. Cyclosporin A, but not FK 506, protects mitochondria and neurons against hypoglycemic damage and implicates the mitochondrial permeability transition in cell death. J Neurosci. 1998 Jul 15;18(14):5151–9.

214. Zhang H, Liu J, Wang X, Duan C, Wang X, Yang H. V63 and N65 of overexpressed α-synuclein are involved in mitochondrial dysfunction. Brain Res. 2016;1642:308–18.

215. Schlatter D, Thoma R, Küng E, Stihle M, Müller F, Borroni E, et al. Crystal engineering yields crystals of cyclophilin D diffracting to 1.7 Å resolution. Acta Crystallogr Sect D Biol Crystallogr. 2005 May 1;61(5):513–9.

216. Yu H. Extending the size limit of protein nuclear magnetic resonance. Proc Natl Acad Sci. 1999 Jan 19;96(2):332–4.

10 Appendix

10.1 Bucket table and identified metabolites

Table 10-1 - List of buckets and the metabolites associated with them for NMR metabolomics of SH-SY5Y cell extracts.

Left	Right	Number	Label
0.835	0.875	1	methyl
0.875	0.883	2	isocaproate_1
0.883	0.888	3	butyrate_2
0.888	0.895	4	isocaproate_3
0.895	0.903	5	butyrate_4
0.903	0.913	6	Miscel_1
0.913	0.933	7	butyrate_5
0.933	0.949	8	Miscel_2
0.949	0.97	9	Ile/alloIle_6
0.97	0.986	10	alloIle_7
0.992	0.986	11	Val_8
0.992	0.998	12	Butanone_9
0.998	1.004	13	Val_10
1.004	1.025	14	Butanone/Ile_11
1.025	1.043	15	Val_12
1.043	1.049	16	2-oxybutyrate_13
1.049	1.054	17	Val_14
1.054	1.076	18	2-oxybutyrate_15
1.076	1.106	19	Miscel_3
1.106	1.113	20	misc_16
1.113	1.132	21	Miscel_4
1.132	1.158	22	misc_17
1.158	1.173	23	Miscel_5
1.173	1.189	24	ethanol_21
1.189	1.19	25	3-aminoisobut_20
1.19	1.196	26	misc-lipid_22
1.196	1.203	27	ethanol_23
1.203	1.222	28	misc-lipid_24
1.222	1.228	29	fucose_25
1.228	1.234	30	misc-lipid_26
1.234	1.238	31	fucose_27
1.238	1.241	32	Miscel_6
1.241	1.245	33	misc-lipid_28

1.245	1.248	34	fucose_29
1.248	1.257	35	misc-lipid/fuc_30
1.257	1.276	36	Miscel_7
1.276	1.283	37	3-hydroxyval_31
1.283	1.306	38	caprate_32
1.306	1.322	39	caprate_34
1.322	1.327	40	lactate_35
1.327	1.331	41	threonine_36
1.331	1.34	42	lactate/thr_37
1.34	1.395	43	Miscel_8
1.395	1.415	44	3-phenprop_38
1.415	1.448	45	Miscel_9
1.448	1.47	46	isocaproate_39
1.47	1.495	47	alanine_40
1.495	1.518	48	isocaproate_41
1.518	1.586	49	butyrate_42
1.586	1.708	50	2-aminoadipat_43
1.708	1.748	51	ethylmalonate_44
1.748	1.761	52	misc_45
1.761	1.786	53	Miscel_10
1.786	1.804	54	4-hydroxybut_46
1.804	1.909	55	2-aminoadipat_47
1.909	1.931	56	acetate_48
1.931	1.976	57	misc_49
1.976	2.016	58	acetamide_50
2.016	2.025	59	homoserine_51
2.025	2.098	60	glutamate_52
2.098	2.137	61	glu/gln_53
2.137	2.142	62	homoser/gln_54
2.142	2.171	63	o-acetylcholi_55
2.171	2.183	64	GSSG/caprate_56
2.183	2.196	65	cap/isoc_57
2.194	2.202	66	iscocaproate_58
2.202	2.212	67	butanone_59
2.212	2.24	68	acetone_60
2.24	2.247	69	4-hydroxybuty_61
2.247	2.254	70	Miscel_11
2.254	2.263	71	thymol_62
2.263	2.278	72	Miscel_12
2.278	2.31	73	3aminoadipate_63
2.31	2.37	74	glu_64

2.37	2.374	75	Miscel_13
2.374	2.382	76	misc_65
2.382	2.399	77	pyruvate_66
2.399	2.441	78	succinate_67
2.441	2.468	79	gln_68
2.468	2.474	80	misc_69
2.474	2.48	81	gln_70
2.48	2.497	82	misc_71
2.497	2.52	83	5-aminolevuli_72
2.52	2.53	84	citrate_73
2.53	2.547	85	misc_74
2.547	2.554	86	citrate_75
2.554	2.584	87	GSSG_76
2.584	2.615	88	3-aminoisobut_77
2.615	2.643	89	misc_78
2.643	2.655	90	citrate_79
2.655	2.668	91	misc_80
2.668	2.7	92	citrate_81
2.7	2.717	93	misc_84
2.717	2.724	94	misc_85
2.724	2.73	95	Miscel_14
2.73	2.738	96	dimethylamine_86
2.738	2.756	97	Miscel_15
2.756	2.768	98	sarcosine_87
2.768	2.816	99	misc_88
2.816	2.826	100	methylguanidin_89
2.826	2.853	101	misc_90
2.853	2.894	102	misc_91
2.894	2.934	103	misc_92
2.934	2.942	104	n-methylhydant_93
2.942	2.947	105	misc_94
2.947	2.992	106	GSSG_95
2.992	3.006	107	ethylmalonate_96
3.006	3.024	108	histamine_97
3.024	3.037	109	creatine-phos_98
3.037	3.044	110	creatine_99
3.044	3.048	111	creatinine_100
3.048	3.121	112	3-aminoisobut_101
3.121	3.165	113	citrulline_102
3.165	3.204	114	misc_103
3.204	3.216	115	choline_104

3.216	3.229	116	o-p-cho/carn_105
3.229	3.24	117	misc_107
3.24	3.25	118	pi-Me-His_108
3.25	3.253	119	taurine_109
3.253	3.259	120	pi-Me-His/bet_110
3.259	3.266	121	taurine_111
3.266	3.273	122	Miscel_16
3.273	3.277	123	TMNO_112
3.277	3.281	124	taurine_113
3.281	3.285	125	myoinisitol_114
3.285	3.292	126	pi-Me-His_115
3.292	3.302	127	_myoinisitol_116
3.302	3.319	128	misc_117
3.319	3.325	129	pi-Me-His/mis_118
3.325	3.349	130	misc_119
3.349	3.356	131	methanol_121
3.356	3.362	132	misc_122
3.362	3.387	133	carnitine_123
3.387	3.41	134	Miscel_17
3.41	3.416	135	taurine_124
3.416	3.422	136	34dihydroxyben_125
3.422	3.428	137	taurine_126
3.428	3.431	138	carnitine_127
3.431	3.439	139	taurine_128
3.439	3.479	140	fucose_129
3.479	3.482	141	3hydroxypheny_130
3.481	3.524	142	arabinose_131
3.524	3.551	143	myoinisitol_132
3.551	3.56	144	lactose_133
3.56	3.565	145	glycine_134
3.565	3.576	146	lactose_135
3.576	3.581	147	theophylline_136
3.581	3.609	148	phosphocholine_137
3.609	3.616	149	myoinisitol_138
3.616	3.625	150	sarcosine_139
3.625	3.631	151	myoinisitol_140
3.631	3.638	152	gly-3-p-chol_141
3.638	3.643	153	fucose_142
3.643	3.647	154	myoinisitol_143

3.647	3.65	155	arabinose_144
3.801	3.812	156	Lac_169/arab/fuc/lac
3.812	3.845	157	arab/fuc/lac_168
3.845	3.86	158	fuc/serine_170
3.86	3.877	159	lac/G3PC_171
3.877	3.893	160	lac/G3PC/arab_172
3.893	3.904	161	G3PC_173
3.904	3.907	162	betaine_174
3.907	3.91	163	G3PC_175
3.91	3.916	164	arabinose_176
3.916	3.923	165	G3PC/arab_177
3.923	3.929	166	G3PC_178
3.929	3.938	167	creatine_179
3.938	3.945	168	lac/G3PC_180
3.945	3.96	169	lac/G3PC/arab_181
3.96	3.97	170	pi-meth-his_182
3.97	3.978	171	PMHis/galol_183
3.978	3.99	172	gal/Ser/hip_184
3.99	3.997	173	Ser/hip_185
3.997	4.056	174	arabinose_186
4.056	4.076	175	myoinisitol_187
4.076	4.133	176	lactate_188
4.133	4.146	177	misc_189
4.146	4.19	178	ophosphochol_190
4.19	4.274	179	Miscel_19
4.274	4.303	180	threonine_191
4.303	4.338	181	gly-3-p-chol_192
4.338	4.343	182	tartrate_193
4.343	4.352	183	gly-3-p-chol_194
5.222	5.25	184	Lactose_195
5.25	5.396	185	Miscel_21
5.396	5.432	186	misc-sugar_196
5.432	5.934	187	Miscel_22
5.934	5.955	188	GTP_197
5.955	5.965	189	Miscel_23
5.965	5.979	190	misc_198
5.979	5.99	191	misc_199
5.99	5.999	192	misc_200
5.999	6.01	193	misc_201

6.01	6.033	194	Miscel_24
6.033	6.043	195	misc_202
6.043	6.053	196	misc_203
6.053	6.084	197	Miscel_25
6.084	6.107	198	adenosine_204
6.107	6.142	199	Miscel_26
6.142	6.162	200	ADP/ATP_205
6.162	6.519	201	Miscel_27
6.519	6.526	202	singlet_206
6.526	7.301	203	Miscel_28
7.301	7.317	204	pi-meth-his_207
7.317	7.328	205	misc_208
7.328	7.479	206	Miscel_29
7.479	7.493	207	benzoate_209
7.493	7.535	208	Miscel_30
7.535	7.597	209	benzoate_210
7.597	7.769	210	Miscel_31
7.769	7.782	211	pi-meth-his_211
7.782	7.797	212	misc_212
7.797	7.846	213	Miscel_32
7.846	7.858	214	hippurate_213
7.858	7.887	215	benzoate_214
7.887	7.947	216	Miscel_33
7.947	7.963	217	misc_215
7.963	7.972	218	misc_216
7.972	7.988	219	misc_217
7.988	8.001	220	theophylline_218
8	8.01	221	methylxanthine_219
8.01	8.02	222	misc_220
8.138	8.15	223	misc_221
8.15	8.161	224	GTP_222
8.161	8.176	225	Miscel_34
8.176	8.186	226	oxypurinol_223
8.186	8.192	227	Miscel_35
8.192	8.204	228	hypoxanthine_224
8.204	8.212	229	Miscel_36
8.212	8.222	230	anserine_225
8.222	8.269	231	Miscel_37
8.269	8.282	232	ADP/ATP/aden_226
8.282	8.346	233	Miscel_38

8.346	8.357	234	adenosine_227
8.357	8.428	235	Miscel_39
8.428	8.438	236	misc_228
8.438	8.454	237	Miscel_40
8.454	8.465	238	formate_229
8.465	8.539	239	Miscel_41
8.539	8.546	240	ATP_230
8.546	8.556	241	ADP_231
8.556	8.582	242	Miscel_42
8.582	8.592	243	misc_232
8.592	8.612	244	Miscel_43
8.612	8.62	245	misc_233

10.2 Principal component analysis of metabolomics data

10.2.1 Peptide toxicity

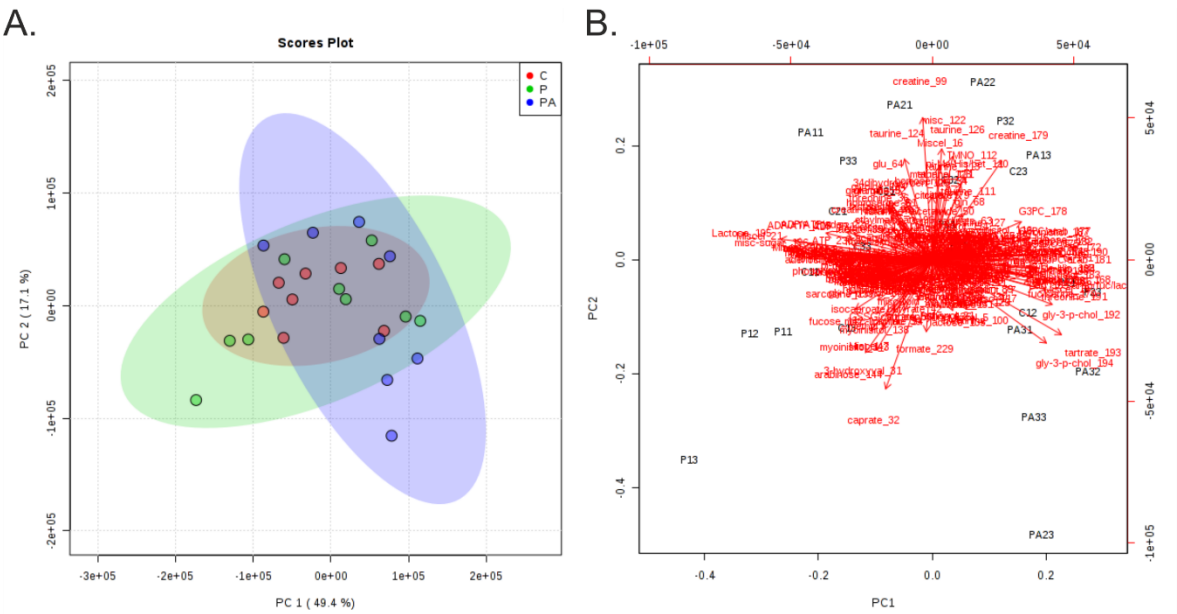

Figure 10-1 - PCA of the effect of KDGIVNGVKA on SH-SY5Y cells. *A PCA scores plot (A) shows that the samples exposed to fresh (green) and aged (red) KDGIVNGVKA are more variable than the control samples (red). The biplot (B) shows that this variance is largely the result of fluctuations in the elevels of caproate, creatine, lactose and glycerol-3-phosphocholine.*

10.2.2 Fibril toxicity

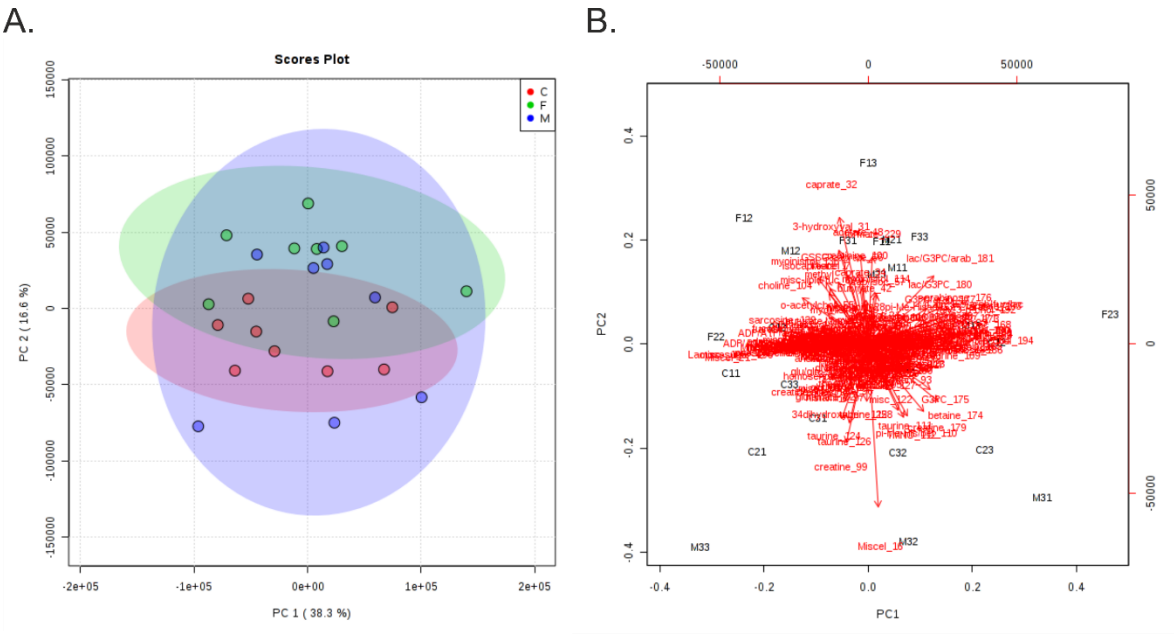

Figure 10-2 - PCA of the differential effects of aSyn monomers and fibrils on SH-SY5Y cells. *The Scores plot (A) showing the variance across different sample conditions: PBS control (red), monomeric aSyn alone (blue), and aSyn fibrils alone (green). The biplot (B) reveals that two of the biggest sources of variance across PC1 are lactose and arabinose, whilst in PC2 the main sources of variance are caproate, creatine and an unknown metabolite.*

10.2.3 Effect of KDGIVNGVKA on fibril toxicity

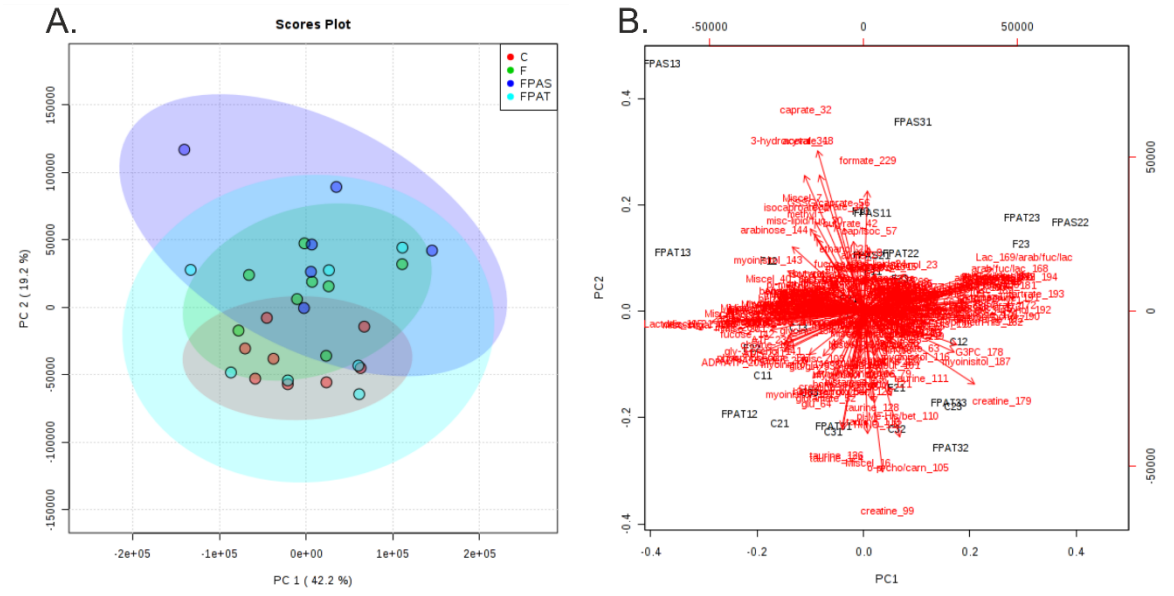

Figure 10-3 - PCA of the differential effects of aSyn fibrils on SH-SY5Y cells in the presence or absence of KDGIVNGVKA. *A Scores plot (A) showing the variance across different sample conditions: PBS alone (red), aSyn fibrils alone (green), fibrils plus independently aged KDGIVNGVKA (blue), and fibrils formed in the presence of KDGIVNGVKA (cyan). A biplot (B) reveals that major contributors to variance in PC1 are lactose and tartrate, and creatine, caprate and taurine in PC2.*

10.3 Circular dichroism spectra and secondary structure estimations of α-synuclein in the presence of detergent micelles and small unilamellar vesicles

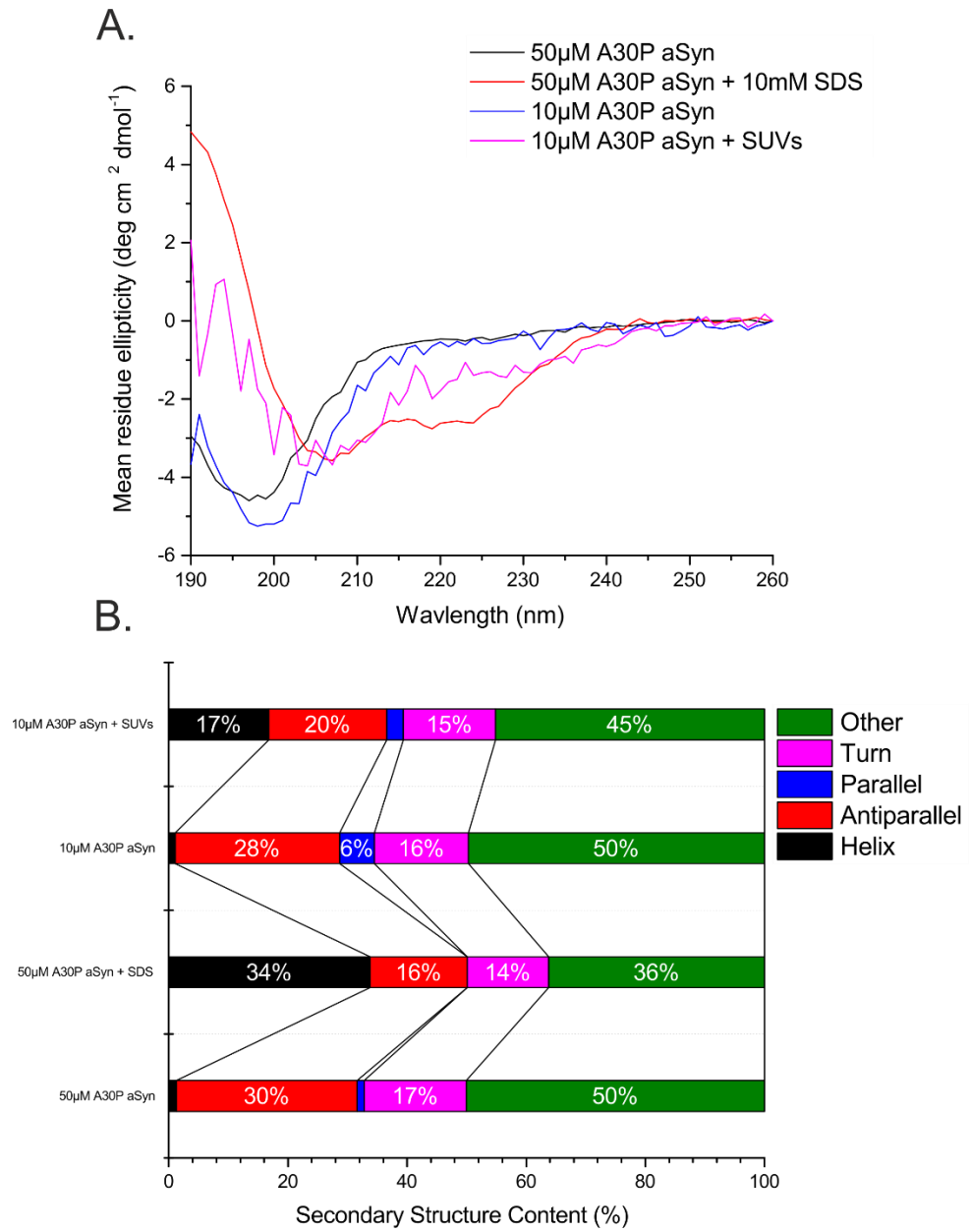

Figure 10-4 - CD spectra and estimations of secondary structural content of A30P aSyn alone, in the presence of SDS micelles, and in the presence of SUVs. *CD spectra (A) of 50μM A30P aSyn alone, of 50μM A30P aSyn with 10mM SDS, of 10μM A30P aSyn alone, and of 10μM A30P aSyn with 1.4mg/mL SUVs (DOPE:DOPS:DOPC 5:3:2). Secondary structural content estimations (B) were carried out using BeStSel* (181,182). *As expected A30P aSyn alone exhibits little helical content, but this rises in the presence of SUVs and more substantially in the presence of SDS micelles. The NRMSD values were 0.02091, 0.00785, 0.04081, and 0.08318 for the samples of 50μM A30P aSyn alone and with SDS, and of 10μM A30P aSyn alone and with SUVs respectively.*

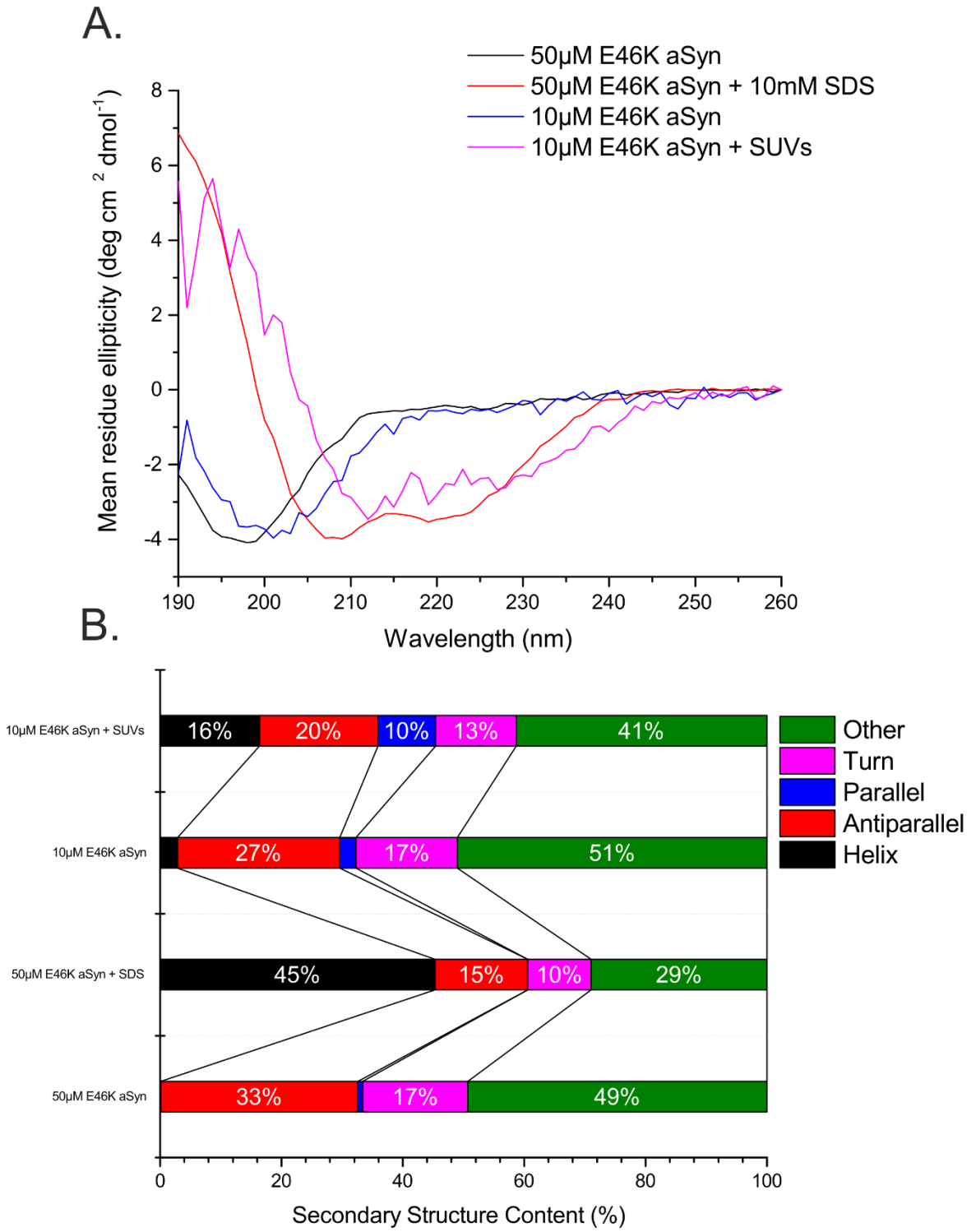

Figure 10-5 - CD spectra and estimations of secondary structural content of E46K aSyn alone, in the presence of SDS micelles, and in the presence of SUVs. *CD spectra (A) of 50μM E46K aSyn alone, of 50μM E46K aSyn with 10mM SDS, of 10μM E46K aSyn alone, and of 10μM E46K aSyn with 1.4mg/mL SUVs (DOPE:DOPS:DOPC 5:3:2). Secondary structural content estimations (B) were carried out using BeStSel* (181,182)*. E46K aSyn alone exhibits little helical content, but this rises extremely significantly in the presence of SDS micelles and to a much lesser extent in the samples containing SUVs. The NRMSD values are 0.01956, 0.00627, 0.05291, and 0.05385 for 50μM E46K aSyn alone and with SDS, and for 10μM E46K aSyn alone and with SUVs respectively.*

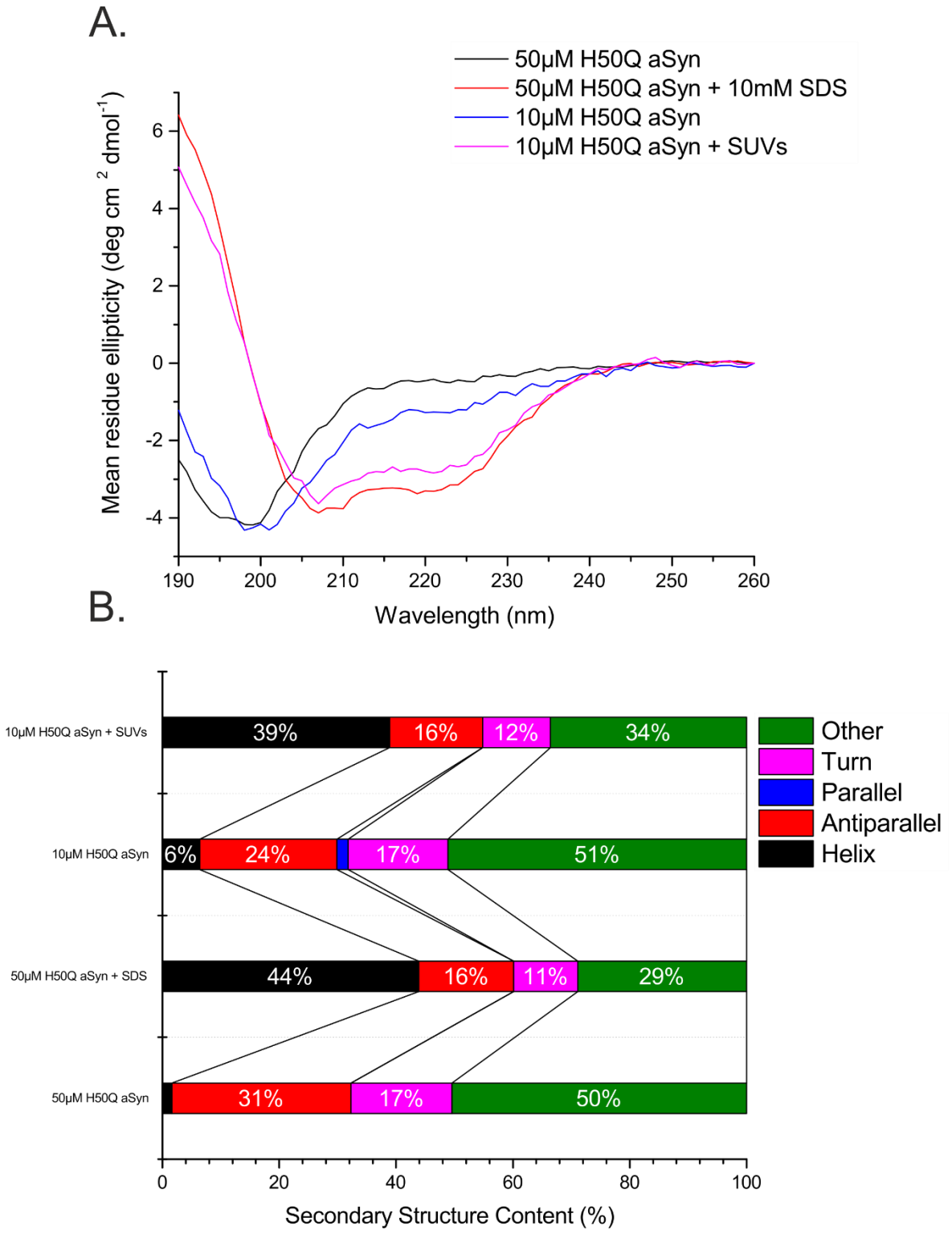

Figure 10-6 - CD spectra and estimations of secondary structural content of H50Q aSyn alone, in the presence of SDS micelles, and in the presence of SUVs. *CD spectra (A) of 50µM H50Q aSyn alone, of 50µM H50Q aSyn with 10mM SDS, of 10µM H50Q aSyn alone, and of 10µM H50Q aSyn with 1.4mg/mL SUVs (DOPE:DOPS:DOPC 5:3:2). Secondary structural content estimations (B) were carried out using BeStSel* (181,182)*. H50Q aSyn alone exhibits little helical content, but this rises substantially in the presence of SDS micelles or SUVs (44% and 39% respectively). This comes at the expense of the proportion in random coil ("other") and antiparallel conformations. The NRMSD values are 0.02143, 0.00673, 0.02621, and 0.00963 for 50µM H50Q aSyn alone and with SDS, and for 10µM H50Q aSyn alone and with SUVs respectively.*

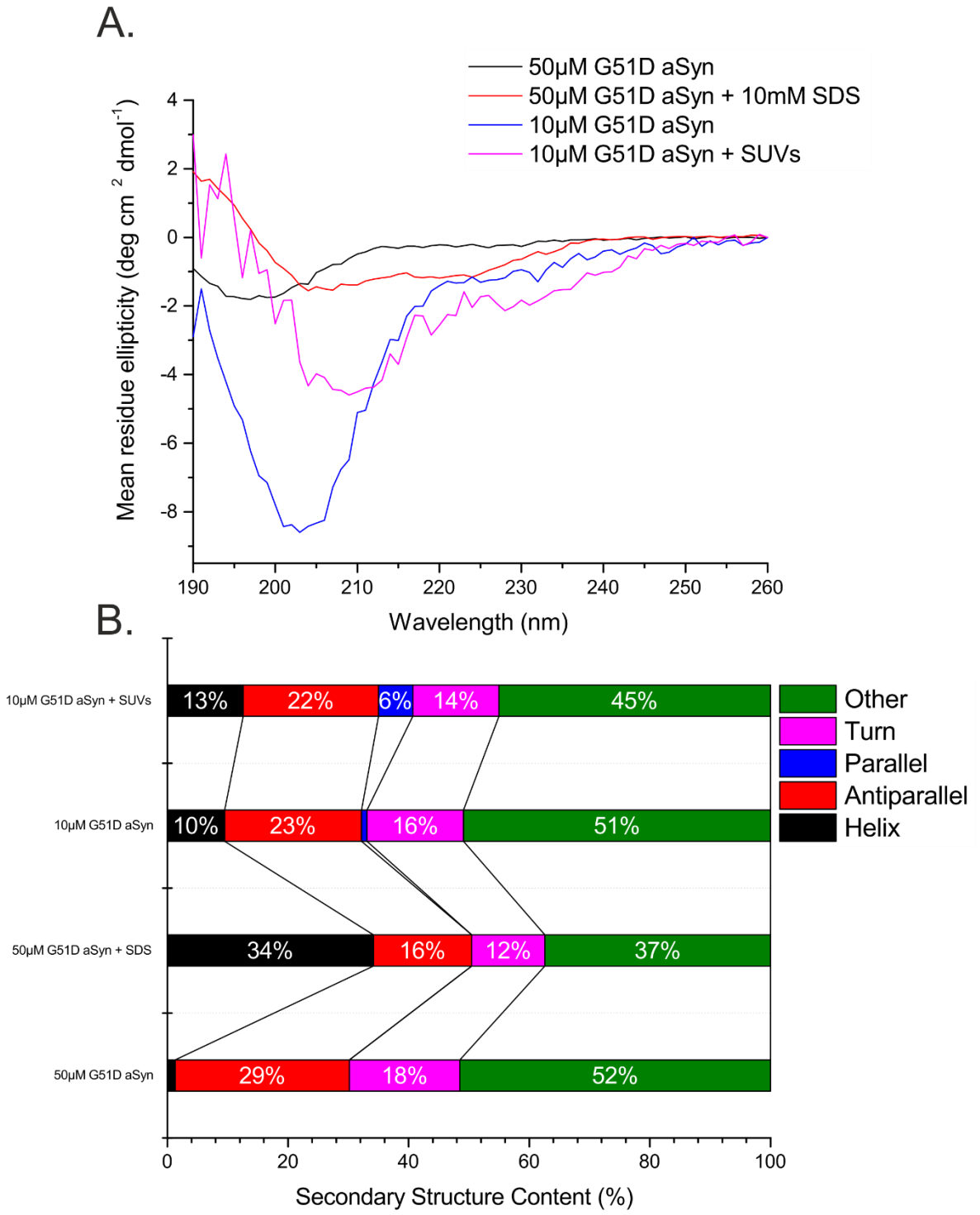

Figure 10-7 - CD spectra and estimations of secondary structural content of G51D aSyn alone, in the presence of SDS micelles, and in the presence of SUVs. *CD spectra (A) of 50μM G51D aSyn alone, of 50μM G51D aSyn with 10mM SDS, of 10μM G51D aSyn alone, and of 10μM G51D aSyn with 1.4mg/mL SUVs (DOPE:DOPS:DOPC 5:3:2). Secondary structural content estimations (B) were carried out using BeStSel* (181,182)*. G51D aSyn alone exhibits little helical content, but this rises in the presence of SDS micelles. There is a small increase in helicity in the presence of the SUVs, but instead a greater proportion of the protein exists in β-strand-like conformations. The NRMSD values are 0.02777, 0.01461, 0.03158, and 0.0721 for 50μM G51D aSyn alone and with SDS, and for 10μM G51D aSyn alone and with SUVs respectively.*

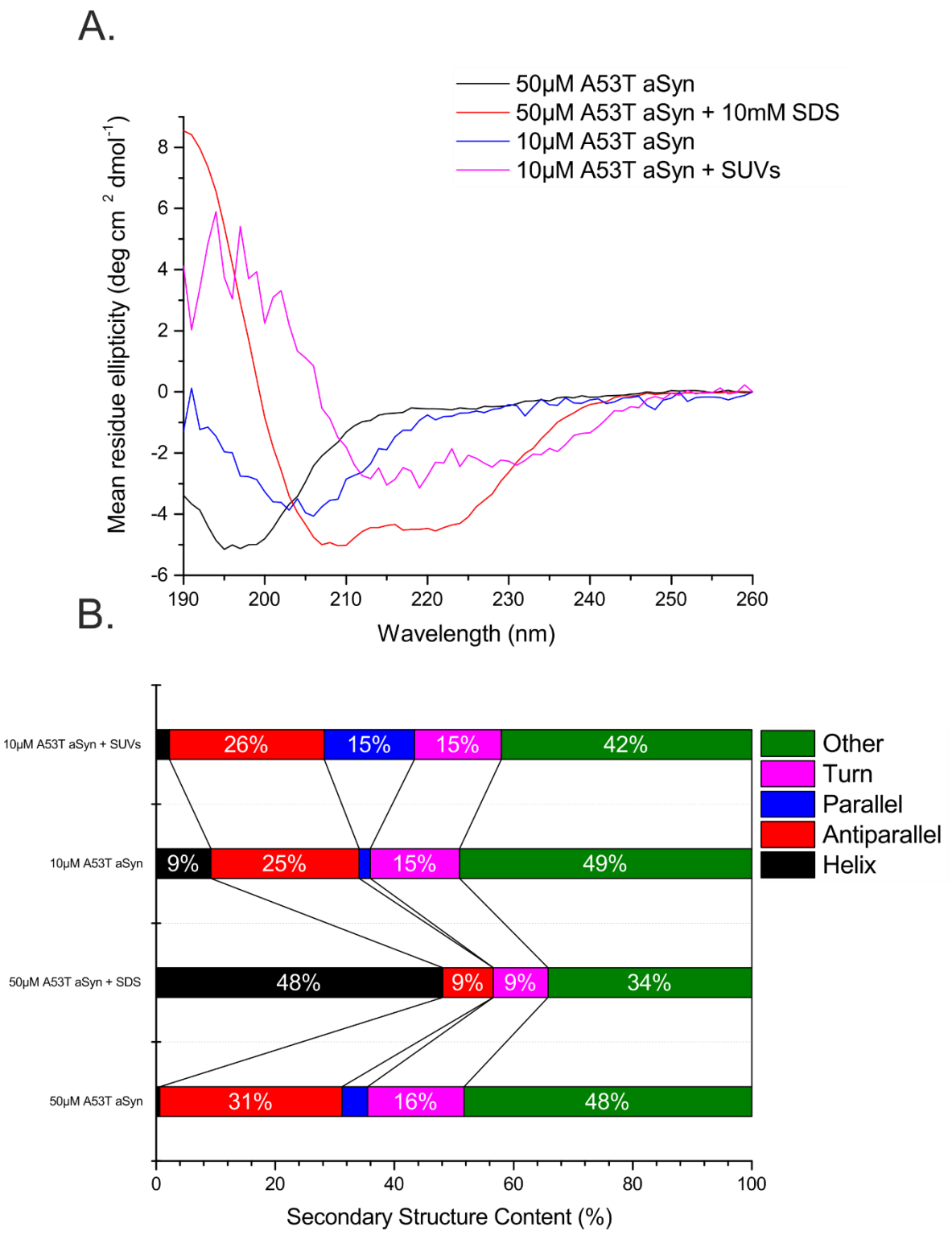

Figure 10-8 - CD spectra and estimations of secondary structural content of A53T aSyn alone, in the presence of SDS micelles, and in the presence of SUVs. *CD spectra (A) of 50μM A53T aSyn alone, of 50μM A53T aSyn with 10mM SDS, of 10μM A53T aSyn alone, and of 10μM A53T aSyn with 1.4mg/mL SUVs (DOPE:DOPS:DOPC 5:3:2). Secondary structural content estimations (B) were carried out using BeStSel* (181,182). *A53T aSyn alone exhibits little helical content, but this increases enormously in the presence of SDS micelles. Intriguingly, the helicity in the presence of SUVs remains below 5%, whilst the level of parallel β-strand has increased to 15%. This may suggest the beginnings of protein aggregation. The NRMSD values are 0.01841, 0.00427, 0.05509, and 0.05994 for 50μM A53T aSyn alone and with SDS, and for 10μM A53T aSyn alone and with SUVs respectively.*

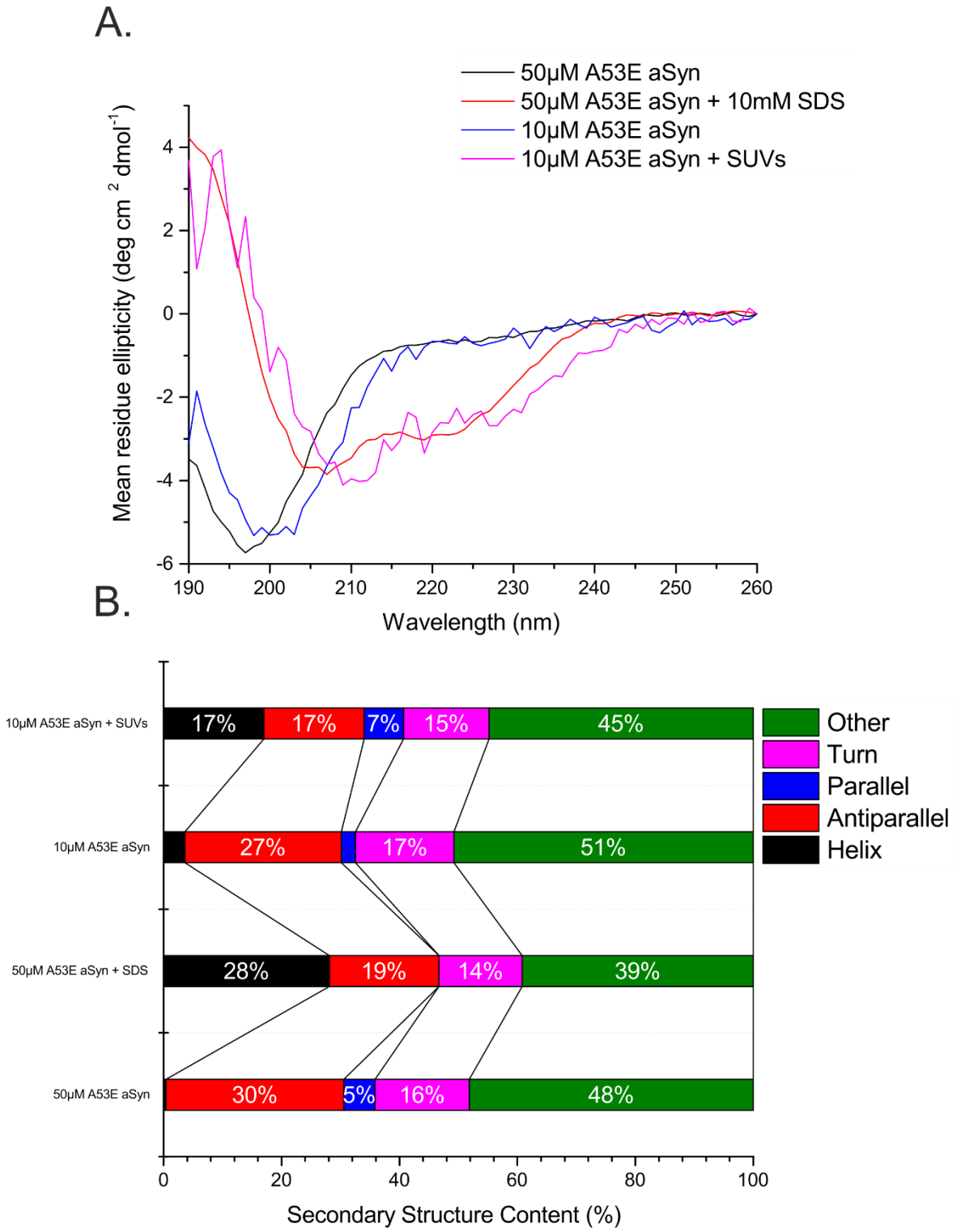

Figure 10-9 - CD spectra and estimations of secondary structural content of A53E aSyn alone, in the presence of SDS micelles, and in the presence of SUVs. *CD spectra (A) of 50μM A53E aSyn alone, of 50μM A53E aSyn with 10mM SDS, of 10μM A53E aSyn alone, and of 10μM A53E aSyn with 1.4mg/mL SUVs (DOPE:DOPS:DOPC 5:3:2). Secondary structural content estimations (B) were carried out using BeStSel* (181,182)*. As expected A53E aSyn alone exhibits little helical content, but this is substantially increased in the presence of SDS micelles or SUVs. Interestingly, in the presence of SUVs the level of helicity is lower than with SDS micelles, but some parallel β-strand characteristics have appeared and there remains 17% antiparallel signal. This may suggest protein aggregation. The NRMSD values are 0.0177, 0.00689, 0.04083, and 0.05726 for 50μM A53E aSyn alone and with SDS, and for 10μM A53E aSyn alone and with SUVs respectively.*

10.4 Effect of tyrosine nitration on the lipid-association of α-synuclein

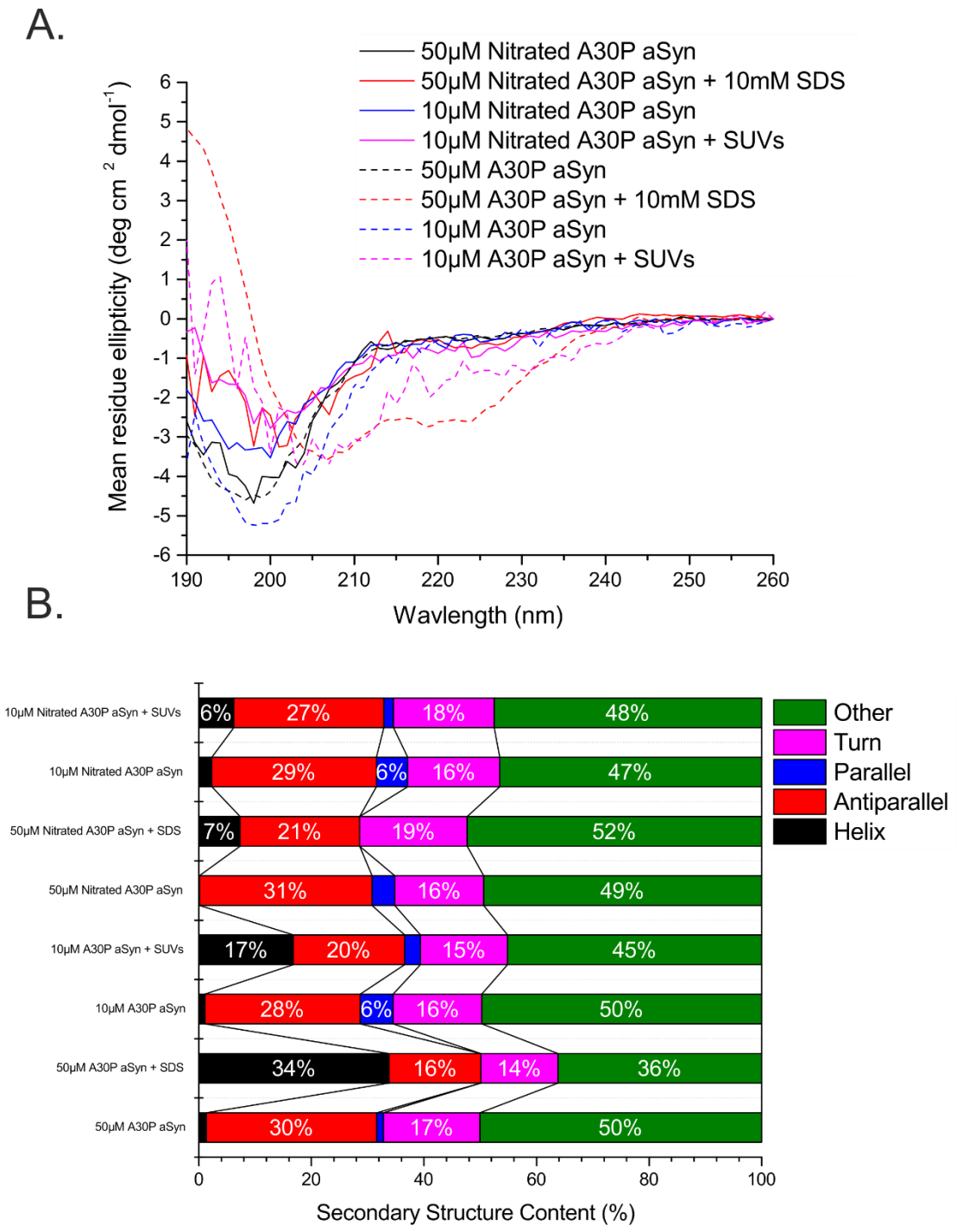

Figure 10-10 - CD spectra and estimations of secondary structural content for nitrated A30P aSyn in comparison to non-nitrated protein. *CD spectra (A) for nitrated (solid line) and non-nitrated (dashed-line) 50μM A30P aSyn alone, 50μM A30P aSyn with SDS micelles, 10μM A30P aSyn alone, and 10μM A30P aSyn with lipid SUVs composed of DOPE:DOPS:DOPC (5:3:2) are shown. Secondary structure estimations from the CD spectra as calculated by the BeStSel server are shown (B)* (181,182). *The NRMSD values are as follows: 50μM A30P aSyn alone (0.02091) and with SDS (0.00785), 10μM A30P alone (0.04081) and with SUVs (0.08318), 50μM nitrated A30P alone (0.03743) and with SDS (0.08103), and 10μM nitrated A30P alone (0.02923) and with SUVs (0.0538).*

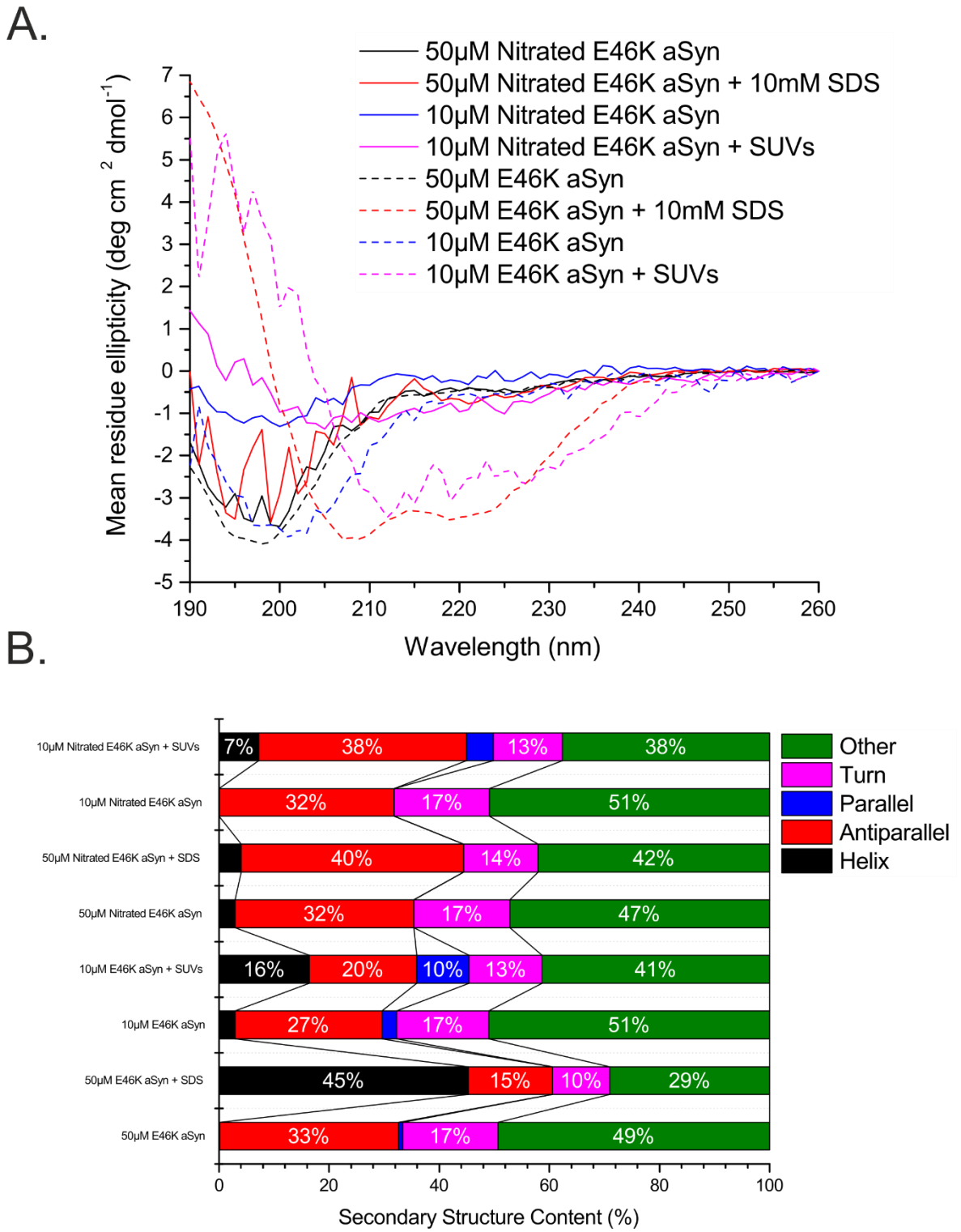

Figure 10-11- CD spectra and estimations of secondary structural content for nitrated E46K aSyn in comparison to non-nitrated protein. *CD spectra (A) for nitrated (solid line) and non-nitrated (dashed-line) 50μM E46K aSyn alone, 50μM E46K aSyn with SDS micelles, 10μM E46K alone, and 10μM E46K aSyn with lipid SUVs composed of DOPE:DOPS:DOPC (5:3:2) are shown. Secondary structure estimations from the CD spectra as calculated by the BeStSel server are shown (B)* (181,182). *The NRMSD values are as follows: 50μM E46K aSyn alone (0.01956), 50μM E46K aSyn with SDS (0.00627), 10μM E46K aSyn alone (0.05291), 10μM E46K with SUVs (0.05385), 50μM nitrated E46K aSyn alone (0.04146), 50μM nitrated E46K with SDS (0.11025), 10μM nitrated E46K aSyn alone (0.06251), and 10μM nitrated E46K aSyn with SUVs (0.0569).*

A.

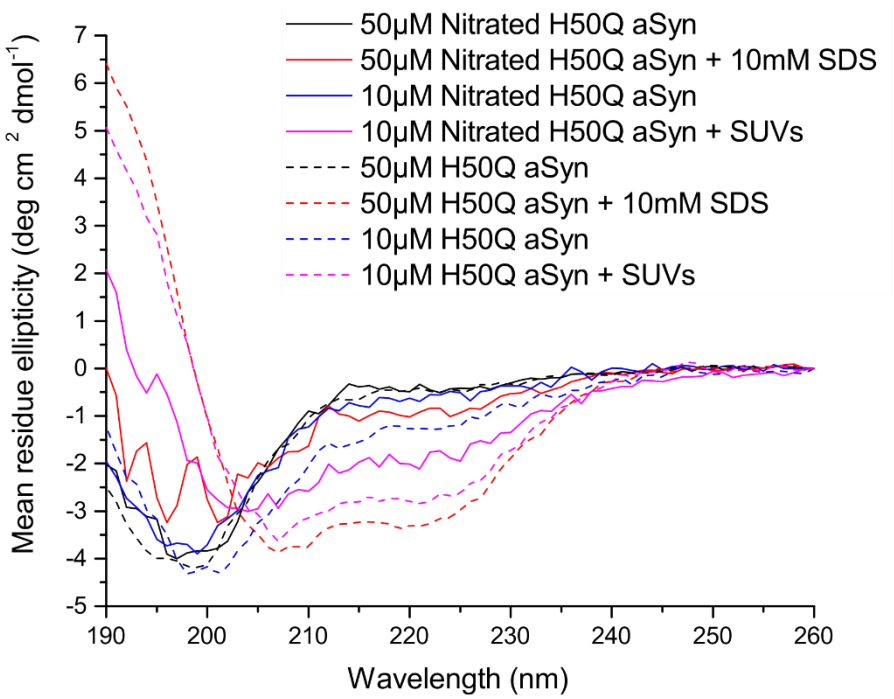

B.

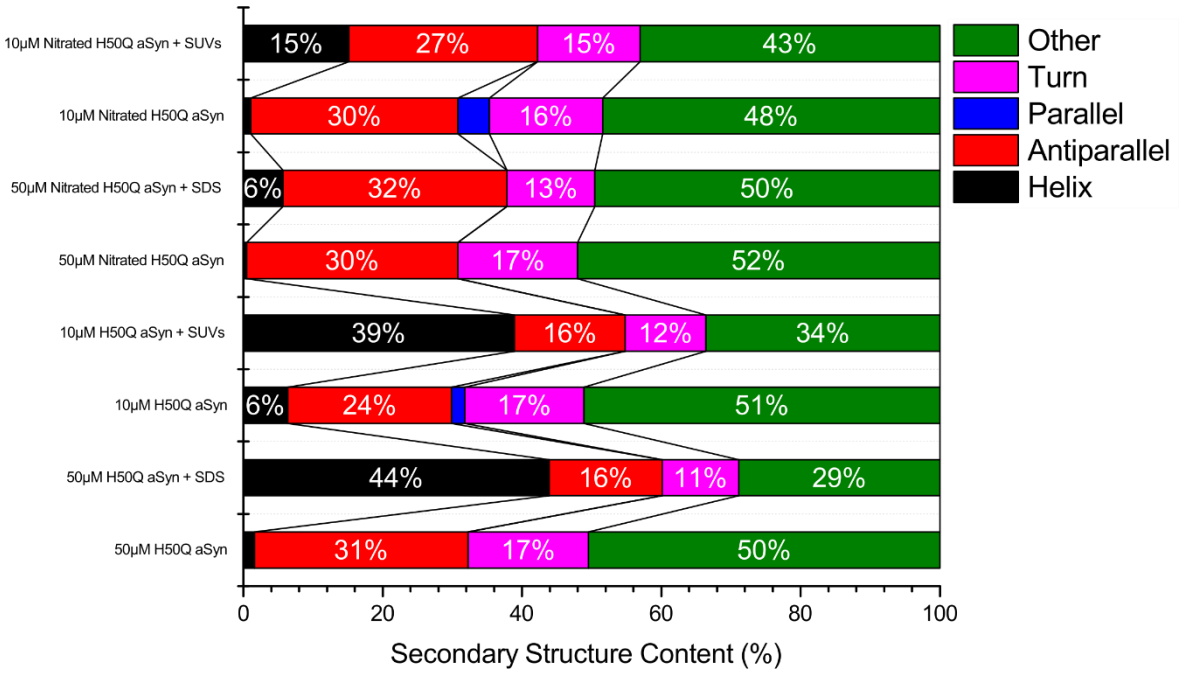

Figure 10-12 - CD spectra and estimations of secondary structural content for nitrated H50Q aSyn in comparison to non-nitrated protein. *CD spectra (A) for nitrated (solid line) and non-nitrated (dashed-line) 50μM H50Q aSyn alone, 50μM H50Q aSyn with SDS micelles, 10μM H50Q aSyn alone, and 10μM H50Q aSyn with lipid SUVs composed of DOPE:DOPS:DOPC (5:3:2) are shown. Secondary structure estimations from the CD spectra as calculated by the BeStSel server are shown (B)* (181,182). *The NRMSD values are as follows: 50μM H50Q aSyn alone (0.02143), 50μM H50Q aSyn with SDS (0.00673), 10μM H50Q aSyn alone (0.02621), 10μM H50Q aSyn with SUVs (0.00963), 50μM nitrated H50Q aSyn alone (0.03003), 50μM nitrated H50Q aSyn with SDS (0.08117), 10μM nitrated H50Q aSyn alone (0.0232), and 10μM nitrated H50Q aSyn with SUVs (0.03809).*

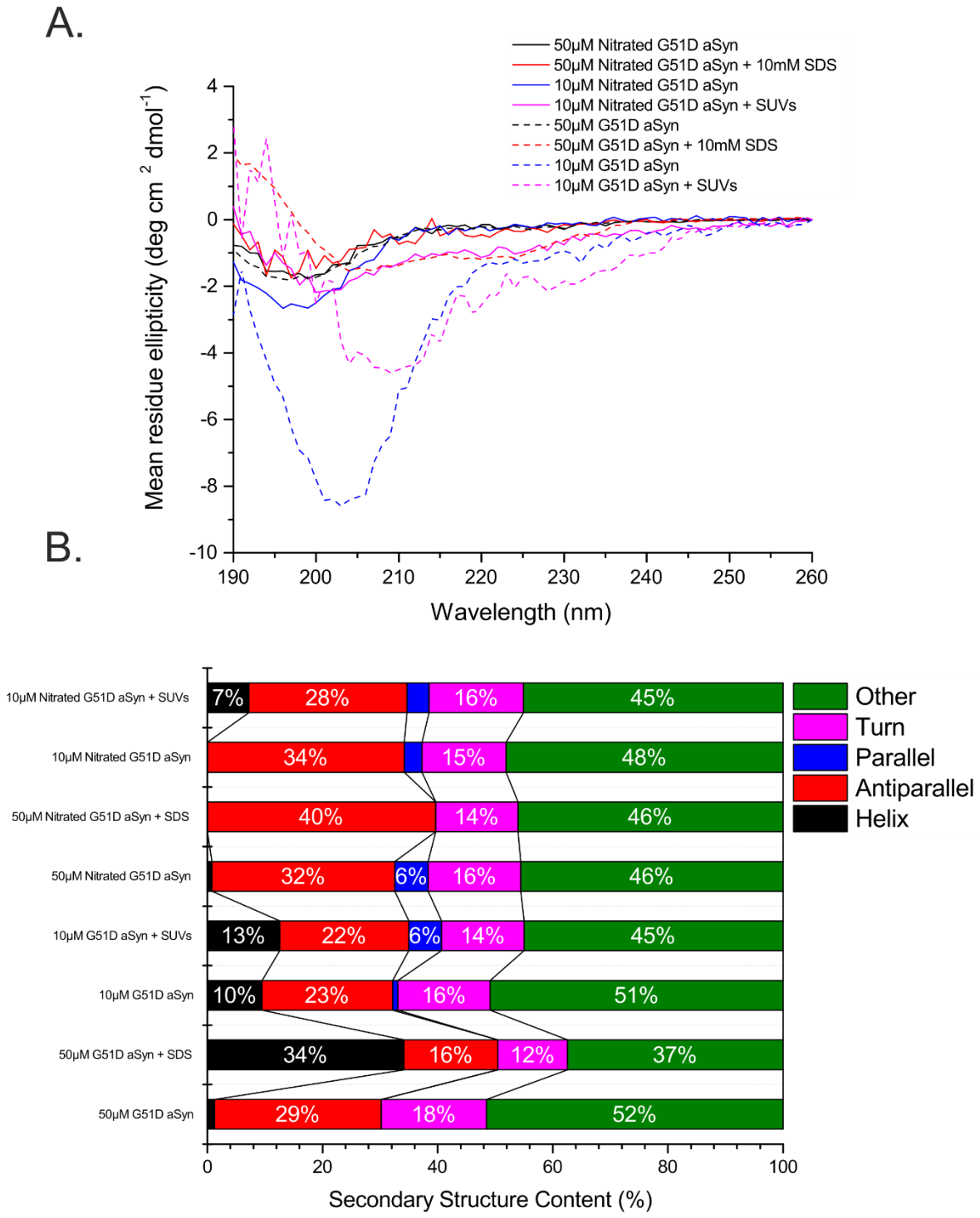

Figure 10-13 - CD spectra and estimations of secondary structural content for nitrated G51D aSyn in comparison to non-nitrated protein. *CD spectra (A) for nitrated (solid line) and non-nitrated (dashed-line) 50μM G51D aSyn alone, 50μM G51D aSyn with SDS micelles, 10μM G51D aSyn alone, and 10μM G51D aSyn with lipid SUVs composed of DOPE:DOPS:DOPC (5:3:2) are shown. Secondary structure estimations from the CD spectra as calculated by the BeStSel server are shown (B)* (181,182). *The NRMSD values are as follows: 50μM G51D aSyn alone (0.02227), 50μM G51D aSyn with SDS (0.01461), 10μM G51D aSyn alone (0.03158), 10μM G51D aSyn with SUVs (0.0721), 50μM nitrated G51D aSyn alone (0.0418), 50μM nitrated G51D aSyn with SDS (0.09259), 10μM nitrated G51D aSyn alone (0.03353), and 10μM nitrated G51D aSyn with SUVs (0.05897).*

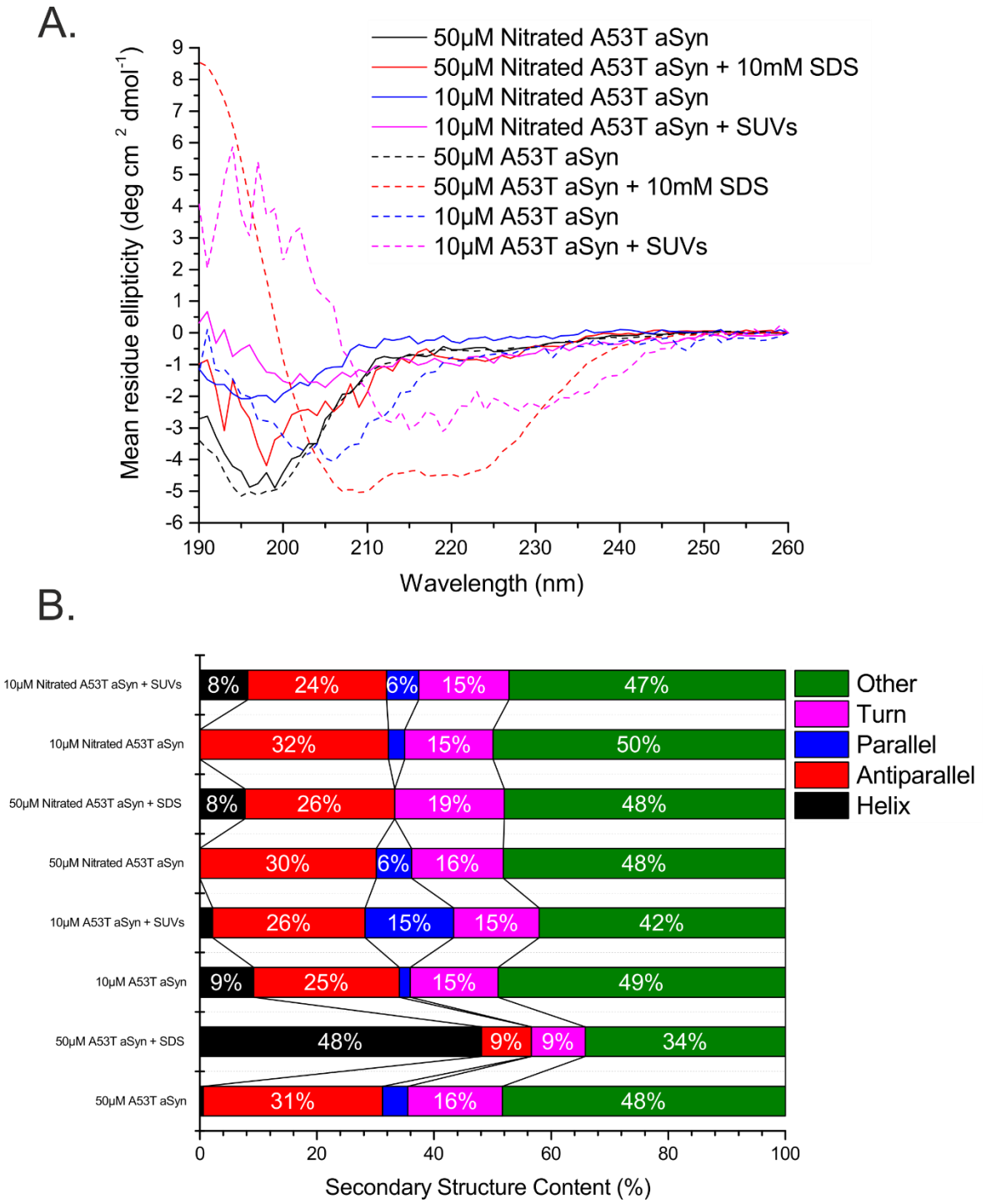

Figure 10-14 - CD spectra and estimations of secondary structural content for nitrated A53T aSyn in comparison to non-nitrated protein. *CD spectra (A) for nitrated (solid line) and non-nitrated (dashed-line) 50μM A53T aSyn alone, 50μM A53T aSyn with SDS micelles, 10μM A53T aSyn alone, and 10μM A53T aSyn with lipid SUVs composed of DOPE:DOPS:DOPC (5:3:2) are shown. Secondary structure estimations from the CD spectra as calculated by the BeStSel server are shown (B)* (181,182). *The NRMSD values are as follows: 50μM A53T aSyn alone (0.01841), 50μM A53T with SDS (0.00427), 10μM A53T aSyn alone (0.05509), 10μM A53T aSyn with SUVs (0.05994), 50μM nitrated A53T aSyn alone (0.02388), 50μM nitrated A53T aSyn with SDS (0.06388), 10μM nitrated A53T aSyn alone (0.03874), and 10μM A53T aSyn with SUVs (0.06684).*

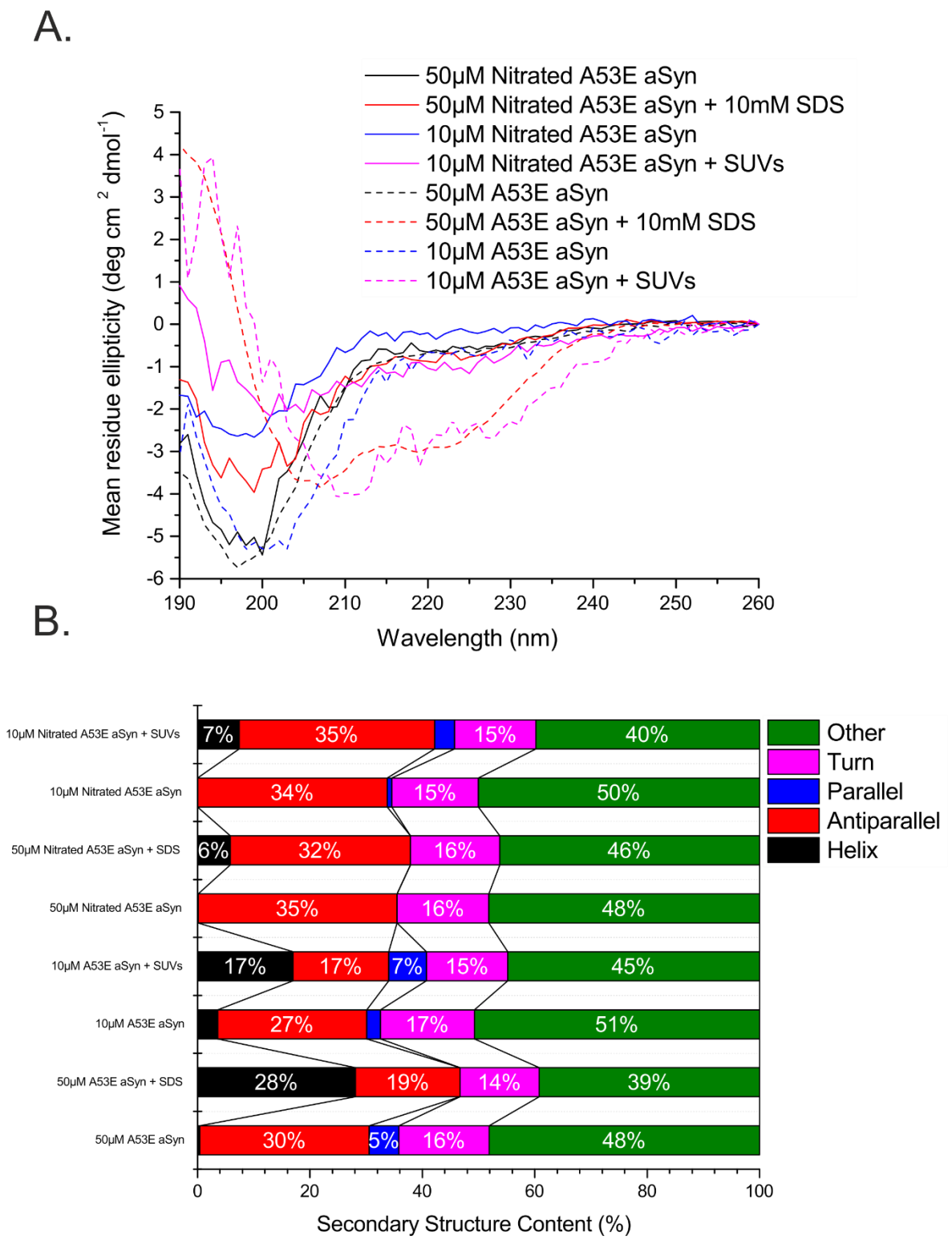

Figure 10-15 - CD spectra and estimations of secondary structural content for nitrated A53E aSyn in comparison to non-nitrated protein. *CD spectra (A) for nitrated (solid line) and non-nitrated (dashed-line) 50μM A53E aSyn alone, 50μM A53E with SDS micelles, 10μM A53E aSyn alone, and 10μM A53E aSyn with lipid SUVs composed of DOPE:DOPS:DOPC (5:3:2) are shown. Secondary structure estimations from the CD spectra as calculated by the BeStSel server are shown (B)* (181,182). *The NRMSD values are as follows: 50μM A53E aSyn alone (0.0177), 50μM A53E aSyn with SDS (0.00689), 10μM A53E aSyn alone (0.04083), 10μM A53E aSyn with SUVs (0.05726), 50μM nitrated A53E aSyn alone (0.03034), 50μM nitrated A53E aSyn with SDS (0.03895), 10μM nitrated A53E aSyn alone (0.03734), and 10μM A53E aSyn with SUVs (0.0641).*